The Development of Anaerobic Setups and Analytical Techniques for the Static Testing of the Oilfield Sulphide Scales

Yaser Khaled Saleh Alduailej

Submitted for the degree of Doctor of Philosophy

Heriot-Watt University

School of Energy, Geoscience, Infrastructure and Society

June 2019

ABSTRACT

The occurrence of oilfield sulphide scale has contributed to the decrease in production and injection rates by reducing the inner diameter of flow lines and causing failures to downhole equipment. The most common remedy for oilfield scale is inhibition, and the design of a scale inhibition treatment usually requires investigative laboratory tests to evaluate and understand the scale inhibition and formation mechanisms. The *static* jar test is one of the primary tests carried out in an evaluation study of a scale inhibitor, where two or more solutions are mixed that form or inhibit the formation of the subject scale(s). Further advancements in the technique for the static tests for sulphide scale have been required, as they are sensitive to oxygen, i.e. the tests result in iron (II) sulphide precipitation, and are prone to evolve $H_2S_{(g)}$ at low pH levels (pH < 8), heightening further the need for special logistical and safety measures.

Several developments of the conventional static bottle test were evaluated, which ultimately led to the development of an anaerobic bench-top static test setup, consisting of airtight tubes and vials. The primary purposes of this setup were to enable the control and monitoring of aqueous sulphide concentrations, as well as minimising the oxidation of sulphide species. This apparatus allows experimentalists to accurately pH-adjust sodium sulphide solutions and retain the evolved $H_2S_{(g)}$, while continuously and non-intrusively quantifying the sulphide concentrations via the UV-Vis spectrophotometer technique. This anaerobic static test setup offers a genuine alternative to costly investment in anaerobic capabilities, *e.g.* glovebox facilities.

The anaerobic setup was used in the determination of the effect of oxygen on the aqueous sulphide, which showed minimum influence in the oilfield scale studies. The formation of FeS, ZnS and PbS was tested under various conditions using the anaerobic setup and the results were validated against a scale prediction model. Dynamic formation tests of iron sulphide showed increasing iron-deficiency with time, which recommends more frequent cleanout treatments to increase dissolution efficiency. The reproducible pH-adjustment of the aqueous sulphide had a significant impact on the scale inhibition tests, which can optimise inhibition treatment design. These results were attained using a safe, compact and highly repeatable setup developed at a fraction of the cost of other anaerobic testing systems.

DEDICATION

To my parents, Khaled and Nawal

To my lovely wife and my other half, Asma, and to my children, Khaled, Salma and Hassan

To my brothers and sisters, Mohammed, Aisha, Suad, Hind and Saleh

ACKNOWLEDGEMENT

All praise is due to Allah, to whom belongs whatever is in the heavens and whatever is in the earth, and to Him belongs all praise in the Hereafter. And He is the Wise, the Acquainted. [Al-Qur'an – Surah Saba' 34: 1]

I want to thank my supervisor, Professor Ken Sorbie, for his *patience* and guidance, and, before that, for accepting me as his student. His contributions to my research have been critical. Professor Sorbie has inspired me to unleash my research-imagination and to go beyond the norm. For all of that, I am grateful and ever so thankful.

Special thanks for Dr Harry Oduro, Dr Mohammed Alkhaldi, and Salman Alqathami, from Saudi Aramco, for their invaluable support in the investigation of sulphide oxidation and the analysis of aqueous sulphide.

I would also like to thank Professor Eric McKay for his welcoming and his very first advice: *"question everything"*, Dr Alexander Graham for his supervision throughout my PhD and support in the publications and thesis revision, Dr Lorraine Boak for her lab supervision and vital support during the development of the UV-Vis method, Mike Singleton for his guidance and support, Duarte Silva for this support in the modelling section, Wendy McEwan and Katherine McIver for their help in the ICP analysis, Tom Clark and Tom McGravie for their support in the fabrication workshop, Alan Beteta for his assistance in the oxygen-free-related tests, Ivan Davis for his help in the ESEM-EDX analysis, Dr Oleg Ishkov for being the most supportive and kindest office- and *coffee*-mate, Heather O'Hara for her tremendous support during my PhD, and for all FAST members who have positively contributed to the beautiful 54-months stay in Edinburgh.

Many thanks for Dr Jim Buckman for his support and facilitation of the ESEM-EDX analysis.

I would like to sincerely thank Alexander and Claire Graham for their exceptional and generous hospitality.

Many thanks to Mr Samer AlAshgar, Mr Saleh Al Ammari, Dr Suha Al-Behaisi, and Mr Abdullah Al-Mohammed, from Saudi Aramco, for their support before and throughout the Advanced Degree Program assignment.

Saudi Aramco is thanked for sponsoring my PhD and for their continuous support throughout my studies.

Sponsoring companies of FAST 4, 5, and 6 are thanked for their continuous contribution to FAST research.

ACADEMIC REGISTRY
Research Thesis Submission

Name*:*	Yaser Alduailej		
School:	EGIS		
Version: *(i.e. First, Resubmission, Final)*	Final	Degree Sought:	PhD

Declaration

In accordance with the appropriate regulations I hereby submit my thesis and I declare that:

1) the thesis embodies the results of my own work and has been composed by myself
2) where appropriate, I have made acknowledgement of the work of others and have made reference to work carried out in collaboration with other persons
3) the thesis is the correct version of the thesis for submission and is the same version as any electronic versions submitted*.
4) my thesis for the award referred to, deposited in the Heriot-Watt University Library, should be made available for loan or photocopying and be available via the Institutional Repository, subject to such conditions as the Librarian may require
5) I understand that as a student of the University I am required to abide by the Regulations of the University and to conform to its discipline.
6) I confirm that the thesis has been verified against plagiarism via an approved plagiarism detection application e.g. Turnitin.

* *Please note that it is the responsibility of the candidate to ensure that the correct version of the thesis is submitted.*

Signature of Candidate*:*		Date:	11/11/2019

Submission

Submitted By *(name in capitals):*	
Signature of Individual Submitting:	
Date Submitted:	

For Completion in the Student Service Centre (SSC)

Received in the SSC by *(name in capitals):*			
Method of Submission *(Handed in to SSC; posted through internal/external mail):*			
*E-thesis Submitted (**mandatory for final theses**)*			
Signature:		Date:	

Please note this form should be bound into the submitted thesis.
Academic Registry/Version (1) August 2016

TABLE OF CONTENTS

LISTS OF TABLES ix
LISTS OF FIGURES x
LIST OF PUBLICATIONS xiv
Nomenclature xv

1 - INTRODUCTION **1**

1.1 Scale Formation in Oilfield Operations 1
1.2 Oilfield Sulphide Scales 2
1.2.1 Hydrogen Sulphide in the Oilfield *2*
1.2.2 Hydrogen Sulphide in Laboratory Studies *3*
1.2.3 Sources of Divalent Metal Cations (Fe^{2+}, Zn^{2+} and Pb^{2+}) *5*
1.3 Scale Inhibition 7
1.4 Scale Prediction Models 8
1.5 Objectives and Research Methodologies 9

2 – Literature Review **10**

2.1 Oilfield Sulphide Scale 10
2.2 Protocols for Sulphide Scale Formation and Inhibition Tests 12
2.2.1 The Static "Jar" Test of Barium Sulphate Scale *12*
2.2.2 Introducing Hydrogen Sulphide Gas to Form Sulphide Scale *13*
2.2.3 The Investigation of Sulphide Scale Using Airtight Vessels *15*
2.2.4 Dynamic Sulphide Scale Tests *16*
2.2.5 Kinetic Turbidity Tests *16*
2.3 Analytical Techniques for Sulphide Determination 16
2.3.1 Titration and Potentiometry *16*
2.3.2 Chromatography *17*
2.3.3 Spectrophotometry *17*
2.3.4 Summary of Analytical Methods for Sulphide Determination *18*
2.4 Oxidation of Aqueous Sulphide 19
2.4.1 Reactions of Aqueous Sulphide and Dissolved Oxygen *19*
2.4.2 Oxidation of Sulphide in the Oil and Gas Fields *21*
2.4.3 Oxygen Sources in Downhole Fluids *22*
2.5 Conclusions 22

3 – Static Bottle Test for Sulphide Scale – Current Practice **24**

Executive Summary 24
3.1 Description of the Static Bottle Test 24
3.1.1 Experimental Description of the Formation Test of ZnS at NSSW and 50°C *24*
3.1.2 Results of the Static Formation Test of ZnS at 50°C *27*
3.2 Development of the Static Scale Test Setup 29
3.2.1 pH Adjustment of Sulphide Solutions *30*
3.2.2 Formation of ZnS Using H_2S Gas *39*
3.2.3 Evaluation of the Efficiency of Inhibiting ZnS Formed by Displacing H_2S gas *44*
3.3 Summary and Conclusions 46

4 – Development of an Analytical Method for Aqueous Sulphide Detection **47**

Executive Summary 47
4.1 Importance of Developing an Alternative Analytical Method 47
4.2 Alternative Sulphide Determination Methods 47
4.3 Description of the Copper Reagent Method 48
4.3.1 Establishment of a Calibration Curve *49*
4.3.2 Further Enhancement of Calibration Curves *53*
4.4 Incompatibilities of the Copper Reagent 57
4.5 Analysis of Samples with Suspended Solids 59
4.6 UV-Vis Method Compared to ICP/Back-Calculation Technique in Detecting Oxidative Loss of Sulphide Concentration 61
4.7 Summary and conclusions 63

5 – The Anaerobic Static Test Setup 64

Executive Summary 64
5.1 Conventional Bottle Test 64
5.2 Description of the Anaerobic Test Setup 65
5.3 Preparation and De-Oxygenation of Stock Solutions 66
5.4 Mixing and Sampling Protocols 67
5.5 pH Adjustment and Stock Solution Mixing Volumes 69
5.5.1 pH Adjustment of Aqueous Sulphide Solutions 69
5.5.2 The Protocols of Mixing Various Solutions 71
5.6 A Comparison of the Different Test Setups 72
5.7 Summary and Conclusions 73

6 – Oxidation of Aqueous Sulphide 74

Executive Summary 74
6.1 Introduction 74
6.2 Preliminary Static Oxidation Tests 75
6.2.1 The Effect of pH on the Magnitude of Oxidative Sulphide in the Presence of Oxygen 75
6.2.2 Results of the Preliminary Oxidation Tests 77
6.3 Extended Static Oxidation Tests 84
6.3.1 Procedural Modifications for the Extended Oxidation Tests 84
6.3.2 Theoretical Quantification of the Oxidative Loss Based on Dissolved Oxygen Content 84
6.3.3 The Extended Oxidative Loss Measured by UV-Vis Method 85
6.3.4 Repeat of the Extended Oxidation Test 88
6.4 Dynamic (Stirring) Oxidation Tests 90
6.4.1 The Preparations and Test Procedure of the Dynamic Oxidation Test 90
6.4.2 Oxidation of 100 mg/L of Aqueous Sulphide at pH_f of 5.61 and 6.42 91
6.4.3 Depletion of Dissolved Oxygen (5 mg/L) and Sulphide (1,000 mg/L) Concentrations at Various pH Levels 93
6.4.4 Oxygen Poisoning Tests 96
6.5 Conclusions and recommendations 100

7 – Formation of FeS 102

Executive Summary 102
7.1 Introduction 102
7.2 Autoscale Profiles of FeS 103
7.2.1 Autoscaling of FeS at Various Sulphide-to-Iron Concentration Ratios 104
7.2.2 FeS Autoscaling Profiles at Fixed Iron concentrations 107
7.3 The Effect of Oxygen on the Formation of FeS 111
7.4 Autoscale Profiles of ZnS, PbS and Combined Scales 113
7.5 Experimental and Prediction Data Comparison 118
7.5.1 FeS Autoscale Profiles 119
7.5.2 Direct FeS Formation vs FeS Autoscale 125
7.5.3 PbS, ZnS and Multiple Scale 126
7.6 Dynamic (Stirring) Tests of FeS Formation 132
7.7 Conclusions 137

8 – Inhibition of FeS 139

Executive Summary 139
8.1 The Inhibition of FeS inhibition at various conditions 139
8.2 Descriptions of MIC Determination Tests at Various Conditions 140
8.2.1 Effect of the Initial Sulphide Concentration on the MIC 141
8.2.2 Effect of Increasing the Iron Concentration on the MIC 145
8.2.3 Effect of Extending the Inhibition Duration on the MIC 146
8.2.4 Effect of Temperature on the MIC 146
8.2.5 Comparison of Two Scale Inhibitors at Two Temperatures in Terms of MIC 147
8.2.6 Effect of Salinity on the MIC 149
8.3 The Effect of Dissolved Oxygen on the Inhibition Efficiency at [SI] = 40 mg/L 150
8.4 Dynamic (Stirring) Test of Inhibited FeS 151
8.5 Conclusions 152

9 – Conclusions and Recommendations 154

References 156

Appendix A - Development of the UV-Vis Spectrophotometric method 165
Appendix B – pH Measurement of Anaerobic Sulphide Solutions 166
Appendix C - Experimental Procedures 168
Appendix D - Sulphide Oxidation 170
Appendix E - Direct Formation of FeS at Variable-pH Solutions 172
Appendix F – ICP Analysis Protocol (for TF-iCAP 6500DV and HJY-U2 Equipment) 175

LISTS OF TABLES

Table 2.1 Literature thermodynamic solubility product constants for FeS, ZnS, and PbS.....11
Table 2.2 Summary of analytical methods for determining the concentration of aqueous sulphide.....18
Table 2.3 Summary of literature review from Weres and Tsao (1983).....21
Table 3.1 H_2S NSSW brine composition for the ZnS formation test.....25
Table 3.2 Zn NSSW brine composition for the ZnS formation test.....25
Table 3.3 $ZnCl_2$ concentration and corresponding weights per 250 mL Zn NSSW.....26
Table 3.4 ICP standard preparation for Zn analysis.....27
Table 3.5 Concentrations of zinc in Zn brines.....32
Table 3.6 Adjustment of pH value for the pH-adjusted H_2S brines.....33
Table 3.7 pH adjustment process and results of 2nd and 3rd Phases.....36
Table 3.8 ICP analysis results of Zn concentration in stock and supernatant solutions and their respective pH values of 2nd and 3rd phases.....38
Table 3.9 ICP analysis of zinc in stock and mixed solutions after saturation with the 300 ppm H_2S gas41
Table 3.10 ICP analysis of zinc in stock and supernatant solutions after sparging with H_2S gas.....42
Table 3.11 EDX analysis of the white precipitates formed from displacing $H_2S_{(g)}$ through Zn NSSW...43
Table 3.12 The individual loadings of scale inhibitors used at separate Zn samples.....44
Table 4.1 Difference summary between the methylene blue and the copper reagent methods.....48
Table 4.2 Groups of different sulphide stock solutions of varying concentration, used for establishing several calibration curves over different ranges.....51
Table 4.3 Various developmental steps of the UV-Vis spectrophotometric method.....55
Table 4.4 The geochemical composition of Glenelg formation water (Al-Harbi *et al.*, 2017).....58
Table 5.1 Features of the used Hungate-type tubes and the culture vials.....66
Table 5.2 Tabled pH adjustment results using 1M HCl and 5 mL of 242 mg/L sulphide solution in NSSW.....70
Table 5.3 Comparison of the features of the static test setups.....73
Table 6.1 Weights and concentration of sulphides in prepared solutions.....75
Table 6.2 Tabled pH adjustment results using 1M HCl and 5 mL of 242 mg/L sulphide solution in NSSW.....77
Table 6.3 Extended static oxidation test of sulphide solutions (40 mg/L of aqueous sulphide) at different conditions.....84
Table 6.4 The geochemical composition of Khuff formation water (Franco *et al.*, 2010).....94
Table 7.1 Scale prediction data for FeS in Khuff Na & Ca ($[Fe^{2+}]_i$ = 48 mg/L and $[S^{2-}]_i$ = 970 mg/L).120
Table 7.2 1st Set - Final sulphide and iron concentrations and pH value after several mixing periods..133
Table 7.3 2nd Set - Final sulphide and iron concentrations and pH value after several mixing periods.133
Table 7.4 ESEM analysis of FeS formed particles in the 1st set after mixing for various periods.....135
Table 7.5 ESEM analysis of FeS formed particles in the 2nd set after mixing for various periods.....136
Table 8.1 Details of the MIC determination sets of samples (concentrations, pH, brine, and temperature).....142
Table 8.2 Final iron concentrations and pH values of the inhibited FeS solutions after several mixing periods.....151
Table 8.3 ESEM analysis of the inhibited FeS formed particles in the 3rd set after two days of mixing.....152

LISTS OF FIGURES

Figure 1.1 Speciation of aqueous sulphide in distilled water as a function of pH.....5
Figure 2.1 Conventional experimental scheme of the static bottle test of sulphide scale starting from the brine preparation, aliquot distribution and addition of metal cation concentrations, heating, mixing the two brines, then heating and frequent analysis.....12
Figure 2.2 Sulphide scaling experimental rig A *(Keogh et al., 2017)*, B (*Keogh et al., 2018*).....14
Figure 2.3 Experimental setup for the scavenging efficiency experiment where H_2S is generated by dissolving FeS *(Al-Duailej et al., 2012)* 15
Figure 3.1 Scale formation profiles of ZnS represented by pH values and zinc concentration in stock and test samples compared to theoretical values in NSSW at 50°C after 24 hours 28
Figure 3.2 ZnS Particle size distribution measured in duplicate samples as a function of Zn/S molar ratio 29
Figure 3.3 Experimental scheme to adjust the pH of sulphide solution before mixing with the scaling metal solution to avoid direct acid addition to sulphide solution which could evolve $H_2S_{(g)}$ 31
Figure 3.4 Losses of H_2S after adjusting pH values 33
Figure 3.5 ICP results of remaining Zn in supernatant solution after mixing with pH-adjusted sulphide brines showing higher $[Zn^{2+}]$ in samples at lower pH values (1000-1 and 1000-2) because of $H_2S_{(g)}$ evolution.....34
Figure 3.6 Final pH values of supernatant solution of both sulphide and zinc excess samples as a function of the pH values of the pH-adjusted H_2S brines.....35
Figure 3.7 Fractions of the initial sulphide concentrations in the pH-adjusted H_2S brines (2^{nd} Phase) before and after heating to represent what remains after the pH adjustment 37
Figure 3.8 Fractions of the initial sulphide concentrations in the pH-adjusted H_2S brines (3^{rd} Phase) before and after heating to represent the remaining sulphide concentrations after pH adjustment 37
Figure 3.9 Mass median diameter (D_{50}) for ZnS precipitates formed at different adjusted pH of the H_2S brines (3^{rd} Phase) 39
Figure 3.10 Experimental setup for H_2S gas flowing through Zn NSSW samples showing the gas bottle on the left side, the manifold at the top, and the connected reaction glass bottles at the bottom..40
Figure 3.11 A sample in a pressure rated glass bottle being bubbled with the 300 ppm H_2S gas.....41
Figure 3.12 White cloudiness after forming ZnS by bubbling H_2S directly through zinc brines.....42
Figure 3.13 Final pH values of the supernatant solution as a function of $H_2S_{(g)}$ bubbling time (dissolving more H_2S gas in solution lowers the pH) 43
Figure 3.14 Mass median diameter (D_{50}) for ZnS precipitate formed at different times by bubbling $H_2S_{(g)}$ through Zn NSSW brine.....44
Figure 3.15 The efficiency of SI-2 in inhibiting ZnS formed by H_2S gas in duplicate samples showing inconsistent results.....45
Figure 3.16 The efficiency of PPCA in inhibiting ZnS formed by H_2S gas in duplicate samples showing inconsistent results.....45
Figure 4.1 CuS solution in a cuvette ready for analysis by UV-VIS spectrophotometer after adding sulphide to the copper reagent (A stirrer appears at the bottom of the cuvette).....49
Figure 4.2 Investigating the preliminary accuracy and limitations of the calibration curves using the recommended linear fit.....50
Figure 4.3 Three individual calibration curves of sulphide stock solutions in distilled water divided by three ranges of aqueous sulphide ranges 51
Figure 4.4 The linear calibration curve of the 0 – 255 mg/L sulphide stock solutions (data points represent different measurements of the same sample).....52
Figure 4.5 The first calibration curves in Figure 4.2 fitted with a second order polynomial correlation as absorbance values against mg/L of aqueous sulphide to show that linearity is not the best fit 53
Figure 4.6 2^{nd} order polynomial equation enhancing the fit of the calibration curve of Figure 4.4 54
Figure 4.7 A calibration curve (2^{nd} order polynomial fit) of absorbance values using copper sulphate reagent against sulphide concentrations in **DW** with error bars representing standard deviations not exceeding 4.23%.....56
Figure 4.8 A calibration curve (2^{nd} order polynomial fit) of absorbance values using copper sulphate reagent against sulphide concentrations in **NSSW** with error bars representing standard deviations not exceeding 3.18% 56
Figure 4.9 A calibration curve (2^{nd} order polynomial fit) of absorbance values using ***copper chloride*** reagent against sulphide concentrations in **DW** with error bars representing standard deviations not exceeding 3.09%.....58

Figure 4.10 A calibration curve (2nd order polynomial fit) of absorbance values using ***copper chloride*** reagent against sulphide concentrations in **Glenelg FW** with error bars representing standard deviations not exceeding 4.69% 59
Figure 4.11 Iron sulphide formation filtered through different filter sizes (a) without scale inhibitor, and (b) with scale inhibitor 60
Figure 4.12 Lead sulphide formation filtered through different filter sizes (a) without scale inhibitor, and (b) with scale inhibitor 60
Figure 4.13 The effect of filtration on the aqueous sulphide concentrations showing that only 0.2µm filter size was able to filter out the solids yet caused losses in aqueous sulphide concentrations. 61
Figure 4.14 Sulphide concentrations of anaerobic and aerobic solutions at different pH values, analysed using UV-Vis method and ICP/back-calculation technique to show ability of detecting of fine differences in concentrations 62
Figure 5.1 (a) Labco Exetainer™ borosilicate round bottom tube, (b) Thermo Scientific™ glass vials with PTFE-lined silicone septum, (c) SGE™ gas tight manual syringes, and (d) SGE™ repeating adapter RAX 65
Figure 5.2 The de-oxygenation of solutions in Hungate-type tubes using N_2 gas bubbling through needles 67
Figure 5.3 Sampling a solution containing formed FeS using a disposable syringe mounted with a sharp needle 68
Figure 5.4 Filtration of the withdrawn sample using a syringe-mounted filter 68
Figure 5.5 Schematics and sequence of the steps of the iron sulphide formation test 71
Figure 5.6 Photos of the experimental steps of forming FeS in a Hungate-type tube using a gastight syringe mounted with a repeating adapter (RAX) 72
Figure 5.7 The formation of FeS in a dynamic (stirring) test showing a vortex caused by the rotation of the stirring bar at the base of the vial 72
Figure 6.1 Simple illustration of adding diluted HCl to sulphide solutions using gastight analytical syringes and airtight tubes 76
Figure 6.2 Sulphide concentrations in aerobic and anaerobic NSSW solutions at different added HCl volumes showing the difference in losses of [H_2S] due to oxidation and evolution 78
Figure 6.3 Sulphide concentrations in aerobic and anaerobic SF-NSSW solutions at different added HCl volumes showing the difference in losses of [H_2S] due to oxidation and evolution 78
Figure 6.4 Sulphide concentrations analysed by UV-Vis spectrophotometer for different pH-adjusted NSSW sulphide solutions to show the losses of [H_2S] in aerobic and anaerobic solutions 79
Figure 6.5 Sulphide concentrations analysed by UV-Vis spectrophotometer for different pH-adjusted SF-NSSW sulphide solutions to show the losses of [H_2S] in aerobic and anaerobic solutions 80
Figure 6.6 ICP analysis of zinc in anaerobic and aerobic solutions at different pH values which did not show conclusive results because difference in concentrations was within the ICP error margin (±10%) 80
Figure 6.7 ICP analysis of barium in anaerobic and aerobic solutions at different pH values where barium chloride was used to quench any sulphate formed as an oxidative product 81
Figure 6.8 Turbidity (elemental sulphur formation) of NSSW anaerobic and aerobic pH-adjusted sulphide solutions to show the effect of oxygen on aqueous sulphide at various pH levels 82
Figure 6.9 Turbidity (formation of elemental sulphur) observed in SF-NSSW anaerobic and aerobic pH-adjusted sulphide solutions to show the oxidation effect of oxygen at various pH levels 83
Figure 6.10 Suspended elemental sulphur, an oxidative product, appeared in the aerobic solution (right) whereas the anaerobic solution (left) remained clear 83
Figure 6.11 The different reductions in the sulphide concentrations caused by the oxidation in the ***aerobic*** solutions as a function of pH and time 86
Figure 6.12 The ***anaerobic*** (oxygen-free) solutions showed minimal reduction in sulphide concentrations at various pH levels and time steps 86
Figure 6.13 Anaerobic and aerobic sulphide solutions at different pH values and time steps showing signs of elemental sulphur formation (turbidity) at low pH values (pH< 6) 87
Figure 6.14 Duplicate results of the ***aerobic*** solutions showing similar reductions in aqueous sulphide concentrations as a result of oxidation at various durations and pH levels 89
Figure 6.15 Duplicate sets of results of the ***anaerobic*** (oxygen-free) solutions showing minimal reduction in aqueous sulphide concentrations as a function of pH and time 89
Figure 6.16 Illustration of the experimental setup for the dynamic oxidation tests where a vial was placed on a stirring plate(left), and oxygen meter was used to measure dissolved oxygen concentrations through an optical fibre cable 91
Figure 6.17 A dynamic (stirring) test showed oxidation effect represented in distinctive sharp reductions of oxygen and aqueous sulphide concentrations after the injection of acid to adjust the pH to ***pH 6.42*** 92

Figure 6.18 A dynamic (stirring) test showed oxidation effect represented in slow reductions of oxygen and aqueous sulphide concentrations after the injection of acid to adjust the pH to ***pH 5.61***.....92
Figure 6.19 A dynamic (stirring) test showed oxidation effect represented in steep reductions of oxygen and sulphide concentration particularly after the injection of acid to a 20 wt. % NaCl sulphide solution at room temperature and ***pH_f 5.72*** 95
Figure 6.20 A dynamic (stirring) test showed oxidation effect represented in steep reductions of oxygen concentration before and after the injection of acid to a 20 wt. % NaCl sulphide solution at room temperature and ***pH_f 11.39*** 95
Figure 6.21 Oxygen poisoning of an anaerobic sulphide solution (***pH_f 6.76***) through injecting air which is represented by the sharp and steady reduction rates of oxygen and sulphide concentrations, respectively.....97
Figure 6.22 ESEM images and EDX semi-quantitative analysis of solids filtered from the first oxygen poisoning test (air injection).....98
Figure 6.23 Oxygen poisoning of an anaerobic sulphide solution (***pH_f 6.64***) through injecting air which is represented by the sharp and steady reduction rates of oxygen and sulphide concentrations, respectively.....99
Figure 6.24 ESEM images and EDX semi-quantitative analysis of solids filtered from the second oxygen poisoning test (aerated HCl injection) 100
Figure 7.1 Autoscale (solubility) profiles of FeS in 3.5 wt. % NaCl at various total sulphide concentrations (1,000, 200 and 100 mg/L) and iron (II) concentrations (25 and 50 mg/L) at room temperature as a function of pH 105
Figure 7.2 Duplicates of FeS (1,000/50 mg/L) autoscale profile as a function of pH at room temperature using Khuff Na & Ca brine.....108
Figure 7.3 Duplicates of FeS (500/50 mg/L) autoscale profile as a function of pH at room temperature using Khuff Na & Ca brine.....108
Figure 7.4 Duplicates of FeS (200/50 mg/L) autoscale profile as a function of pH at room temperature using Khuff Na & Ca brine.....109
Figure 7.5 Duplicates of FeS (100/50 mg/L) autoscale profile as a function of pH at room temperature using Khuff Na & Ca brine.....109
Figure 7.6 Combined FeS autoscale (solubility) profiles as a function of pH and aqueous sulphide concentration in Khuff Na & Ca brine at room temperature.....110
Figure 7.7 Distribution of aqueous sulphide species at $\{S^{2-}\}_T = 10^{-3}$ in terms of pH. (Rickard and Luther, 2007).....111
Figure 7.8 The autoscale profile of FeS at an aerobic aqueous sulphide solution ($[S^{2-}]_i$ = 1,000 mg/L and $[Fe^{2+}]_i$ = 50 mg/L).....112
Figure 7.9 Comparing the autoscale profiles of FeS formed at anoxic and oxic conditions ($[S^{2-}]_i$ = 1,000 mg/L and $[Fe^{2+}]_i$ = 50 mg/L, Filtered).....113
Figure 7.10 ZnS (100/50 mg/L) autoscale profile at room temperature using Khuff Na & Ca brine 114
Figure 7.11 PbS (100/50 mg/L) autoscale profile at room temperature using Khuff Na & Ca brine.....114
Figure 7.12 PbS (100/50 mg/L) autoscale profile at room temperature using different concentrations of stock HCl at room temperature to lower the pH to pH 0.....115
Figure 7.13 Autoscaling profiles of FeS, ZnS and PbS in Khuff Na & Ca brine represented as reactants' concentrations against pH values ($[M^{2+}]_i$= 50 mg/L, $[S^{2-}]_i$ = 100 mg/L) 116
Figure 7.14 Comparison between the autoscaling profiles of FeS in single or combined scale solution in Khuff Na & Ca brine ($[Fe^{2+}]_i$= 50 mg/L, $[S^{2-}]_i$= 100 mg/L).....117
Figure 7.15 Comparison between the autoscaling profiles of ZnS in single or combined scale solution was inconclusive because of missing data points between pH 1.5 – 2.8 ($[Zn^{2+}]_i$= 50 mg/L, $[S^{2-}]_i$= 100 mg/L) 117
Figure 7.16 Comparison between the autoscaling profiles of PbS in single or combined scale solution both showing the extreme low solubility of PbS in brine at pH > 1 ($[Pb^{2+}]_i$= 50 mg/L, $[S^{2-}]_i$= 100 mg/L) 118
Figure 7.17 The interface of the scale prediction model showing the input fields and produced results 119
Figure 7.18 Plotted data from the scale prediction model listed in Table 7.1 ($[Fe^{2+}]_i$ = 48 mg/L and $[S^{2-}]_i$ = 970 mg/L).....121
Figure 7.19 Plotted data from the scale prediction model ($[Fe^{2+}]_i$ = 48 mg/L and $[S^{2-}]_i$ = 480 mg/L)...122
Figure 7.20 Plotted data from the scale prediction model ($[Fe^{2+}]_i$ = 48 mg/L and $[S^{2-}]_i$ = 190 mg/L)...122
Figure 7.21 Plotted data from the scale prediction model ($[Fe^{2+}]_i$ = 48 mg/L and $[S^{2-}]_i$ = 95 mg/L).....123
Figure 7.22 Prediction data of Fe^{2+} depletion during the FeS autoscale at various total sulphide concentrations showing different solubilities at pH 4 - 6.....124
Figure 7.23 Experimental and prediction model data of Fe^{2+} depletion during FeS autoscale at various sulphide concentrations showing excellent agreement.....124

Figure 7.24 A Comparison between the direct formation and the autoscale of FeS at 1,000 mg/L of sulphide showing slightly lower solubility profile of the direct formation over the autoscale formation 125
Figure 7.25 Overlaid experimental results on prediction data for ZnS autoscale profile in Khuff Na & Ca ($[Zn^{2+}]_i$ = 50 mg/L and $[S^{2-}]_i$ = 100 mg/L) 126
Figure 7.26 Overlaid experimental results on prediction data for PbS autoscale profile in Khuff Na & Ca ($[Pb^{2+}]_i$ = 50 mg/L and $[S^{2-}]_i$ = 100 mg/L) 127
Figure 7.27 Overlaid experimental results on prediction data for PbS autoscale profile in DW ($[Pb^{2+}]_i$ = 50 mg/L and $[S^{2-}]_i$ = 100 mg/L) 127
Figure 7.28 The interface of the 3rd version of scale prediction model showing the added input fields for K_{sp} values 129
Figure 7.29 Data comparison of autoscale profiles of ZnS in Khuff Na & Ca using $K_{sp, ZnS} = 2.03 \times 10^{-25}$ 130
Figure 7.30 Data comparison (experimental and predicted) of autoscale profiles of PbS in HCl using $K_{sp, PbS} = 2.50 \times 10^{-29}$ 130
Figure 7.31 Experimental data from combined autoscale tests overlaid with 1st version of the prediction model showing discrepancies in the agreements with prediction data 131
Figure 7.32 Prediction data of combined autoscale using $K_{sp, FeS} = 1.29 \times 10^{-19}$, $K_{sp, ZnS} = 2.03 \times 10^{-25}$, and $K_{sp, PbS} = 2.50 \times 10^{-29}$ 131
Figure 7.33 Prediction data of combined autoscale using $K_{sp, FeS} = 5.08 \times 10^{-21}$, $K_{sp, ZnS} = 2.03 \times 10^{-25}$, and $K_{sp, PbS} = 2.50 \times 10^{-29}$ showing better agreements than in Figure 7.31 and Figure 7.32 132
Figure 7.34: Decline in measured aqueous sulphide concentrations at different mixing durations 134
Figure 8.1 Determining MIC (80% or more Fe C/C_0 – Eq 8.1) of SI-2 to inhibit FeS at various pH and initial total sulphide concentrations in 3.5 wt.% NaCl ($[Fe^{2+}]_i$= 50 mg/L) 142
Figure 8.2 Effect of pH on total iron in solution (percentage) against the scale inhibitor concentration at $[S^{2-}]_i$ = 100 mg/L, $[Fe^{2+}]_i$ = 50 mg/L in 3.5 wt.% NaCl (Unfiltered samples) 143
Figure 8.3 Effect of pH on iron concentration in filtered samples (through 0.2 µm filter size) against the scale inhibitor concentration at $[S^{2-}]_i$ = 100 mg/L, $[Fe^{2+}]_i$ = 50 mg/L in 3.5 wt.% NaCl 143
Figure 8.4 Effect of pH on total iron in solution (percentage) against the scale inhibitor concentration at $[S^{2-}]_i$ = 200 mg/L, $[Fe^{2+}]_i$ = 50 mg/L in 3.5 wt.% NaCl (Unfiltered samples) 144
Figure 8.5 Effect of pH on iron concentration in filtered samples (through 0.2 µm filter size) against the scale inhibitor concentration at $[S^{2-}]_i$ = 200 mg/L, $[Fe^{2+}]_i$ = 50 mg/L in 3.5 wt.% NaCl 144
Figure 8.6 The scale inhibition efficiency (percentage) at 50 and 100 mg/L Fe^{2+}, pH ~ 6.1, and $[S^{2-}]_i$ = 1,000 mg/L in 3.5 wt.% NaCl at room temperature 145
Figure 8.7 Scale inhibition efficiency (percentage) after two durations at $[Fe^{2+}]_i$ = 50 mg/L, pH 6, and $[S^{2-}]_i$ = 1,000 mg/L in 3.5 wt.% NaCl at room temperature 146
Figure 8.8 Scale inhibition efficiency at 50ºC and room temperature in 3.5 wt.% NaCl to show the effect of temperature on inhibition at various sulphide concentrations 147
Figure 8.9 The effect of temperature on the MIC of SI-2 in Khuff Na & Ca ($[Fe^{2+}]_i$ = 50 mg/L and $[S^{2-}]_i$ = 100 mg/L) 148
Figure 8.10 The effect of temperature on the MIC of SI-3 in Khuff Na & Ca ($[Fe^{2+}]_i$ = 50 mg/L and $[S^{2-}]_i$ = 100 mg/L) 149
Figure 8.11 Tube lids loosened/removed as a result of high temperature (95ºC) and pressure 149
Figure 8.12 Scale inhibition efficiency of SI-2 at room temperature and 50ºC using 3.5 wt.% NaCl and Khuff formation brine to show the effect of brine composition on inhibition 150
Figure 8.13 The scale inhibition of FeS in terms of $[Fe^{2+}]_{aq}$ at various pH levels using an aerated aqueous sulphide solution and [SI] = 40 mg/L 151

LIST OF PUBLICATIONS

Alduailej, Y., Graham, A., Oduro, H., Sorbie, K., 2017. Oxidation of Sulphides and its Effect on Sulphide Scale Formation, in: Tekna Oil Field Chemistry Symposium. Tekna, Geilo, Norway, pp. 1–20.

Alduailej, Y., Boak, L.S., Alharbi, B., Graham, A.J., Sorbie, K.S., Oduro, H., Alkhaldi, M., Alqathami, S., 2018. Development of an UV-Vis Spectrophotometric Method for Accurate Determination of Aqueous Sulphides in Exotic Scale Studies, in: SPE International Oilfield Scale Conference and Exhibition. Society of Petroleum Engineers, Aberdeen, UK.

Alduailej, Y., Alharbi, B., Graham, A., Sorbie, K., Oduro, H., Alkhaldi, M., Alqathami, S., 2018. A New Insight into the Static Inhibition and Formation of Iron(II) Sulphide Scale, in: 17th Middle East Corrosion Conference & Exhibition. Manama, Bahrain.

Al-Harbi, B., **Alduailej, Y.**, Graham, A., Sorbie, K., 2018. Systematic Investigation of Iron Sulfide and Iron Hydroxide Inhibition, in: 17th Middle East Corrosion Conference & Exhibition. Manama, Bahrain.

Nomenclature

pH	A number expressing the acidity or basicity of a solution
CO_2	Carbon dioxide
H_2S	Hydrogen sulphide
FeS	Iron (II) sulphide
ZnS	Zinc sulphide
PbS	Lead sulphide
Fe^{2+}	Ferrous iron
Fe^{3+}	Ferric iron
M^{2+}	Divalent metal cation
MS	Metal sulphide
SRB	Sulphate reducing bacteria
$_{(g)}$	subscript - Gaseous
$_{(aq)}$	subscript - Aqueous
HS^-	Bisulphide ion
S^{2-}	Sulphide ion
S	Sulphur
S_8	Elemental Sulphur
H^+	Hydrogen proton
HCl	Hydrochloric acid
NaCl	Sodium chloride
$CaCl_2$	Calcium chloride
NSSW	North Sea seawater
SF-NSSW	Sulphate free North Sea seawater
MF-NSSW	Magnesium free North Sea water
Khuff Na & Ca	Khuff formation water prepared with NaCl and $CaCl_2$
S_n^{2-}	Polysulphide ion
SO_4^{2-}	Sulphate ion
K_1	Reaction rate
K_2	Reaction rate
DW	Distilled water
K_{sp}	Solubility product
$K_{sp,\ MS}$	Solubility product of metal sulphide
$K_{sp,\ FeS}$	Solubility product of iron (II) sulphide
$K_{sp,\ ZnS}$	Solubility product of zinc sulphide
$K_{sp,\ PbS}$	Solubility product of lead sulphide
SR	Saturation ratio
MIC	Minimum inhibition concentration
ICP	Inductively coupled plasma
ESEM	Environmental scanning electron microscopy
PVT	Pressure/Volume/Temperature

ft	Feet
HPHT	High pressure/High temperature
°C	Degrees centigrade
K_{eq}	Equilibrium constant
M	Molar
bar	Metric unit of pressure
psi	Pound per square inch
nm	Nanometre
mM	Milli-molar
mL	Millilitre
µM	Micro-molar
µL	Microlitre
µm	Micrometre
min	Minute
g	gram
µg	Microgram
mg/L	Milligrams per litre
ppm	Parts per million
ppb	Parts per billion
AW	Atomic weight
MW	Molecular weight
Δ	Delta (the change of quantity or value)
UV	Ultra-violet
Vis	Visible
$_f$	subscript – Final value
$_i$	subscript – Initial value
TDS	Total dissolved solids
SI	Scale inhibitor
RT	Room temperature
T test	A statistical function used to determine the significance in difference between the means of two groups with similar features
P or $P_{T\text{-test}}$	A value between 0 and 1, with $P \leq 0.05$ typically indicates a significant difference in the T test
STD	Standard Deviation

1 - INTRODUCTION

1.1 Scale Formation in Oilfield Operations

Oilfield mineral scale can be defined as the particles depositing on or coating a surface of a metal, such as pipes and equipment, the formation rock in the reservoir or near wellbore, or any other material available in the production system of the oil and gas industry. Scale deposition in oilfield processes leads to flow hindrance during well production or injection. The loss of flow occurs as a result of an internal diameter reduction in pipes, or as a downhole equipment failure due to mechanical restrictions (Kelland, 2016). Any hindrance of flow is often associated with financial losses, such as production decline or extended workover processes.

The oilfield scale could form as a result of commingling two or more incompatible fluids, leading to solids formation and deposition. The changes in conditions, such as temperature and pressure or simply by evaporation of water from the brine, could cause a single fluid to form scale, commonly referred to as self-scaling or autoscale (Orski *et al.*, 2007). These phenomena can occur at different locations in any oilfield process involving water, for example: before injecting a mixture of two or more waters for water-flooding, around the well-bore where injected water encounters formation water, or deep in the reservoir as a result of displacement, to mention a few (Jordan and Mackay, 2005). Autoscaling occurs during the production of sour hydrocarbons, where the decrease in pressure causes the dissolved gases, such as carbon dioxide (CO_2) and hydrogen sulphide (H_2S), to partition from the aqueous liquid phase to the gas phase, leading to the increase in the aqueous fluid's pH, and, consequently, the formation of sulphide and carbonate scales (Orski *et al.*, 2007). Therefore, the associated water, produced alongside the gaseous hydrocarbons, poses a potential for scaling, particularly in sour environments.

The production of sour fields incurs extra costs due to the involvement of additional processes such as sweetening of the hydrocarbons and sulphide scale prevention treatments (Henni, 2013). Individual sulphide and carbonate scales can be categorised as pH-sensitive scales, i.e. their formation is highly governed by pH (Kan and Tomson, 2012). Barium sulphate, calcium sulphate, strontium sulphate, and halite are pH-independent scales, which, as suggested by the name, do not predominantly depend on the in-situ pH (Kan and Tomson, 2012). Other conditions, such as pressure, temperature

and salinity may influence the alkalinity of the water, and the magnitude of scale formation.

At equilibrium, the reservoir fluids, oil, gas and water, are not susceptible to scale formation. The scaling potential exists when this equilibrium is interrupted, such as through drilling, well-intervention or production. Once interrupted, the reservoir fluids are forced towards equilibrium, throughout which scales form and precipitate (Okocha and Sorbie, 2013). The formation of sulphide scale follows chemical reactions that have been extensively reported in the literature. Iron (II) sulphide (FeS), zinc sulphide (ZnS) and lead sulphide (PbS) are the common oilfield sulphide scales. To form these scales, the sulphide anion (H_2S, HS^-, or S^{2-}) reacts with the metal cation (M^{2+}) to create the sulphide scale (MS), where M can be iron (II) (Fe^{2+}), zinc (Zn^{2+}), or lead (Pb^{2+}).

The comprehension of the oilfield scale formation mechanism is the first part of the solution, as subsequent steps, such as scale inhibition or removal, rely exclusively on how such scale deposition has occurred. Preventing oilfield scale from forming and depositing has been mostly agreed upon as a more advantageous method over scale removal treatments (Bhandari *et al.*, 2016, Bybee, 2001, Lopez *et al.*, 2005, Przybylinski, 2001, Crabtree *et al.*, 1999).

. The latter may include mechanical, such as scrapers, and chemical means, such as acids and chelating agents. For certain scale types, this statement is indisputable, particularly the exotic scales such as iron, zinc and lead sulphides.

1.2 Oilfield Sulphide Scales

1.2.1 Hydrogen Sulphide in the Oilfield

Hydrogen sulphide is one of the most hazardous gases, and hence poses extreme safety, health and environmental risks. It is highly associated with corrosion, pitting, and steel cracking challenges. The formation of hydrogen sulphide in the oil and gas fields can occur through biotic and abiotic processes. An example of the biotic process is the generation of H_2S by sulphate reducing bacteria (SRB) which metabolises sulphate ions in injected water to produce H_2S via a reduction mechanism. An abiotic process can be a thermochemical reduction of sulphur, thermal hydrolysis of organic sulphur compounds, or hydrolysis of metal sulphide compounds (Barré *et al.*, 2018; Lamoureux-Var *et al.*,

2018). A third source of H_2S can be the result of acid treatment of sour gas wells that have deposited iron sulphide (Nasr-El-Din and Al-Humaidan, 2001). The concentration levels of hydrogen sulphide vary from one field to another and can reach extreme percentages, as reported in the Middle East and Canada (Burt and Susanna, 2015, Ghaderi *et al.*, 2011, Ramachandran *et al.*, 2015a, 2015b, Verri *et al.*, 2017).

As a gas, hydrogen sulphide is not directly involved in the formation of sulphide scale. However, once dissolved in an aqueous fluid, aqueous hydrogen sulphide ($H_2S_{(aq)}$) dissociates into two other sulphide species, bisulphide (HS^-) and sulphide (S^{2-}), and all three species co-exist at equilibrium and contribute to the formation of the sulphide scale. Depending on the pH of the fluid, each sulphide species composes a certain fraction of the total sulphide to honour the rate constants of the speciation reactions. The hydrogen sulphide speciation reactions have been well investigated, and the rates of these two reactions have been documented. However, the values of the second speciation reaction rate K_2 have been highly disputed in the literature (Morse *et al.*, 1987). When H_2S dissolves in water, the following reactions occur to reach equilibrium:

$$H_2S_{aq} \overset{K_1}{\Leftrightarrow} HS^- + H^+ \tag{1.1}$$

$$K_1 = \frac{[H^+][HS^-]}{[H_2S]} = 9.632 \times 10^{-8} \quad (\mathrm{K_1} \text{ value recommended by Okocha, 2011}) \tag{1.2}$$

$$HS^- \overset{K_2}{\Leftrightarrow} S^{2-} + H^+ \tag{1.3}$$

$$K_2 = \frac{[H^+][S^{2-}]}{[HS^-]} = 1 \times 10^{-17} \quad (\mathrm{K_2} \text{ value recommended by Okocha, 2011}) \tag{1.4}$$

All speciation reactions are directly dependent on the pH, or $[H^+]$, which determines the sulphide species distribution (O'Brien and Birkner, 1977). In downhole conditions, the pH is majorly governed by dissolved carbon dioxide (CO_2), thus driving the equilibrium of reactions (1.1) and (1.3) towards $H_2S_{(aq)}$. Once these gases evolve, due to pressure drop, the proton concentration starts to decrease, causing the speciation of sulphide to shift slightly towards HS^-.

1.2.2 Hydrogen Sulphide in Laboratory Studies

The chemistry of aqueous sulphide in laboratory investigation relies on the source of the sulphide ions, which is commonly a sodium sulphide salt (basic conditions) or a hydrogen

sulphide gas (neutral to acidic conditions). The use of sulphide salt is widely associated with assumptions to maintain a moderate level of test complexity, such as screening inhibition products, where the initial pH of sulphide solutions is considered ineffectual to the test objectives. On the other end of the complexity spectrum, specific objective-oriented tests, such as determining the effect of various parameters on an inhibitor performance, require more representative chemistry of the aqueous sulphide. Therefore, H_2S gas is used in such studies to saturate brines with aqueous sulphide, or sodium sulphide solutions are pH-adjusted from basic to neutral-acidic conditions, for example via CO_2 saturation. Consequently, the involvement of H_2S and CO_2 gases entails advanced safety and experimental procedures, commonly through the use of anaerobic pressurised systems.

The speciation of hydrogen sulphide gas in aqueous solutions has been discussed in the previous section. The dissolution of sodium sulphide nonahydrate ($Na_2S.9H_2O$) salt in water follows these reactions:

$$Na_2S.9H_2O \rightleftharpoons 2\,Na^+ + S^{2-} + 9H_2O \tag{1.5}$$

$$S^{2-} + H^+ \rightleftharpoons HS^- \tag{1.6}$$

The second reaction is favoured, because of the low second speciation constant K_2 (Eq. 1.4), during which hydrogen protons are consumed, thus reducing the overall $[H^+]$ in solution, and subsequently raising the pH value to ~ pH 10-12, normally, but depending on the sulphide concentration. On the other hand, shifting the speciation towards $H_2S_{(aq)}$ in laboratory experiments requires an abundance of hydrogen protons following Equation (1.7):

$$HS^- + H^+ \rightleftharpoons H_2S_{(aq)} \tag{1.7}$$

Several reports have discussed the existence of all three sulphide species concurrently, yet the concentration of sulphide ion (S^{2-}) is low compared to the other two species. Based on the speciation reaction rates K_1 and K_2, the following speciation chart, Figure 1.1, can be generated to indicate the zones and fractions of each species at any given pH value using distilled water (DW) as a solvent.

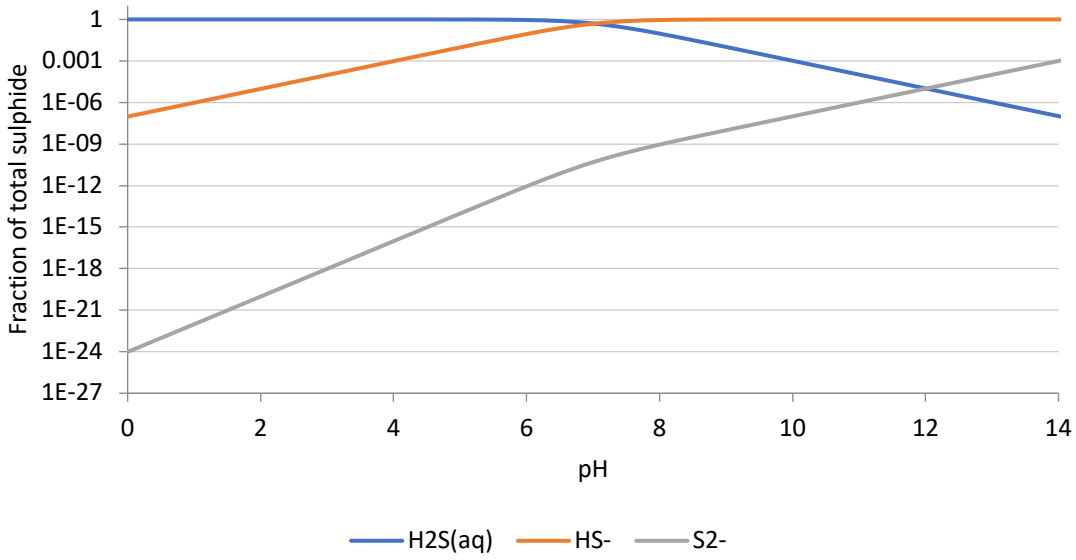

Figure 1.1 Speciation of aqueous sulphide in distilled water as a function of pH

Under acidic conditions, pH < 6, the dominant sulphide species is $H_2S_{(aq)}$, while HS^- and S^{2-} exist at low and deficient concentrations, respectively. Around circumneutral pH, both $H_2S_{(aq)}$ and HS^- exist at considerable concentration fractions (0.1 – 0.9), while S^{2-} remains at low concentrations, ~ 10^{-11}. At high alkalinity, pH ≥ 12, the $H_2S_{(aq)}$ concentration becomes less than 10^{-5}, the concentration of S^{2-} becomes more abundant compared to $H_2S_{(aq)}$, while the dominant species at this alkalinity is HS^-. Although the sulphide species can be mathematically interchangeable, according to Equations (1.1) – (1.4), studies have suggested that HS^-, rather than S^{2-}, is the sulphide species involved in the kinetics of the iron sulphide formation reaction (Przybylinski, 2001; Rickard, 1989).

1.2.3 Sources of Divalent Metal Cations (Fe^{2+}, Zn^{2+} and Pb^{2+})

Iron, zinc and lead, like heavy metals, can potentially originate from reaction products of minerals in the formation, the reaction of injected water with formation minerals, or heavy brine completion fluids (Collins and Jordan, 2003). The primary sources of iron in the oil and gas fields can be natural, such as from the formation rock, or artificial, such as corrosion or iron sulphide scale (Verri and Sorbie, 2017). The formation rock can be dissolved in low pH water, releasing free iron ions, whilst corrosion and scale are caused mainly by injecting acids downhole for well stimulation or formation damage removal purposes (Kasnick and Engen, 1989, Nasr-El-Din and Al-Humaidan, 2001). The acid can cause corrosion to the steel pipes, which enriches the acid with dissolved iron, and can dissolve the sulphide scale, thus releasing iron and sulphide into the aqueous fluid.

The main reactions of sulphides with iron, zinc and lead can be written in terms of H_2S, HS^-, or S^{2-}. Assuming M^{2+} represents the divalent metal cation, these are the potential reactions and the solubility product constant $K_{sp,\ MS}$ equation:

$$M^{2+} + S^{2-} \rightleftharpoons MS_{(s)} \tag{1.8}$$

$$M^{2+} + HS^{-} \rightleftharpoons MS_{(s)} + H^{+} \tag{1.9}$$

$$M^{2+} + H_2S \rightleftharpoons MS_{(s)} + 2H^{+} \tag{1.10}$$

$$K_{sp,\ MS} = [M^{2+}][S^{2-}] \tag{1.11}$$

All three reactions are expressively correct and can be written interchangeably using the concentration of hydrogen protons $[H^+]$, which can be drawn from the pH, and the equilibrium constants of the speciation reactions of sulphide in water: K_1 and K_2. Since these reactions can be written using sulphide species interchangeably, the pH of the solution, or $[H^+]$, is the vital factor, determining whether a sulphide scale would form, and to what extent. Equations (1.12) and (1.13), which are rearranged from equations (1.2) and (1.4), can be used to show the interchangeability of sulphide species in equation (1.14):

$$[HS^-] = K_1 \times \frac{[H_2S]}{[H^+]} \tag{1.12}$$

$$[S^{2-}] = K_2 \times \frac{[HS^-]}{[H^+]} = K_2 \times \frac{[K_1 \times \frac{[H_2S]}{[H^+]}]}{[H^+]} = \frac{K_1K_2\,[H_2S]}{[H^+]^2} \tag{1.13}$$

$$K_{sp,\ MS} = [M^{2+}][S^{2-}] = [M^{2+}]\frac{K_2[HS^-]}{[H^+]} = [M^{2+}]\frac{K_1K_2\,[H_2S]}{[H^+]^2} \tag{1.14}$$

The solubility product constants of sulphide scales, although extremely low, vary significantly: $K_{sp,\ FeS} = 2.88 \times 10^{-18}$, $K_{sp,\ ZnS} = 2.03 \times 10^{-25}$, $K_{sp,\ PbS} = 3.80 \times 10^{-28}$ (Okocha, 2011). Based on these values, these sulphide scales are extremely insoluble in water but can dissolve in strong acids. Zinc and lead sulphide scales are known to have single equimolar forms, while iron sulphide can exist in stoichiometric and non-stoichiometric forms, each having their unique properties and solubility profiles (Rickard and Luther, 2007). Several forms of iron sulphide found in oil and gas fields have been reported in the literature (Hajj *et al.*, 2015; Ramachandran *et al.*, 2015a, 2015b). In general, the iron sulphide deposited in pipes tends to have a greater iron-to-sulphur ratio closer to the inner wall and an increasing sulphur-to-iron ratio whilst moving towards the centre of the pipe.

This change in composition occurs as a result of continuously exposing iron sulphide to the flow of sulphide-rich fluids, causing the elements of the formed scale to change their oxidation states and react further with sulphide, thus, shifting the molar ratio beyond unity, while pipe walls provide an abundant source of iron.

1.3 Scale Inhibition

Scale inhibition includes preventing scale crystal particles from forming (nucleation), stopping crystal growth, or suspending/dispersing particles in solution (preventing deposition). For sulphide scale, studies showed that crystal growth-blocking and dispersion were the optimum mechanisms (Bhandari *et al.*, 2016). Inhibitors can be squeezed into the formation to adsorb on the rock, and then desorb and flow back with the fluids providing the inhibition effect. Another implementation of inhibitors can be a direct feed into a flow line, commonly above the surface, to avoid scale deposition in upstream pipes, equipment and tanks. Each implementation would involve a specific set of conditions, at which deployed inhibitors should perform efficiently.

Inhibiting sulphide scale has proven to be challenging, as many studies have shown the lack of performance of iron chelating agents and dispersant chemicals. During recent research, however, a few chemicals have produced promising results in laboratory evaluations and field trials (Bhandari *et al.*, 2016; Wylde *et al.*, 2015).

Inhibition tests are commonly performed under static (e.g. static bottle test) or dynamic conditions (e.g. tube/filter blocking test). The conventional static tests provide the minimum inhibition concentration (MIC), commonly at 2 and 22 hours, and can be used for the screening of several scale inhibitors. The dynamic tests investigating sulphide scale determine the time required to block a filter/tube after forming the scale, which usually is less than two hours. The MIC is considered the primary outcome from the static bottle tests, where different concentrations of inhibitors and scaling ions are tested to determine the minimum inhibitor concentration required to prevent/disperse the sulphide scale. Usually, MICs are further evaluated in dynamic tests and used as thresholds in the scale inhibitor retention tests. Associated analysis techniques include but are not limited to: Inductively coupled plasma (ICP), pH measurement, particle size distribution, and environmental scanning electron microscopy (ESEM). Physical appearance can be used, positively, to confirm the formation of scale, or the difference between settled and dispersed particles.

The advanced static tests of sulphide scale have specific applications and test conditions including the use of pressurised gasses and anaerobic systems. These test conditions were applied in the investigation of the effect of pH on the sulphide formation and dispersion using sodium sulphide solutions saturated with carbon dioxide gas (Lehmann and Firouzkouhi, 2008). Similar conditions were used in the investigation of anti-fouling surfaces to prevent PbS deposition using a strictly closed system to saturate vessels, containing lead chloride solutions, with 1% H_2S/99% CO_2 gas mixture (Keogh *et al.*, 2017). These studies exemplify the strict conditions associated with modifying the static test to achieve more representative conditions, such as pH adjustment, or avoid interferences by using anaerobic conditions.

Other means of preventing sulphide scaling include the desulphation of injected seawater, using biocides for SRBs, or using H_2S scavengers (Kelland, 2016). All three techniques contribute to the reduction of H_2S generation, and, consequently, minimize the scaling potential. Eliminating the intake (sulphate) through desulphation of seawater, or the SRBs through the use of biocides lead to stopping reservoir souring. In addition, H_2S scavengers, directly target aqueous H_2S through various reaction mechanisms, thus reducing its content in produced water (Kelland, 2016). In extreme sour environments, as in the Middle East, these techniques could have limited impact on the scaling potential.

1.4 Scale Prediction Models

Scale prediction models are calculations that solve a system of equations involving dissolution and scaling reactions, and mass/charge balances. Various experimental values, including reaction rates and dissolution constants, often available in the literature, are required to solve these equations. Once the system of equations is solved, the model is tested for boundaries based on the objective of the model. Experimental data reported in the literature provides a starting point to confirm the accuracy of any prediction model.

Several scale prediction models have been used in the past, such as MultiScale and ScaleChem, which provide an accurate prediction for aqueous systems (Silva, 2017). However, sulphide scale is dependent on pH, which in return is highly influenced by dissolved gases, i.e. CO_2 and H_2S. The incorporation of these gases into the model requires pressure/volume/temperature (PVT) systems that can deal with hydrocarbons, gases, and water (three phases) (Silva *et al.*, 2018; Verri and Sorbie, 2017).

Most prediction models used for oilfield brines are based on Pitzer's extension of the Debye–Hückel theory, which considers the activities of ions, rather than concentrations. When different ions are dissolved in a solution, their solubilities are affected by their concentrations and their activity coefficients, which are factors calculated experimentally to account for attraction and repulsion forces associated with ionic charges. Therefore, a prediction model based on activity is considered more accurate than a concentration model (Silva, 2017). Nonetheless, both models similarly process the input data to produce a prediction, based on the used system of equations.

Although this work did not include the development of a prediction model, one was used for elaborating certain solubility behaviours of sulphide scales, which will be discussed in Chapter 8.

1.5 Objectives and Research Methodologies

Several reports have determined the impact of the chemistry of the aqueous sulphide on the sulphide scale formation and inhibition (Keogh *et al.*, 2017; Lehmann and Firouzkouhi, 2008). Therefore, it is intuitive to consider the introduction of aqueous sulphide at a representative pH level and an anaerobic environment in every test involved in the sulphide scale investigative studies. However, achieving these conditions is currently limited to the *advanced* testing methodologies, which, quite often, cannot be used for *standard* static "jar" tests.

The objective of this study is to develop a flexible, accessible, safe and affordable bench-top static test setup for the formation and inhibition of oilfield sulphide scale at a representative pH and anaerobic conditions. The research methodology involved determining the gap in the literature, proposing an alternative setup and a supportive analytical method, and validating the proposed setup through scale formation and inhibition tests.

2 – Literature Review

2.1 Oilfield Sulphide Scale

The first scale problems with a "sulphide root cause" in the oil and gas industry were reported in the late 19th century in Indiana, Illinois, USA (Rogers and Rowe Jr., 1955). However, it became a more significant concern at the beginning of the 20th century (Bignell, 1930; Devine *et al.*, 1934; Headlee, 1945; Mills, 1926; Murphy, 1949; Plummer and Walling, 1946). At that time, the main sulphide scale challenges were either a result of or a cause of, corrosion. Therefore, iron sulphide was the dominant type of sulphide scale during that period. Later, when secondary oil recovery was reaching its prime (Thakur and Satter, 1998), sulphide scaling was reported to plug the formation, thus causing a decline in injection rates whilst using untreated seawater or turbid water as a source (Ellenberger and Holben, 1959). Consequently, it was essential to maintain the quality of injected water by controlling various factors such as the dissolved iron and pH, in an attempt to prevent such scaling situations from occurring.

Iron sulphide, zinc sulphide and lead sulphide can precipitate anywhere in the system from production tubing to topside processing facilities, resulting in production decline and limited accessibility to downhole tools. Consequently, an additional cost is required for implementing effective scale mitigation and removal strategies, for example, various iron sulphide scales formed in the lower part of tubing within the Khuff sour gas wells in Saudi Arabia and Bahrain (Kasnick and Engen, 1989; Mirza *et al.*, 1999). The composition of iron sulphide was found to vary with depth, even in the same well, e.g. two samples were collected from 34 and 680 ft and identified to be predominately pyrite and mackinawite, respectively (Nasr-El-Din and Al-Humaidan, 2001). Several comprehensive studies supported this observation such as those by Franco *et al.* (2010) and Wang *et al.* (2013).

In HPHT systems, zinc sulphide and lead sulphide have been reported as forming in the upper part of the well and several other locations including produced water control valves, surface controlled subsurface safety valves, surface cooler and separator and the overboard water line in different HT/HP fields within North Sea and Gulf of Mexico (Baraka-Lokmane *et al.*, 2014; Hartog *et al.*, 2002; Jordan *et al.*, 2000; Lopez *et al.*, 2005; Orski *et al.*, 2007). It is well known that the solubilities of ZnS and PbS are strongly influenced by pH and temperature; therefore, the tendency of ZnS and PbS to deposit in

the upper part of the well may be a direct consequence of temperature and pressure reduction (Jordan *et al.*, 2000). As pressure decreases, dissolved carbon dioxide liberates from the produced water and thus pH increases, causing the formation of calcite and sulphide scales.

Sulphide scales have very low solubility products, Table 2.1, which makes them extremely insoluble in water. Relatively, iron sulphide is more soluble than zinc or lead sulphides. Increasing temperature and the solution salinity tends to increase the solubility values of lead and zinc sulphides. Over the range of 25-300 °C, zinc sulphide is more soluble than lead sulphide. The increase of salinity from 3 to 5M NaCl increases the solubility by five folds while increasing temperature by only 15°C increases the solubility further than that caused by increasing salinity (Barrett and Anderson, 1988). Moreover, sulphide solubility increases with decreasing pH; hence acid treatments tend to be effective in dissolving scale deposits (Collins and Jordan, 2003).

Table 2.1 Literature thermodynamic solubility product constants for FeS, ZnS, and PbS

Scale Type	*Thermodynamic solubility product constants (K_{sp}) at 25°C*	*Recommended Equilibrium constants (K_{eq})*
Iron(II) Sulphide	Amorphous 1.44 x 10^{17} Mackinawite 2.88 x 10^{-18} (Harmandas *et al.*, 1998)	1.29 x 10^{-19} (Okocha and Sorbie, 2013)
Lead(II) Sulphide	2.5 x 10^{-29} (a) (Clever and Johnston, 1980)	3.80 x 10^{-28} (Okocha and Sorbie, 2013)
Zinc(II) Sulphide	1.6 x 10^{-24} (b) (Clever *et al.*, 1992)	2.03 x 10^{-25} (Okocha and Sorbie, 2013)

(a) Tentative value
(b) According to the author, the best value of its time (1952).

Although iron sulphide solubility behaviours have several similarities to those of ZnS and PbS (in terms of temperature, pH and salinity effects), it may exist in one or more forms. Consequently, these forms have different solubility values based on their stoichiometric composition. Troilite (FeS), for example, can be quickly dissolved in acid whilst pyrite (FeS_2) dissolves less and more slowly in acid, hence the use of mechanical means for scale removal (Leal *et al.*, 2007; Nasr-El-Din and Al-Humaidan, 2001).

2.2 Protocols for Sulphide Scale Formation and Inhibition Tests

2.2.1 The Static "Jar" Test of Barium Sulphate Scale

Several studies on the formation and inhibition of sulphide scale followed the experimental procedure developed by Graham *et al.* (1997) with slight modifications to address different approaches (Collins and Jordan, 2001; Jordan *et al.*, 2000; Okocha *et al.*, 2008; Okocha and Sorbie, 2010; Savin *et al.*, 2014). The procedure mainly involves two brines, one containing sulphide and the other containing cation(s). At a specific set of conditions, these two brines were mixed, as illustrated in Figure 2.1 (a setup based on the work of Graham *et al.* (1997) and modified by Okocha (2011)), and a set of analysis techniques were used to determine the formation or inhibition efficiencies at different periods. The metal concentrations are prepared at various concentrations, i.e. C1 – C4, while the sulphide concentration was maintained constant.

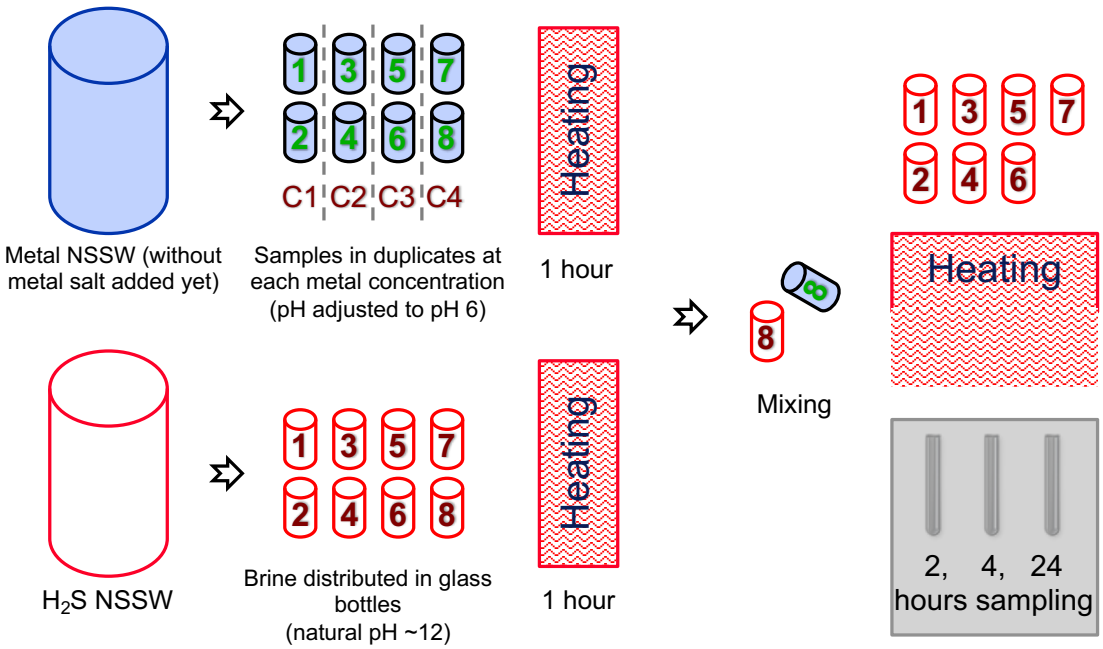

Figure 2.1 Conventional experimental scheme of the static bottle test of sulphide scale starting from the brine preparation, aliquot distribution and addition of metal cation concentrations, heating, mixing the two brines, then heating and frequent analysis

In all of these studies, hydrogen sulphide (or any of the sulphide species, which might be H_2S, HS^- and S^{2-}), was introduced usually via the sodium sulphide salt, which is highly soluble in brine. As observed in the reported data from these experiments, the addition of sodium sulphide increases the pH value of the brine to ~ pH 11 - 12, depending on the

amount of added sulphide salt. Achieving the right conditions for the metal sulphide scale formation/inhibition starts with adjusting the pH for better representation and compatibility. Mixing a low pH cation solution with a high pH sulphide solution should facilitate a moderate pH value. Okocha (2011) developed a model to determine at what pH value the cation/metal solution should be to reach a final pH of 7 after mixing with the sulphide solution. The author maintained the sulphide concentration in his work in excess to the counter cation, and he reported excellent agreement between the model and the experimental pH values and masses of sulphide precipitate obtained.

The main reason for mixing a low pH cation/metal solution with the high pH sulphide solution is to avoid the liberation of H_2S when pH-adjusting the sulphide solution. In sulphide scale static tests conducted at atmospheric pressure, this means loss of sulphide concentration as H_2S gas evolves from solution. Furthermore, sulphide species are extremely sensitive to pH adjustment, and a small variation could result in a significant deviation from desired final pH (Al-Harbi *et al.*, 2018). Introducing pressure to the sulphide static tests will elevate the current high safety requirements further. Hence, a compromise is needed to achieve the required pH value of the sulphide solutions without further health and safety reformations.

2.2.2 Introducing Hydrogen Sulphide Gas to Form Sulphide Scale

The use of hydrogen sulphide gas to form sulphide scale has been investigated using a closed system to evaluate anti-fouling services in terms of preventing PbS deposition in single and multiple phases (Keogh *et al.*, 2017, 2018). The bespoke system, shown in Figure 2.2, utilised a 1% H_2S/99% CO_2 gas mixture to saturate the gaseous phases and dissolve nearly 30 ppm of aqueous hydrogen sulphide in the lead chloride solution under 1.1-1.2 bar of constant pressure. The authors reported gradual formation of PbS, represented by the darkening of the solution's colour.

A

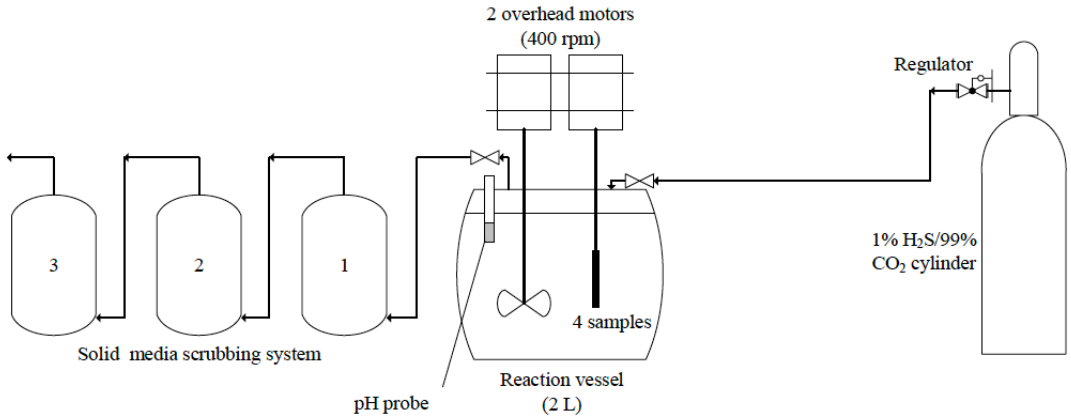

B

Figure 2.2 Sulphide scaling experimental rig A *(Keogh et al., 2017)*, B (*Keogh et al., 2018*)

An easier method of introducing a finite amount of high concentration H_2S gas in a bench-top static test was achieved by adding a specific volume of 10 wt. % hydrochloric acid (HCl) to a known weight and purity of iron sulphide in a volumetric flask sealed by a stopper (Al-Duailej *et al.*, 2012, 2010; Nasr-El-Din and Al-Humaidan, 2001). The H_2S gas was displaced to the reaction vessel by a continuous flow of ultra-pure nitrogen (N_2) gas through rubber tubes and glass pipettes previously inserted through the stoppers, as seen in Figure 2.3. This scheme was used primarily for evaluating the performances of

H_2S scavengers at various solutions. The principal drawback of this technique, which affected the overall accuracy, was the inconsistent dissolution of iron sulphide, which lead to variable H_2S gas generation.

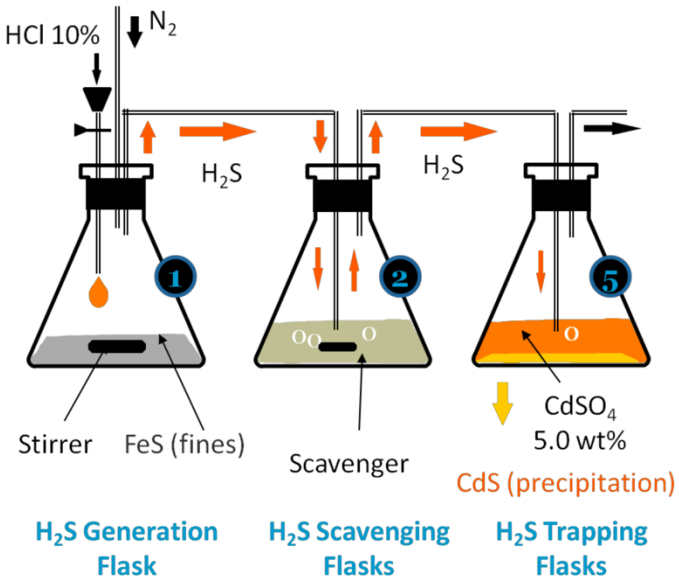

Figure 2.3 Experimental setup for the scavenging efficiency experiment where H_2S is generated by dissolving FeS *(Al-Duailej et al., 2012)*

2.2.3 The Investigation of Sulphide Scale Using Airtight Vessels

The septum-sealed bottles were used to evaluate the formation and inhibition of the oilfield iron sulphide scale (Przybylinski, 2001, 2003). In these studies, the iron and sulphide containing solutions were carried out at their respective natural pH. The iron solution was acidic, while the sulphide solution was basic and containing imidazole (non-interfering buffer) to neutralise the final pH of the mixed solution. The oxygen level in the mixed solution was lowered down to ~ 1 ppm.

A similar setup was used inside an anaerobic chamber while using carbon dioxide gas to saturate brines and adjust their pH before mixing them in septum-sealed bottles (Lehmann and Firouzkouhi, 2008). The maximum hydrogen sulphide concentration used in this study was nearly 80 ppm, and the lowest pH of the sulphide brine was pH 5.5. The study also showed an effect of pH, under which the iron sulphide formed, on the particle size distribution. The study concluded that low-pH solutions produced smaller FeS particle sizes.

2.2.4 Dynamic Sulphide Scale Tests

Dynamic scale tests, on the other hand, often require pressure above atmospheric to control the flow through the filter or the tube (Okocha, 2011). In addition to pressure, advanced dynamic testing of iron(II) sulphide (FeS) formation and inhibition required the use of oxygen traps to ensure the mixing of the two reacting solutions was in an anaerobic environment (Liu *et al.* 2017), which is essential for tests involving iron to prevent oxygen ingress (Baraka-Lokmane *et al.*, 2015; Okocha and Sorbie, 2010; Rickard and Luther, 2007; Savin *et al.*, 2014; Wang *et al.*, 2012). Dissolved oxygen reacts with and oxidises ferrous iron (Fe^{2+}) to produce ferric iron (Fe^{3+}) through the following reaction (Stumm and Lee, 1961):

$$Fe^{2+} + {}^{1}/_{4}\,O_2 + 2OH^- + {}^{1}/_{4}\,H_2O \rightarrow Fe(OH)_3 \qquad (2.1)$$

2.2.5 Kinetic Turbidity Tests

A kinetic turbidity test was used as an alternative method to determine the difference between various scales, including PbS and ZnS, and to determine the efficiency and mechanism of various scale inhibitors (Kerr *et al.* 2017). This method uses kinetic cells or cuvettes, and an ultra-violet visible (UV-Vis) spectrophotometric technique to detect and interpret the turbidity caused by suspended scale particles in the test solutions, as well as determine the settling time for different inhibited scale particles. Several test conditions were investigated, such as variable temperatures, ion concentrations, and stirring speeds.

2.3 Analytical Techniques for Sulphide Determination

Since the mid-20th century, the determination of sulphide concentration in water samples has been performed through several procedures for different applications. These procedures were based on various techniques including titration, spectrophotometry, gas chromatography or potentiometry. Below are brief descriptions of each method, and the application in which it was used.

2.3.1 Titration and Potentiometry

Samples of sulphide in water-suspended sediments were analysed by a titration technique using sodium thiosulfate and potassium iodide (Fishman and Friedman, 1985). Through their investigation, the authors have reported interferences with oxygen and heavy metals. In addition, the method lacked precision in the published data, which could be considered

the main limitation of this technique. A high-precision potentiometric procedure using ion-selective electrodes for determining di-anion sulphide concentrations in distilled water samples was described with a detection limit of 1 part per million parts (ppm) over a range of 0.1 - 12,000 ppm (US Environmental Protection Agency, 1996). In this procedure, the samples required storing at 4ºC before analysis, and distillation of the samples was needed if they contained silver or mercury since they cause interferences with the electrodes. Apart from the lack of practicality, this method had a remarkable accuracy of 94 – 103 % in the range of 1 - 6,000 ppm.

2.3.2 Chromatography

Gas and ion chromatographic techniques offered detection limits in the range of nano- to micro-moles (Casella *et al.*, 2000; Cutter and Radford-knoery, 1993). As a requirement for the chromatographic techniques, sulphide ions were stripped out from water samples to be analysed by flame photometric or amperometric detectors. Although this method provides favourable accuracy, it adds a step of extracting sulphide from aqueous samples, which eventually obstructs the practicality when used in sulphide scale studies. Moreover, the aqueous sulphide concentrations in the oil and gas fields usually range from a few milligrams per litre (milli-moles) to thousands of mg/L (multiple orders of moles), which will require further dilutions to the samples to fit the detection range of this technique.

2.3.3 Spectrophotometry

The spectrophotometric methods for detecting sulphide concentrations depend on measuring the absorbance of solutions, made from different reagents and sulphide samples, at various wavelengths (e.g. Barzegar *et al.*, 2003; Cline and Richards, 1969; Cord-Ruwisch, 1985; Emami *et al.*, 2004; Shanthi and Balasubramanian, 1996; Wallace *et al.*, 2007). Some of the reagents used in this technique included salts of copper sulphate, N,N-dimethyl-p-phenylenediamine (DPD) and pararosaniline (PRA), which, once mixed with sulphide samples, were analysed at wavelengths of 480, 670, and 520 nm, respectively (Cline and Richards, 1969; Cord-Ruwisch, 1985; Shanthi and Balasubramanian, 1996). Calibration curves have to be constructed for each reagent, and the sample needs to be compatible with these reagents, by only forming the solids responsible for the measurement-targeted absorbance. Other reagents have also been used for sulphide determination using a back-calculation approach. For example, the loss of absorbance of thionine at 600 nm, and Methyl green at 637 nm once reacted with sulphide, was used to detect sulphide concentrations (Barzegar *et al.*, 2003; Emami *et al.*, 2004).

2.3.4 Summary of Analytical Methods for Sulphide Determination

All of the reported techniques have limitations and interferences. Nonetheless, a few, such as the spectrophotometric methods using copper sulphate and DPD could be applicable in sulphide scale studies. Table 2.2 shows a summary of the reviewed techniques, their main features and limitations with regards to sulphide scale studies.

Table 2.2 Summary of analytical methods for determining the concentration of aqueous sulphide

Title	*Technique*	*Reagent*	*Range*	*Accuracy*	*Limitations*	*Reference*
Sulphide, titrimetric, iodometric	Titration	Potassium Iodide	-	Not reported	Oxygen-sensitive, no precision data	Fishman and Friedman 1985
Method 9215	Ion-Selective Electrode	-	0.1 - 12,000 ppm	High at 1 – 6,000 ppm	Only distilled samples, Pre-test Storing	US Environmental Protection Agency 1996
Cline's Reagent (Methylene Blue)	Spectrophotometry (670nm)	N,N-dimethyl-p-phenylenediamine (Absorbance)	0.032 – 32 ppm (4 regions)	3% SD	Thiosulphate partially inhibits the reaction	Cline 1969
Sulphide Determination in SRB cultures	Spectrophotometry (480nm)	Copper sulphate (Absorbance)	3.2 – unknown ppm	5% SD	Applicable only while stirring, not tested with other anions	Cord-Ruwisch 1985
Colorimetric Response to Hydrogen Sulfide	Spectrophotometry (multiple values)	Two Copper(II) chromophores	10-1000 ppm (10)	-	A thin film made, with numerous peaks	Wallace *et al.* 2007
Determination of Sulphide in Spring and Wastewater	Spectrophotometry (600nm)	Thionine (Loss of Absorbance)	0.4 - 38 ppm (4 regions)	0.8 - 2.7% (region-dependent)	Interference of Cu^{2+}, Cd^{2+}, Pb^{2+}, Pd^{2+}, and Ag^{+}	Emami *et al.* 2004
Kinetic Spectrophotometric Determination of sulphide	Spectrophotometry (637nm)	Methyl Green (Loss of Absorbance)	0.03 - 1.2 ppm	0.85 - 2.3% RSD	Low range, Interference of Hg^{2+}, Hg^{+}, Pb^{2+}, Ag^{+}, IO_3^{-}, and SO_3^{2-}	Barzegar *et al.* 2003
Spectrophotometric Determination of H_2S Based on Schiff's Reaction	Spectrophotometry (520nm)	Pararosaniline (Absorbance)	0-0.04 ppm	2.4%	Designed for air samples, Low range, Sulphide dioxide interference	Shanthi and Balasubramanian 1996
Determination of Carbonyl Sulfide (OCS)	Gas Chromatography (Flame Photometric Detector)	-	In nano-moles	5%	Indirect, Shallow range, Pressurized water samples	Cutter and Radford-knoery 1993
Sulfide Measurements by Flow Injection Analysis	Ion Chromatography (Ampeometric Detector)	-	In micro-moles	4.7%	Indirect, Shallow range, Lead interference	Casella *et al.* 2000

2.4 Oxidation of Aqueous Sulphide

2.4.1 Reactions of Aqueous Sulphide and Dissolved Oxygen

At the right conditions, aqueous sulphides undergo oxidation in the presence of oxygen (Almgren and Hagström, 1974; Broderius and Smith, 1980; Fishman and Friedman, 1985; Halfyard and Hawboldt, 2011; Harmandas *et al.*, 1998; Headlee, 1945; Kamyshny *et al.*, 2008; Kamyshny and Ferdelman, 2010; Lawrence *et al.*, 2000; Lefers *et al.*, 1978; Luther *et al.*, 2011; Oduro *et al.*, 2013; Wang *et al.*, 2016; Zerkle *et al.*, 2010). The concept of sulphide oxidation is well investigated in the literature under different disciplines, including geochemistry, microbiology and chemical engineering. Oxidation of sulphides ultimately produces elemental sulphur (S_8), polysulphide (S_n^{2-}) and sulphate (SO_4^{2-}). The rate of oxidation is controlled by several factors including temperature, pH, and the concentrations of oxygen and sulphides (Almgren and Hagström, 1974). Headlee (1945) suggested the following equations for the oxidation of hydrogen sulphide:

$$2H_2S + O_2 \rightarrow 2H_2O + 2S \quad (2.2)$$

$$H_2S + 2O_2 \rightarrow H_2SO_4 \quad (2.3)$$

Lefers *et al.* (1978) have discussed the reactions of bisulphides (HS^-) and referred to other studies (Avrahami and Golding, 1968; Chen and Morris, 1972) in which these reactions were categorised based on alkalinity and pH level:

In neutral, weak acid or weak basic solutions (circumneutral conditions):

$$2HS^- + O_2 \rightarrow 2S + 2OH^- \quad (2.4)$$

$$HS^- + (n-1)S \rightarrow H^+ + S_n^{2-} \quad (2.5)$$

One of the assumptions was the oxidation of sulphide to form sulphur and polysulphide at pH > 9 is improbable, and the formation of stable thiosulphates at pH > 11 can occur based on the following reactions:

$$2HS^- + 3O_2 \rightarrow 2SO_3^{2-} + 2H^+ \quad (2.6)$$

$$2SO_3^{2-} + O_2 \rightarrow 2SO_4^{2-} \quad (2.7)$$

$$2SO_3^{2-} + 2HS^- + O_2 \rightarrow 2S_2O_3^{2-} + 2OH^- \quad (2.8)$$

Nonetheless, Avrahami and Golding (1968) reported results suggesting an increase in oxidation rate with increase in pH values from 11 to 14, at temperatures 25 and 45ºC. Several studies in the literature have reported inconsistent sulphide oxidation rates in the sea and fresh waters. Unfortunately, the focus in these studies was mainly on solutions with pH values 6 - 13, with lower pH values remaining not thoroughly studied (Almgren and Hagström, 1974; Broderius and Smith, 1980; Fishman and Friedman, 1985; Halfyard and Hawboldt, 2011; Harmandas *et al.*, 1998; Headlee, 1945; Kamyshny *et al.*, 2008; Kamyshny and Ferdelman, 2010; Lawrence *et al.*, 2000; Lefers *et al.*, 1978; Luther *et al.*, 2011; Oduro *et al.*, 2013; Zerkle *et al.*, 2010). Details of the sulphide oxidation reaction(s) have been reported in the work of Weres and Tsao (1983), Zangh and Millero (1992), Steudel (1996), and Nielsen *et al.* (2003). According to these studies, the sulphide oxidation occurs through two mechanisms, viz. a polar mechanism and a free radical chain mechanism. Weres and Tsao (1983) reviewed the literature of sulphide oxidation at different brines, conditions, and concentrations, and Table 2.3 shows a summary of that review.

Table 2.3 Summary of literature review from Weres and Tsao (1983)

Study	*Solution*	*pH*	*[Sulphide]*	*Oxidation products*		*Remarks*
				Intermediate	*Final*	
(Avrahami and Golding, 1968)	-	11-14	100μM	Sulphite, which reacts with either O_2 to form sulphate, or O_2 and HS^- to form thiosulphate	Thiosulphate and sulphate	-Rate of HS^- consumption: doubled with one-unit pH increase, or tripling $[O_2]$
(Chen and Morris, 1972)	-	6-13	50μM - 20mM	Polysulphides	-pH<6: colloidal sulphur -pH>8.5: thiosulphate -$[H_2S]$>1mM: colloidal sulfur -$[H_2S]$<1mM: thiosulphate and sulphate	-Free radical chain mechanism -Maxima: pH6.8-8 and pH11
(O'Brien and Birkner, 1977)	-	4, 7.55, 10	10-80μM	Sulphite	Sulphite, sulphate and thiosulphate	Colloidal sulphur was not observed
(Cline and Richards, 1969)	Lake water	-	60μM	-	10-15% Sulphite, sulphate and 30-35% thiosulphate	-No turbidity (no colloidal sulphur) -5μM added iron (II) accelerated the reaction
(Almgren and Hagström, 1974)	Seawater	-	1-200μM	-	-	Increased rate at pH 8-8.5

2.4.2 Oxidation of Sulphide in the Oil and Gas Fields

The oil and gas industry has moved towards producing challenging natural gas reservoirs with high sour profiles. In recent years, sour oil and gas reserves in the Middle East have become of significant interest, after the production from less challenging reserves has passed its peak (Canty, 2012). Kuwait, Oman, Saudi Arabia and the UAE have started the development of sour gas fields, comprising more than 60% of natural gas fields, of which some are expected to reach 23% H_2S (Boschee, 2014). With the industry's shift towards more technically difficult sour gas reservoirs, it is essential to investigate sulphur-related challenges in production, transportation and treatment.

The oxidation of sulphide has not been thoroughly investigated in the oil and gas industry. (Przybylinski, 2001 and 2003) briefly discussed, from the perspective of iron sulphide

formation and inhibition, the oxidation of sulphide by either oxygen or ferric iron in the oilfield. Przybylinski has stated that the impact of small amounts of dissolved oxygen on the inhibition results was insignificant. A recent study discussed H_2S loss in reservoir fluid samples in terms of the sample's chamber coatings, temperature, pressure, and agitation (Khan *et al.*, 2017). The authors mentioned a possible solubility/reaction of H_2S with drilling mud contamination. Nonetheless, the study could not conclude as to what caused the sulphide concentration to decrease with time.

On the other hand, several reports have discussed the deposition of elemental sulphur, which could be an oxidative product based on equation (2.2), in the reservoir, near wellbore area, or in production pipelines (Al-Jaberi *et al.*, 2017; Brunner *et al.*, 1980; Fadairo *et al.*, 2012; Guo *et al.*, 2006; Hands *et al.*, 2002; Liu *et al.*, 2012; Mahmoud, 2014, 2012; Mei *et al.*, 2006; Roberts, 1997; Shedid and Zekri, 2002; Sun *et al.*, 2011; Tang *et al.*, 2011; Zekri *et al.*, 2009). The deposition of sulphur can occur mostly due to the reduction in pressure and temperature, and occasionally due to oxygen ingress or decline in the production of a gas well (Al-Mutairi *et al.*, 2007; Boivin and Oliphant, 2011; Fadairo *et al.*, 2012; Headlee, 1945; Liu *et al.*, 2012; Mahmoud, 2014; Mahmoud and Al-Majed, 2012; Mei *et al.*, 2006; Roberts, 1997; Shedid and Zekri, 2002; Sun *et al.*, 2011; Tang *et al.*, 2011; Xiao *et al.*, 2010).

2.4.3 Oxygen Sources in Downhole Fluids

The source of oxygen in the downhole environment is mainly the injected fluids. Although de-oxygenation and oxygen scavenging methods are often applied, fluids with high oxygen solubility, monoethylene glycol (MEG) for example, occasionally transfer oxygen to the system when injected for hydrate inhibition treatments (Kan and Tomson, 2012). A second source of oxygen is leaking joints or valves above ground, which consequently causes sulphur deposition in surface facilities (Boivin and Oliphant, 2011; Kan and Tomson, 2012).

2.5 Conclusions

The literature contains excellent testing techniques of sulphide scale, various determination techniques of aqueous sulphide concentrations, and a different effect of oxygen on aqueous sulphide species depending on test conditions. However, the findings of the literature survey cannot be introduced directly into the static testing of the oilfield sulphide scale. Therefore, a gap has been acknowledged between the levels of static tests,

which can be occupied with an anaerobic bench-top apparatus that confidently enables the pH-adjustment of sodium sulphide solutions while retaining evolved H_2S gas. Furthermore, the proposed setup required a reassuring assaying of aqueous sulphide concentrations and a theoretical validation of the sulphide scale formation tests.

3 – Static Bottle Test for Sulphide Scale – Current Practice

Executive Summary

The conventional static jar test has been used to identify the scale formation patterns of ZnS by varying the Zn:S molar ratios. However, the testing method did not represent the reactants in realistic conditions, i.e. pH and sulphide ion species. Therefore, modifications to this testing method were carried out to produce results similar to those of pressurised rigs and closed anaerobic systems. These modifications involved pH adjustments of the sodium sulphide brines and using H_2S gas to saturate brines with sulphide. Both techniques provided closer conditions to the in-situ conditions in terms of pH and ion species, however, they had major disadvantages such as the loss of H_2S from solution during pH adjustment, and the low solubility of bubbled H_2S gas during the saturation step. As a result, inhibition tests using the gas saturation method showed very inconsistent efficiencies at various scale inhibitor concentrations. In addition, tracing the concentrations of aqueous sulphide was not practical and could be further improved.

3.1 Description of the Static Bottle Test

The sulphide scale studies primarily consist of static and dynamic investigative tests. The current static bottle test was described in Section 2.2, where the original schematics of the test were developed by Graham *et al.* (1997) for barium sulphate scale, then further modified to address other objectives. The three common sulphide scales (FeS, ZnS and PbS) can be tested at static conditions using this experimental setup. However, iron sulphide requires anaerobic conditions to minimise oxidising the ferrous iron (Fe^{2+}) to ferric iron (Fe^{3+}) upon exposure to oxygen. Zinc sulphide formation was tested first to evaluate the setup, since zinc was less toxic than lead, and did not initially require anaerobic conditions. The evaluation of the static bottle test should highlight the areas which could be improved to achieve a *hybrid* static test setup that offers comparable test conditions at lesser cost and complexity of anaerobic systems and bespoke rigs.

3.1.1 Experimental Description of the Formation Test of ZnS at NSSW and 50ºC

Before describing the experimental procedures, it is important to mention that the preparation of sodium sulphide and zinc chloride brines must be carried out with caution inside fume cupboards. The sodium sulphide nonahydrate salt is considered corrosive to the skin and acutely toxic to dermal and oral exposure, and to aquatic life. Zinc chloride salt may cause eye and skin burns and is harmful upon swallowing and inhalation.

For general purposes, North Sea-sea water (NSSW) was selected as the brine for the scale formation experiment. The salinity of NSSW is close to 35,000 mg/L, and it mainly contains sodium chloride, calcium chloride, potassium chloride, and sodium sulphate. Two versions of NSSW were prepared in 5 L each: H_2S NSSW and Zn NSSW, according to the compositions shown in Table 3.1 and Table 3.2. The main difference between these brines was the magnesium concentrations: zero and 2,736 mg/L for H_2S NSSW and Zn NSSW brines, respectively. The exclusion of magnesium from the H_2S NSSW prevented the formation of magnesium hydroxide after the addition of sodium sulphide salt, which raised the pH to ~ pH 11 - 12. The addition of sodium sulphide salt, however, took place just before the mixing of these two brines. The pH of Zn NSSW brine was further adjusted by adding diluted NaOH, to reach pH 6.

Table 3.1 H_2S NSSW brine composition for the ZnS formation test

Ion	*Concentration, mg/L*
Na	10,890
Ca	428
Mg	0
K	460
SO_4	2,960
$H_2S^{(a)}$	300
Zn	0
HCO_3	0

(a) Sodium sulphide salt was added separately after preparing the brine from other salts. It was added on the same day as mixing the two brines.

Table 3.2 Zn NSSW brine composition for the ZnS formation test

Ion	*Concentration, mg/L*
Na	10,890
Ca	428
Mg	2,736
K	460
SO_4	2,960
H_2S	0
Zn	See Table 3.3
HCO_3	0

The Zn NSSW was created without addition of $ZnCl_2$. Subsequently, 250 mL of each of the $ZnCl_2$ concentrations detailed in Table 3.3 were made, of which two duplicate 100

mL samples were transferred into plastic bottles and labelled accordingly. The stock solution samples were made up of what was left from the original 250 mL solution. Similarly, the H_2S NSSW was prepared initially without adding $Na_2S.9H_2O$, and then the latter was added according to the desired concentration. The pH value was measured and recorded. Afterwards, samples of 100 mL were transferred to glass bottles and labelled as well.

Table 3.3 $ZnCl_2$ concentration and corresponding weights per 250 mL Zn NSSW

Sample No.	*[$ZnCl_2$], mg/L*
1	100
2	250
3	500
4	575
5	600
6	625
7	700
8	750
9	1,000
10	1,500
11	2,000
12	2,500

The varying zinc and constant sulphide concentrations provided several molar ratios of Zn:S, representing various scaling scenarios in the oil and gas field. The glass bottles containing H_2S NSSW were placed in a water bath, and plastic bottles containing Zn NSSW were placed in an oven, where both sets were heated for one hour at 50ºC. Afterwards, plastic and glass bottles were taken out, one at a time and Zn NSSW was added to H_2S NSSW in the glass bottle, shaken vigorously, and placed back in the water bath. Sampling, where 1 mL of the ZnS supernatant solution was transferred to 9 mL of DW (10x dilution), was performed at 2, 4 and 24 hours to track the progress of the reaction. The samples, stock solutions, and ICP standards, shown in Table 3.4, were analysed by ICP to measure the concentrations of subject ions, which were in this experiment: Zn, Mg and Ca. The ICP standards were prepared to match the diluted samples; therefore, the maximum ICP standard was 150 mg/L of zinc. Final pH measurements were made after cooling the supernatant solutions. *(For ICP analysis protocol, refer to Appendix F).*

Table 3.4 ICP standard preparation for Zn analysis

Chemical	*Volumes used for 250 mL in DW (mL)*			
	Standard 1 (0 mg/L)	*Standard 2 (50 mg/L)*	*Standard 3 (100 mg/L)*	*Standard 4 (150 mg/L)*
Zinc 10,000 ppm ICP standard	0	1.25	2.5	3.75

Solids precipitated during the experiment were analysed using a particle size distribution analyser to determine whether different molar ratios of sulphide and zinc would influence the size of deposited solid particles.

3.1.2 Results of the Static Formation Test of ZnS at 50ºC

The ICP analysis of zinc sulphide formation samples followed the theoretical values of zinc concentrations in solution. The zinc concentrations and pH values were plotted as a function of Zn:S molar ratio, as shown in Figure 3.1. It was noticeable that zinc has completely precipitated in the sulphide excess region, where zinc to sulphur ratio is less than 1. Excess zinc concentration was detected as the molar ratio increased beyond Zn:S ratio of 1. The difference in zinc concentrations between stock and test samples was constant (261 mg/L ± 5 %) throughout the samples in the zinc excess region. This difference is equivalent, in moles, to the actual sulphide added to the brine solution, since the reaction is governed by a 1:1 molar ratio. The added sulphide concentration was calculated, based on the measured weight of $Na_2S.9H_2O$, to be 141 mg/L; however, it was found to be ranging between 128 - 131 mg/L, using back-calculation of average consumption of zinc moles. The experimental data showed excellent agreement with the theoretical values of zinc concentrations confirming the 1:1 molar ratio of the reaction.

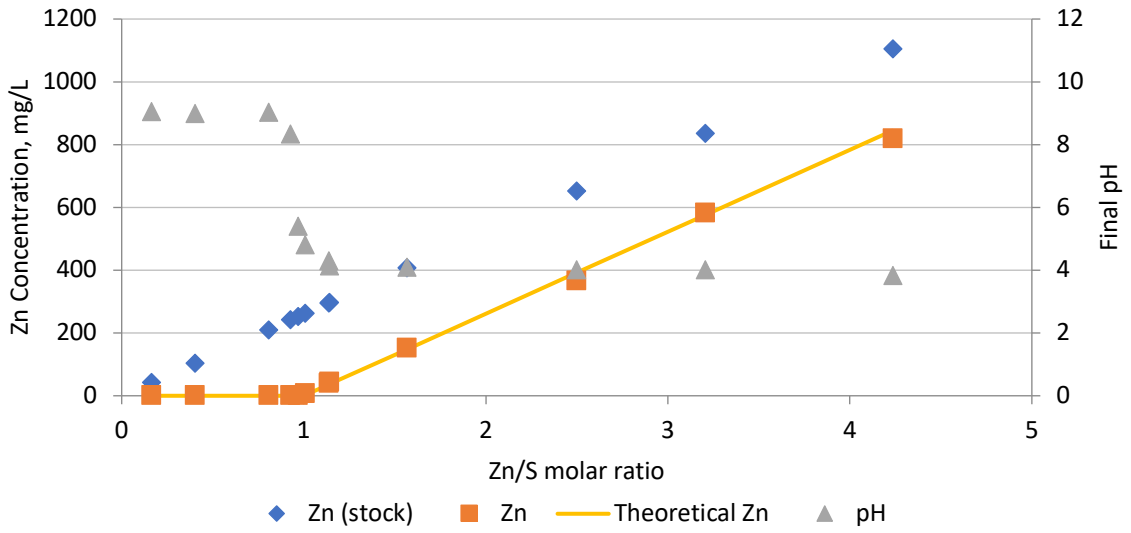

Figure 3.1 Scale formation profiles of ZnS represented by pH values and zinc concentration in stock and test samples compared to theoretical values in NSSW at 50°C after 24 hours

The pH values of test samples were distinctively dependant on the dominant ion. In the sulphide excess region, pH was level at 9, since the initial sulphide brine concentration was as high as pH 11.8, and the decrease in pH was a result of the dilution and consumption of the initial sulphide concentration. At such pH, the dominant sulphide species was HS^-, while $H_2S_{(aq)}$ and S^{2-} were at significantly lower concentrations, based on the sulphide distribution shown in Figure 1.1. The pH value remained constant as long as the molar ratio between zinc and sulphide was below 1. An inflection point occurred in the range of 0.93 - 1.14 Zn:S molar ratios. In this range, the sulphide influence over pH diminished and zinc became dominant, hence the drop in pH values from 8.35 to 4.31. Beyond the inflection point, the increase in zinc concentrations shows a negligible effect on the pH value. In all samples, aqueous sulphide acted as a buffer maintaining a relatively high final pH, and once the aqueous sulphide was completely depleted, the pH was governed by the Zn NSSW solution.

The collected solids from test samples were analysed using a particle size distribution analyser. Figure 3.2 shows a broad and inconclusive trend suggesting either an increase in the mean median diameter or a consistent size of the deposited solids as the molar ratio between zinc and sulphide increased. However, because of the scattered nature of these results, it remained inconclusive. Running a statistical T-test on these results showed

significant variations between the repeated (paired) measurements of each molar ratio (P-value = 0.004 < 0.05).

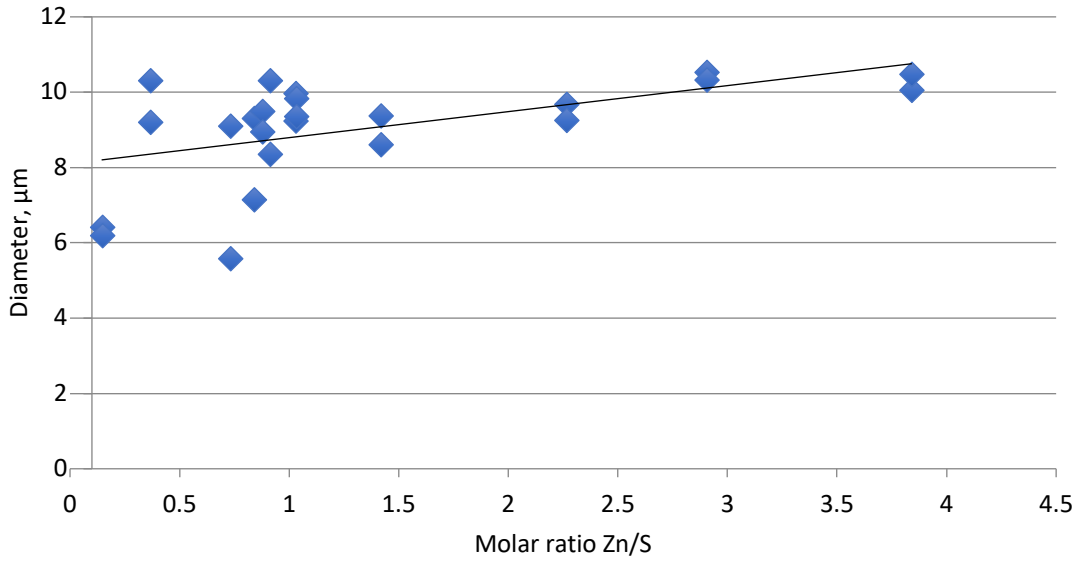

Figure 3.2 ZnS Particle size distribution measured in duplicate samples as a function of Zn/S molar ratio

3.2 Development of the Static Scale Test Setup

The development of the static jar test was based on identifying the areas that could be improved to provide an advanced testing environment, comparable to that of dedicated closed systems. Below are the two areas that could enhance the testing methodology:

(i) The aqueous sulphide system is exceptionally susceptible to the pH of the solution and controlling the pH of the sulphide solutions provides better representation to the oilfield conditions.

(ii) The determination of the aqueous sulphide concentrations is required throughout the test stages to identify the changes in the concentration, such as the evolution of $H_2S_{(g)}$, and the causes behind these changes.

The traceability of sulphide concentration was achievable through quenching with a zinc chloride solution which was analysed by ICP to identify the difference against a stock solution. The decrease in zinc concentration can be back-calculated to determine the sulphide content as follows:

$$\Delta[Zn] = [Zn]_{Stock} - [Zn]_{aq} \quad (3.1)$$

$$\Delta[Sulphide] = \Delta[Zn] \times \frac{MW_{H2S}}{AW_{Zn}} \quad (3.2)$$

where MW_{H2S} is the molecular weight of H_2S, and AW_{Zn} is the atomic weight of zinc. This method could provide sufficient accuracy within the precision of the ICP method (± 10% error). The quenching could be done at different stages of the test to trace any changes in the sulphide concentration, especially throughout the pH adjustment steps. However, the quenching/back-calculation technique only offered the results after the test completion.

3.2.1 pH Adjustment of Sulphide Solutions

3.2.1.1 Description of the proposed mechanism for pH adjustment

The use of sodium sulphide solution at natural pH (pH 10 - 12) was not representative of the oilfield sulphide species, and it required a pH adjustment to simulate the effect of dissolved sour gases, mainly CO_2, on the solution pH. The addition of acid or the dissolution of CO_2 gas into the sulphide result in increasing the population of $[H^+]$ to shift the speciation towards the preferred form of sulphide, namely $H_2S_{(g)}$ and HS^-, as seen in Equations (1.1) and (1.3). However, acidifying (or lowering the pH of) the sodium sulphide solution results in the evolution of $H_2S_{(g)}$, which, in addition to the health and safety risks, changes the concentrations of the aqueous sulphide.

Okocha (2011) has proposed a less direct technique of lowering the pH of aqueous sulphide, compared to the addition of acid. The suggested procedure involved a high pH sulphide solution (pH 11-12) mixed with a scaling metal brine (sulphide-free) at a low pH (pH 1-2) to produce a mixed sulphide solution with circumneutral pH (pH ~ 7). Alternatively, Przybylinski (2001) used imidazole (non-interfering buffer) in the basic sodium sulphide solution to reach a final circumneutral pH of the mixed iron sulphide solution. Both techniques did not initially affect the speciation of sulphide and only neutralised the pH after forming the scale in question. Lehmann and Firouzkouhi (2008) used CO_2 gas to saturate and lower the pH of the sodium sulphide brines prior to adding the iron, which required a pressurised system inside an anaerobic chamber.

The necessity of introducing the right species of sulphide at the correct pH value stems from the direct effect on the solubility products and the subsequent impact on the inhibition performance through the varying sizes or masses of formed scale particles. In general, Lehmann and Firouzkouhi (2008) have concluded that the particle size of FeS increase with increasing the pH of the sodium sulphide brines. Such a conclusion directly impacts scale inhibitors, especially dispersants, as their apparent inhibition efficiencies are influenced by the particle size and the particles agglomeration.

The conventional bottle test procedure received an additional step to adjust the sulphide solution before mixing the scaling solutions while maintaining minimum H_2S evolution due to pH reduction. The following scheme, Figure 3.3, was proposed to offer a subtler shift in the pH compared to the direct addition of acid, thus reducing the expected evolution of $H_2S_{(g)}$.

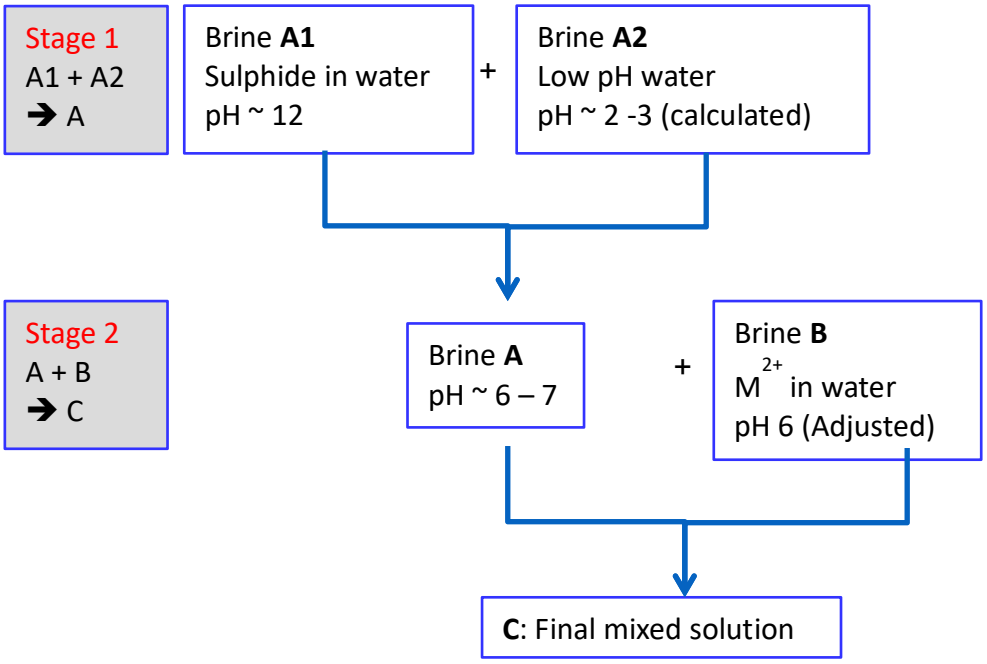

Figure 3.3 Experimental scheme to adjust the pH of sulphide solution before mixing with the scaling metal solution to avoid direct acid addition to sulphide solution which could evolve $H_2S_{(g)}$

The sulphide concentration in Brine A1 was doubled, to account for the extra mixing step. Brine A2 was prepared from the same brine as Brine A1 without adding the sodium sulphide salt. This brine (A2) was pH adjusted by adding HCl, and the expected pH range

was pH 2 – 3, which was established using a simple spreadsheet model to calculate the final pH after the mixing of the two different solutions. Brine A1 and A2 were mixed to produce Brine A of pH 6 – 7. Brine A was then combined with Brine B, which contained the cation, to form the sulphide scale and reach a final circumneutral pH.

3.2.1.2 The experimental procedure of the pH adjusted ZnS scale formation test

Zinc chloride was added to Zn NSSW (Brine B) at two concentrations, according to Table 3.5, the initial sulphide concentration in brine A1 (or RAW H_2S NSSW) was doubled to 600 mg/L. The final sulphide concentration remained fixed at 150 mg/L. The test was carried out at room temperature, and the mixing ratio throughout the steps was 1:1.

Table 3.5 Concentrations of zinc in Zn brines

Samples	*[$ZnCl_2$], mg/L in NSSW*	*[Zn^{2+}], mg/L in NSSW*	*[Zn^{2+}], mg/L in mixed solution*	*Adjusted pH*
50-x	100	44	22	6
1000-x	2,000	904	452	6

Several attempts were made to achieve a pH ranging between pH 6 - 7 for the pH-adjusted H_2S brine (Brine A). As a result, different initial low pH values were chosen to scope out the best range of initial low pH. The first phase of this test included two sets of varying zinc chloride concentrations (100 and 2,000 mg/L), which produced zinc to sulphide molar ratios (Zn/S) of 0.07 and 1.56, respectively. Three pH values were prepared for the sulphide brine, as shown in Table 3.6. The sets were labelled 50 and 1,000 as a roundup of the zinc concentration in solution. Slight variations of initial pH resulted in a substantial difference in the final pH values (Note that this was as expected from earlier modelling work carried out to design these experiments). Each of these pH-adjusted H_2S brines was mixed with both concentrations of zinc in Zn brine.

Table 3.6 Adjustment of pH value for the pH-adjusted H_2S brines

Low pH NSSW (0 mg/L H_2S)	*RAW H_2S NSSW (600 mg/L H_2S)*	*pH-adjusted H_2S brine (300 mg/L)*	*Samples No.*
pH 1.82	pH 12.18	pH 7.17	50-1, 50-2
		pH 7.16	1000-1, 1000-2
pH 1.88		pH 8.14	50-3, 50-4
		pH 8.29	1000-3, 1000-4
pH 1.98		pH 11.01	50-5, 50-6
		pH 11.05	1000-5, 1000-6

3.2.1.3 Results of the ZnS formation test using pH adjusted sulphide solutions

The quenching of sulphide excess samples (50-1 to 50-6) revealed the loss of H_2S during the lowering of pH of the sodium sulphide solutions before mixing with Zn brines. In Figure 3.4, the decrease in initial sulphide concentration reached 18% at pH 7.16, and 8% at pH 8.29 and pH 11.5. The sulphide species distribution was, theoretically and by referring to Figure 1.1, roughly 40% as $H_2S_{(aq)}$ and 60% as HS^- at pH of 7.2, hence the large loss percentage. On the other hand, at pH 8.29, the percentage of $H_2S_{(aq)}$ was expected to be around 5%, and much smaller losses would be expected. The ICP analysis of the outcome supernatant solutions concurred the effect of loss of sulphide concentrations on the formation of ZnS at various pH levels, as seen in Figure 3.5.

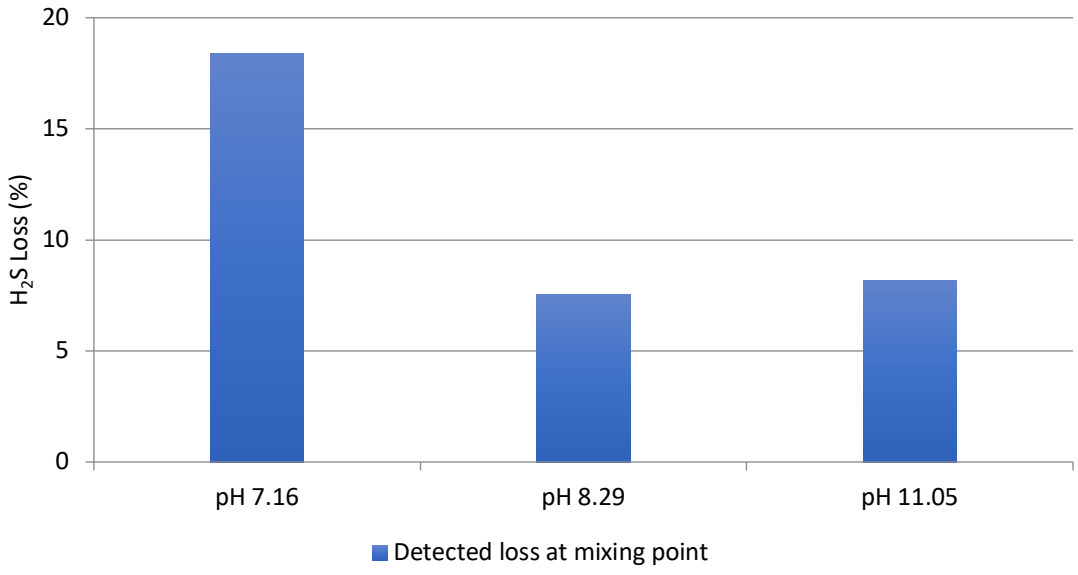

Figure 3.4 Losses of H_2S after adjusting pH values

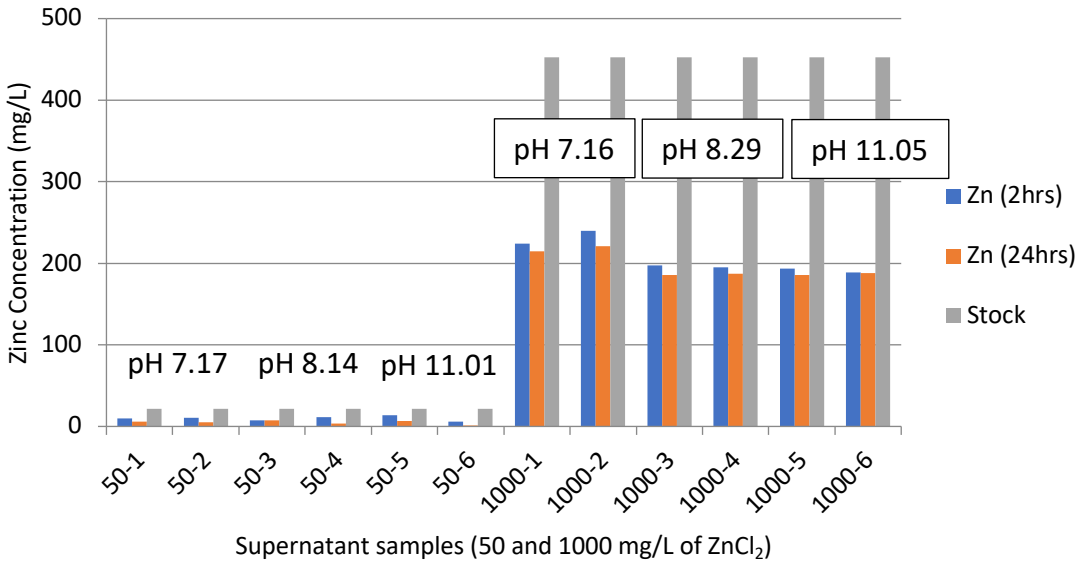

Figure 3.5 ICP results of remaining Zn in supernatant solution after mixing with pH-adjusted sulphide brines showing higher [Zn^{2+}] in samples at lower pH values (1000-1 and 1000-2) because of $H_2S_{(g)}$ evolution

The pH behaviour of both sets of samples, 50 and 1000, is shown in Figure 3.6. The zinc excess samples, 1000-1 to 1000-6, have demonstrated similar pH behaviour to that in the first test seen in Figure 3.1, where H_2S brine was at natural pH. Apart from a generally lower pH value for these zinc excess samples, i.e. ~ pH 2.3, there was not an observable effect of the initial pH value of sulphide brine on the pH value of supernatant solutions. On the other hand, the sulphide excess samples, 50-1 to 50-6, were positively dependent on the initial pH value of sulphide brine. The pH-adjusted H_2S brines had pH values of ~7.2, 8.2 and 11, and correspondingly, the pH values of supernatant solutions were measured at ~7.5, 8 and 9.2, respectively. The pH value of 9.2 was very close to the value achieved in the sulphide excess region in the first test, as seen in Figure 3.1.

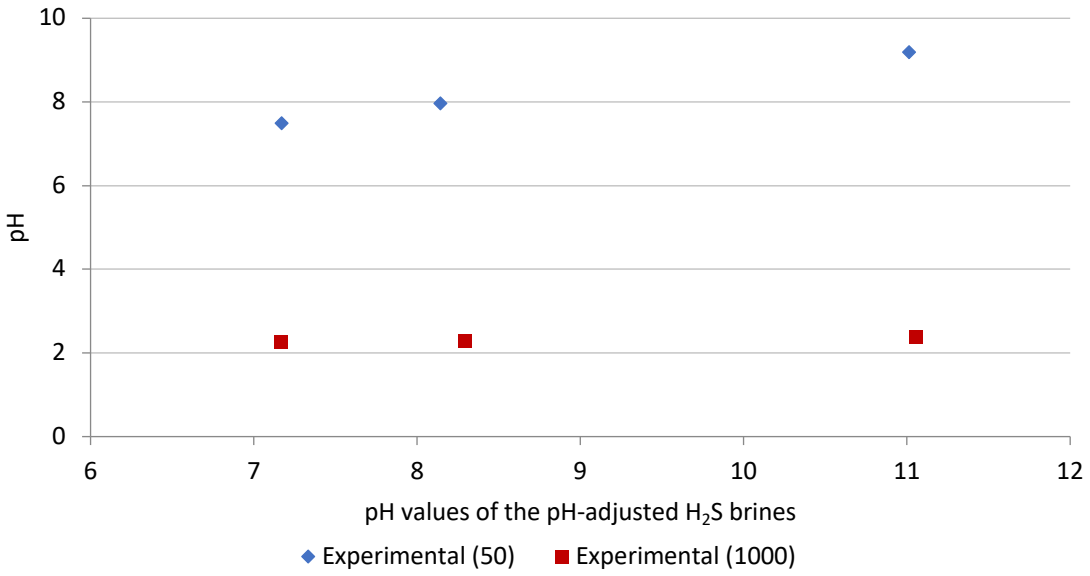

Figure 3.6 Final pH values of supernatant solution of both sulphide and zinc excess samples as a function of the pH values of the pH-adjusted H_2S brines

The primary impact of evolving $H_2S_{(g)}$, or decreasing the aqueous sulphide concentration, was observed in the zinc-excess solutions, as the zinc concentration in supernatant solutions were averaging ~ 217 mg/L at pH 7.16, and ~ 186 mg/L at pH 8.29 and pH 11.05. Furthermore, this decrease in aqueous sulphide levels will have detrimental effect on sulphide scale formation and inhibition tests where a 15 - 20 % reduction of the sulphide concentrations makes a difference in the outcome.

The next phases of this test were carried out at 50ºC and were limited to sulphide excess samples to achieve better traceability of the loss of sulphide. Similarly, initial pH values were prepared for the pH-adjusted H_2S brines (brine A2), as listed in Table 3.7. The pH values were selected with small increments between them, and the resulting pH value for the mixture has further proven the severe sensitivity of the aqueous sulphide system to pH variations.

Table 3.7 pH adjustment process and results of 2nd and 3rd Phases

	Low pH NSSW (0 mg/L H_2S)	*RAW H_2S NSSW (600 mg/L H_2S)*	*pH-adjusted H_2S brine (300 mg/L)*
2nd Phase	1.70	11.92	2.72
	1.78		5.71
	1.82		6.21
	1.85		6.56
3rd Phase	1.52	12.12	6.63
	1.54		6.50
	1.57		7.04
	1.65		7.23
	1.75		10.65
	1.77		10.79

The sensitivity of the sodium sulphide solutions to pH adjustment was observed in and Table 3.7. These pH variations and the excessive loss of sulphide concentration in the pH adjusted sulphide solutions, blue bars in Figure 3.7 and Figure 3.8, were the primary drawbacks of this technique. The decline in sulphide concentration was mainly due to the liberation of H_2S, as these losses were correlated with the adjusted pH of the sulphide solutions, as shown in Figure 3.7 and Figure 3.8. The difference in aqueous sulphide concentration between the samples at room temperature and at 50°C was a result of reduced solubility due to the increase in temperature (Rickard, 2012).

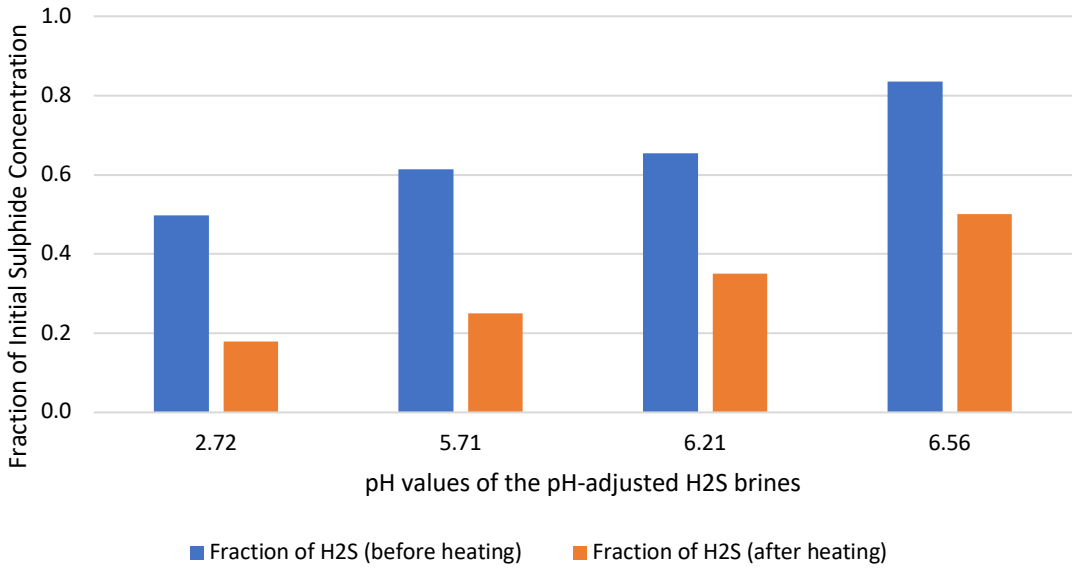

Figure 3.7 Fractions of the initial sulphide concentrations in the pH-adjusted H_2S brines (2^{nd} Phase) before and after heating to represent what remains after the pH adjustment

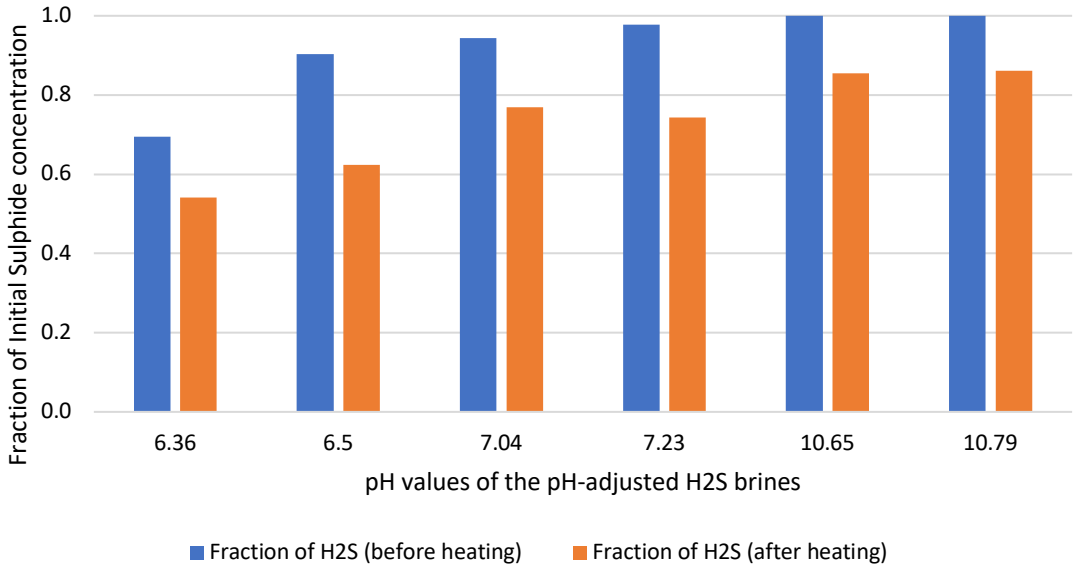

Figure 3.8 Fractions of the initial sulphide concentrations in the pH-adjusted H_2S brines (3^{rd} Phase) before and after heating to represent the remaining sulphide concentrations after pH adjustment

The ICP analysis of the supernatant solutions, after mixing H_2S brines and Zn brines, showed a total consumption of Zn in most samples, and the final pH values are listed in Table 3.8. The least ZnS formation was observed in the lowest pH sample, where more

than 80% of the initial sulphide concentration was lost in the pH adjusted H_2S brine (pH 2.72) after heating, as seen in Figure 3.7.

Table 3.8 ICP analysis results of Zn concentration in stock and supernatant solutions and their respective pH values of 2nd and 3rd phases

Zn Concentrations (mg/L)			*pH_f of supernatant solution*
Stock solution		*Supernatant solution*	
2nd Phase	21.2	5.3	2.76
		1.4	3.46
		0.8	3.5
		2.5	4.79
		1.3	5.28
		0.5	6.49
		1.5	6.57
3rd Phase	22.8	0.5	6.37*
		0.2	6.69*
		1.0	7.14*
		0.5	7.41*
		0.4	8.45*
		0.8	8.73*

* Averages of two measured pH values

The particle size distribution of the 3rd phase of this test was measured, and the effect of pH adjustment of the sulphide solutions on the size was apparent as shown in Figure 3.9. It was evident that at high pH, the particle size was more substantial and in agreement with the general findings of FeS formation reported by Lehmann and Firouzkouhi (2008) who used carbon dioxide to adjust the pH of the sulphide brines. Consequently, the particle size variation due to the pH of the aqueous sulphide solution will have an impact on the inhibition evaluation outcome.

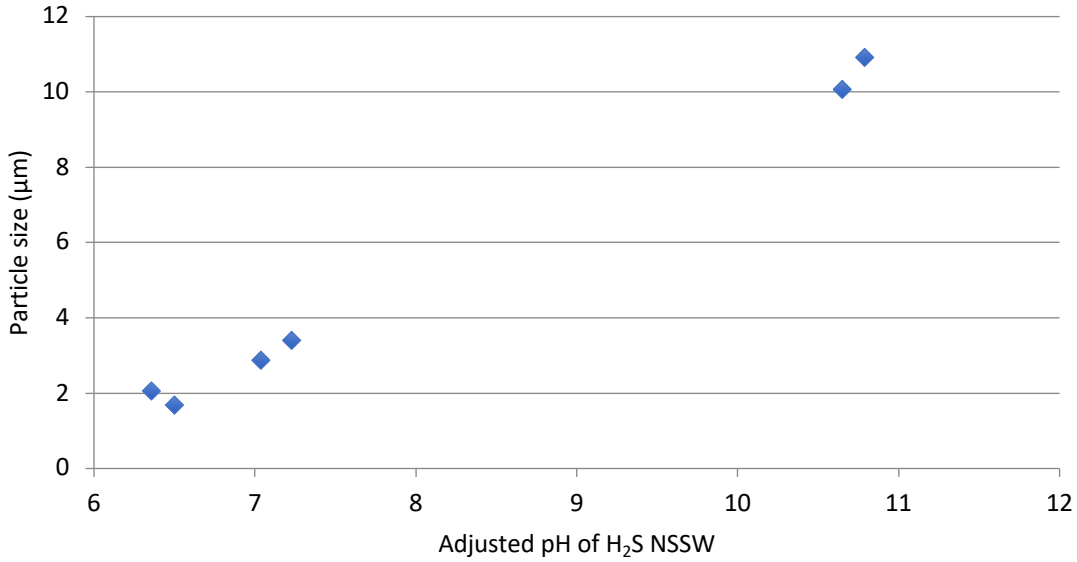

Figure 3.9 Mass median diameter (D_{50}) for ZnS precipitates formed at different adjusted pH of the H_2S brines (3rd Phase)

3.2.2 Formation of ZnS Using H_2S Gas

Using H_2S gas as a source of sulphide was considered as an alternative to the addition of sodium sulphide salt and the subsequent pH adjustment steps. The objective was to use hydrogen sulphide gas in a bench-top static test (in a fume cupboard) for oilfield sulphide scale formation and inhibition. However, the handling of H_2S gas in a laboratory environment has proven to be challenging and, consequently, several approaches have been devised to dissolve the sour gas in test brines at room temperature.

The first approach was similar to the first zinc sulphide scale test (Section 3.1.1), where two brines, H_2S NSSW (without H_2S) and Zn NSSW, were prepared from the compositions in Table 3.1 and Table 3.2. Then, to saturate the brine with H_2S, an H_2S/N_2 gas mixture of 300 ppm of $H_2S_{(g)}$ in $N_{2(g)}$ was bubbled through pressure-compatible glass bottles containing the H_2S NSSW brine. Since the H_2S gas concentration was significantly lower than the 10,000 ppm of H_2S used by Keogh *et al.* (2017), the gas was displaced through the liquid phase, rather than saturating the gaseous phase only, to enhance the dissolution of the hydrogen sulphide. In addition, the gas mixture flowed through different samples for different periods, namely 30 and 60 minutes, at a regulated pressure of two pound-per-square inch (psi) to avoid rupturing the 1.5 bar pressure rated glass bottles. After the saturation, the bottles were mixed with Zn NSSW brine to form

the sulphide scale. The ICP analysis of zinc concentrations was used to determine the loss in initial zinc concentration due to ZnS formation.

The second approach followed a different mechanism, where the 0.03% H_2S gas was bubbled directly into the Zn NSSW brine. This procedure was proposed to minimise the preparation steps by taking out the mixing of two brines, which might disrupt the aqueous H_2S. The volume of H_2S displaced through the brines was varied by fixing the pressure regulator at 2 psi and changing the flow durations for each sample, which, theoretically, created a range of Zn/S molar ratios. Five pressure-rated glass bottles containing the Zn NSSW brine were used in this test at different sparging durations, namely 30, 60, 90, 120 and 150 minutes. The concept of displacing H_2S gas through a solution to react and form either soluble or insoluble products was previously tested in the literature (Al-Duailej *et al.*, 2012, 2010). Figure 3.10 and Figure 3.11 show the setup used for this experiment and how gas was dispalced through Zn NSSW.

Figure 3.10 Experimental setup for H_2S gas flowing through Zn NSSW samples showing the gas bottle on the left side, the manifold at the top, and the connected reaction glass bottles at the bottom.

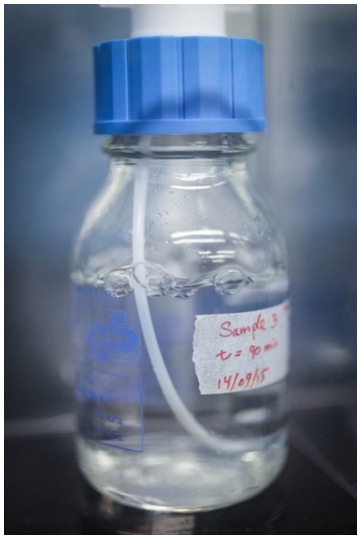

Figure 3.11 A sample in a pressure rated glass bottle being bubbled with the 300 ppm H_2S gas

The first approach to carrying out this test attempted to saturate NSSW with aqueous H_2S before mixing it with the Zn NSSW brine ($[Zn^{2+}]_i$ = ~ 1,200 mg/L). The high zinc concentration was intentionally used as excess to avoid any residual H_2S in solution. Although the sparging periods extended up to 60 minutes, none of these samples visibly formed precipitates. Furthermore, the ICP analysis of the mixed samples in Table 3.9 showed no loss of zinc concentration compared with the stock solutions. The main reason of the lack of ZnS formation resided in the solubility of H_2S gas in water at atmospheric pressure and room temperature, which was calculated to be around 1.2 mg/L, given the 300 ppm H_2S gas source. Such solubility was in agreement with the reported ~ 30 mg/L of aqueous sulphide using 10,000 mg/L of H_2S gas to saturate the headspace (Keogh *et al.*, 2017).

Table 3.9 ICP analysis of zinc in stock and mixed solutions after saturation with the 300 ppm H_2S gas

H_2S gas sparging duration (min)	*Zn concentrations (mg/L)*	
	Stock solution	*Supernatant solution*
30	633	629.92
30	633	629.91
60	633	634.55
60	633	599.94

In the second approach, the 300 ppm H_2S gas was bubbled through Zn NSSW directly, and white precipitates were observed after approximately 10 – 15 minutes of sparging, as seen in Figure 3.12. The ICP analysis of zinc in supernatant and stock solutions (Table 3.10) showed no discernible difference in zinc concentrations, largely because the difference falls into the marginal error percentage of ICP (±10%). Nonetheless, the ESEM-EDX analysis of the filtered white precipitates revealed zinc and sulphur components at nearly 1:1 molar ratio, as seen in Table 3.11.

Figure 3.12 White cloudiness after forming ZnS by bubbling H_2S directly through zinc brines

Table 3.10 ICP analysis of zinc in stock and supernatant solutions after sparging with H_2S gas

Samples Sparging Duration (min)	*Zn Concentrations (mg/L)*	
	Stock solution	*Supernatant solution*
30	1174.49	1194.93
30	1174.49	1187.78
60	1174.49	1124.56
60	1174.49	1178.58
90	1174.49	1182.67
90	1174.49	1159.16
120	1174.49	1178.58
120	1174.49	1174.49
120	1174.49	1183.69
150	1174.49	1177.56

Table 3.11 EDX analysis of the white precipitates formed from displacing $H_2S_{(g)}$ through Zn NSSW

Element	*Atomic%*
S	54.42
Zn	45.58

In addition to the ICP and ESEM/EDX, pH measurements were taken after the introduction of H_2S gas, and the pH values of the supernatant solution are shown in Figure 3.13. This set of results showed that the resultant pH was remarkably consistent for the original and repeat experiments. The extended periods of H_2S sparging showed a slight decrease in the pH values of the sparged solutions. This minor decrease in pH values could be explained by the slight dissolution of H_2S gas into the brines which is typically accompanied by an increase in the hydrogen proton concentration.

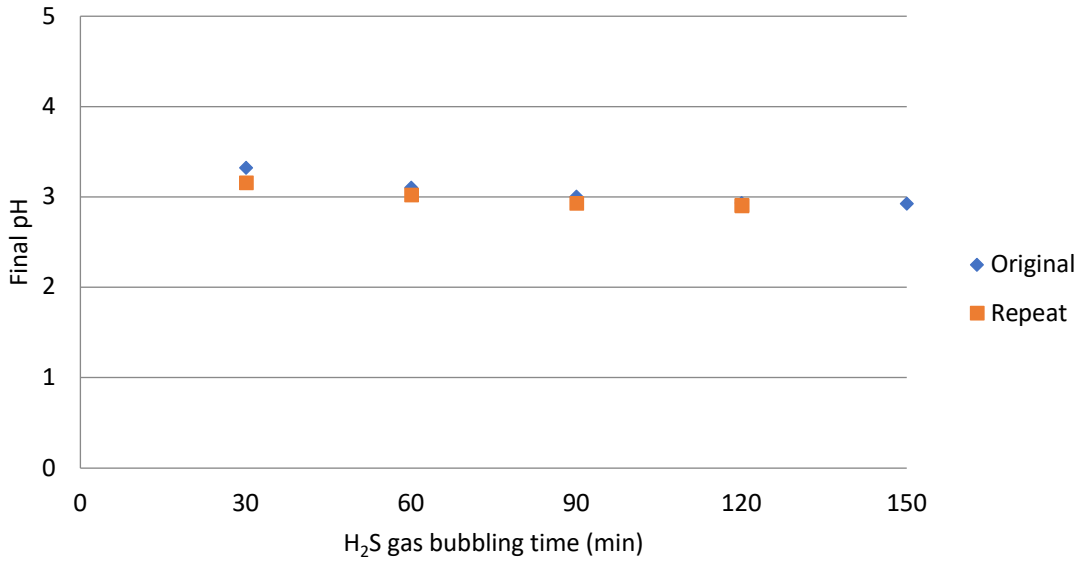

Figure 3.13 Final pH values of the supernatant solution as a function of $H_2S_{(g)}$ bubbling time (dissolving more H_2S gas in solution lowers the pH)

The particle size distribution of the ZnS precipitates in the direct sparging of H_2S gas into Zn solutions is shown in Figure 3.14. The average particle size showed a slight dependency on exposure to H_2S. The average sizes of particles in this test were similar to

those formed at pH 6 - 7 (Figure 3.9) and very distinctive from particles formed at higher pH values (Figure 3.2).

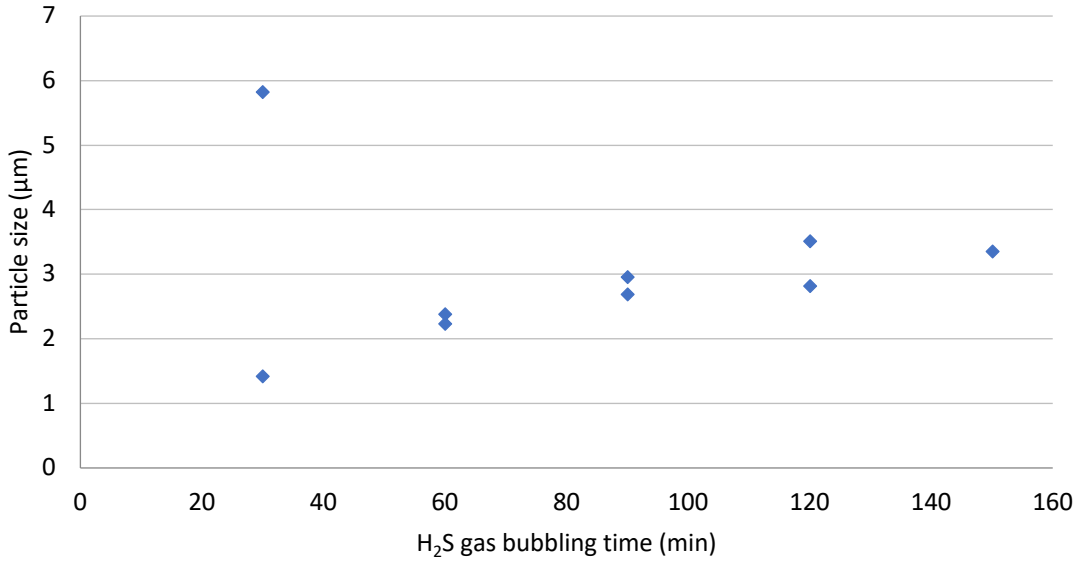

Figure 3.14 Mass median diameter (D_{50}) for ZnS precipitate formed at different times by bubbling $H_2S_{(g)}$ through Zn NSSW brine

3.2.3 Evaluation of the Efficiency of Inhibiting ZnS Formed by Displacing H_2S gas

The direct sparging of H_2S into a zinc chloride brine has shown a formation of ZnS confirmed by ESEM-EDX analysis yet was not verified by the ICP analysis. Therefore, the initial zinc concentration was lowered to 91 mg/L, to highlight the decrease in zinc concentration, in an inhibition test of ZnS using a high molecular weight sulphonated copolymer, SI-2, and a polyphosphino carboxylic acid (PPCA). The inhibitors were used at various loadings, as seen in Table 3.12, in the zinc brines, which were sparged with the 300 ppm H_2S gas for one hour. The zinc concentrations (dissolved Zn^{2+} and dispersed ZnS) were determined in the supernatant solutions and shown in Figure 3.15 and Figure 3.16.

Table 3.12 The individual loadings of scale inhibitors used at separate Zn samples

Tested concentrations of scale inhibitors, mg/L	
SI-2	*PPCA*
5	100
25	500
50	1,000
100	1,500

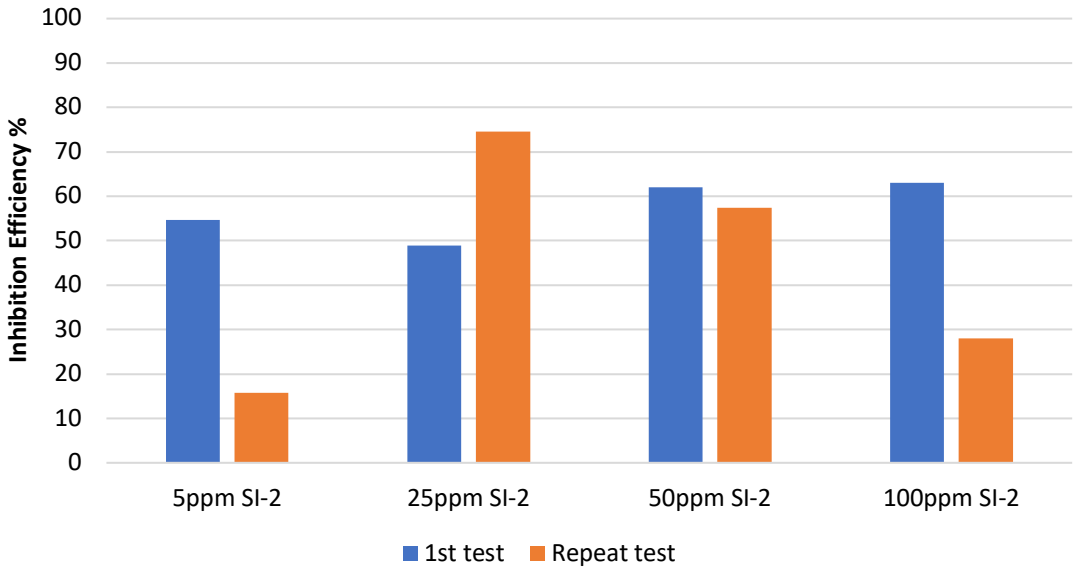

Figure 3.15 The efficiency of SI-2 in inhibiting ZnS formed by H_2S gas in duplicate samples showing inconsistent results

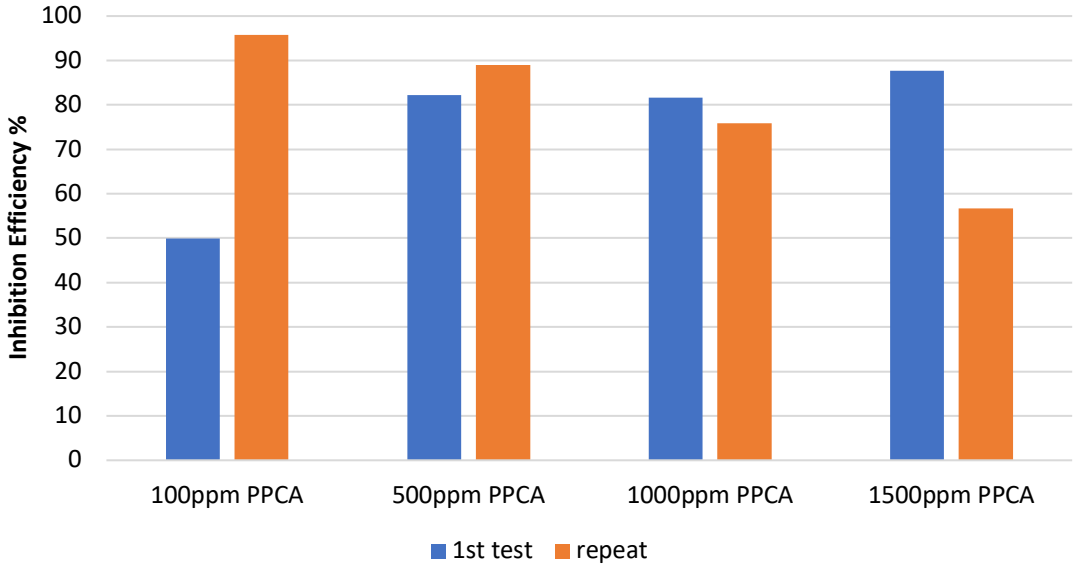

Figure 3.16 The efficiency of PPCA in inhibiting ZnS formed by H_2S gas in duplicate samples showing inconsistent results

The formation and inhibition of ZnS were observed in this test, as the measured zinc concentrations revealed varying levels, which was not seen at previous tests where the initial zinc concentrations were higher by more than ten folds. Nevertheless, the performance of the subject inhibitors fluctuated between test repeats and the various loadings, which was primarily due to the ambiguous dissolved H_2S gas levels in the zinc

brines. As it stands, the evaluated gas introduction technique was not yet suitable for the sulphide scale studies. The direct sparging of H_2S into zinc brines did not allow for the accurate measurement of the introduced sulphide concentrations, while the saturating method required a large increase of the H_2S gas concentration.

3.3 Summary and Conclusions

The conventional static bottle test, also known as the barium sulphate jar test, was evaluated to highlight potential modifications. The objective was to enhance the experimental setup and deliver an outcome comparable to that achieved using more sophisticated techniques, such as anaerobic chambers and pressurised system, at lower logistical and safety measures. The leading areas for improvement were the pH-adjustment of the sulphide brines and the quasi-continuous monitoring of the sulphide concentrations.

Two techniques were tested to prepare the brines: a subtler pH-adjustment of the sodium sulphide brine and saturating the solutions with a 300 ppm H_2S gas. While the former technique resulted in the adequate formation of ZnS, the latter did not initially form sufficient ZnS. Lowering the concentration of zinc in an inhibition test revealed both formation and inhibition of ZnS using the direct sparging of H_2S. However, the results lacked repeatability and correlation with the inhibitors' loadings. Based on the findings of these tests, the following conclusions were made:

(i) The conventional static "jar" test was evaluated and developed using 1) pH adjusted sodium sulphide brines, and 2) H_2S gas to saturate brines, under ambient conditions, to form and inhibit zinc sulphide scale.

(ii) The developed technique, using pH adjusted sodium sulphide brines and 300ppm H_2S-sparged brine experienced loss of dissolved sulphide and low H_2S solubility, respectively. Nonetheless, findings related to particle size were agreeing with other studies which used advanced pressurised anaerobic setups.

(iii) The setup still required further modifications, which lead to the development of the anaerobic bench-top setup using airtight vials and tubes.

4 – Development of an Analytical Method for Aqueous Sulphide Detection

Executive Summary

The shortcomings of the static jar test were discussed the previous chapter, including the impractical traceability of aqueous sulphide concentrations. This chapter provided an alternative method to assay the aqueous sulphide concentrations using UV-Vis spectrophotometer and a copper sulphate reagent. This method has been discussed in the literature in microbial studies (Cord-Ruwisch, 1985) and has been further modified in this study to accommodate the sulphide scale studies. The modifications involved several factors such as mixing regimes, linearity of calibration curves, and geochemical composition effect on analysis. The final outcome of these modifications provided calibration curves with R^2 values of 0.9999 and an average standard deviation of 2.0%. This method provided a quantitative measure to the newly developed method described in the next chapter.

4.1 Importance of Developing an Alternative Analytical Method

The need for an analytical technique which can directly and accurately determine the concentration of aqueous sulphide in scale studies was discussed at the end of Chapter 3. The current method of determining aqueous sulphide concentration in exotic sulphide scale studies was quenching aqueous sulphide in a cation-in-excess solution, mainly $ZnCl_2$, and back-calculating the sulphide concentration from the ICP analysis of the difference between the solution's cation concentration and a stock solution. This method was both reliable and moderately accurate within a marginal error of ± 10 % generally associated with the ICP analysis. However, it lacked the fast-quantitative measurement that could improve the accuracy and practicality of sulphide scale tests.

4.2 Alternative Sulphide Determination Methods

Other analytical methods that are used less often include Draeger-Tubes®, generally used for drilling fluids flow-back, continuous on-line analysers which are exclusively used in field and plants applications, and wet chemistry methods such as titration. Various testing methods are used for different applications depending on criteria such as the concentrations and the analysis duration. From the comparison of sulphide determination methods in Section 2.3, only a few techniques were practically suitable for the proposed bench-top experimental setup to investigate the sulphide scales. The copper reagent and

methylene blue spectrophotometric methods were favoured for their quick preparation and analysis time and overall accuracy. Table 4.1 shows the main differences between the methylene blue (Cline, 1969) and the copper reagent (Cord-Ruwisch, 1985) methods, and the latter was preferred for the sulphide scale studies.

Table 4.1 Difference summary between the methylene blue and the copper reagent methods

Comparison	*(Cord-Ruwisch, 1985)*	*(Cline, 1969)*
Reagent	Copper sulphate in diluted HCl	N,N-dimethyl-p-phenylenediamine (DPD)
Waste	Less harmful	Harmful
Analysis duration	40 seconds	20 min
Mixing mechanism	Stirring while adding the sulphide sample	Normal addition
Detection limit	0.1 mMole	0.01 mMole
Wavelength	480nm	670nm

4.3 Description of the Copper Reagent Method

The copper cation in the reagent (copper sulphate and diluted HCl) reacts with aqueous sulphide anions (H_2S, HS^- or S^{2-}) in the sample, following the reaction equation (1.8), to form copper sulphide (CuS), which is the third least soluble metal sulphide compound after mercury sulphide and silver sulphide (William, 2010; Kolthoff, 1930). Therefore, samples containing aqueous sulphide and metal sulphide particles, other than mercury and silver, will form CuS, which turns the solution from pale blue into yellow-brown, as seen in Figure 4.1. The intensity of the colour is dependent on the concentration of sulphide in the sample, which establishes a correlation between the sulphide concentration and the measured absorbance using a UV-Vis spectrophotometer.

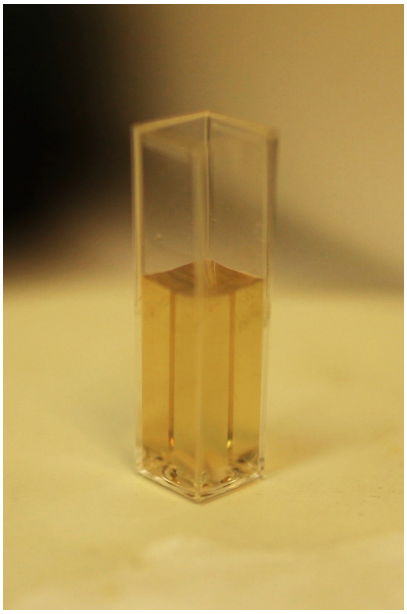

Figure 4.1 CuS solution in a cuvette ready for analysis by UV-VIS spectrophotometer after adding sulphide to the copper reagent (A stirrer appears at the bottom of the cuvette)

The copper reagent was prepared by adding 5 mMol of copper sulphate ($CuSO_4$) to 50 mMol of HCl in DW. The CuS solution was prepared by adding 0.1 mL of the sulphide sample to 1.9 mL (20x dilution) of the cupper reagent in, initially, a reusable clear glass cuvette with a stirrer bar rotating at ~1,000 revolutions per minute (rpm). The sample was stirred for 5 seconds to disperse the CuS nano-particles evenly, then analysed within 40 seconds after stopping stirring.

4.3.1 Establishment of a Calibration Curve

The copper reagent method requires a calibration curve prepared from measured absorbance values of stock sodium sulphide solutions, as a reference, to determine the sulphide concentration in the study samples. The first calibration curves were established over five different levels of sulphide ranging from 1.16 – 28.7 mMol (37 – 920 mg/L) and a DW blank, and the measurements were carried out using two dilution factors: 20x and 40x. The sulphide sample, 0.1 mL (or 0.05 mL) was added by an Eppendorf volumetric pipette to 1.9 mL (or 1.95 mL) of the copper sulphate reagent in a clear-glass cuvette, then analysed by the UV-Vis spectrophotometer at a wavelength of 480 nm. Figure 4.2 shows adequate introductory results, yet the calibration curves of both dilution factors did not produce accurate correlation factors.

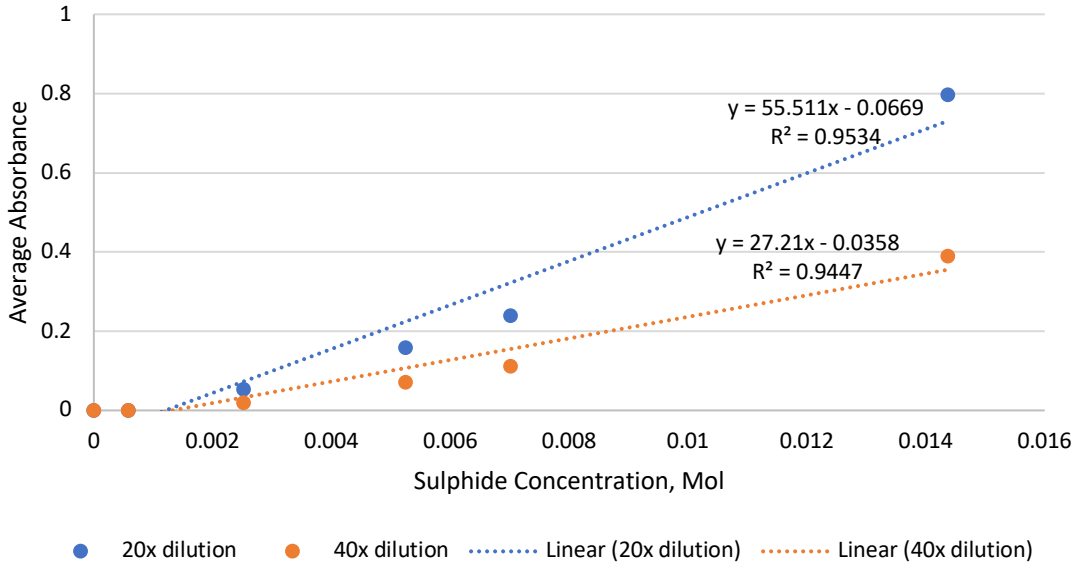

Figure 4.2 Investigating the preliminary accuracy and limitations of the calibration curves using the recommended linear fit

The main remark from this draft was the direct measurement of the absorbance values of the sulphide samples which is vastly more practical compared to the ICP/back-calculation technique. However, the targeted accuracy and repeatability of the UV-Vis method was not yet achieved, mandating further investigation. The range of measured concentrations was assumed to be extensive; thus, the second calibration curve was proposed to be segmented into three groups of sulphide concentrations, which are listed in Table 4.2. This proposal was aimed at preserving the linear profile which was reported in the original method below an absorbance value of 0.5. In addition, a mixture of 0.1 mL DW and 1.9 mL $CuSO_4$ reagent (pale blue) was measured as blank. The resultant curves representing the stock solutions are shown in Figure 4.3, where each data point is the average of 3 – 5 individual sample measurements of the same solution.

Table 4.2 Groups of different sulphide stock solutions of varying concentration, used for establishing several calibration curves over different ranges

Stock No.	*Sulphide concentrations*		*Weights of $Na_2S.9H_2O$*	*Different Calibration ranges*
	mMole / litre	*mg/L*	*g/ 250 ml DW/NSSW*	
1	0.6	19.2	0.036	*Group 1*
2	0.8	25.6	0.048	
3	1	32	0.06	
4	1.2	38.4	0.072	
5	1.4	44.8	0.084	
6	1.5	48	0.09	*Group 2*
7	2	64	0.12	
8	2.5	80	0.15	
9	3	96	0.18	
10	3.5	112	0.21	
11	4	128	0.24	*Group 3*
12	5	160	0.30	
13	7	224	0.42	
14	8	256	0.48	

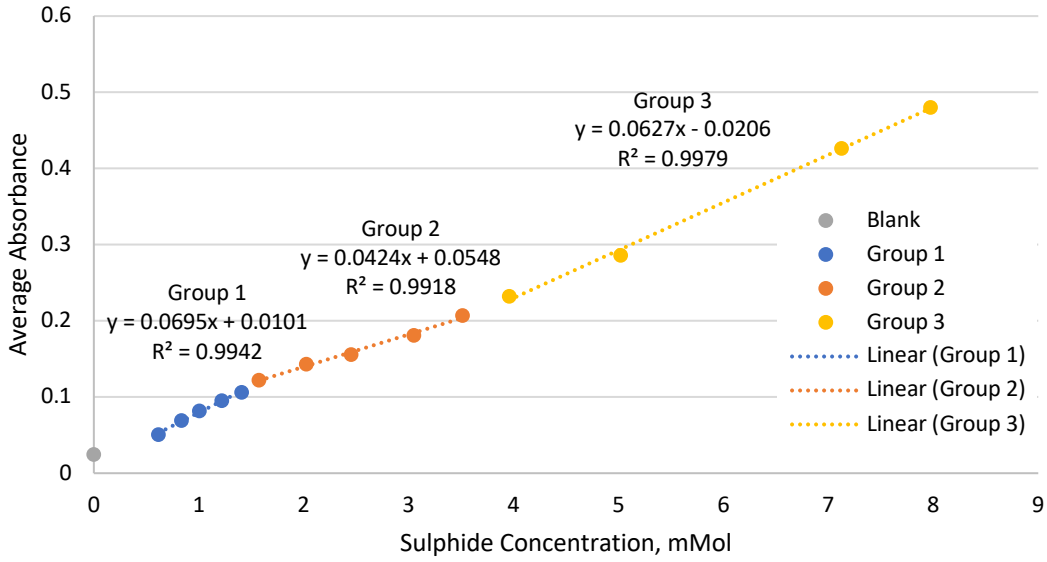

Figure 4.3 Three individual calibration curves of sulphide stock solutions in distilled water divided by three ranges of aqueous sulphide ranges

The correlation factors of these curves were improved using a lower range of concentrations, compared to the first calibration curves in Figure 4.2. Nonetheless, these improvements to the data fit still needed perfecting. The combination of the three calibration curves shaped a single curve extending from 0 – 255 mg/L, a maximum

absorbance value of 0.480 and a linear correlation factor $R^2 = 0.9953$, as seen in Figure 4.4. The repeatability of these measurements required further finessing as it lacked precision for a few concentrations. Nonetheless, running a statistical analysis shows that the T test of these values (repeated measurements of the same samples) produce insignificant variances ($p > 0.05$).

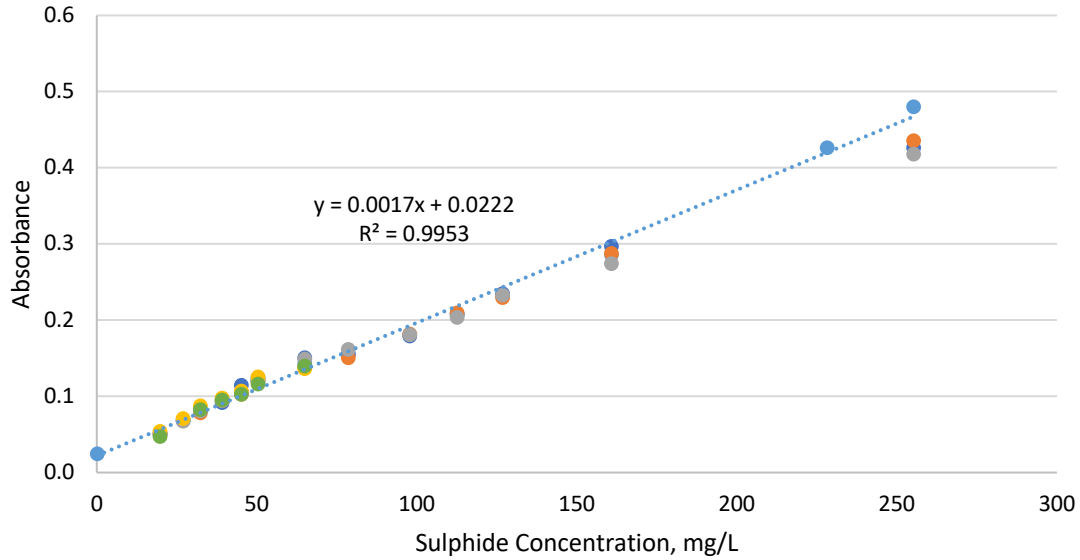

Figure 4.4 The linear calibration curve of the 0 – 255 mg/L sulphide stock solutions (data points represent different measurements of the same sample)

One of the causes of poor repeatability in measuring test samples was a noticeable residue of CuS particles observed on the inner walls of the glass cuvette which introduced a positive error to the absorbance measurement. Therefore, a frequent blank measurement was introduced after every other concentration measurement (every 6 – 10 samples) and the correction calculation was accomplished according to the following equation:

$$Corrected\ A_{x,\ (n\ of\ m)} = A_x - \frac{x}{y} \times (A_{blank\ after\ m} - A_{\ blank\ before\ n}) \qquad (4.1)$$

where A_x was the absorbance of sample x, "n" was the sequence number of sample x, "m" was the number of samples between two blanks' readings: $A_{\ blank\ before\ n}$ and $A_{blank\ after\ m}$. This correction simply eliminated the gain in absorbance caused by the deposited CuS residue on the cuvette's inner walls. However, this practice was abandoned after the introduction of the disposable cuvettes.

4.3.2 Further Enhancement of Calibration Curves

The pursuit of an accurate and repeatable analytical technique demanded further development of the Cord-Ruwisch's (1985) method and a few were discussed in the previous section. Therefore, three primary aspects were stressed for more enhancement:

(i) Expanding the concentration range
(ii) Reducing the minor fluctuation in the repeat measurements
(iii) Increasing the practicality of the method

A few steps were taken to minimise the discrepancies in the measurements, such as fixing the cuvette's position on the stirring plate, evenly distributing the CuS nano-particles by increasing the stirring duration to 7 seconds and avoiding dispensing the sample at the cuvette's inner walls. One of the main considerations was using a second order polynomial profile instead of the linear fit. The calibration curves shown in Figure 4.5 and Figure 4.6 have $R^2 = 0.9999$ and 0.9972, respectively, compared to $R^2 = 0.0953$ and 0.9953 of the linear calibration curves in Figure 4.2 (20x) and Figure 4.4, respectively. Table 4.3 summarises the major developmental steps (not necessarily in the same order) taken during the evaluation of the copper reagent method.

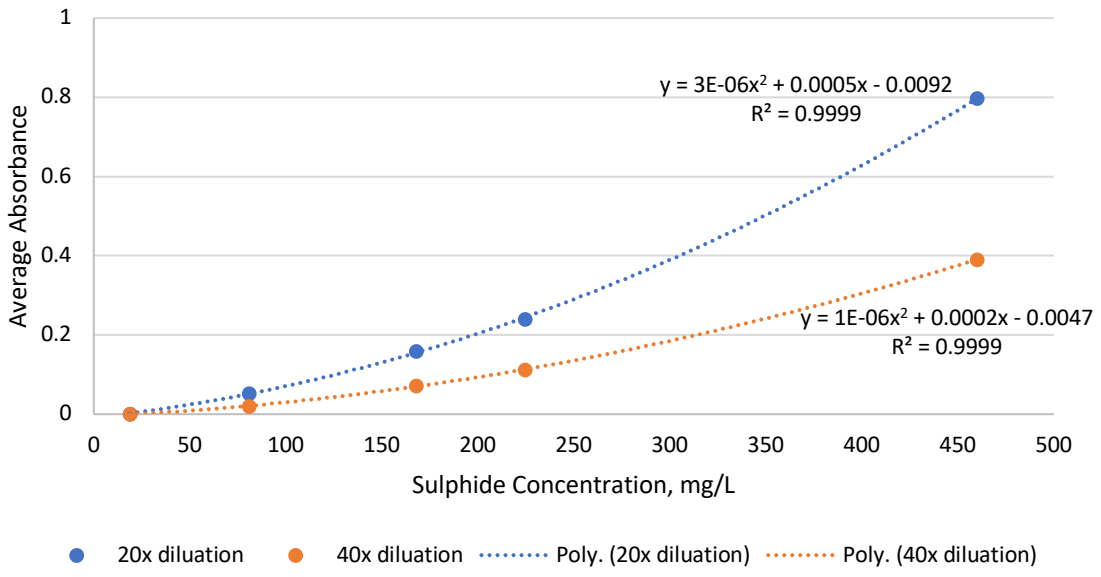

Figure 4.5 The first calibration curves in Figure 4.2 fitted with a second order polynomial correlation as absorbance values against mg/L of aqueous sulphide to show that linearity is not the best fit

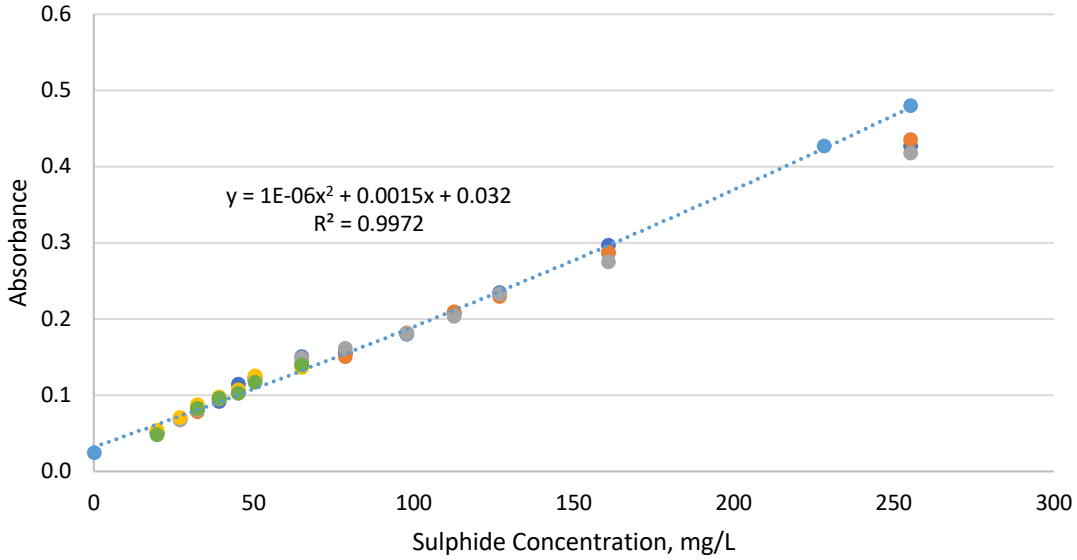

Figure 4.6 2nd order polynomial equation enhancing the fit of the calibration curve of Figure 4.4

Table 4.3 Various developmental steps of the UV-Vis spectrophotometric method

	Step	*Initial practice*	*Updated practice*	*Comments*
1	Cuvette location on a stirrer plate	Approximately at the centre	Fixed location at the centre using marked masking tape	Might not be the optimum location, but provides consistency
2	Sampling sulphides	Using 1ml volumetric pipette	Using 100µL SGE gastight analytical syringe	A syringe was needed to penetrate septa
3	Sampling sulphides	Using 100µL SGE gastight analytical syringe	With a mounted repeating adapter (SGE RAX)	To increase precision, see Appendix A
4	Reference measurement (Glass cuvette)	Once before starting sample measurements	Cuvettes cleaned with a tissue first. Reference then measured at the start, end, and every two-three samples	Copper sulphide nano-particles accumulate on cuvettes walls, not always noticeable to the eye. References are used to correct drift.
5	Dispensing sample into the cuvette	Just avoiding hitting cuvette walls	Using one corner to support the syringe needle and dispensing uniformly at the centre of cuvette while avoiding walls.	Sample on the wall is not reflected in measurement. Using cuvette upper corner for support helps practicality and for repeatability.
6	Stirring time	5 seconds	7 seconds	Longer stirring time allows for more uniform distribution of copper sulphide nano-particles
7	Cuvette	Glass cuvettes	Disposable polystyrene cuvettes	To avoid film-accumulation on cuvette wall
8	Stock solutions	100 – 250 mL plastic bottle	Hungate-type airtight tubes	To control sampling, H_2S evolution, and oxygen contamination

After implementing these developmental steps, the correlation of the samples' absorbance values and stock concentration was significantly improved. Glass cuvettes were replaced with disposable polystyrene ones, and the calibration curves were reconstructed to cover, in more samples, the common used concentration ranges (7 - 387 mg/L and 7 – 386 mg/L) of aqueous sulphides in DW and NSSW, respectively, as seen in Figure 4.7 and Figure 4.8. The comparison between linear and 2^{nd} order polynomial profiles continued to confirm the advantage of extending the maximum limit of absorbance measurement accompanied by a non-linear correlation.

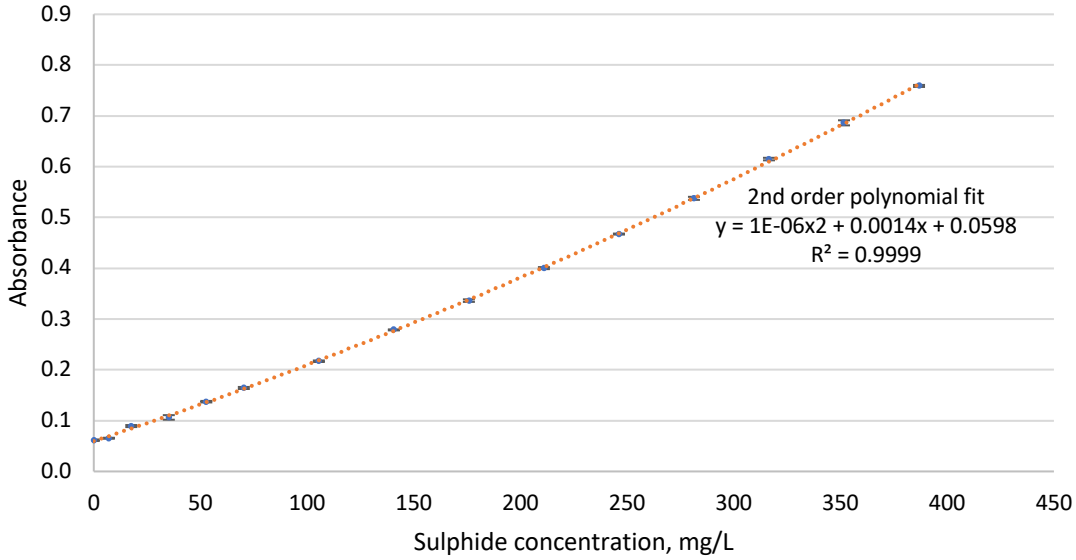

Figure 4.7 A calibration curve (2nd order polynomial fit) of absorbance values using copper sulphate reagent against sulphide concentrations in **DW** with error bars representing standard deviations not exceeding 4.23%

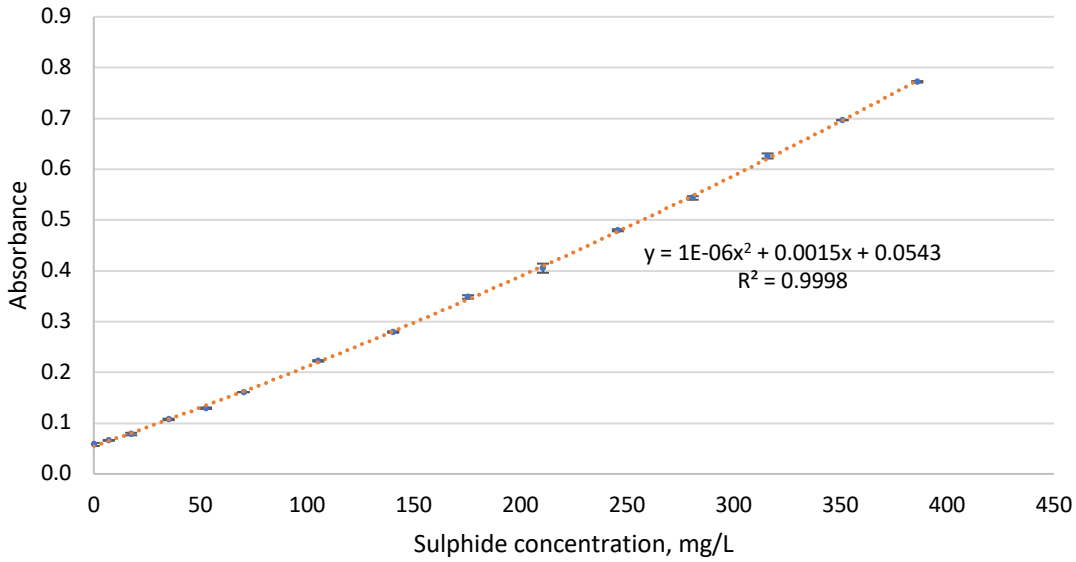

Figure 4.8 A calibration curve (2nd order polynomial fit) of absorbance values using copper sulphate reagent against sulphide concentrations in **NSSW** with error bars representing standard deviations not exceeding 3.18%

After achieving outstanding correlation factors for DW and NSSW solutions, the generated equations were rewritten to determine the sulphide concentration from the obtained absorbance measurements. Equations (4.2) and (4.3) of the calibration curves in

Figure 4.7 and Figure 4.8, respectively, were written in terms of x (the sulphide concentration) in equations (4.4) and (4.5) where y is the average absorbance value. These equations were used to determine the aqueous sulphide concentrations in test samples.

$$Absorbance, y_{DW} = 1 \times 10^{-6}\, x^2 + 0.0014x + 0.0596 \quad (4.2)$$

$$Absorbance, y_{NSSW} = 1 \times 10^{-6}\, x^2 + 0.0015x + 0.0542 \quad (4.3)$$

$$Total\ sulphide\ concentration, x_{DW} = \frac{-0.0014 + \sqrt{(0.0000017216 - 0.000004y}}{0.000002} \quad (4.4)$$

$$Total\ sulphide\ concentration, x_{NSSW} = \frac{-0.0014 + \sqrt{0.000004y + 0.000001738}}{0.000002} \quad (4.5)$$

4.4 Incompatibilities of the Copper Reagent

The original method by Cord-Ruwisch (1985) used a copper sulphate reagent as it was intended for determining colloidal sulphide concentrations in cultures with sulphate-reducing bacteria in the possible presence of Fe^{2+}. In oilfield scale studies, however, the sulphide brines might contain barium (Ba^{2+}) and strontium (Sr^{2+}) which would precipitate upon mixing with the $CuSO_4$ reagent. An alternative and compatible source of copper, the main ingredient of the reagent, is needed for solutions containing such sulphate scale inducing cations.

A copper chloride salt was used as the replacement for the copper sulphate as it was more compatible with the brines. However, precautions had to be taken during its handling and solution preparation because it is harmful upon ingestion or skin and eye contact, and very toxic to aquatic organisms. The copper chloride reagent was prepared and tested against sets of stock sulphide solutions (9 – 400 mg/L) to establish new calibration curves. The calibration curve of the copper chloride reagent and DW sulphide stock solutions in Figure 4.9 is similar to the calibration curves previously determined for the copper *sulphate* reagent. However, the correlation factor and the lower detection limit were affected when a high salinity brine, described in Table 4.4, was used to establish the calibration curve, as seen in Figure 4.10.

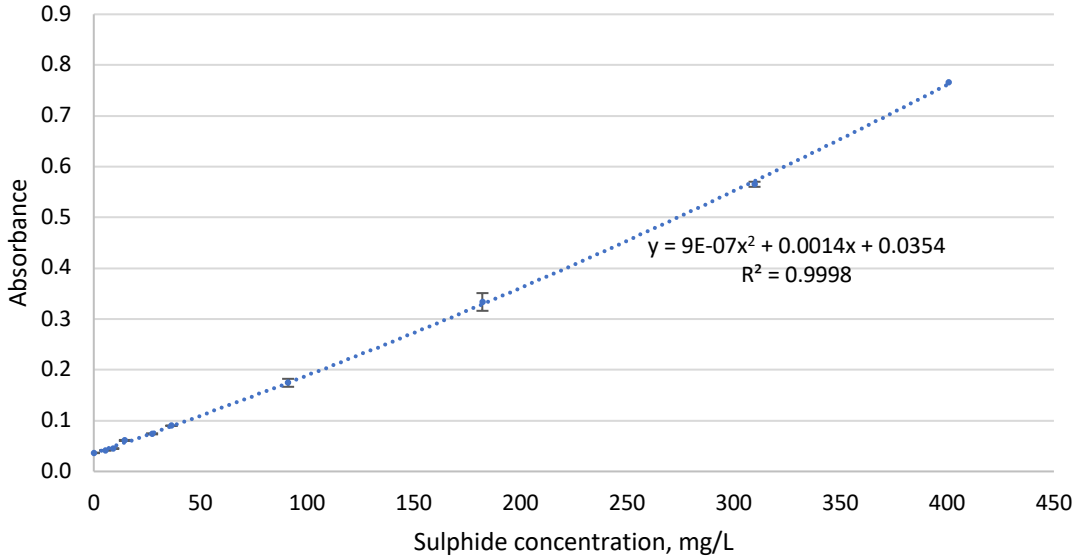

Figure 4.9 A calibration curve (2nd order polynomial fit) of absorbance values using ***copper chloride*** reagent against sulphide concentrations in **DW** with error bars representing standard deviations not exceeding 3.09%

Table 4.4 The geochemical composition of Glenelg formation water (Al-Harbi *et al.*, 2017)

Ions	*Concentration, ppm*
Na	80,520
Ca	20,000
Mg*	0
SO_4	0
Cl	170,275
HCO_3	0
Ba	3,700
K	8,000
Sr	2,000
TDS	284,525

* Magnesium was not added to sulphide brines used to avoid the formation of magnesium hydroxide at high pH values (pH>11.5)

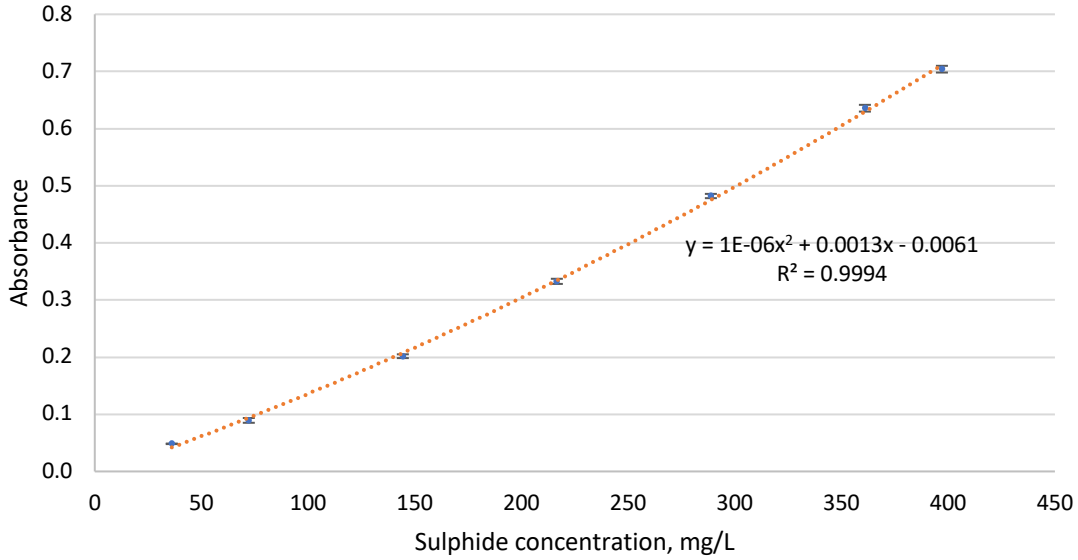

Figure 4.10 A calibration curve (2nd order polynomial fit) of absorbance values using ***copper chloride*** reagent against sulphide concentrations in **Glenelg formation water** with error bars representing standard deviations not exceeding 4.69%

4.5 Analysis of Samples with Suspended Solids

One of the main requirements for the UV-Vis analytical method is to have clear and colourless samples since any cloudiness, turbidity or colour shade will interfere with the absorbance measurement. Therefore, samples with suspended particles, such as formed iron sulphide, lead sulphide or zinc sulphide, must be filtered or centrifuged to produce transparent samples. Otherwise, these sulphide scale particles would either directly interfere with the absorbance measurement or undergo a cation exchange with the copper ions in the reagent. Both interferences would result in an inaccurate measurement of the aqueous sulphide concentration.

The filtration of samples was performed using syringe filters of various sizes, such as 5, 0.45 or 0.2 µm. Different solutions were found to require a different filter size, as shown in Figure 4.11 and Figure 4.12. Some of the uninhibited FeS supernatant solutions were clear, because the solids had settled down, and the supernatant solutions were transferred to new Hungate-type tubes via a volumetric pipette. Inhibited and uninhibited lead sulphide particles were suspended in solution and were only filtered out using 0.2 µm. For both types of scale, 0.45 µm generally filtered out the uninhibited particles, and 0.2 µm managed to filter out the inhibited solids. However, a few uninhibited FeS solutions,

mostly at pH < 5, were filtered through 0.2 µm and the FeS particles managed to pass through the filter.

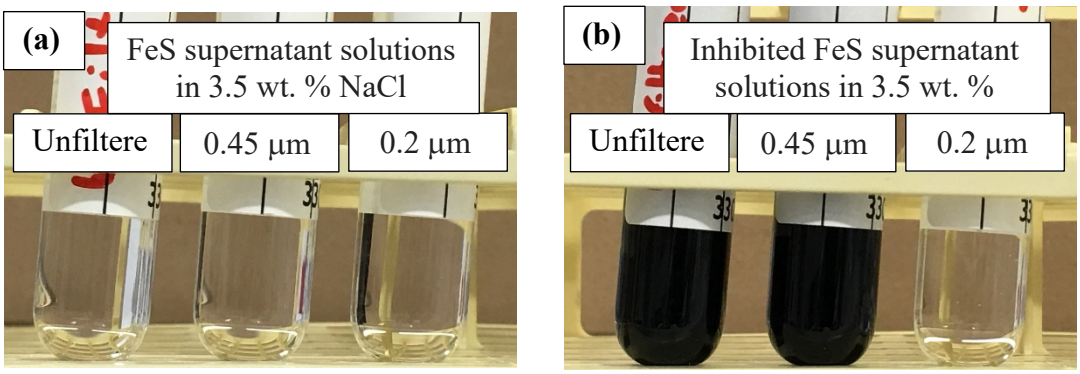

Figure 4.11 Iron sulphide formation filtered through different filter sizes (a) without scale inhibitor, and (b) with scale inhibitor

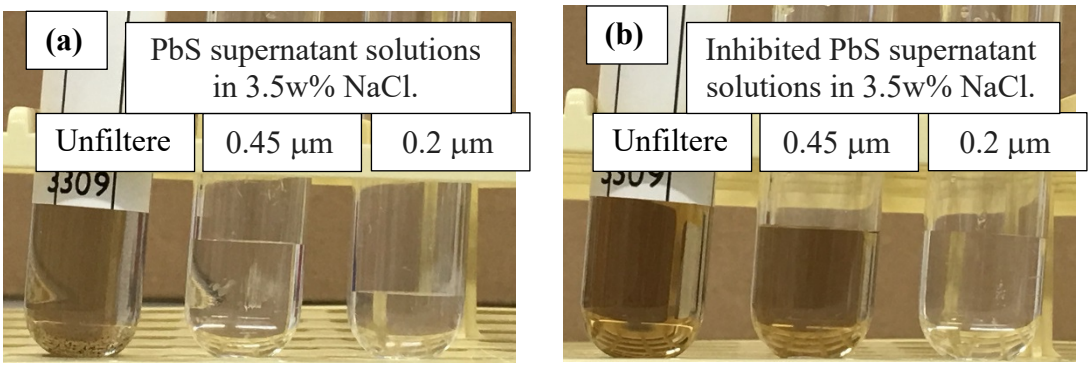

Figure 4.12 Lead sulphide formation filtered through different filter sizes (a) without scale inhibitor, and (b) with scale inhibitor

The analysis of aqueous sulphide in filtered samples has been investigated to determine the impact of filtration on the accuracy of the analytical method. Similar to the solutions in Figure 4.11, FeS and inhibited FeS, initially formed in 3.5 wt. % NaCl solutions inside Hungate-type tubes then filtered using 5.0, 0.45 and 0.2 µm filters into new tubes. The sulphide and iron concentrations were set at 100 and 18 mg/L, respectively, while the inhibitor's concentrations were 0, 50 and 100 mg/L of SI-2. The filtration step, however, resulted in a loss of aqueous sulphide concentrations at the tested values (pH < 7) primarily due to the disrupting the solubility of aqueous H_2S through agitation.

The analysis of cloudy samples in Figure 4.13 showed an interference affecting the absorbance measurements by increasing the supposedly dissolved sulphide levels beyond the stock sulphide concentrations. The only solution that was measurable with and without filtration was the clear stock solution. The analysis of the stock sulphide concentration showed similar losses of 7.4 and 8.4 % when filtered through 5 and 0.2 µm, respectively, while the 0.45 µm filter did not cause losses. The aqueous sulphide concentrations in the inhibited FeS solutions were expected to reach ~ 76 mg/L, based on the molar ratio of iron-to-sulphide, yet they showed a 10 - 20 % decrease in the expected concentrations. The loss of sulphide concentrations due to filtration did not directly reduce the accuracy of the method, as the evolution of $H_2S_{(g)}$ occurred before the measurement. Nonetheless, given the high percentage error, the UV-Vis method could be used as a semi-quantitative analysis technique for filtered samples.

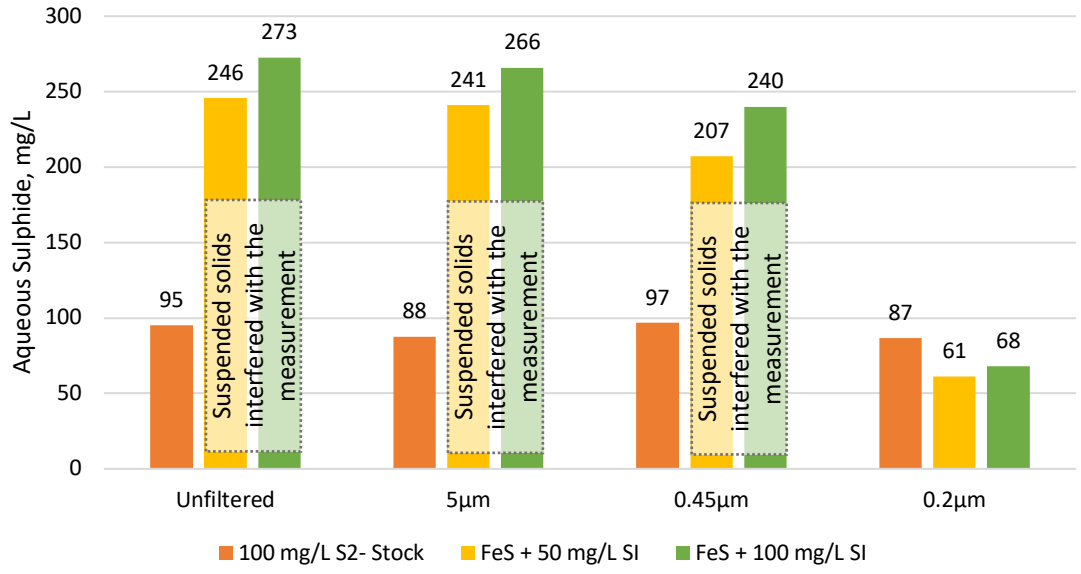

Figure 4.13 The effect of filtration on the aqueous sulphide concentrations showing that only 0.2µm filter size was able to filter out the solids yet caused losses in aqueous sulphide concentrations

4.6 UV-Vis Method Compared to ICP/Back-Calculation Technique in Detecting Oxidative Loss of Sulphide Concentration

The accessibility to an instant measurement of aqueous sulphide was previously mentioned as an advantage over the current ICP/back-calculation technique. However, the accuracy of both methods was investigated to determine which provides a more reliable outcome. Both methods were employed to determine the oxidative loss in

aqueous sulphide concentration between two different types of solutions: aerobic and anaerobic. The sulphide oxidation, including the experiment described below, will be discussed further in Chapter 5, where an anaerobic setup, comprised of the Hungate-type tubes and culture vials, was used to highlight the impact of oxygen on the sulphide solutions. Two sulphide solutions were prepared, in 40-mL culture vials, one of which was de-oxygenated (anaerobic). Aliquots (5 mL) of the aerobic and anaerobic solutions were transferred to the 12-mL airtight tubes then adjusted by adding HCl to achieve various pH values (pH 3 - 12). Afterwards, each aliquot was analysed via the two analytical methods to determine the sulphide concentrations.

The two techniques equivalently determined the decrease of aqueous sulphide concentrations due to liberating $H_2S_{(g)}$, as seen in Figure 4.14. However, the small difference between the anaerobic and aerobic sulphide, due to the oxidative loss, was only verified via the UV-Vis method, as seen in Figure 4.14. These findings proved that the UV-Vis method was more accurate and practical than the ICP/back-calculations technique, since that the latter required a lot more time for sampling, preparation and setting up the ICP machine.

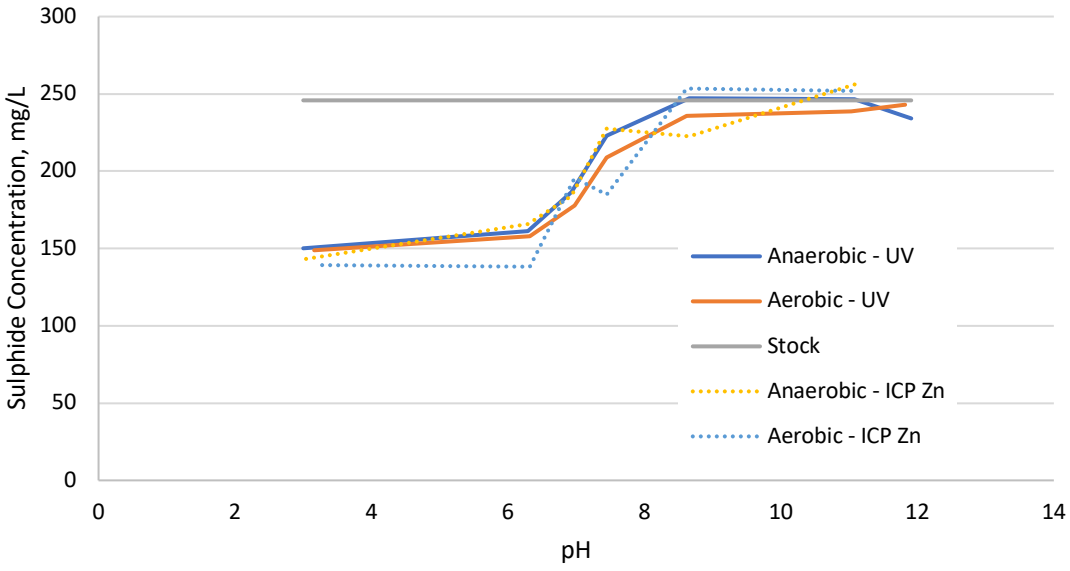

Figure 4.14 Sulphide concentrations of anaerobic and aerobic solutions at different pH values, analysed using UV-Vis method and ICP/back-calculation technique to show ability of detecting of fine differences in concentrations

4.7 Summary and conclusions

A direct analytical method was required to assay the aqueous sulphide concentrations in the oilfield sulphide scale studies. The conventional analysis of aqueous sulphide was carried out by quenching the sulphide solutions with zinc chloride solutions, then determining the sulphide concentration through the ICP/back-calculation technique. The Cord-Ruwisch (1985) UV-Vis spectrophotometric method was evaluated and modified to address the objectives of the oilfield sulphide scale studies. The constructed calibration curves for the UV-Vis method achieved correlation factors R^2 varying between 0.9994 and 0.9999. The nonintrusive quantification of aqueous sulphide through the UV-Vis method was found to be limited to clear-transparent solutions, and filtration of turbid solutions can provide a semi-quantitative analysis. The following conclusions were made based on the findings of the method development:

(i) The UV-Vis spectrophotometric method using copper reagents, mostly used in microbiology, is the first modified technique used to directly and confidently determine the aqueous sulphide concentrations in the oilfield sulphide scale studies.

(ii) The UV-Vis method has shown significant improvement in terms of accuracy and practicality over the current ICP/back-calculation technique.

5 – The Anaerobic Static Test Setup

Executive Summary

The objective of this chapter was to develop an anaerobic experimental setup for static testing of sulphide scale that has the advantages of the conventional jar test and the complex pressurised and anaerobic systems. Chapter 3 discussed the conventional jar test setup and sections 2.2.2 and 2.2.3 discussed the advanced setups. Combining the advantages of these two extreme ends of the experimental setup spectrum should provide a convenient and accurate method which provides closer representation to in-situ conditions while allowing accessibility for sampling at relatively low costs. The new anaerobic setup comprises of airtight tubes and vials and gastight analytical syringes, which provided containment of aqueous and volatile sulphide and isolation of atmospheric oxygen. Such combination of features provided a significant advancement of the pH adjustment of the sulphide brines, which couldn't be successfully achieved in previous chapters.

5.1 Conventional Bottle Test

The conventional bottle test, described in Chapter 3, provides simplicity in terms of preparations, mixing patterns, sampling for analysis, and interpretation. However, these features are limited sulphide scale tests involving high-pH (> pH 8) sodium sulphide solutions. Extending the test conditions to include low-pH Na_2S and H_2S-saturated solutions highlighted the shortcomings of the conventional bottle test. Therefore, an alternative static test setup was sought to accommodate the extended test conditions, where H_2S comprises a significant fraction of the total aqueous sulphide concentrations.

Aqueous sulphide studies in geochemistry (e.g. analysis of sulphide in lake water) and microbiology disciplines (e.g. investigating SRBs) utilised airtight tubes and vials, usually in an anoxic environment, to maintain the sulphide species intact for further analysis or testing. Although these tests involve different procedural steps to the sulphide scale studies, the used setup was a robust candidate for an anaerobic sulphide scale test setup. Similar configurations have been previously used for sulphide scale formation and inhibition tests (Lehmann and Firouzkouhi, 2008; Przybylinski, 2001, 2003), yet little is reported with regards of using such setup as a bench-top system for static tests.

5.2 Description of the Anaerobic Test Setup

The main components of this setup are the 12-mL borosilicate round bottom airtight tubes with chlorobutyl septum (Labco Exetainer™), the 40-mL airtight glass vials with PTFE-lined silicone septum (Thermo Scientific™), and the variable sizes of gas-tight manual syringes (SGE™), namely 100 – 1,000 µL, as seen in Figure 5.1. Whereas the culture vials can be reused after fitting a new septum disc, the Hungate-type tubes are potentially disposable. In the following tests included in Chapters 6, 7, and 8, the culture vials were mainly used with stirring bars, while the Hungate-type tubes were treated as a direct alternative to the traditional static test bottles. The primary features of these tubes and vials are summarised in Table 5.1.

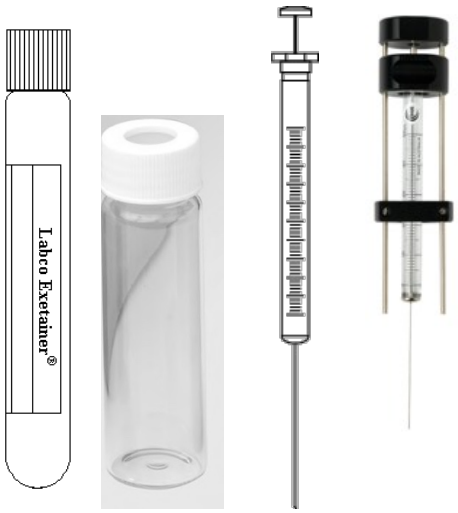

(a)* (b)** (c)*** (d)****

Figure 5.1 (a) Labco Exetainer™ borosilicate round bottom tube, (b) Thermo Scientific™ glass vials with PTFE-lined silicone septum, (c) SGE™ gas tight manual syringes, and (d) SGE™ repeating adapter RAX

* image source: https://www.labco.co.uk/media/com_hikashop/upload/vial3_boro_gaslabel.gif
** image source: https://assets.fishersci.com/TFS-Assets/LCD/product-images/Economy-Processed-Clear-And-Amber.tif-650.jpg
*** image source: http://www.sge.com/root/images/syringes/gc_manual/schematic_fixed_needle_20_21.gif
**** image source: http://www.sge.com/root/images/syringes/accessories/syringe-repeating-adaptor

Table 5.1 Features of the used Hungate-type tubes and the culture vials

Feature	*Hungate-type Tube*	*Culture Vial*
Manufacturer	Labco Exetainer™	Thermo Scientific™
Volume, mL	12	40
Pressure	Up to 3 bars	unknown
Heat	Up to 50ºC	unknown
Test condition	Static	Static and Semi-dynamic (stirring)
Reusability	No	Yes (requires new septum)

The advantages of using tubes and vials of small capacities include lower cost, less required space, and less wasteful outcome compared to the conventional jar test setup. A single tray can accommodate 72 tubes, or 12 vials, in a space that can only fit 6 – 8 of the 50 – 250 mL glass bottles. The volumes of a single test containing 12 tubes add up to a maximum of 144 ml, which is less than the conventional bottle test volume of 200 mL. Reducing the wasteful outcome has a significant impact on the cost of environmental waste management. It is needless to say that the use of the gastight syringes has shown greater confidence in the test accuracy, especially when mounted with a repeating adapter, e.g. SGE RAX, compared to using the Eppendorf volumetric pipettes or disposable syringes fitted with needles (See Appendix A). The repeating adapter is mounted on the syringe and adjusted to the required volume to maximise the repeatability and reduce the human error.

5.3 Preparation and De-Oxygenation of Stock Solutions

The vials and tubes can be used directly to prepare the sulphide and the metal solutions or to receive aliquots of said solutions after preparation. The stock solutions, the ferrous chloride and the sodium sulphide, in particular, are preferably prepared by dissolving appropriate salts on de-oxygenated water, then de-oxygenating again using N_2 gas sparged through septum-puncturing needles inserted below the liquid level. The dissolution of sodium sulphide salt has been revised, and new preparation steps have been included. Crystals of $Na_2S.9H_2O$ were washed by immersing briefly in DW, then dried thoroughly using lab roll paper. This step is essential to ensure an oxidation-free, new crystal surface for the tests, thus minimising the “oxidative” contamination involvements.

The de-oxygenation of solutions, shown in Figure 5.2, is expected for every component of the anaerobic experiments, whether the main reactant, such as the sulphide and iron (II) solutions, or an additive, such as HCl, NaOH, and scale inhibitors. The oxidation state

of iron might affect the scale inhibition performance as suggested by Kelland (2011). The zinc and lead cation solutions are less affected by oxygen, yet it is preferred to maintain an oxygen-free environment throughout the sulphide scale formation reaction. Typically, the de-oxygenation is carried out prior to adding the additives to the stock solutions, namely the addition of HCl to Na_2S solutions, to avoid evolving the gaseous H_2S. It is preferable to have a positive pressure inside the vials and tubes containing the metal stock solutions to prevent oxygen contamination and to ease the successive withdrawals of aliquots.

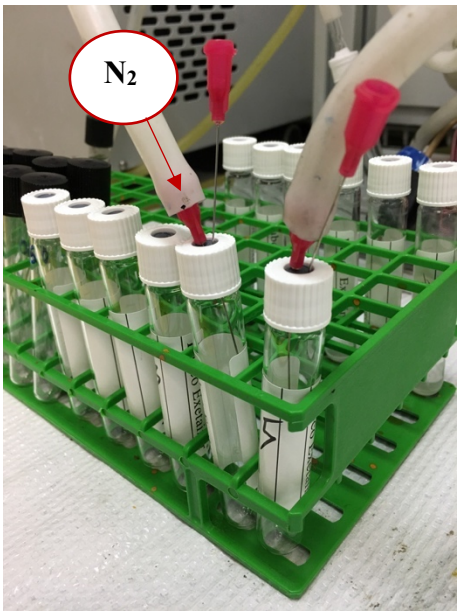

Figure 5.2 The de-oxygenation of solutions in Hungate-type tubes using N_2 gas bubbling through needles

5.4 Mixing and Sampling Protocols

The proposed anaerobic static setup offers the flexibility to perform various tests by changing the sequences of adding/mixing multiple solutions. The direct formation of iron sulphide, for example, can be achieved by adding the de-oxygenated iron (II) solution to the pH-adjusted sulphide solution or vice versa. On the other hand, the investigation of the scale inhibition efficiency can be achieved by adding a scale inhibitor prior to mixing the iron (II) and sulphide solutions. Using variable scale inhibitor concentrations can determine the MIC of said inhibitor. Furthermore, adding HCl and NaOH can either dissolve or precipitate the sulphide scale, based on the final pH, while conserving the aqueous sulphide concentrations, to indicate dissolution and formation configurations.

The gastight syringes are used to puncture the septum and add the iron solution and additives to the sulphide solution. Disposable syringes mounted with sharp needles are used for sampling the final solutions, as in Figure 5.3. These syringes can be equipped with filters, Figure 5.4, to indicate the particle size qualitatively and to filter samples before the ICP analysis.

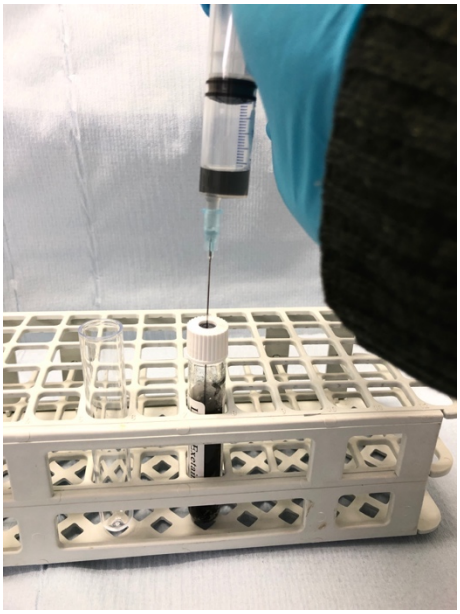

Figure 5.3 Sampling a solution containing formed FeS using a disposable syringe mounted with a sharp needle

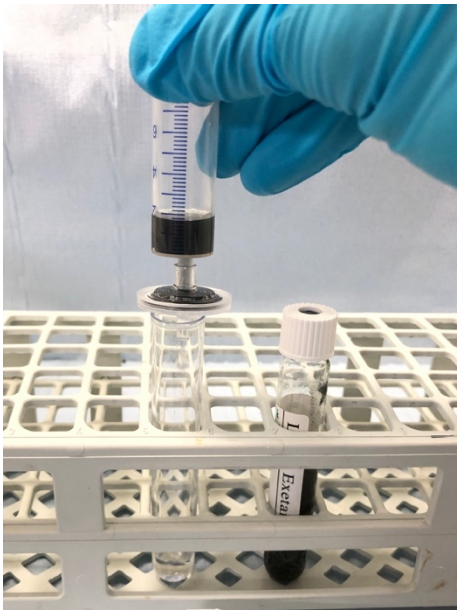

Figure 5.4 Filtration of the withdrawn sample using a syringe-mounted filter

5.5 pH Adjustment and Stock Solution Mixing Volumes

The volumes of solutions, whether in the vials and tubes or added through the needles, required a new mixing technique, as the 1:1 addition followed in the conventional setup can no longer be used given the closed nature of vessels and the limited volumes of gastight syringes. Therefore, the aqueous sulphide solution was selected to be the leading solution (~ 10 – 11 mL) while the metal cation and SI stock solutions were added at lower volumes (~ 10 – 200 μL). Therefore, Fe^{2+}, Zn^{2+} and Fe^{2+} stock solutions, as well as the investigated SI, were prepared in DW at concentrations exceeding 5,000 mg/L to reach the designed final concentration (after dilution in the sulphide solution).

5.5.1 pH Adjustment of Aqueous Sulphide Solutions

The pH adjustment of the aqueous sulphide solution was carried out using aerobic and anaerobic solutions using a de-oxygenated 1M HCl. A stock sulphide solution of 242 mg/L in NSSW was prepared (0.0727 g of $Na_2S.9H_2O$ in 250 mL NSSW), and 5 mL aliquots were transferred to 30 Hungate-type tubes labelled aerobic and anaerobic. The anaerobic solutions were de-oxygenated prior to the acid addition. Various volumes of 1M HCl were added to these tubes, and the pH was measured for the supernatant solutions after 24 hours. Table 5.2 shows the final pH of the sulphide solutions after adding the corresponding acid volumes.

Table 5.2 Tabled pH adjustment results using 1M HCl and 5 mL of 242 mg/L sulphide solution in NSSW

Brine	NSSW (Mg-free)			
HCl concentration	1 M			
Sulphide concentration	242 mg/L			
NSSW volume	5 ml			
V_n HCl, µL	*pH_n*			
	1st set (anaerobic)	*1st set (aerobic)*	*2nd set (anaerobic)*	*2nd set (aerobic)*
0	11.85	11.78	11.91	11.82
30	-	-	11.08	11.03
40	8.83	9.14	8.66	8.62
50	7.73	7.55	7.45	7.45
60	7.25	6.98	6.93	6.98
70	6.53	6.45	6.29	6.32
80	3.7	3.71	3.00	3.16
90	2.67	2.69	-	-
100	2.43	2.36	-	-

An equation was devised to pH-adjust sulphide solutions with varying concentrations and volumes, by calculating the required volume of 1 M HCl based on the results in

$$V_{HCl}\ to\ achieve\ pH_n = \frac{C \times V_n}{242} \times \frac{V_{H_2S}}{5} \quad (5.1)$$

where V_{HCl} is the required volume of 1M HCl to achieve pH_n for a solution of sulphide concentration C and volume V_{H_2S}, and V_n is the volume of 1M HCl from associated with pH_n in s. Table 5.2 shows the final pH of the sulphide solutions after adding the corresponding acid volumes.

. Further testing revealed that reducing the head spaces in the airtight tubes and vials is mandatory to reduce the evolution of H_2S from solution during the addition of acid.

The pH measurement was normally done using a probe immediately at the end of each test. Airtight vials (40 mL) were opened, and the probe was inserted to the top third of the liquid volume level. The pH value was recorded within one minute, once the reading

stabilized. As for the Hungate-type tubes, 3.5 - 4 mL of the sample was extracted with a syringe and transferred to a small beaker (30 mL), then the probe was inserted and the pH was recorded within a minute, once the reading stabilized. The latter technique theoretically could involve H_2S gas release, thus slightly influencing the pH. However, such evolution was thought to be insignificantly impactful on pH, and by maintaining the same procedure for all samples a high level of precision was reserved. *(For pH measurement of sulfidic samples, refer to Appendix B).*

5.5.2 The Protocols of Mixing Various Solutions

The addition of a highly concentrated iron (II) solution to the sulphide solution could present a localised extreme interface between the two solutions before reaching the final (diluted) concentration. For example, adding 100 µL of 5,000 mg/L of Fe^{2+} to a 10 mL of 1,000 mg/L of an aqueous sulphide solution, according to the schematic in Figure 5.5, should result in final concentrations of 50 and ~ 990 mg/L of the two reactants, respectively. However, the first interaction will be between the initial stock concentrations, as seen in Figure 5.6 (b). Therefore, the formation of FeS, which is highly sensitive to the molar ratios of the iron and sulphide, is almost instantaneous, Figure 5.6 (c), and can form according to molar ratios different than the designed ones, affecting the chemical composition (stoichiometry) and the particle size of formed iron sulphide. An alternative approach can be used to overcome this challenge, which will be discussed further in Chapter 7.

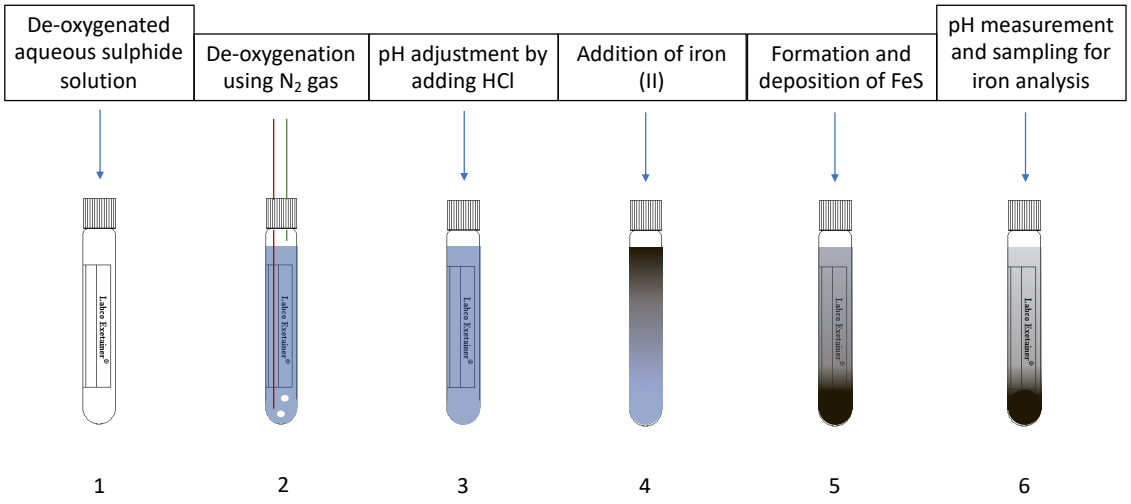

Figure 5.5 Schematics and sequence of the steps of the iron sulphide formation test

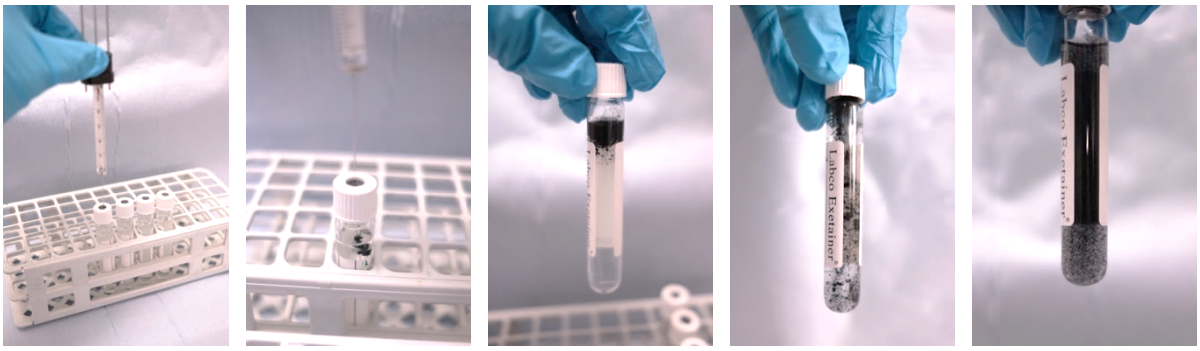

(a) (b) (c) (d) (e)

Figure 5.6 Photos of the experimental steps of forming FeS in a Hungate-type tube using a gastight syringe mounted with a repeating adapter (RAX)

The formation of FeS in a dynamic (stirring) test follows similar steps to the static test described above. However, given the dynamic nature of the stirring test, the mixing of the two solutions differ from that in the static test, as seen in Figure 5.7. The static and the dynamic (stirring) techniques became the base of the formation, inhibition and oxidation tests, as will be discussed in the following chapters.

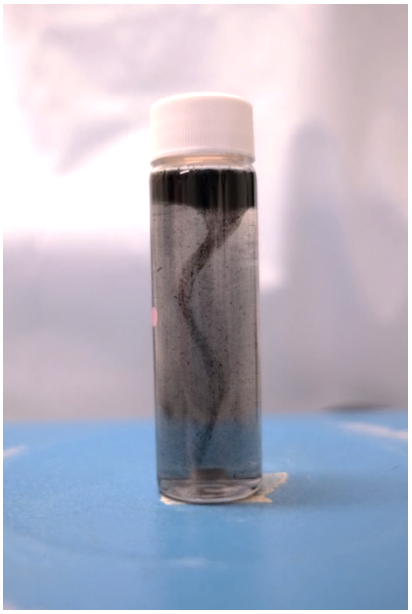

Figure 5.7 The formation of FeS in a dynamic (stirring) test showing a vortex caused by the rotation of the stirring bar at the base of the vial

5.6 A Comparison of the Different Test Setups

A summary of the features of the conventional test setup, the new anaerobic setup and the pressurised systems, i.e. glove box, is shown in Table 5.3.

Table 5.3 Comparison of the features of the static test setups

Features	*Conventional*	*Anaerobic*	*Pressurised systems*
Practicality	Fast (hassle free)	Fast (hassle free)	Impractical for repeatable tests
Sampling	Accessible	Accessible	Inaccessible
Conditions (pH)	Not representative	Representative	Representative
Sulphide concentrations	Up to 600 mg/L	Up to 1,000 mg/L	Up to 10,000 mg/L
Heating of samples	Doable	Limited (up to 50ºC)	Doable
Particle size analysis	Quantitative	Qualitative	Quantitative
Wasteful outcome	50 – 200 mL/sample	10 – 40 mL/ sample	-
Safety	Depends on the pH	Safe	Safe
Cost	Inexpensive	Inexpensive	Costly

5.7 Summary and Conclusions

A new alternative static test setup was proposed to increase the repeatability of pH adjustment of sulphide solutions and to minimise H_2S evolution and oxygen contamination. The new anaerobic setup is based on airtight tubes and vials, and gastight syringes, replacing the conventional glass bottles and Eppendorf volumetric pipettes.

The proposed setup was found to be inexpensive, flexible, representative, and more accessible to sampling than the other reported setups. The reliable pH adjustment step of sodium sulphide solutions and the retaining of total sulphide concentrations were the two main advantages of this setup, which provides higher confidence in test results. Further tests involving the pH adjustment of aqueous sulphide solutions, namely the oxidation of aqueous sulphides, and the formation and inhibition of sulphide scales, were carried out exclusively using this setup.

6 – Oxidation of Aqueous Sulphide

Executive Summary

The effect of oxygen on ferrous iron (Fe^{2+}) is well documented and investigations of FeS scale has always been conducted in oxygen-free conditions. However, the effect of oxygen on aqueous sulphide has not been thoroughly investigated. This chapter discussed the implications of oxygen-sulphide reactions and the impact of sulphide concentration and form, as well as the formed scale. The main outcome of this chapter was the identification of two effects of sulphide oxidations, namely 1) the formation of elemental sulphur at pH < 6.5, and 2) the severe reduction of sulphide concentrations at pH > 6.5. Therefore, it is recommended to maintain anaerobic conditions to sulphide scales, particularly when sulphide is the limiting reactant or if formed particles, i.e. elemental sulphur, could cause misleading results.

6.1 Introduction

One of the main features of the new anaerobic setup, described in Chapter 5, is the isolation of atmospheric oxygen. As discussed in Section 2.4, aqueous sulphide species undergo oxidation in the presence of oxygen resulting in the formation of elemental sulphur (S_8), polysulphide (S_n^{2-}) and sulphate (SO_4^{2-}). The new anaerobic setup should allow an investigative comparison to determine the effect of oxygen on the aqueous sulphide solutions in the oilfield sulphide scale studies.

In this chapter, several test procedures have been conducted identically on aerobic and anaerobic sulphide solutions, which were analysed afterwards to detect changes and compare results. These tests included static tests, where multiple solutions were pH adjusted to various pH levels, followed by a settling period, and finally analysed using the ICP, the UV-Vis method and a pH meter. Another type of tests involved a dynamic factor and oxygen monitoring, where solutions were stirred while oxygen levels were continuously monitored, and the aqueous sulphide levels were frequently analysed.

The new anaerobic setup discussed in the previous chapter was used for these experiments to validate the main features of this setup: 1) the oxygen isolation, and 2) the containment of hydrogen sulphide gas during pH adjustment of the sulphide solutions. Aerobic and anaerobic sulphide solutions were tested at similar sets of conditions to determine the

primary changes due to sulphide oxidation. The analytical tools used in these tests mainly included UV-Vis method (using copper reagents), pH measurements, ICP and ESEM.

6.2 Preliminary Static Oxidation Tests

The initial oxidation tests were focused on identifying the effect of the presence of oxygen on the aqueous sulphide concentration at various pH levels. The solutions were mainly analysed by ICP and UV-Vis method to determine the changes in the sulphide levels. The dissolved oxygen concentrations were not monitored in these initial tests.

6.2.1 The Effect of pH on the Magnitude of Oxidative Sulphide in the Presence of Oxygen

The test procedure consisted of four key stages: 1) the preparation of the stock sulphide solution, 2) the de-oxygenation of the anaerobic sulphide solutions, 3) the acid addition, and 4) the analysis using ICP/back-calculation and the UV-Vis techniques.

6.2.1.1 The Preparation and De-Oxygenation of the Aqueous Sulphide Stock Solution

Four 242 mg/L stock sulphide solutions were prepared by dissolving ~ 0.0727 g (as in Table 6.1) of freshly washed, and dried $Na_2S.9H_2O$ salt crystals in 40 mL of de-oxygenated (N_2-sparged) magnesium-free (MF-NSSW) and sulphate-free (SF-NSSW) North Sea seawater brines in culture vials. The stock solutions were then transferred into Hungate-type tubes in 5 mL aliquots. Half of the tube set was labelled aerobic, and the second half was labelled anaerobic and de-oxygenated for 15 min by sparging with N_2 gas. The duration of de-oxygenation, determined using an oxygen meter, is described in Appendix C.

Table 6.1 Weights and concentration of sulphides in prepared solutions

Set	*Solution*	*$Na_2S.9H_2O$ Weight in 40 ml (g)*	*Theoretical sulphide concentration (mg/L)*	*pH*
1st Set (NSSW)	Anaerobic	0.0727	242	11.85
	Aerobic	0.0728	242	11.78
2nd Set (SF-NSSW)	Anaerobic	0.0726	242	11.91
	Aerobic	0.0730	243	11.82

6.2.1.2 The pH-Adjustment of Aqueous Sulphide Solutions by Acid Addition

Both aerobic and anaerobic solutions were injected with various volumes of 1M de-oxygenated HCl, as shown in Figure 6.1, according to the quantities listed in Table 6.2. The injection of different amounts of HCl produced samples with various pH values, while almost duplicating the same pH value for the aerobic and the anaerobic solutions to allow for further comparison.

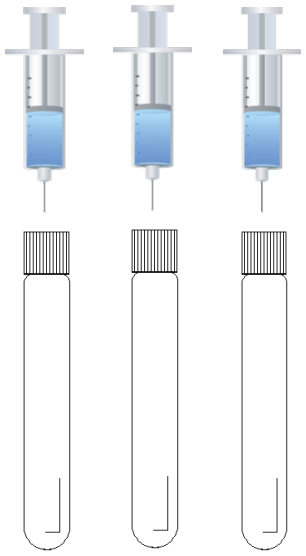

Figure 6.1 Simple illustration of adding diluted HCl to sulphide solutions using gastight analytical syringes and airtight tubes

Table 6.2 Tabled pH adjustment results using 1M HCl and 5 mL of 242 mg/L sulphide solution in NSSW

Brine	NSSW & SF-NSSW (Mg-free)			
HCl concentration	1 M			
Sulphide concentration	242 mg/L			
NSSW volume	5 ml			
V_n HCl, µL	*pH_n*			
	1st set (anaerobic)	*1st set (aerobic)*	*2nd set (anaerobic)*	*2nd set (aerobic)*
0	11.85	11.78	11.91	11.82
30	-	-	11.08	11.03
40	8.83	9.14	8.66	8.62
50	7.73	7.55	7.45	7.45
60	7.25	6.98	6.93	6.98
70	6.53	6.45	6.29	6.32
80	3.7	3.71	3.00	3.16
90	2.67	2.69	-	-
100	2.43	2.36	-	-

6.2.1.3 The Analysis of Aqueous Sulphide Concentrations

The two analytical techniques, ICP/back-calculation and UV-Vis, were used to identify the concentrations of aqueous sulphide in the final pH-adjusted solutions. A quenching solution of Ba and Zn excess was prepared, and the sulphide sample was diluted ten times in the quenching solution, then analysed by ICP. The calculated difference in the aqueous sulphide concentration from both techniques could be attributed to the oxidation process in the aerobic solutions. The comparison between the two analytical methods in this test has been discussed previously in Section 4.6.

6.2.2 Results of the Preliminary Oxidation Tests

6.2.2.1 Oxidative Loss Measured by UV-Vis and ICP/Back-Calculation Techniques

The aqueous sulphide concentrations, determined by the UV-Vis method, were initially plotted against the added volumes of 1M HCl, as seen in Figure 6.2 and Figure 6.3 for the aerobic and anaerobic solutions in the 1st and 2nd sets, respectively. The levels of sulphide concentrations were observed to drop collectively due to the headspaces in the tubes which allowed for the liberation of $H_2S_{(g)}$ during the addition of HCl. Nonetheless, a difference between the aerobic and anaerobic sulphide concentrations can be seen in these two figures, reflecting an oxidative loss. Further testing was done to compare aerobic,

semi-anaerobic, anaerobic and degassed sodium sulphide solutions in terms of depleting sulphide concentration during the injection of HCl, which are shown in Appendix D.

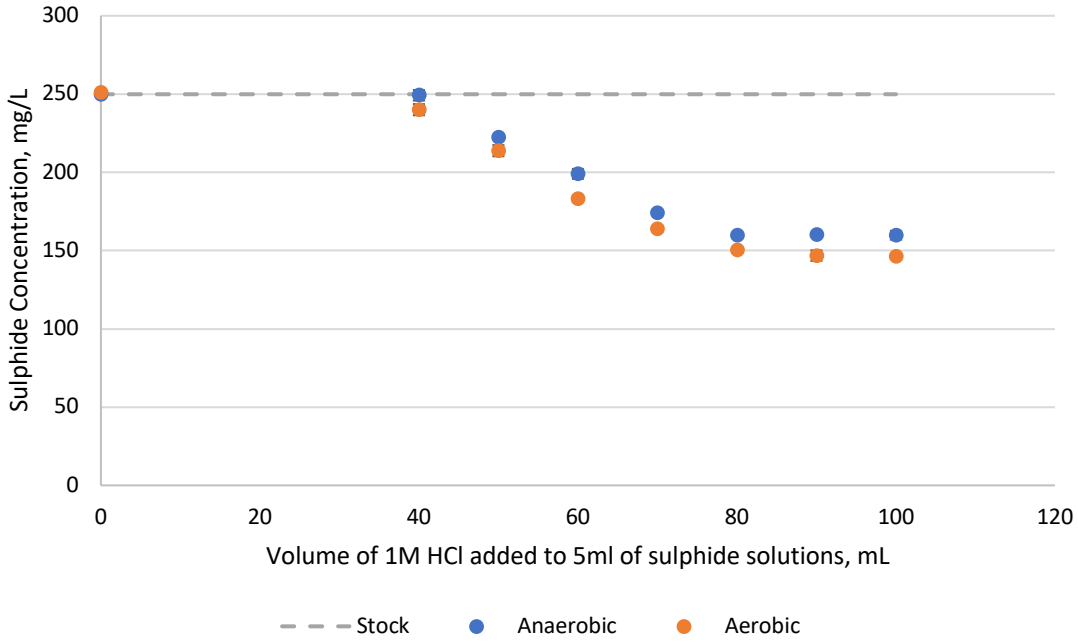

Figure 6.2 Sulphide concentrations in aerobic and anaerobic NSSW solutions at different added HCl volumes showing the difference in losses of [H_2S] due to oxidation and evolution

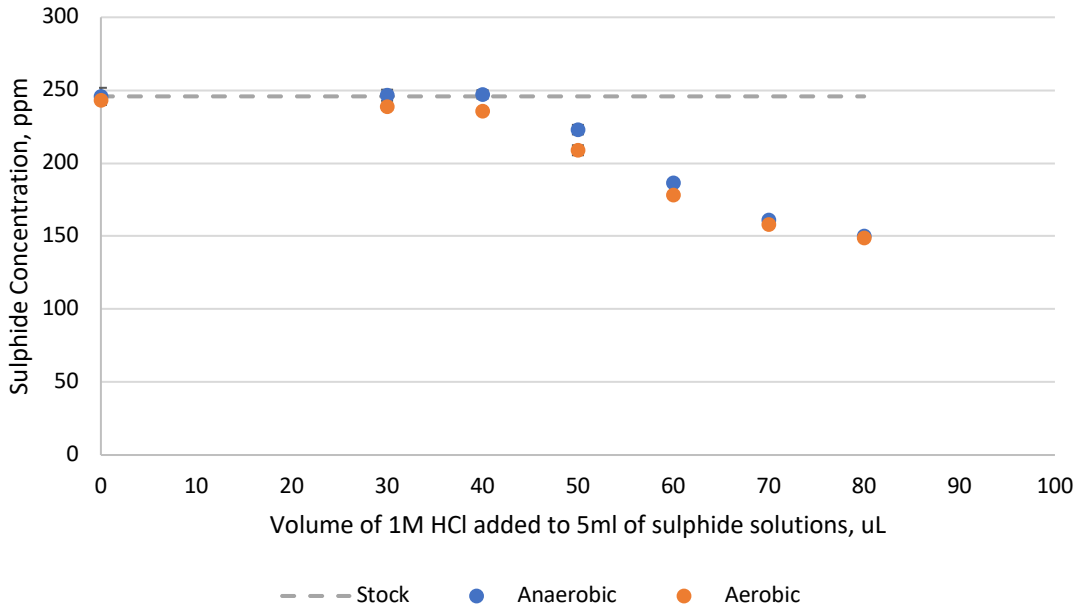

Figure 6.3 Sulphide concentrations in aerobic and anaerobic SF-NSSW solutions at different added HCl volumes showing the difference in losses of [H_2S] due to oxidation and evolution

The effect of the pH on the oxidative loss was qualitatively indicative, yet inconclusive, from the plotted graphs in Figure 6.4 and Figure 6.5, where the sulphide concentrations were plotted against the final pH of their respective solutions. The evolution of H_2S combined with an incomplete de-oxygenation of the anaerobic sulphide solutions resulted in an inconspicuous relationship between the pH and the oxidation process in this test. The qualitative determination of the oxidative loss was concluded for the preliminary tests. The ICP/back-calculation of the sulphide and concentrations from the zinc and barium concentrations, respectively, did not indicate a valid outcome, as seen in Figure 6.6 and Figure 6.7. The potential difference in aqueous sulphide concentration, in Figure 6.6, was within the ICP's error margin, thus it was not detected clearly. The concentrations of barium and sulphate was thought to be lower than the solubility product of barium sulphate, hence the lack of barium sulphate precipitation or $[Ba^{2+}]$ reduction in Figure 6.7.

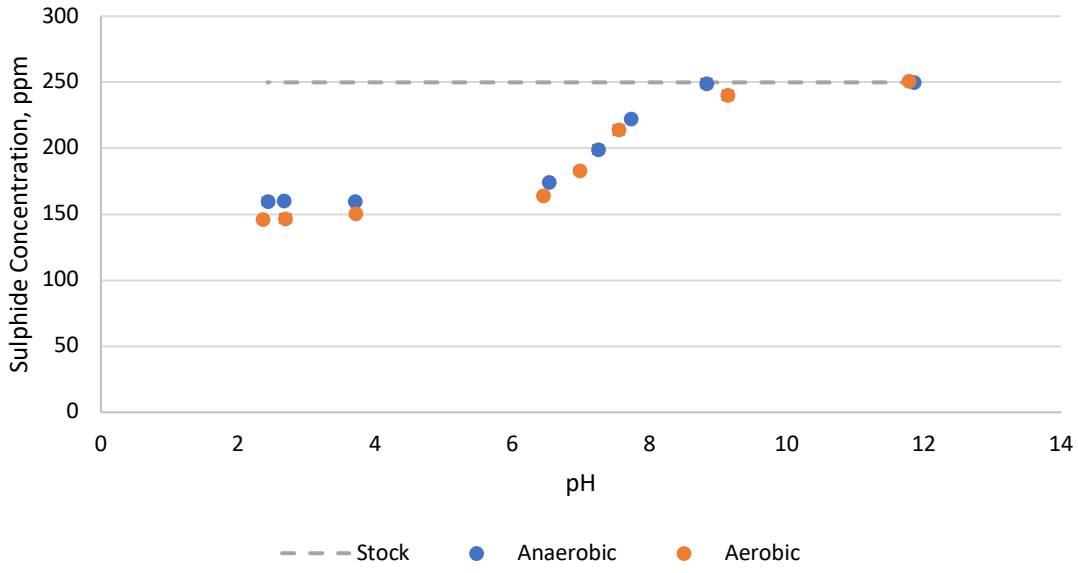

Figure 6.4 Sulphide concentrations analysed by UV-Vis spectrophotometer for different pH-adjusted NSSW sulphide solutions to show the losses of $[H_2S]$ in aerobic and anaerobic solutions

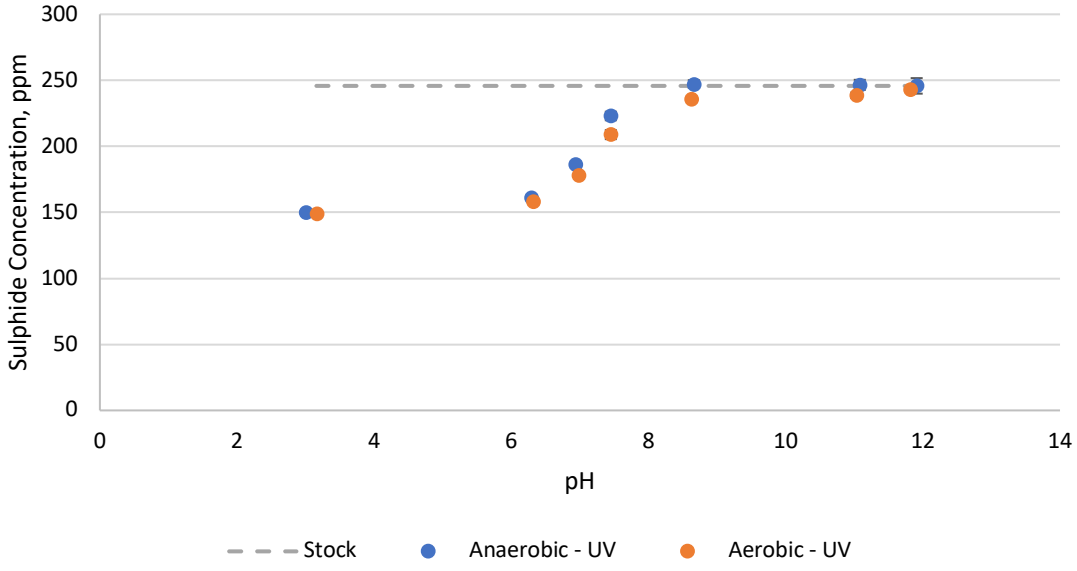

Figure 6.5 Sulphide concentrations analysed by UV-Vis spectrophotometer for different pH-adjusted SF-NSSW sulphide solutions to show the losses of [H_2S] in aerobic and anaerobic solutions

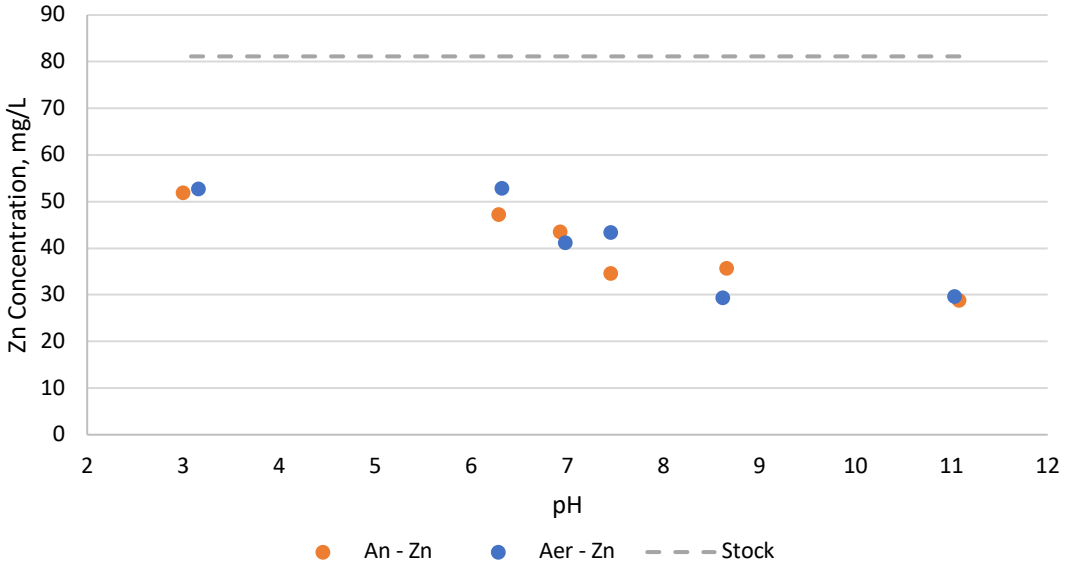

Figure 6.6 ICP analysis of zinc in anaerobic and aerobic solutions at different pH values which did not show conclusive results because difference in concentrations was within the ICP error margin (±10%)

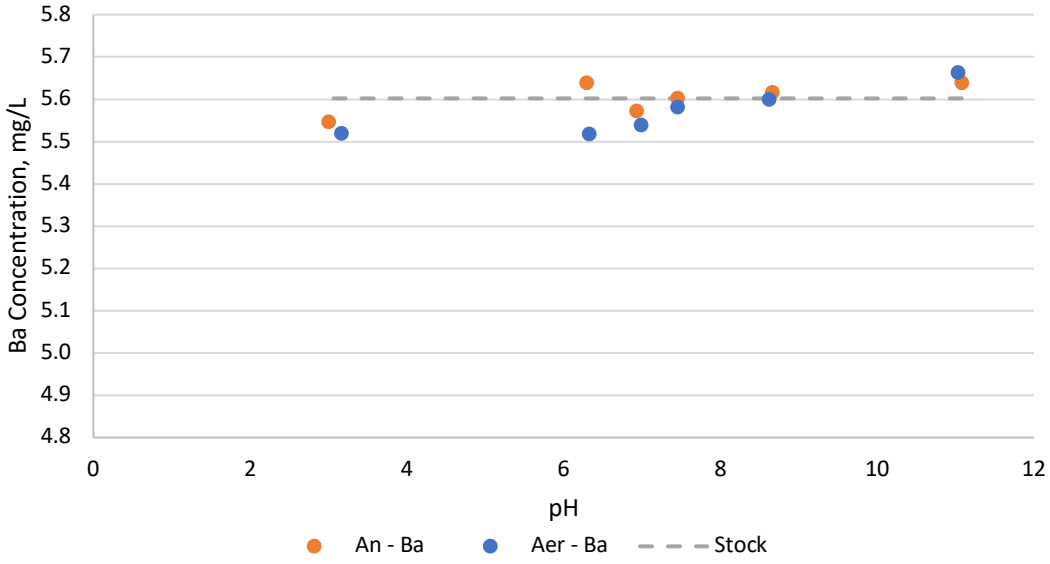

Figure 6.7 ICP analysis of barium in anaerobic and aerobic solutions at different pH values where barium chloride was used to quench any sulphate formed as an oxidative product

6.2.2.2 Visual Indications of Oxidative Products

The visual observations of the Hungate-type tubes revealed some degree of white turbidity in the aerobic solutions, while the anaerobic solutions remained completely clear, as shown in Figure 6.8 and Figure 6.9. Despite the loss in sulphide concentrations in the aerobic solutions, the turbidity only appeared in solutions at pH ≤ 6.5, whilst solutions with higher pH values were clear. The only plausible explanation of this cloudiness was the formation of elemental sulphur, which was observed in earlier work; as seen in Figure 6.10, where the sulphide solutions were prepared in DW. Nevertheless, the sulphide concentrations at pH values ≤ 6.5 in the SF-NSSW solutions were almost identical for aerobic and anaerobic solutions, while the solutions were visually dissimilar in terms of clarity and turbidity.

pH	8.83	7.73	7.25	6.53	3.70	2.67	2.43
NSSW Anaerobic Solutions	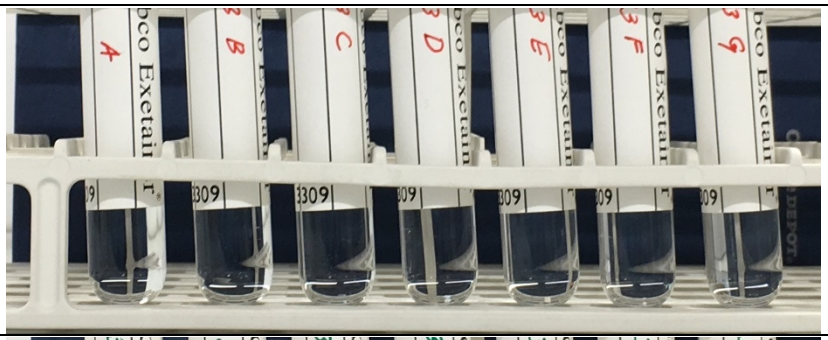						
NSSW Aerobic Solutions	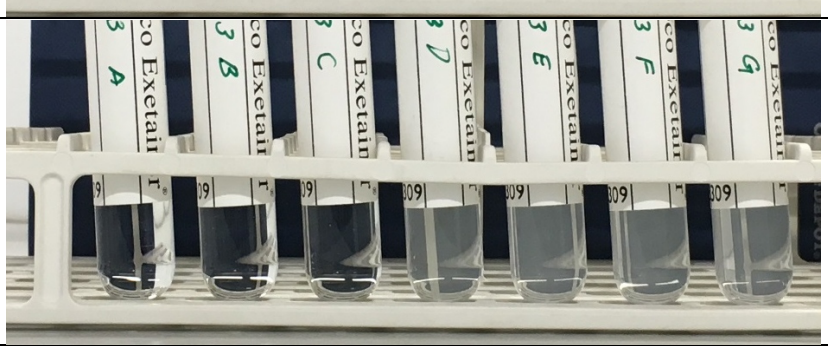						
pH	9.14	7.55	6.98	6.45	3.71	2.69	2.36

Figure 6.8 Turbidity (elemental sulphur formation) of NSSW anaerobic and aerobic pH-adjusted sulphide solutions to show the effect of oxygen on aqueous sulphide at various pH levels

pH	11.08	8.66	7.45	6.93	6.29	3.00
SF-NSSW Anaerobic Solutions	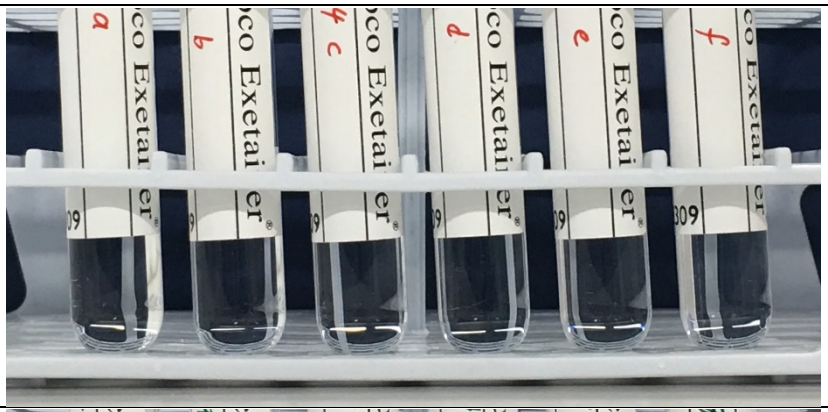					
SF-NSSW Aerobic Solutions	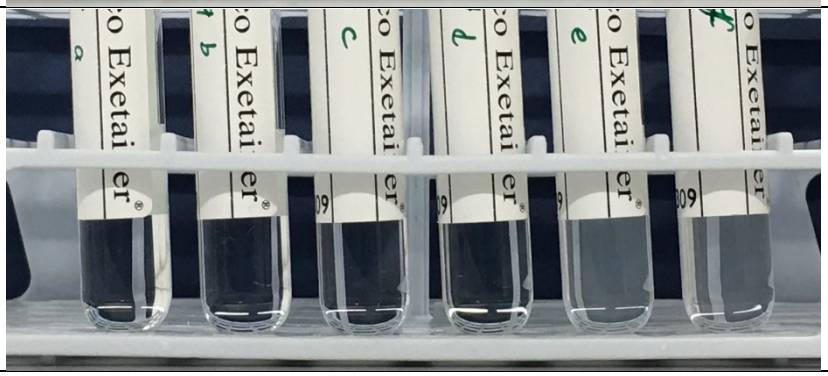					
pH	11.03	8.62	7.45	6.98	6.32	3.16

Figure 6.9 Turbidity (formation of elemental sulphur) observed in SF-NSSW anaerobic and aerobic pH-adjusted sulphide solutions to show the oxidation effect of oxygen at various pH levels

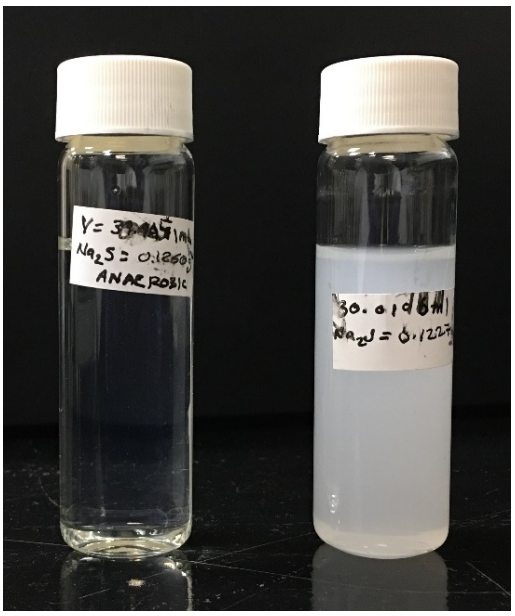

Figure 6.10 Suspended elemental sulphur, an oxidative product, appeared in the aerobic solution (right) whereas the anaerobic solution (left) remained clear

6.3 Extended Static Oxidation Tests

The quantitative determination of the oxidative loss in aqueous sulphide concentration was described and discussed in the previous test. However, the large headspace and the incomplete de-oxygenation of the anaerobic solutions reduced the correlation between the pH values of solutions and the magnitude of oxidative loss. Therefore, procedural modifications were made to minimise the interference of these factors. In addition, the range of pH levels was reduced, and a time factor was introduced.

6.3.1 Procedural Modifications for the Extended Oxidation Tests

The modifications in this test involved increasing the volumes of aqueous sulphide solutions to 11 mL in the 12-mL Hungate-type tubes, thus reducing the headspace. In addition, the de-oxygenation step was extended to 18 minutes at 4 psi, instead of 15 min at 2 psi, according to Appendix C. The aerobic and anaerobic solutions were pH adjusted to three different pH levels, and individual samples were designated to each time step, namely one hour, one day and one week. The analysis was limited to the UV-Vis method and pH measurement. Finally, the aqueous sulphide concentration was lowered to 40 mg/L (0.09g $Na_2S.9H_2O$ in 250 ml NSSW) to increase the quantification of the oxidative loss throughout the samples. A summary of the test conditions is shown in Table 6.3.

Table 6.3 Extended static oxidation test of sulphide solutions (40 mg/L of aqueous sulphide) at different conditions

Target pH	*1M HCl, µL*	*Analysis after one hour*		*Analysed after one day*		*Analysed after one week*	
		Aerobic	*Anaerobic*	*Aerobic*	*Anaerobic*	*Aerobic*	*Anaerobic*
pH 3	36	11 ml	11 ml	11 ml	11 ml	11 ml	11 ml
pH 6.5	26	11 ml	11 ml	11 ml	11 ml	11 ml	11 ml
pH 8	18	11 ml	11 ml	11 ml	11 ml	11 ml	11 ml

6.3.2 Theoretical Quantification of the Oxidative Loss Based on Dissolved Oxygen Content

The dissolved oxygen concentration in water at atmospheric pressure and room temperature normally varies between 6 - 8 mg/L, depending on factors such as the salinity of the solution. In these static tests, dissolved oxygen concentration was not measured, however, by assuming $[O_{2(aq)}]$ to be 6 - 8 mg/L (187 - 250 µMol), then the maximum

stoichiometric ratio (2:1 sulphide-to-oxygen) of the reactions below should consume 12 - 17 mg/L (~ 375 - 500 μMol) of bisulphide anion, yielding elemental sulphur (Nielsen *et al.*, 2003).

$$2HS^- + O_2 \rightarrow 2S^0 + 2OH^- \quad (5.2)$$

$$2HS^- + 2O_2 \rightarrow S_2O_3^{2-} + H_2O \quad (5.3)$$

$$2HS^- + 3O_2 \rightarrow 2SO_3^{2-} + 2H^+ \quad (5.4)$$

$$2HS^- + 4O_2 \rightarrow 2SO_4^{2-} + 2H^+ \quad (5.5)$$

6.3.3 The Extended Oxidative Loss Measured by UV-Vis Method

The results of aqueous sulphide analysis were plotted in Figure 6.11 and Figure 6.12 against pH to show the changes of sulphide concentrations in the aerobic and anaerobic solutions with time. In the sealed aerobic samples with stock concentrations of 40 mg/L, the reduction in sulphide concentrations was seen to be a maximum at pH 6.45, which was quantified as 6, 20 and 27 mg/L after one hour, one day and one week, respectively. It is worth mentioning that the reported oxidation maxima are at pH 6.8 – 8 and at pH 11, as shown in Table 2.3. This reduction was beyond that expected from the stoichiometric highest ratio of the reaction between bisulphide and oxygen, i.e. 2:1, which suggested additional reactions were occurring to further consume the bisulphide anion. The modifications to the test procedure have significantly impacted the outcome by revealing a pH-dependent trend.

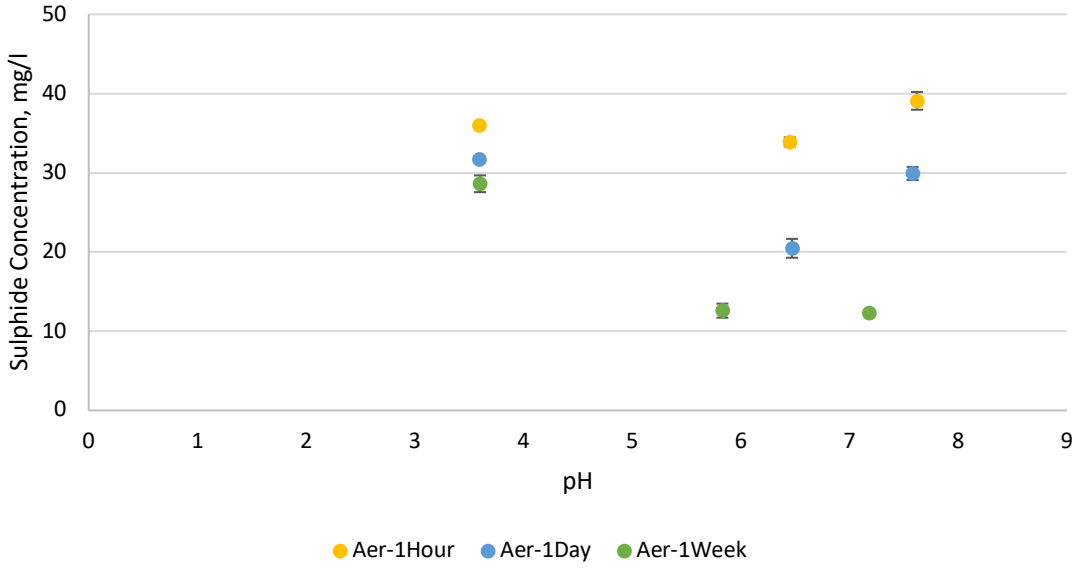

Figure 6.11 The different reductions in the sulphide concentrations caused by the oxidation in the ***aerobic*** solutions as a function of pH and time

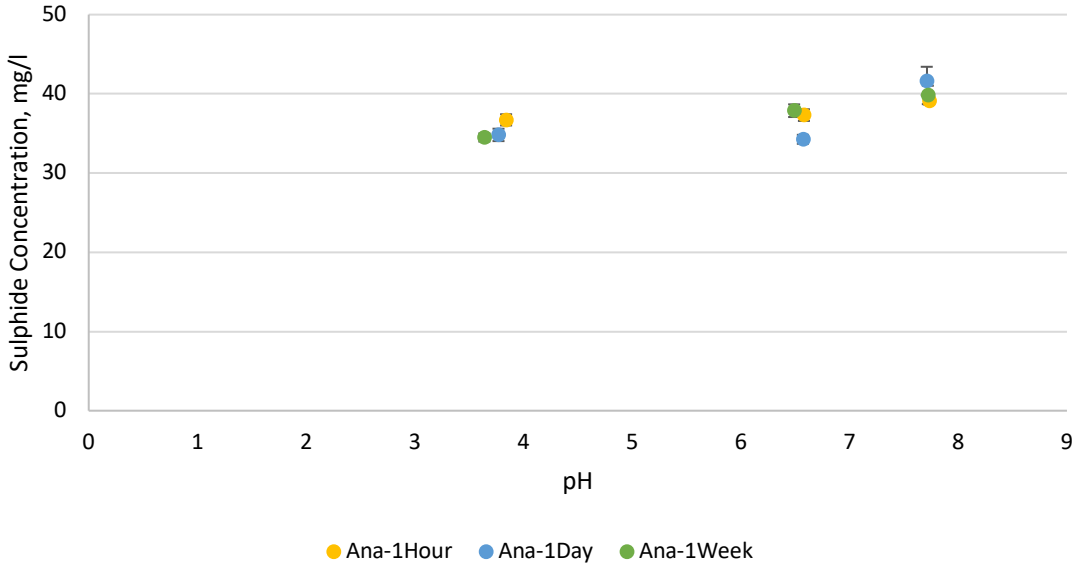

Figure 6.12 The ***anaerobic*** (oxygen-free) solutions showed minimal reduction in sulphide concentrations at various pH levels and time steps

The slightly acidic samples at pH 3.6 in Figure 6.11 showed minimum losses at nearly 4, 8 and 11 mg/L, which were proportional to the test durations. On the contrary, the anaerobic samples maintained losses of 4 – 5 mg/L of sulphide concentrations throughout the test periods, as seen in Figure 6.12. The colloidal elemental sulphur observed in the

aerobic solutions, as seen in Figure 6.13 (b), (d) and (f), was insignificant compared to what was reported in Figure 6.8 and Figure 6.9 using 242 m/L of sulphide, mainly due to the significant difference in initial sulphide concentration. Slight cloudiness can be seen in the sample of pH 3.84, Figure 6.8 (a), and samples of pH 3.59, Figure 6.8 (b) and (d). This cloudiness was assumed to be the result of the formation of elemental sulphur in the aerobic samples after one hour, and one day, however, this turbidity settled after one week of the acid injection. The anaerobic sample at pH 3.84, Figure 6.8 (a), which was thought to be oxygen-free, should not have formed elemental sulphur. Further testing followed a more rigorous deoxygenation procedure, as reported in Appendix C. Based on Appendix C, this sample was assumed to have nearly 1 ppm of dissolved oxygen, hence the sulphur depositin.

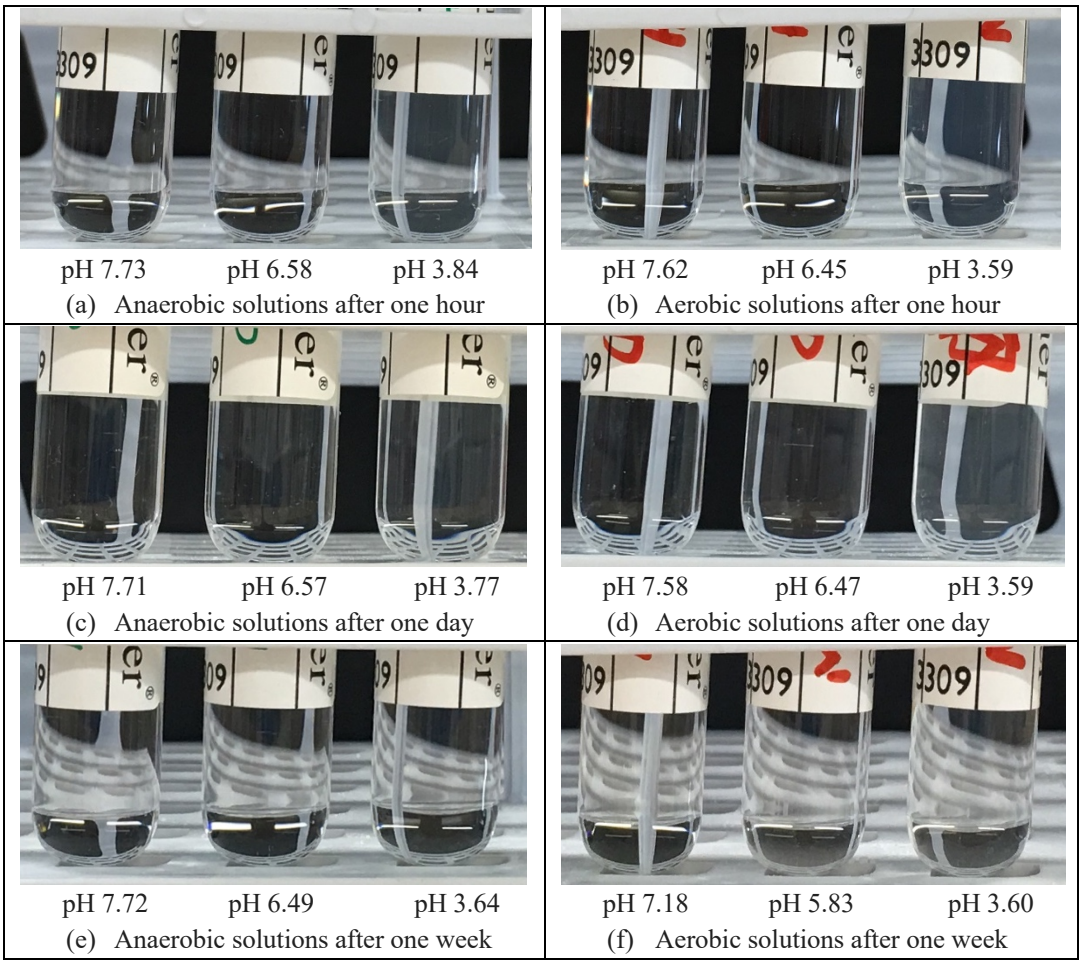

Figure 6.13 Anaerobic and aerobic sulphide solutions at different pH values and time steps showing signs of elemental sulphur formation (turbidity) at low pH values (pH< 6)

The results from the extended oxidation test were potentially impacting the oilfield sulphide scale tests and in agreement with the literature findings. Similar results have

been reported in the literature, where maximum oxidation rates were observed at pH 6 – 8 (Chen and Morris, 1972), where sharp decrease of aqueous sulphide concentrations have occurred. In addition, colloidal sulphur formation was reported at pH < 6.5 depending on initial sulphide concentration (Almgren and Hagström, 1974; Chen and Morris, 1972; Cline and Richards, 1969; O'Brien and Birkner, 1977; Weres and Tsao, 1983). Each observation in the static oxidation test was explained or discussed in these studies. The formation of colloidal sulphur was observed at samples with initial sulphide concentrations of 242 mg/L (~7.3 mM) at pH values below 6.45, which agreed with the suggestion made by Chen and Morris (1972), as well as the absence of sulphur colloidal sulphur at initial sulphide concentrations of 40 mg/L (~1.2 mM). Table 2.3 summarised the conditions that govern the formation of elemental sulphur, and also mentioned the oxidation maximum rates at pH 6.8 – 8 and at pH 11 (Chen and Morris, 1972). In addition, samples at pH of ~3.6 showed less oxidation effect, which was explained by the assumption of forming sulphanes, hydrogen sulphide dimers H_4S_2, from polysulphides at pH < 6, which in return decomposed into H_2S and colloidal sulphur (Chen and Morris, 1972).

6.3.4 Repeat of the Extended Oxidation Test

These static tests were repeated at a slightly higher sulphide concentration, namely 50 mg/L, and the results were remarkably repeatable and confirmative, as seen in Figure 6.14 and Figure 6.15. The lowest point in Figure 6.14 was not expected to show such losses of sulphide, and it could be referred to a human error during the acidizing (pH adjustment) step, which could have placed the solution in the maximum oxidation rate conditions at pH 8, as described by Chen and Morris (1972) and Almgren and Hagström (1974).

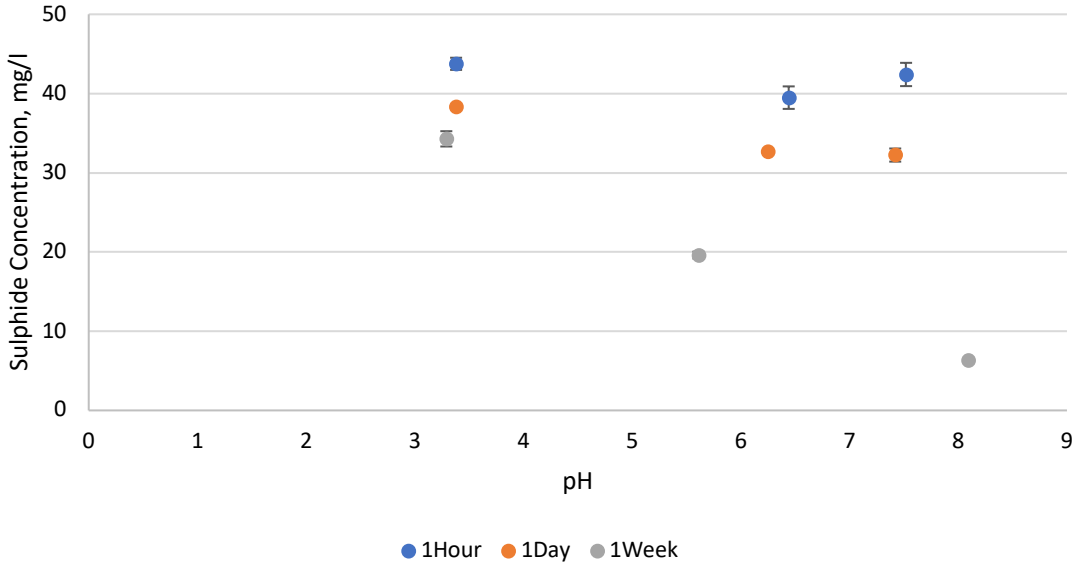

Figure 6.14 Duplicate results of the ***aerobic*** solutions showing similar reductions in aqueous sulphide concentrations as a result of oxidation at various durations and pH levels

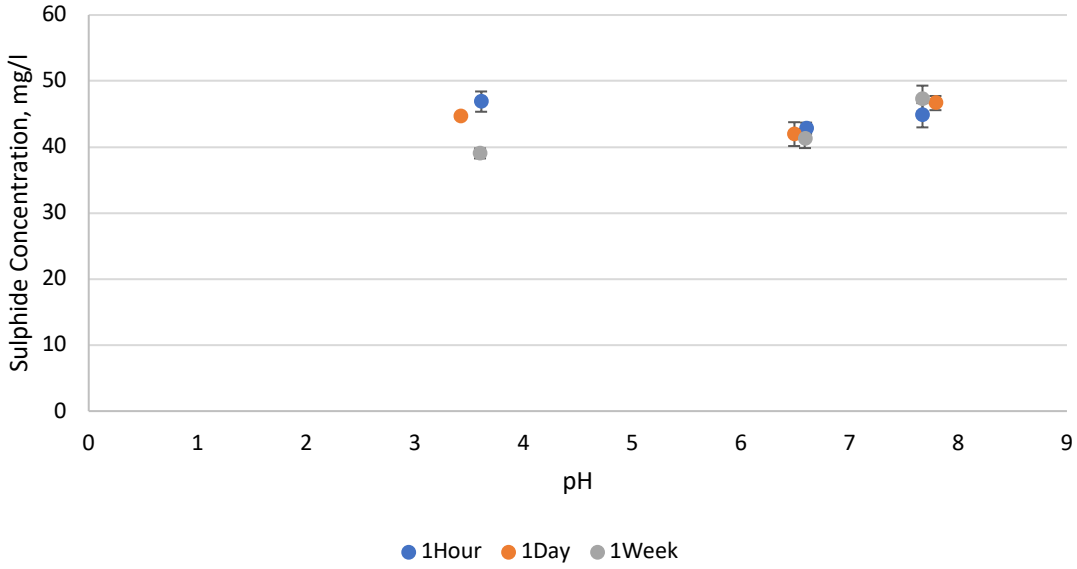

Figure 6.15 Duplicate sets of results of the ***anaerobic*** (oxygen-free) solutions showing minimal reduction in aqueous sulphide concentrations as a function of pH and time

Based on these test conditions (40 – 50 mg/L of sulphide), the oxidative loss of aqueous sulphide could reach more than 20 % of the initial concentration within one hour, 50 % after one day, and 67 % after one week. Such losses can only be significant in tests where the sulphide is the limiting reactant. However, most sulphide scale tests are carried out

immediately after preparing the sulphide solutions, thus minimising the risk of oxidising the aqueous sulphide.

The elemental sulphur formation was confirmed visually at conditions similar to those described in the literature, as summarised in Table 2.3. The presence of a white colloidal could interfere with the formation of sulphide scale particles, namely ZnS. On the other hand, the formation of sulphate, as an oxidative product, was not confirmed via quenching with barium to form barium sulphate.

6.4 Dynamic (Stirring) Oxidation Tests

The static tests revealed an oxidative loss with time and the formation of elemental sulphur at low pH levels. The dynamic (stirring) was designed to provide a closer look at the depletion of aqueous sulphide and dissolved oxygen with the kinetics. Aerobic sulphide solutions were prepared and tested one at a time to allow for many sulphide analysis and continuous dissolved oxygen measurement while the solution is stirred. Various test conditions were investigated, including pH of solution, the sulphide and oxygen concentrations.

6.4.1 The Preparations and Test Procedure of the Dynamic Oxidation Test

The concentrations of dissolved oxygen inside the culture vials were monitored and logged using a Presens portable O_2 meter (Fibox 4 trace) with an optical fibre cable and sensor spots (SP-PSt6 and SP-PSt3-SA). Figure 6.16 shows an illustration of the experimental setup, which was comparable to that reported in the experimental work of Nielsen *et al.* (2003). The logging of dissolved oxygen concentrations started along with the analysis of the initial concentration of aqueous sulphide. Afterwards, various volumes of 1M HCl were added to aerobic solutions to adjust the pH values (pH 5 – 11). The addition of HCl was initially assumed to be the beginning of the aqueous sulphide oxidation. The sulphide analysis was performed every 5 - 10 min, at least for the first 90 minutes, then samples analysed less frequently. At the end of the test, the pH of the solution was measured. Both oxygen and sulphide concentrations were plotted against time to show the depletion trends and any possible correlations.

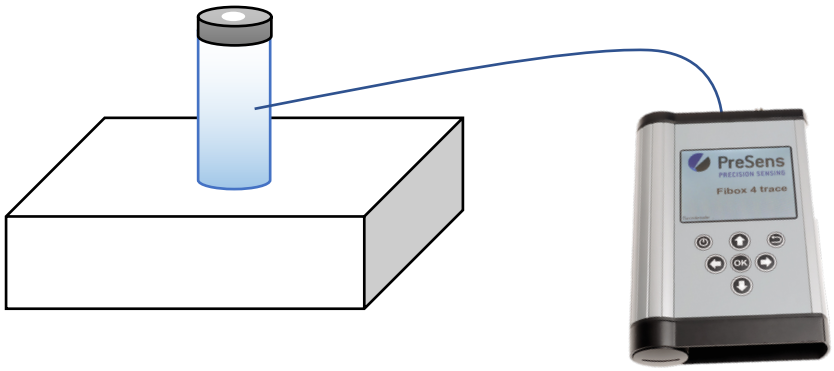

Figure 6.16 Illustration of the experimental setup for the dynamic oxidation tests where a vial was placed on a stirring plate(left), and oxygen meter was used to measure dissolved oxygen concentrations through an optical fibre cable

6.4.2 Oxidation of 100 mg/L of Aqueous Sulphide at pH_f of 5.61 and 6.42

The first two experiments that were tested using the dynamic setup initially agreed with and confirmed results obtained from the static tests. The collected data plotted in Figure 6.17 and Figure 6.18 for solutions with pH_f 6.42 and 5.61, respectively, show the depletion of dissolved oxygen and aqueous sulphide before and after the pH adjustment. In Figure 6.17, the maximum difference in the sulphide concentration was ~ 34 mg/L after 142 minutes of continuous stirring. However, the dissolved oxygen was depleted at a different fashion as it started to decrease dramatically only after 15 minutes of injecting the acid, which could be explained by the reaction equations (6.2) – (6.5). After 100 minutes of acid injection, the curve reached a plateau, and the oxygen concentration remained constant at ~ 650 µg/L. At this level, the sulphide concentration was still decreasing at a low yet steady rate, which suggested the occurrence of reactions other than that between the aqueous sulphide and dissolved oxygen. Steudel (1996) and Zangh and Millero (1992) have reported several reactions between bisulphide and radical sulphur compounds, and between bisulphide and oxidation intermediates, such as sulphite.

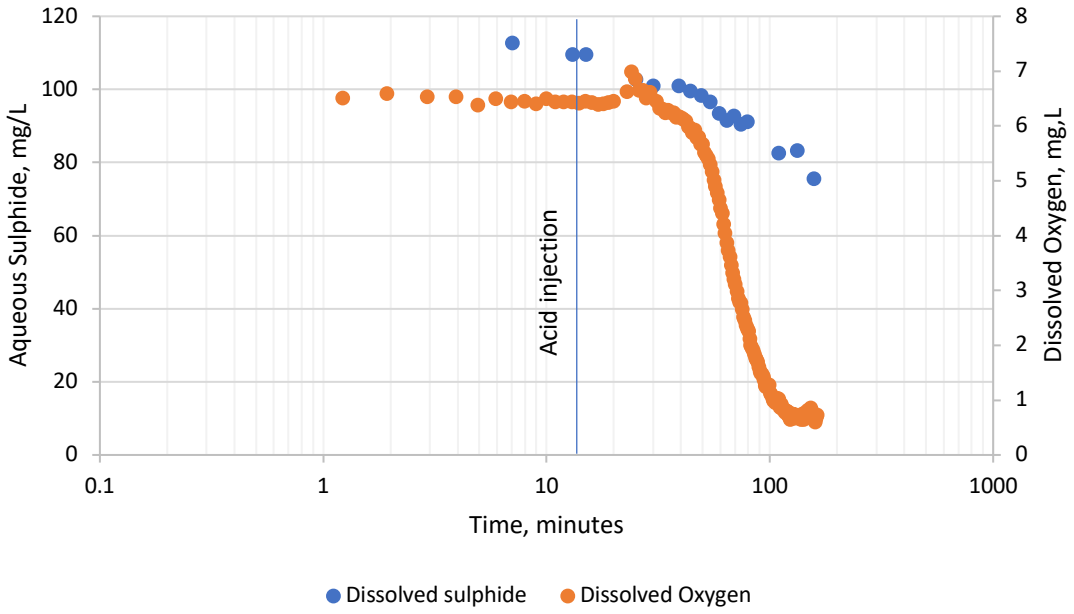

Figure 6.17 A dynamic (stirring) test showed oxidation effect represented in distinctive sharp reductions of oxygen and aqueous sulphide concentrations after the injection of acid to adjust the pH to ***pH 6.42***

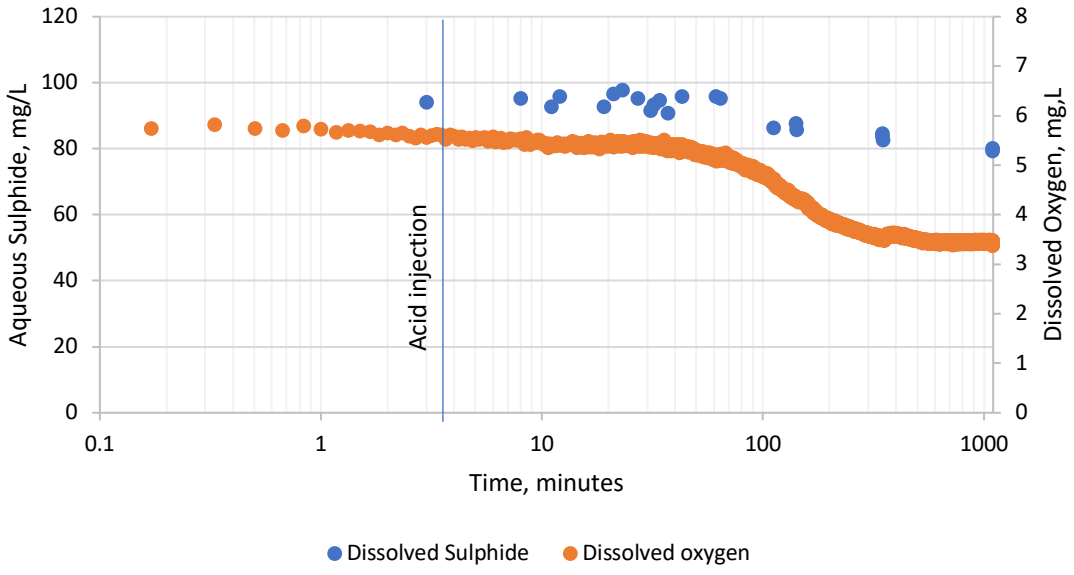

Figure 6.18 A dynamic (stirring) test showed oxidation effect represented in slow reductions of oxygen and aqueous sulphide concentrations after the injection of acid to adjust the pH to ***pH 5.61***

The plotted data in Figure 6.18 illustrates the depletion rates of the aqueous sulphide and dissolved oxygen during the oxidation reaction for 18 hours. The final pH was recorded

as pH_f 5.61 after stopping the experiment. The dissolved oxygen concentration dropped from 5.8 mg/L to 3.6 mg/L over nearly 6 hours, whilst only 11 mg/L of aqueous sulphide concentration was consumed over the same period. The rest of the reaction duration, ~12 hours, showed a slight drop in the sulphide concentration, ~ 3 mg/L, while the oxygen concentration remained constant. These findings agreed with that in the static oxidation tests, at samples of pH 3.6. Although the data showed sufficient concentrations of oxygen and sulphides, the oxidation reaction did not progress, which was reported in the literature for solutions with pH < 6 (Chen and Morris, 1972). Rickard (2012) described the oxidation rates of $H_2S_{(aq)}$ and HS^- and their dependence on the pH. The literature review in his article stated that the oxidation of HS^- is faster than that of $H_2S_{(aq)}$. This statement could explain the vast difference in the depletion rates of the dissolved oxygen and aqueous sulphide in the tested solutions at pH_f 6.42 and 5.61. From Figure 1.1, at pH 6.5, the theoretical percentages of [$H_2S_{(aq)}$] and [HS^-] are 76 and 23 %, respectively, while these percentages change to 97 and 3 %, respectively, at pH 5.5.

6.4.3 Depletion of Dissolved Oxygen (5 mg/L) and Sulphide (1,000 mg/L) Concentrations at Various pH Levels

The oxidation magnitude is affected by the concentrations of oxygen and sulphide, and in these tests, the latter was investigated. Two additional experiments were performed using ~ 1,000 mg/L of aqueous sulphide in 20 wt. % NaCl at two final pH values: pH_f 5.71 and 11.39. A few tests were initially performed using Khuff Na & Ca (14.9 wt. % NaCl - 4.2 wt. % $CaCl_2$, equivalent TDS to Khuff formation brine), during which the initial concentration of dissolved oxygen started to deplete before the acid addition. The complete geochemical composition of the Khuff formation water, shown in Table 6.4, could induce incompatibility complications, such as the formation of magnesium hydroxide at initial high pH values, hence the simplified version. Therefore, the sodium chloride brine was used instead of the simplified Khuff Na & Ca to avoid any possible formation of calcium hydroxide at the high initial pH associated with the dissolution of the sodium sulphide salt to achieve high concentrations of aqueous sulphide.

Table 6.4 The geochemical composition of Khuff formation water (Franco *et al.*, 2010)

Ions	*Concentration, ppm*
Na	54936.0
Ca	14259.0
Mg	1524.0
SO_4	100.0
Cl	114055.0
HCO_3	436.0
Ba	21.6
K	5887.0
Sr	1047.0
pH	5.7
CO_2 *	7.7
H_2S *	7.9

* at 14.7 Pound-force per square inch (Psig) and 77ºF

The aqueous sulphide solutions were prepared by dissolving nearly 0.300 g of sodium sulphide salt in 37.5 and 38.8 mL of 20 wt. % NaCl for the first and second solutions, respectively. The monitoring of dissolved oxygen began during the dissolution of the sodium sulphide crystals. The acid was injected when the dissolved oxygen concentration reached ~ 2.4 – 2.5 mg/L. The volumes of injected 1M HCl were 2.5 and 1.2 mL for the first and second solutions, respectively, and the aqueous sulphide concentrations were immediately recorded as ~ 979 and 1,061 mg/L, respectively. The oxygen monitoring was stopped when the concentrations reached 130 and 8 µg/L of dissolved O_2 in the first and second solutions, respectively.

Figure 6.19 and Figure 6.20 show the depletion rates of the dissolved oxygen and aqueous sulphide in the first and second solutions, respectively. The dissolved oxygen concentrations were initially at ~ 5,000 µg/L in both solutions, yet, the depletion rates of dissolved oxygen were different. In Figure 6.19, the depletion rates of oxygen before and after injecting acid were 105 and 63 µg/L.min, respectively, whilst the rates in Figure 6.20 were calculated to be 154 and 199 µg/L.min, respectively.

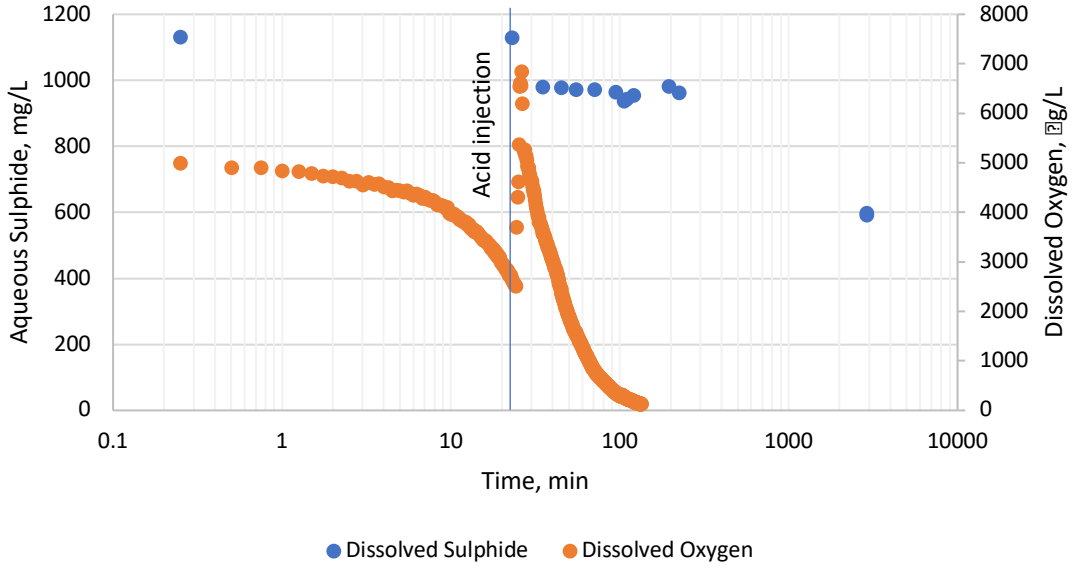

Figure 6.19 A dynamic (stirring) test showed oxidation effect represented in steep reductions of oxygen and sulphide concentration particularly after the injection of acid to a 20 wt. % NaCl sulphide solution at room temperature and ***pH_f 5.72***

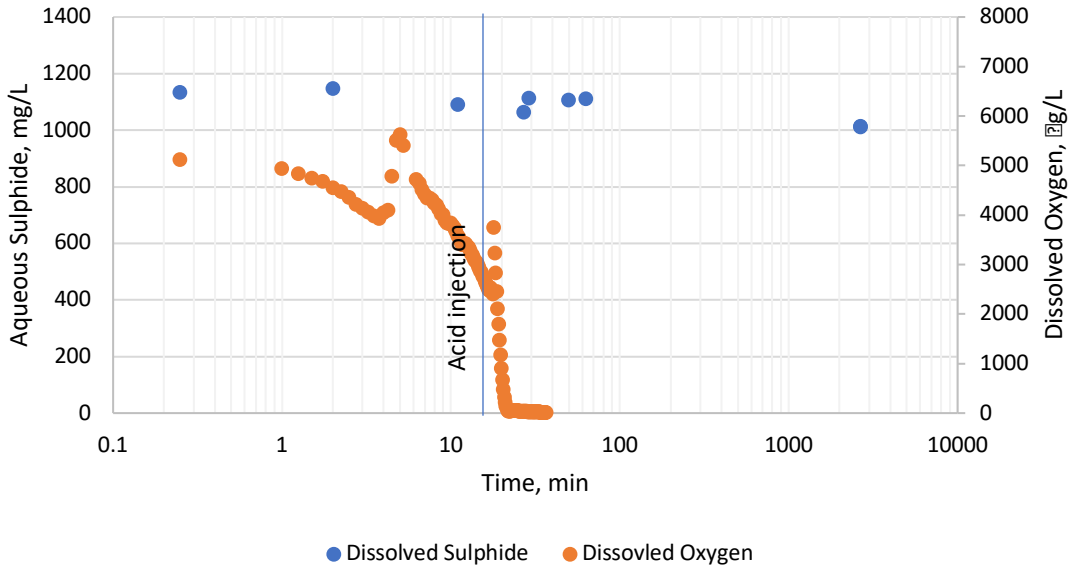

Figure 6.20 A dynamic (stirring) test showed oxidation effect represented in steep reductions of oxygen concentration before and after the injection of acid to a 20 wt. % NaCl sulphide solution at room temperature and ***pH_f 11.39***

On the other hand, the differences in the aqueous sulphide concentrations were negligible in both solutions after the injection of acid. The significant difference in the concentration of aqueous sulphide was only noticeable ~ 45 hours after the pH adjustment, where the

first and second solutions showed decreases of ~ 370 mg/L (*pH 5.72*) and 100 mg/L (*pH 11.39*), respectively. The depletion of aqueous sulphide in Figure 6.19 was similar to that observed in Figure 6.18, albeit having different depletion profiles of the dissolved oxygen. Nonetheless, based on the observations reported in the work of Rickard (2012), the second solution (*pH 11.39*) should have experienced a more significant loss of aqueous sulphide given that the bisulphide ion, the dominant sulphide species at such pH, oxides faster than $H_2S_{(aq)}$.

Although the dissolved oxygen concentrations showed dramatic depletion rates, there was negligible effect on the aqueous sulphide concentrations during the first hour of the tests. There was a slight disagreement while comparing the oxidation of 100 and 1,000 mg/L of sulphide at pH 5.61 and 5.72, respectively. Given the close pH levels, the solutions were anticipated to show similar sulphide depletion behaviours, yet one decreased by ~ 8 mg/L (8.5 %) while the second decreased by ~ 25 mg/L (2.5 %) in the first 100 minutes. The brine salinity and the aqueous sulphide concentration could be contributing to the discrepancies in the results.

6.4.4 Oxygen Poisoning Tests

The decrease in initial dissolved oxygen and sulphide concentrations due to the oxidation reaction was observed in the previous tests. Another set of experiments was designed to identify the effect of oxygen poisoning on aqueous sulphide solutions. These tests involved de-oxygenated (anaerobic) aqueous sulphide solutions in 38 ml of high TDS brine (14.9 wt.% NaCl and 4.2 wt.% $CaCl_2$) in culture vials (40 ml), then one was injected with de-oxygenated 1M HCl, followed by the injection of 2 and 12 cubic centimetre (cc) of air consecutively, while the second test was directly injected with a slightly aerated 1M HCl. The initial sulphide concentrations were 1,000 mg/L for both solutions, and the injected 1M HCl was maintained at 2.0 mL to reach ~ pH_f 6.5. The dissolved sulphide and oxygen concentrations were monitored using UV-Vis method and the Presens portable O_2 meter, respectively.

The first oxygen poisoning test was extended to nearly 67 hours before stopping the experiment. The initial dissolved sulphide and oxygen concentrations were ~ 961 mg/L and ~ 3 μg/L respectively. After acidifying the sulphide solution by adding 2 mL of anoxic 1M HCl, the concentration of sulphide decreased to 908 mg/L primarily due to the

dilution effect. Nonetheless, the sulphide concentration was constant until the air was injected, after which a steady decrease was observed, as seen in Figure 6.21. A total of 48 mg/L of sulphide was depleted from solution over 112 minutes, and an additional loss of 242 mg/L was observed over 52 hours. The preliminary calculated depletion rates of aqueous sulphide were very distinct, 0.0126 mMol/min (0.43 mg/L.min) for the first two hours, and 0.00227 mMol/min (0.08 mg/L.min) for the next 52 hours. On the other hand, the dissolved oxygen levels increased from ~ 4 to 45 µg/L after injecting 2 cc of air followed by an increase to ~ 168 µg/L after injecting 12 cc of air. The dissolved oxygen concentration showed a sharp decrease from 168 to ~ 70 µg/L in just 12 minutes; then it continued to decrease until it reached ~ 4 µg/L after 66.6 hours of injecting air.

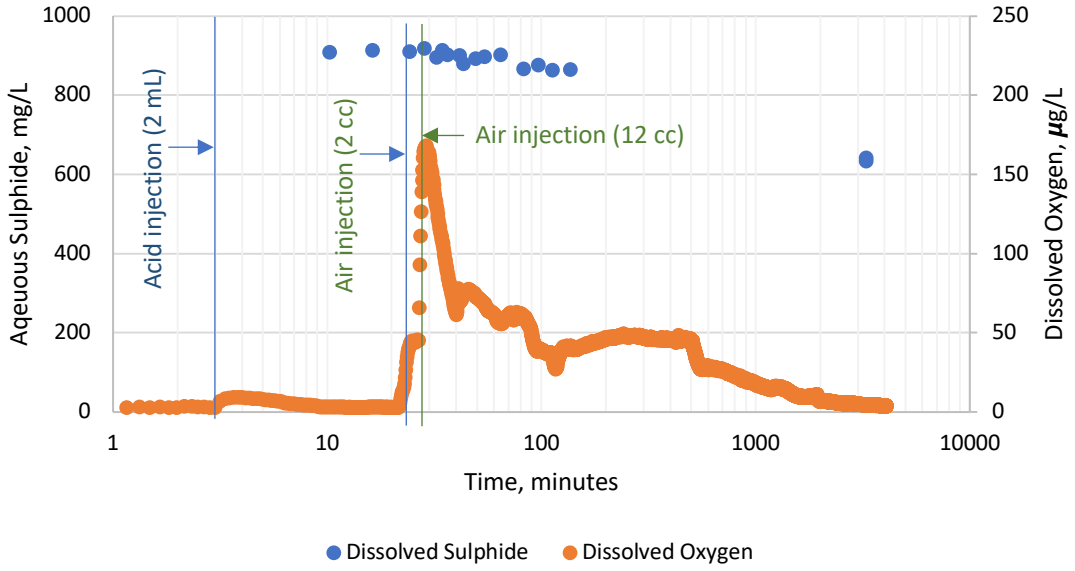

Figure 6.21 Oxygen poisoning of an anaerobic sulphide solution (***pH$_f$ 6.76***) through injecting air which is represented by the sharp and steady reduction rates of oxygen and sulphide concentrations, respectively

The reaction rates of the aqueous sulphide and dissolved oxygen were dissimilar and could not be correlated, which was in agreement with the findings from Figure 6.17 - Figure 6.20. The ESEM-EDX analysis in Figure 6.22 showed that elemental sulphur was a noticeable component in the analysed solids, given that the carbon and oxygen contents were sourced from the filter paper, and the calcium, sodium and chloride were residuals from the high TDS brine.

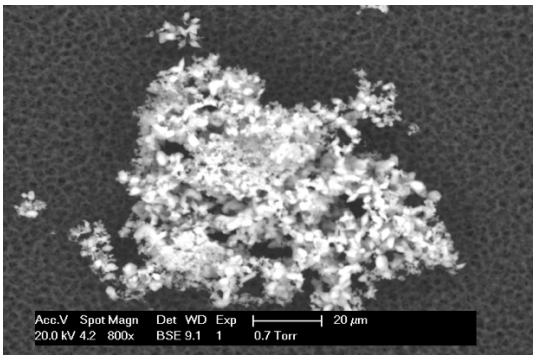

a) 800x magnification

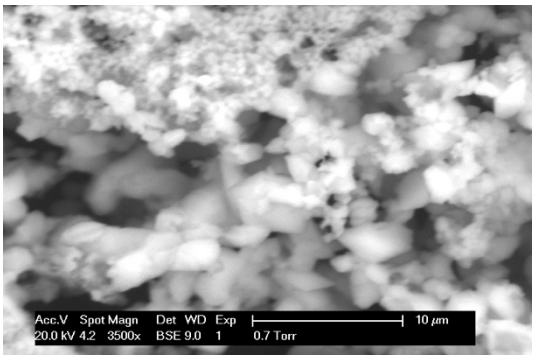

b) 3,500x magnification

Element	Atomic %	Element	Atomic %
O	87.73	C	69.76
Na	2.78	O	13.92
S	**4.25**	Si	0.18
Cl	4.68	**S**	**15.96**
Ca	0.56	Cl	0.17

Figure 6.22 ESEM images and EDX semi-quantitative analysis of solids filtered from the first oxygen poisoning test (air injection)

The second oxygen poisoning test was limited to the injection of a slightly aerated 1M HCl (initially de-oxygenated HCl exposed to air for 30 min) to adjust the pH of the aqueous sulphide solution to ~ pH 6.5. The concentration of dissolved oxygen in HCl was not initially measured. Figure 6.23 shows the depletion of both dissolved ions' concentrations throughout the test duration. The highest level of dissolved oxygen was noticeably lower than that observed in the test of oxygen poisoning by air injection, 38 and 168 µg/L, respectively. Nonetheless, the rate of aqueous sulphide depletion was remarkably faster, at almost double the rate, reaching 0.0248 mMol/min (0.84 mg/L.min) in the first 103 minutes. This high depletion rate was followed by a slower rate of 0.00284 mMol/min (~0.1 mg/L.min), similar to that of the first test, over the next 21.5 hours. The reaction was stopped once the dissolved oxygen level reached a plateau at ~ 4 µg/L.

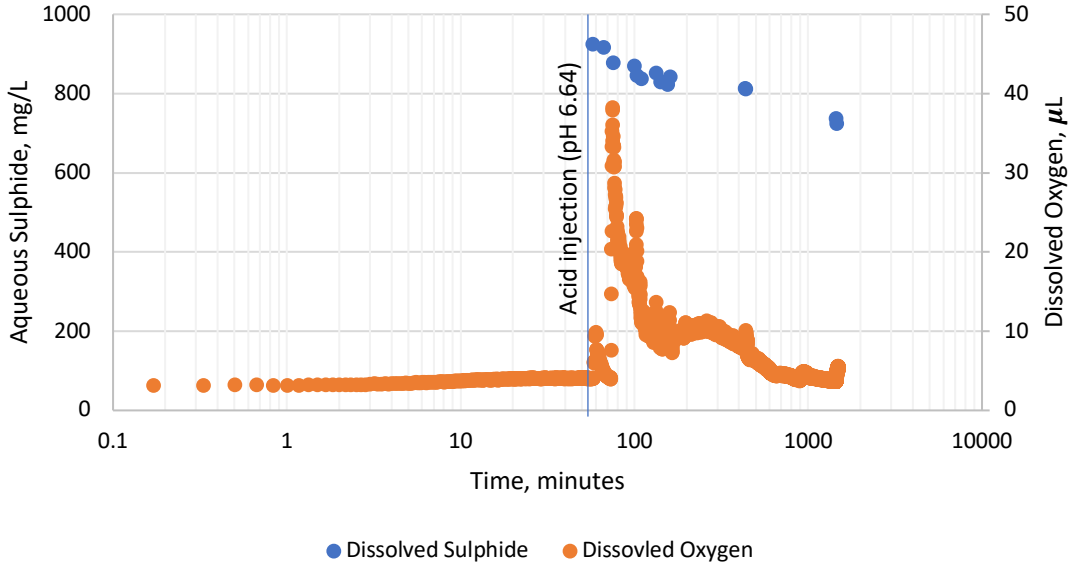

Figure 6.23 Oxygen poisoning of an anaerobic sulphide solution (***pH$_f$ 6.64***) through injecting air which is represented by the sharp and steady reduction rates of oxygen and sulphide concentrations, respectively

The filtered solids were analysed by ESEM-EDX to identify the main elemental components, and Figure 6.24 shows the image and the semi-quantitative analysis of the solids. The sulphur was a substantial component of the formed solids, which confirmed the formation of elemental sulphur at the test conditions. Both oxygen poisoning tests showed similarities to the first dynamic oxidation test of aqueous sulphide solutions in Figure 6.17.

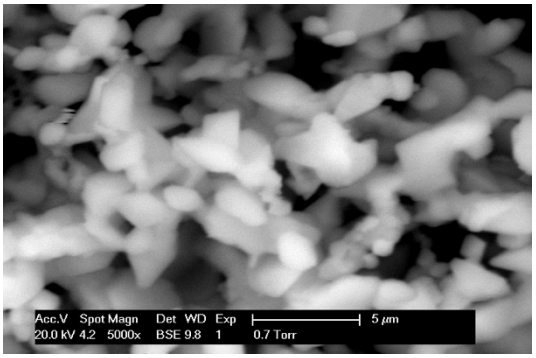

5,000x magnification

Element	Atomic%
O	33.92
Na	0.43
Si	0.19
S	**64.19**
Cl	1.27

Figure 6.24 ESEM images and EDX semi-quantitative analysis of solids filtered from the second oxygen poisoning test (aerated HCl injection)

6.5 Conclusions and recommendations

The new anaerobic test setup was used to perform static and dynamic (stirring) tests to investigate the oxidation of aqueous sulphide due to the exposure to oxygen. The main observed oxidative product was elemental sulphur, manifested as white turbidity forming in solutions of sulphide concentrations higher than 1.2 mM (~ 40 mg/L of $H_2S_{(aq)}$) and at ~ pH ≤ 6. The formation of sulphate as an oxidative product was not confirmed at the investigated conditions. The concentration of aqueous sulphide experienced different depletion behaviours, potentially governed by the test conditions, and the highest rates were observed in 100 and 1,000 mg/L sulphide solutions at pH 6.42 and 6.64, respectively. Based on the findings of these static and dynamic (stirring) oxidation tests of aqueous sulphide solutions, the following conclusions were drawn:

(i) The effect of oxygen on aqueous sulphide brines in oilfield sulphide scale tests was investigated at variable pH values and sulphide concentrations using the developed anaerobic static test setup.

(ii) The primary interference of sulphide oxidation can be the formation of elemental sulphur, which was similar to the formation of ZnS.

(iii) The decrease in sulphide concentration due to oxidation was found to be marginal (up to 10 %) in short test durations (< 2 hours) yet the continuous

decrease in sulphide levels may impact more extended tests (up to 35% after 24h).

(iv) Tests where the aqueous sulphide is the limiting reactant could be affected by the decrease in sulphide levels, while it can be negligible in sulphide-excess tests.

Based on these findings and conclusions, the de-oxygenation of aqueous sulphide solutions was generally recommended to avoid interferences, such as the formation of elemental sulphur, and the depletion of aqueous sulphide in sulphide-deficient solutions.

7 – Formation of FeS

Executive Summary

The experimental setup described in Chapter 5 showed advantageous features in terms of retaining sulphide concentrations and repeatable pH adjustment of sulphide brines. Therefore, various iron sulphide scaling tests have been conducted using the newly developed anaerobic setup to verify its effectiveness. Varying the sulphide excess has showed an effect on the formation of FeS, which was further confirmed using a scale prediction model developed within FAST. The formation of zinc and lead sulphide has been also investigated and compared the prediction data. Long exposure of formed iron sulphide has been observed to change in terms of Fe:S molar ratio as well as the crystal structure. These findings were further investigated in Chapter 8 through the inhibition tests of FeS.

7.1 Introduction

The triggers of sulphide scale formation are primarily the mixing of two or more fluids each containing either a scaling cation (Fe^{2+}, Zn^{2+} and Pb^{2+}) or anion ($H_2S_{(aq)}$, HS^- and S^{2-}), or the changes of conditions occurring to a single fluid containing both scaling ions, such as the decrease in pressure. The formation of sulphide scales by mixing two fluids has been investigated in the literature, as reviewed in Section 2.2, through static and dynamic tests. However, the formation of sulphide scale in a single fluid, also referred to as ***autoscaling***, was rarely investigated in the literature, to the best of the author's knowledge. The autoscaling of sulphide scale, unlike carbonate scale for example, is not common given the extreme low solubility which often drives the reaction towards instant formation of the solid sulphide scale. However, the autoscaling profiles could be used as solubility trends at various pH values and conditions, which aids the understanding of the formation of such scales.

The main complications of investigating the autoscaling of metal sulphide involved the preparation of the test solutions, where both scaling ions should co-exist at equilibrium without forming the sulphide scale. Such co-existence required lowering the pH of the solution, which needed either dissolving sour gases, CO_2 and H_2S, in the liquid phase as in field conditions, or acidifying the solution in investigative laboratory tests. Both routes were considered unfavourable due to the associated health risks and the experimental uncertainty of the conventional glass bottle tests discussed in Section 3.2. Therefore, the

autoscaling of metal sulphide (FeS, ZnS and PbS) solutions was investigated using the new anaerobic static test setup, described in Chapter 5. The analytical techniques used in these tests included the UV-Vis spectrophotometric technique, described in Chapter 4, and ICP-OES to determine aqueous sulphide and total iron concentrations, respectively, and pH meters. These autoscale profiles were compared and validated against theoretical patterns generated using a sulphide scale prediction (concentration) model. This model has been developed by and described in details by Silva (2017) in his PhD thesis.

The investigation of FeS formation involved autoscaling profile determination and the extended exposure of FeS to aqueous sulphide to identify changes in S:Fe ratio of the formed scale. These changes were determined by ESEM-EDX analysis of the samples extracted at different time steps. The autoscale profiles were established for each specific set of conditions, which included the concentrations of ferrous iron, zinc and lead, and aqueous sulphide and brine composition. Afterwards, the determined autoscale profiles were compared to theoretical results generated using a sulphide scale prediction (concentration) model.

7.2 Autoscale Profiles of FeS

The reaction between aqueous sulphides and iron, zinc and lead has been described extensively in the literature. These reactions have been reported in various forms depending on the conditions and existing sulphide species and metal forms (iron in particular). For iron sulphide, the simplest form of this reaction is:

$$Fe^{2+} + S^{2-} \rightleftharpoons FeS_{(s)} \tag{7.1}$$

where ferrous iron reacts with sulphide ion to form and precipitate iron sulphide solids. Because the speciation constant for S^{2-} has been reported to be extremely low $K_2 = 1 \times 10^{-17}$ (Okocha, 2011), and is difficult to quantify experimentally (Rickard and Luther, 2007), the other two equivalent forms of the above reaction would be:

$$Fe^{2+} + HS^{-} \rightleftharpoons FeS_{(s)} + H^{+} \tag{7.2}$$

$$Fe^{2+} + H_2S \rightleftharpoons FeS_{(s)} + 2H^{+} \tag{7.3}$$

In both reactions, iron sulphide is formed, while releasing protons into solution, and, subsequently, lowering the pH. Pinpointing which sulphide species reacts with iron, or whether it is a collective reaction, has been highly debatable in the literature. Regardless, the objective of this work was to investigate experimentally and theoretically the autoscale formation of FeS, ZnS and PbS at various conditions.

The sulphide solutions used in these experiments were prepared in 3.5 wt. % NaCl (equivalent to NSSW), in Khuff formation water, or Khuff Na & Ca brines. Iron, zinc, and lead were then added to 100 – 1,000 mg/L sulphide solutions at low pH, achieved by adding calculated volumes of 1M HCl. At this point, all cations should be dissolved in solution, and, theoretically, no solids should form. Then, the pH was raised by adding specific volumes of NaOH to reach target pH levels in each experiment. As the pH was increased, the formation of PbS, ZnS, and FeS was observed. Each of these scales has a specific range of reported values of its formation constant, and each range is different than the other by multiple orders; hence, they were expected to form over different pH ranges. The final solutions were filtered, measured for their respective pH values, and analysed for cation and sulphide concentrations, using ICP and UV-Vis spectrophotometric techniques, respectively. The analytical results were plotted as cation/anion concentrations. Experimental results were subsequently compared to theoretical results from the scale prediction model.

7.2.1 Autoscaling of FeS at Various Sulphide-to-Iron Concentration Ratios

Preliminary results of FeS formation at variable sulphide and iron concentrations are plotted in Figure 7.1, which shows different sets of (100, 200 and 1,000 mg/L) sulphide and (25 and 50 mg/L) iron (II) in 3.5 wt. % NaCl brine. These concentrations were chosen to demonstrate different molar ratios of sulphide to iron, and throughout all samples, the total sulphide was always in excess (from ~3.3 to 65 folds of sulphide to iron) to ensure the full consumption of iron through FeS precipitation. In these samples, however, dissolved iron was consumed at various levels, depending on the total sulphide concentration and the pH value. The behaviour of these sets of samples suggested that the formation of FeS was influenced by factors besides its solubility at tested pH levels. The primary evidence for such a claim was the presence of varying dissolved iron concentrations in the same range of pH values, i.e. pH 4.6 to 5. Theoretically, iron should have been consumed given the excess of sulphide concentration. Similar results were observed in the direct formation of FeS described in Appendix E.

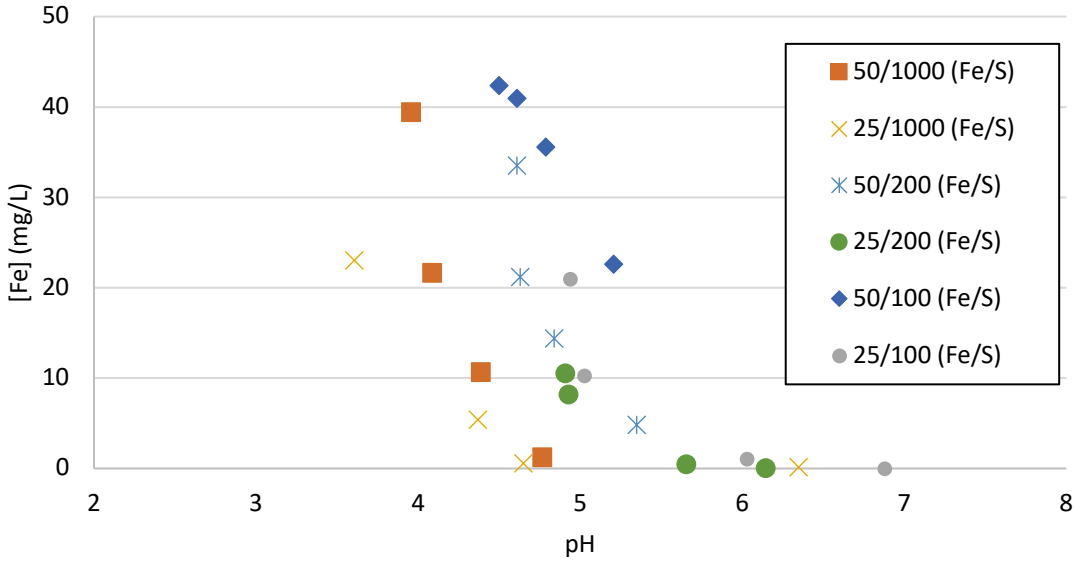

Figure 7.1 Autoscale (solubility) profiles of FeS in 3.5 wt. % NaCl at various total sulphide concentrations (1,000, 200 and 100 mg/L) and iron (II) concentrations (25 and 50 mg/L) at room temperature as a function of pH

Figure 7.1 shows that as the pH increased, the aqueous Fe^{2+} concentration was depleted from solution due to $FeS_{(s)}$ formation. The pH values at which iron depletion took place varied with the initial iron and sulphide concentrations. At $[S^{2-}]_{i,\ total}$ = 1,000 mg/L samples, the dissolved iron was completely consumed from solution at pH 4.65 and 4.77 for $[Fe^{2+}]_i$ = 25 and 50 mg/L, respectively. At similar pH values and 100 and 200 mg/L of total S^{2-}, the concentrations of iron in solution were between 50 and 85% of the initial concentration. For these samples, total consumption/deposition of iron (as FeS) was not observed until pH 5.66 and above.

At any given set of conditions, the solubility product (K_{sp}) of iron(II) sulphide should remain constant. Based on the simplified form of the FeS formation reaction (Equations 7.1 – 7.3), $FeS_{(s)}$ should start to form once the product of $[Fe^{2+}][S^{2-}]$ is equal to or greater than the reported value of $K_{sp,\ FeS}$. The sulphide species can be used interchangeably in the calculation of the solubility product using the speciation constants. Since the pH and the concentrations of iron and aqueous sulphide were known, H_2S could be used to calculate the solubility product. In addition, Rickard (1989) suggested that the reaction rate between iron and sulphide is dependent on bisulphide, as the rate increased with increasing pH. Moreover, H_2S and HS^- are the most abundant sulphide species in the

oilfield conditions (Przybylinski, 2001). Therefore, representing aqueous sulphide in terms of HS^- and H_2S in the solubility product calculations might be more appropriate. Below are the steps followed to substitute $[S^{2-}]$ with $[H_2S]$:

$$K_1 = \frac{[HS^-][H^+]}{[H_2S]} \tag{1.2}$$

Rearranging the equation to find $[HS^-]$:

$$[HS^-] = K_1 \times \frac{[H_2S]}{[H^+]} \tag{7.4}$$

$$K_2 = \frac{[H^+][S^{2-}]}{[HS^-]} \tag{1.4}$$

Rearranging the equation to find $[S^{2-}]$:

$$[S^{2-}] = K_2 \times \frac{[HS^-]}{[H^+]} \tag{7.5}$$

Substituting the value of $[HS^-]$ in the last equation yields:

$$[S^{2-}] = K_2 \times \frac{[K_1 \times \frac{[H_2S]}{[H^+]}]}{[H^+]} = \frac{K_1K_2\,[H_2S]}{[H^+]^2} \tag{7.6}$$

Through these substitutions, $[H_2S]$ can be used to calculate the solubility product of FeS. For example; at pH 4.63, where $[Fe^{2+}]$ = 0.379622 mMol, $[H_2S_{(aq)}]$ = 4.4852 mMol, and given that $[H^+] = 10^{-pH}$:

$$K_{sp,FeS} = [Fe^{2+}][S^{2-}] = [Fe^{2+}]\frac{K_1K_2\,[H_2S]}{[H^+]^2} =$$

$$[0.000379622]\frac{(9.632 \times 10^{-8})(1.0 \times 10^{-17})\,[0.0044852]}{[10^{-4.63}]^2} = 2.79027 \times 10^{-21} \tag{7.7}$$

This value, two orders lower than the reported $K_{sp,\,FeS}$ value of 1.29×10^{-19} (Okocha, 2011), represented the formation constant at equilibrium after precipitating nearly 28 mg/L of iron from solution. At such low calculated K_{sp}, iron sulphide theoretically should not

form, yet approximately 44% of the initial iron concentration was consumed. It has been hypothesised that this discrepancy in the K_{sp} value could be related to the high TDS of the solution, which might have resulted in reducing the solubility of FeS, hence the consumption of iron at a K_{sp} value lower than the literature value. This explanation is in agreement with the reported formation of FeS at pH values as low as pH 2 in spent acid solutions in the presence of excess H_2S (Crowe, 1987). Based on the previous calculations, Equations (7.4) – (7.6), the various total sulphide concentrations in these samples, at any specific pH value, provided different *reactive* aqueous sulphide to react with Fe^{2+}.

7.2.2 FeS Autoscaling Profiles at Fixed Iron concentrations

The autoscaling test was repeated multiple times, using more samples and sulphide concentrations, and various brines, to confirm this phenomenon. The initial total sulphide concentrations in the repeated tests were 100, 200, 500, and 1,000 mg/L, while iron concentration was fixed at 50 mg/L. The molar ratios of total sulphide to iron were ranging from 3:1 to 30:1 across the tested concentrations. However, having total sulphide concentrations in excess to iron did not necessarily ensure the total consumption of iron, as was observed in Figure 7.1, as the pH had a significant influence. The brines in the repeat tests were made from 14.9 wt. % sodium chloride and 4.2 wt. % calcium chloride, which represented a simpler version of the Khuff formation water (Khuff Na & Ca: similar TDS using only NaCl and $CaCl_2$). The tests were carried out in duplicates to ensure data precision and experimental repeatability. The following plots, Figure 7.2, Figure 7.3, Figure 7.4, and Figure 7.5, show the duplicate sets of samples, which will be combined later for simplicity. The pH was measured immediately after the test completion by removing the Hungate-type tube cap and carefully decanting the fluid content into a 30 mL beaker. Tests conducted using 40mL vials were pH-measured inside the vial by just removing the cap and inserting the probe into the first third of the liquid level (See Appendix F). Small errors could be introduced through the pH measurement, nonetheless, these errors were consistent throughout the tests.

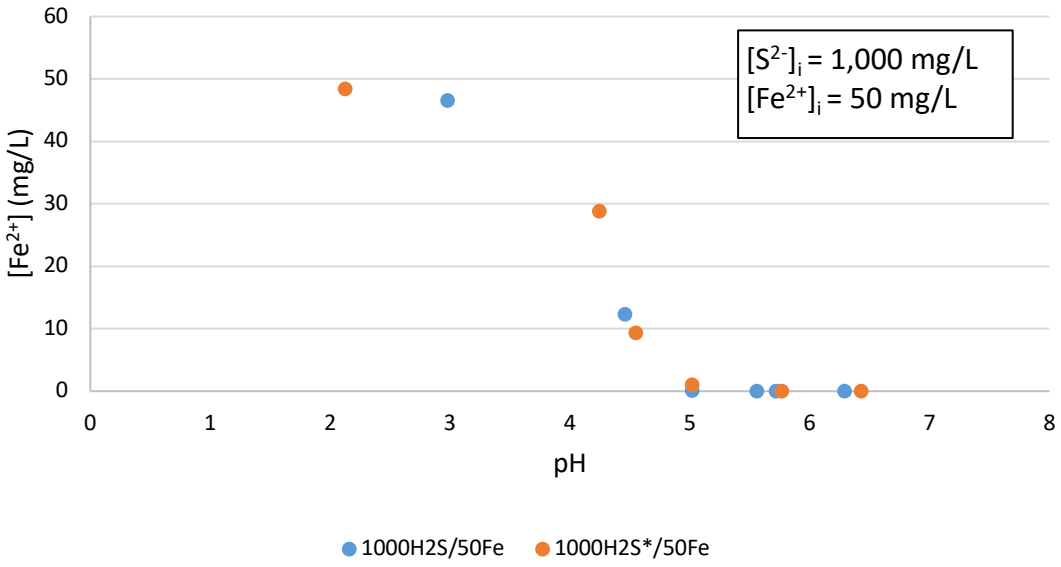

Figure 7.2 Duplicates of FeS (1,000/50 mg/L) autoscale profile as a function of pH at room temperature using Khuff Na & Ca brine

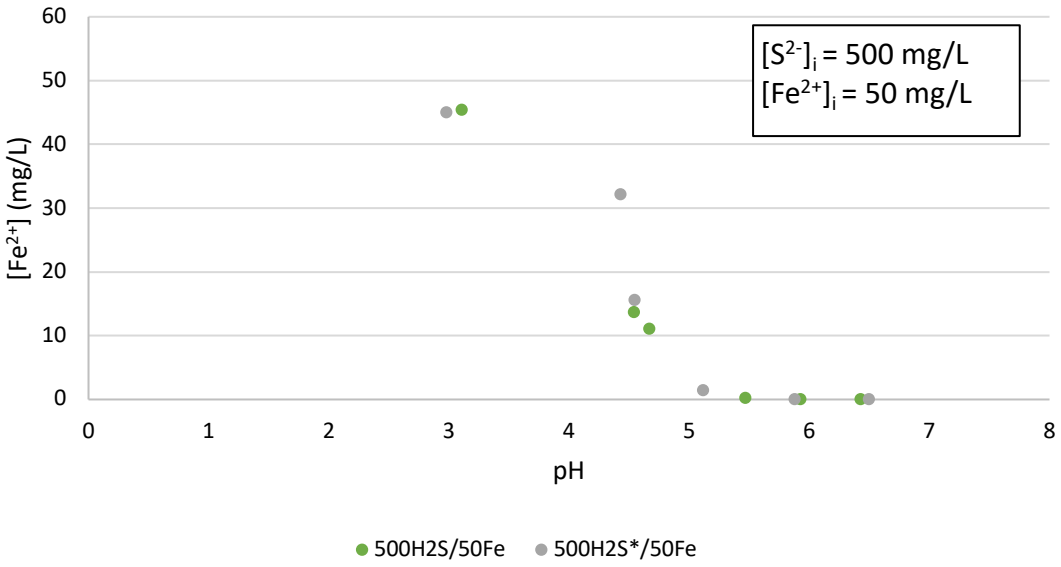

Figure 7.3 Duplicates of FeS (500/50 mg/L) autoscale profile as a function of pH at room temperature using Khuff Na & Ca brine

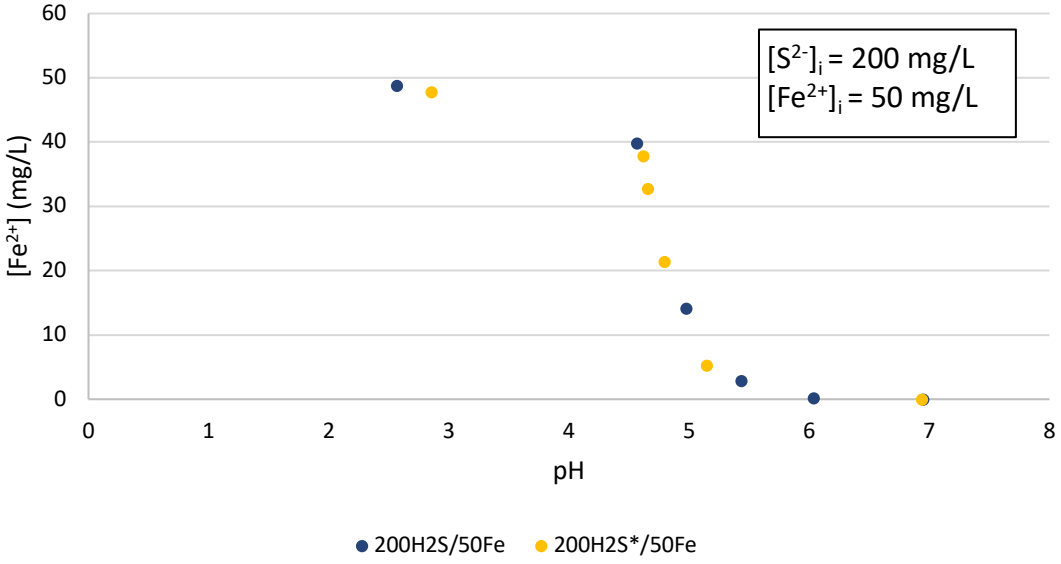

Figure 7.4 Duplicates of FeS (200/50 mg/L) autoscale profile as a function of pH at room temperature using Khuff Na & Ca brine

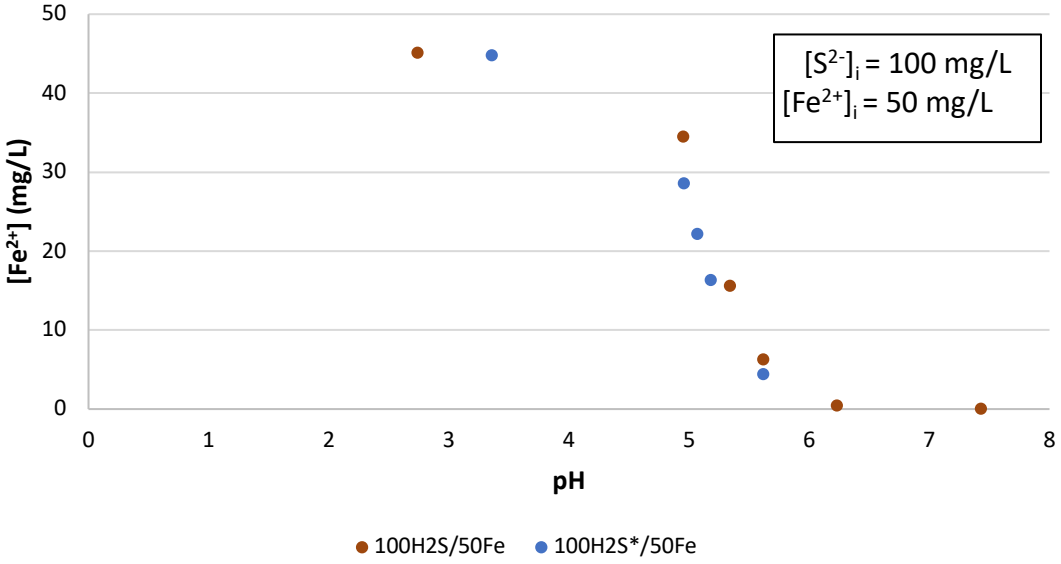

Figure 7.5 Duplicates of FeS (100/50 mg/L) autoscale profile as a function of pH at room temperature using Khuff Na & Ca brine

The plotted data show an excellent match between the duplicate samples and, given that the conditions were the same, these data were combined to achieve comprehensive profiles (Figure 7.6). The initial scale formation was distinct for each combination of H_2S-to-Fe ratio, with the 1,000 mg/L of aqueous sulphide showing a 40% drop in iron

concentration at pH 4.25, while the same drop was observed at pH 4.43, 4.66 and 4.96 for the 500, 200 and 100 mg/L of aqueous sulphide concentrations, respectively. This behaviour demonstrated the effect of varying total sulphide concentration, as the reaction was more favourable at higher sulphide concentration, which could be explained by the following equation:

$$[S^{2-}] = K_2 \times \frac{[K_1 \times \frac{[H_2S]}{[H^+]}]}{[H^+]} = \frac{K_1 K_2 [H_2S]}{[H^+]^2} \quad (6.8)$$

As the pH decreased, the concentration of protons increased $[H^+] = 10^{-pH}$, which decreased $[S^{2-}]$, and consequently lowered the product of $[Fe^{2+}][S^{2-}]$ below the K_{sp} value. However, the increased $[H_2S]$ counterbalanced the decrease in pH and allowed for FeS formation at such low pH. On the other hand, lower $[H_2S]$ excess required higher pH, or lower concentrations of hydrogen protons, to reach enough $[S^{2-}]$ to form FeS.

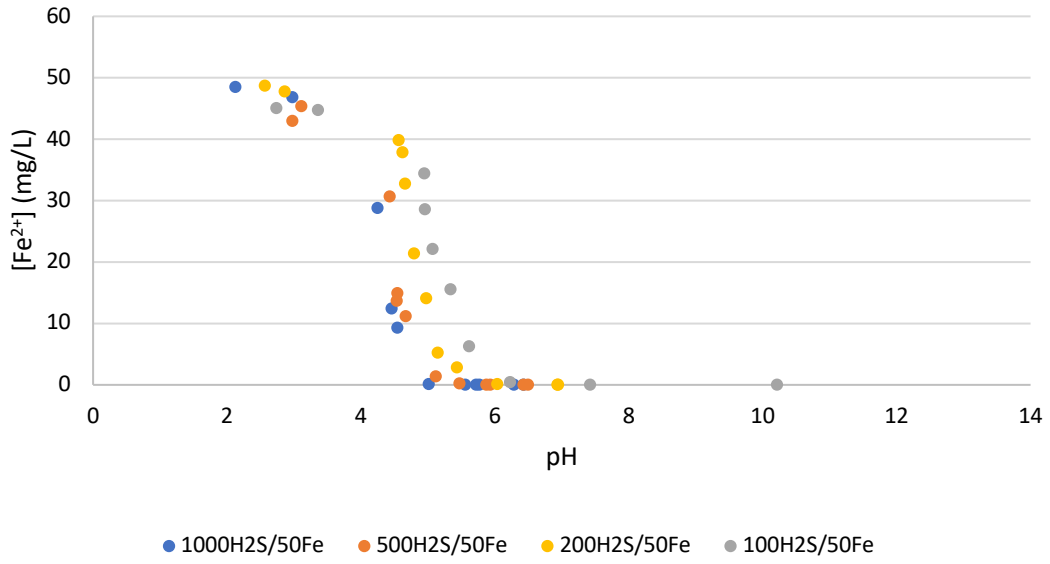

Figure 7.6 Combined FeS autoscale (solubility) profiles as a function of pH and aqueous sulphide concentration in Khuff Na & Ca brine at room temperature

The combined data sets for each H_2S:Fe ratio were plotted together to elaborate the different scaling trends. Figure 7.6 shows these variations in scale profiles. At any given pH value below pH 6, only a fraction of the total sulphide concentration reacted with iron, which was a function of pH and initial sulphide concentration. The dominant sulphide concentration at acidic pH is $H_2S_{(aq)}$, with a small percentage of HS^- and traces of S^{2-}. The

speciation of H_2S in aqueous solutions was modelled using the dissolution reaction rates, and the speciation of sulphides in aqueous solution was shown in Figure 1.1. Furthermore, Rickard and Luther (2007) demonstrated the distribution of sulphide species by plotting their activities against pH (pH 4 to 10), as seen in Figure 7.7. As the actual concentrations of HS^- and S^{2-} increased in these samples, the product of $[Fe^{2+}][S^{2-}]$ was approaching the K_{sp} value, leading to the formation of FeS. The gap in pH values (pH 3.3 – 4.5) in Figure 7.6 was attributed to the extreme pH-sensitivity of the sulphide solution, and such range could be considered a shifting zone, where insignificant additions of HCl would cause substantial shifts towards lower pH values.

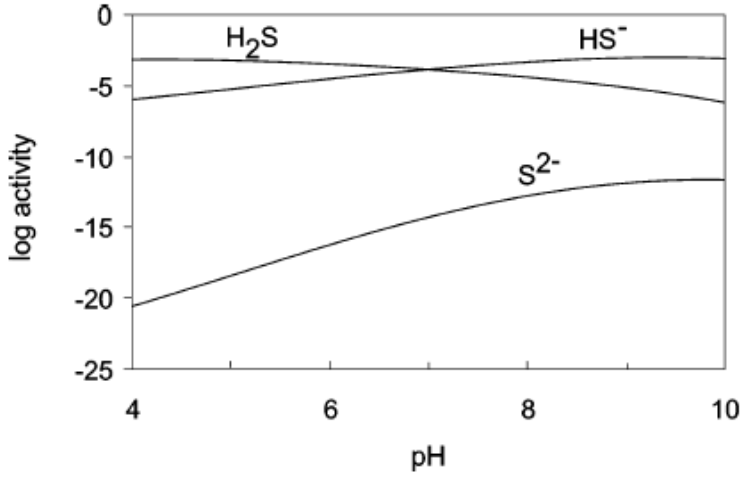

Figure 7.7 Distribution of aqueous sulphide species at $\{S^{2-}\}_T = 10^{-3}$ in terms of pH. (Rickard and Luther, 2007)

7.3 The Effect of Oxygen on the Formation of FeS

The effect of oxygen on the aqueous sulphide has been previously investigated in Chapter 6. The formation and inhibition studies of FeS are typically performed in an anoxic environment to avoid oxidising the ferrous iron to ferric. However, an excess of aqueous sulphide can prevent the formed iron (ii) sulphide from oxidising to iron (iii) sulphide. Therefore, a test of forming ferrous sulphide was carried out using an anaerobic iron chloride solution and an aerobic sulphide solution at low initial pH (pH < 3). The test aimed to determine the effect of dissolved oxygen on the formation of FeS in terms of particle size at various pH levels by adding NaOH.

The ICP analysis of supernatant solutions to identify the iron concentrations after forming FeS at various levels is shown in Figure 7.8. The profile followed a similar trend as the ones seen in Figure 7.6, and the filtration through a 0.2 μm filter showed a similar particle size dependence on the pH level. A further comparison between the FeS formed in the presence and the absence of oxygen in the sulphide solution is shown in Figure 7.9. The slight difference between the blue dots and the rest of the data sets was expected to be a result of the loss of the initial sulphide concentration as the elemental sulphur formed in the presence of oxygen.

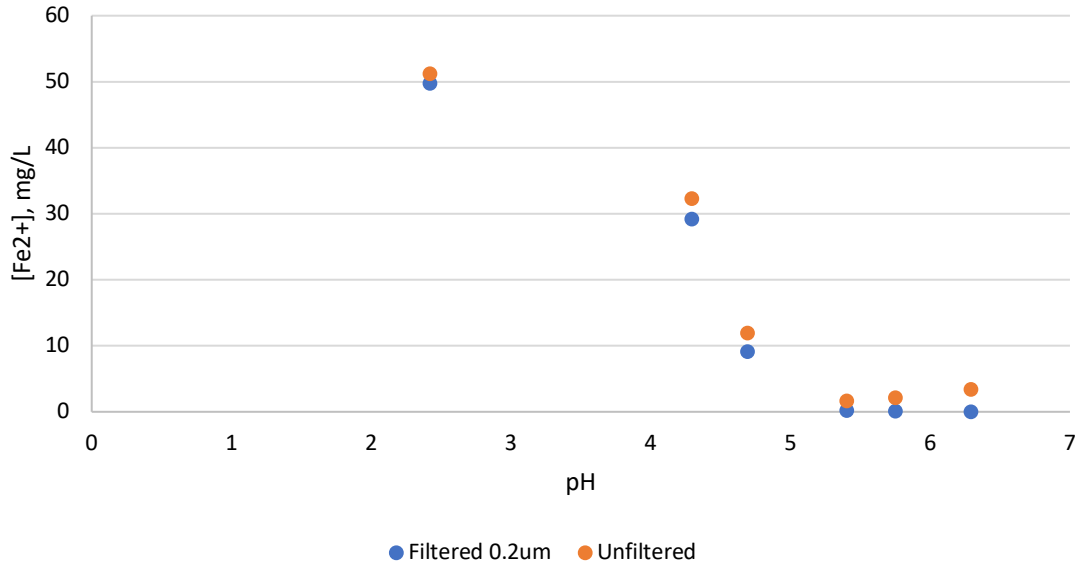

Figure 7.8 The autoscale profile of FeS at an aerobic aqueous sulphide solution ($[S^{2-}]_i$ = 1,000 mg/L and $[Fe^{2+}]_i$ = 50 mg/L)

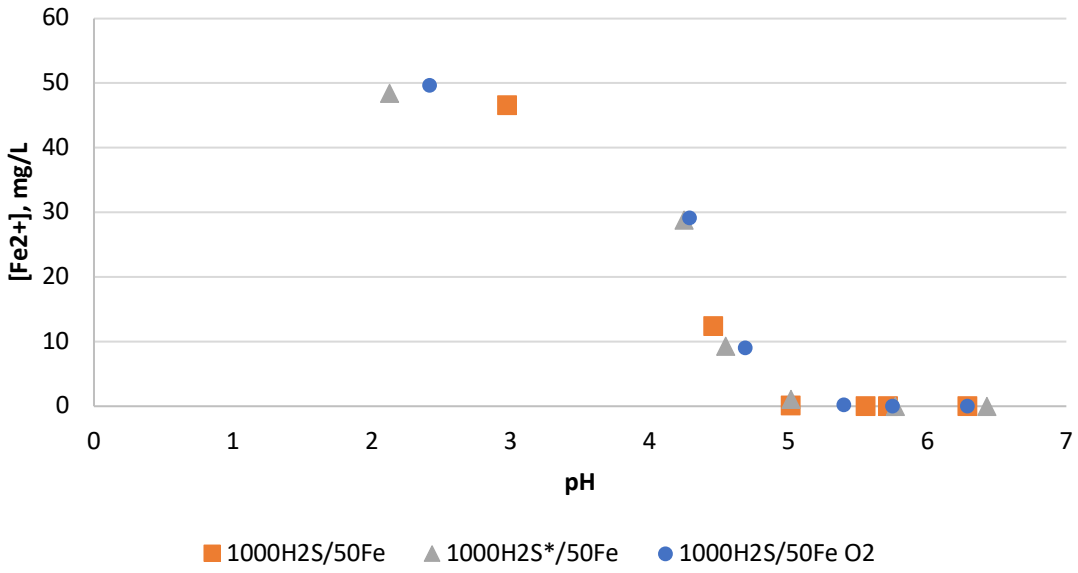

Figure 7.9 Comparing the autoscale profiles of FeS formed at anoxic and oxic conditions ($[S^{2-}]_i$ = 1,000 mg/L and $[Fe^{2+}]_i$ = 50 mg/L, Filtered)

7.4 Autoscale Profiles of ZnS, PbS and Combined Scales

Before describing the autoscaling profiles of ZnS and PbS, it is important to mention that lead acetate salt, which is used to prepare the lead brine, is very hazardous and must be handled with caution inside of fume cupboards. Lead acetate is considered irritant to the skin, respiratory and digestive systems, and may cause permanent eye damage upon contact. Chronic exposure to lead may cause blood effects and kidney damage, thus require frequent monitoring of blood health in a medical centre.

The autoscale profile was not limited to FeS, as similar behaviours were observed for ZnS and PbS. The Khuff Na & Ca brine was used for the autoscaling of ZnS and PbS; however, the trends were not as straightforward as it was for FeS. Since the formation constants for ZnS and PbS are significantly lower than that of FeS, their initial formation occurred at lower pH values, which can be observed in Figure 7.10 and Figure 7.11. The lowest data point for ZnS autoscale was at pH 2.22; nonetheless, at this point, nearly 25% of the initial zinc concentration was consumed to produce ZnS. However, a similar trend to FeS was observed from the latter pH upwards. The autoscale profile of PbS was not as well defined as FeS or ZnS, since dissolved lead was not seen at any sample starting from pH 1.7 upwards, suggesting that PbS forms below this pH value.

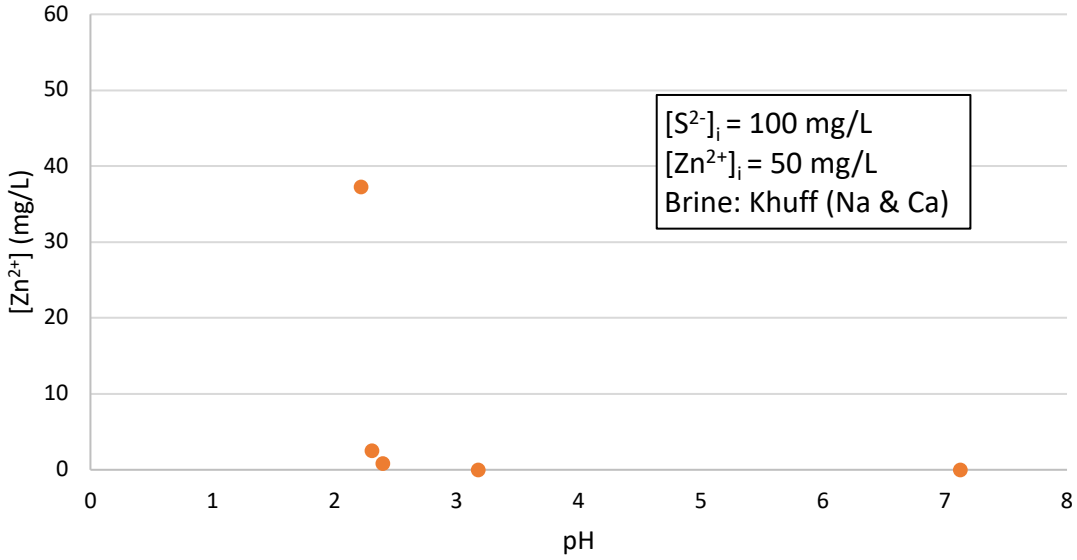

Figure 7.10 ZnS (100/50 mg/L) autoscale profile at room temperature using Khuff Na & Ca brine

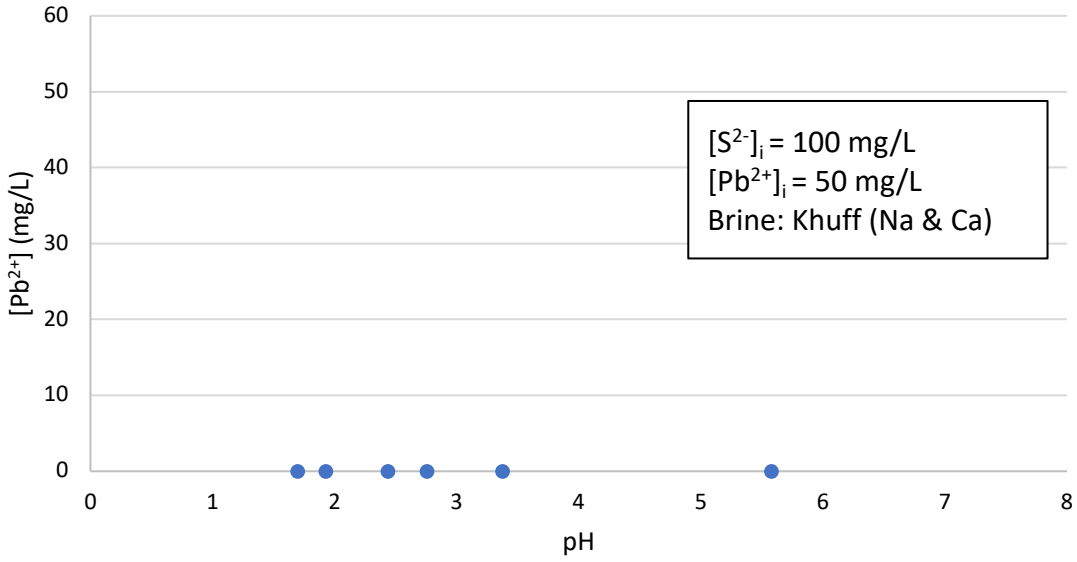

Figure 7.11 PbS (100/50 mg/L) autoscale profile at room temperature using Khuff Na & Ca brine

As the ICP analysis did not register any dissolved Pb^{2+} in solution, the test was repeated at harsher (lower pH) conditions, as seen in Figure 7.12, to provide an improved insight into the autoscale formation of PbS, although these conditions might not be realistic (except in the application of a very strong acid, e.g. in an acidisation treatment). The sulphide solutions were prepared by diluting 1,000 mg/L H_2S Khuff Na & Ca solution

into various concentrations of HCl (35, 17.5, 11.7, 8.8, 3.9, 1.9, 1.6, 1.2, and 0.8 wt.%). The lead stock solution (10,000 mg/L) was then added to these sulphide solutions to form PbS either immediately or after further addition of NaOH. The produced PbS autoscale profile was similar to that of FeS and ZnS yet starting at extremely low pH values. As seen in Figure 7.12, the initial formation of PbS began at a point between pH 0.76 and pH 1.01, and complete depletion of dissolved Pb was observed at pH 1.56.

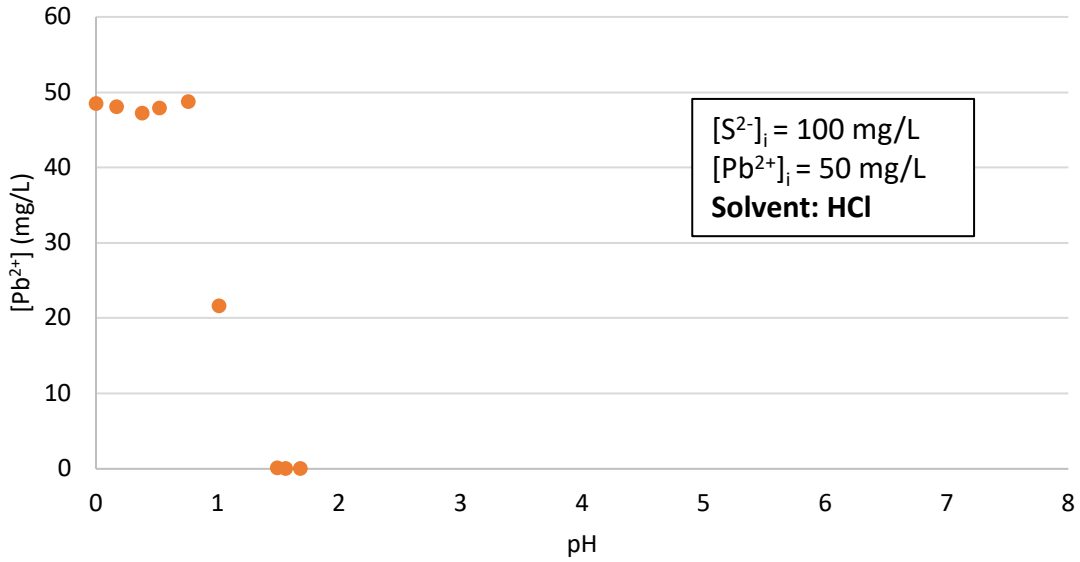

Figure 7.12 PbS (100/50 mg/L) autoscale profile at room temperature using different concentrations of stock HCl at room temperature to lower the pH to pH 0

After confirming the autoscale profiles of PbS, ZnS, and FeS separately, an autoscale test where all three scales were combined was performed, Figure 7.13. In this test, Khuff Na & Ca brine was used as the scaling solution, with 100 mg/L of sulphide initially at pH 1.14 (pH adjusted by adding HCl). The scaling cations were added from stock solutions to reach 50 mg/L of each (Pb^{2+}, Zn^{2+}, and Fe^{2+}). All solutions demonstrated immediate black solids formation after adding Pb^{2+}, whilst they had remained clear during the prior addition of Fe^{2+} and Zn^{2+}. Afterwards, various volumes of 1M NaOH were added to increase the pH. The highest pH achieved in this test was pH 4.99. The ICP analysis, in Figure 7.13, shows different levels of zinc and iron throughout the samples, whilst the lead was only present in trace concentrations. Plotting the concentrations against pH revealed the combined autoscaling profiles of PbS, ZnS, and FeS.

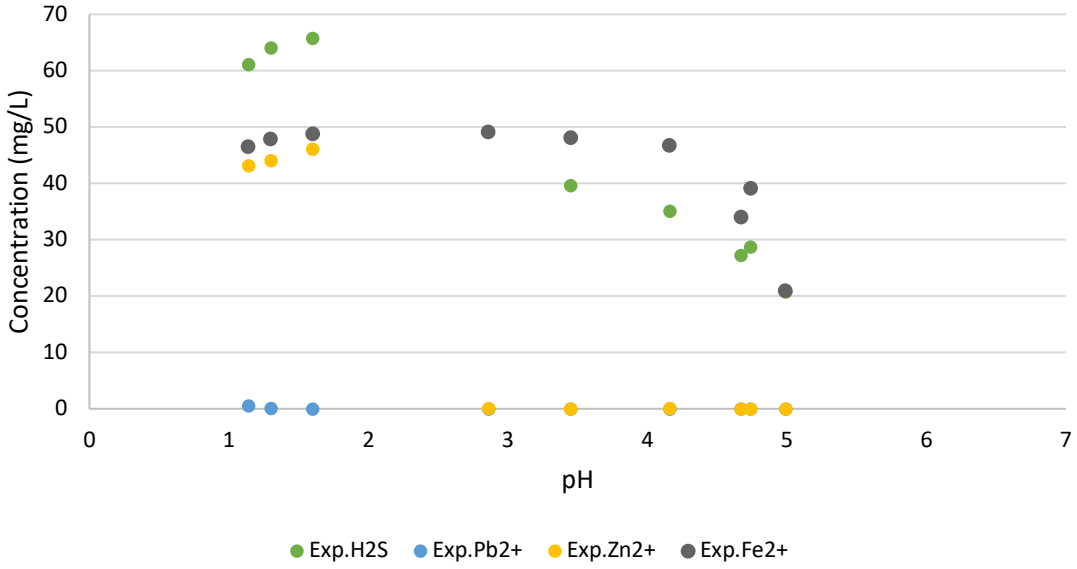

Figure 7.13 Autoscaling profiles of FeS, ZnS and PbS in Khuff Na & Ca brine represented as reactants' concentrations against pH values ($[M^{2+}]_i$= 50 mg/L, $[S^{2-}]_i$ = 100 mg/L)

Due to the lack of data point in specific ranges of pH, only FeS formations scenarios (individually or conjointly) were available for comparison, as seen in Figure 7.14. At pH 4.96, the FeS single scale solution contained 28.6 mg/L Fe, while it was 21 mg/L at pH 4.99 in the combined scaling solution. The difference in iron concentrations might reach 15% of the initial content. However, given these steep scaling profiles in this pH range, dramatic changes in concentrations could be observed over small changes in pH. It was systematically anticipated to find a scaling profile for FeS at a higher pH range in the combined scale solution, mainly as the concentration of sulphide was consumed during the formation of PbS and ZnS. However, overlapping both data sets revealed matching or even slightly lower pH scaling profile for the combined scale solution. Comparing ZnS and PbS single and combined scale formation did not contribute more than a general agreement, as seen in Figure 7.15 and Figure 7.16.

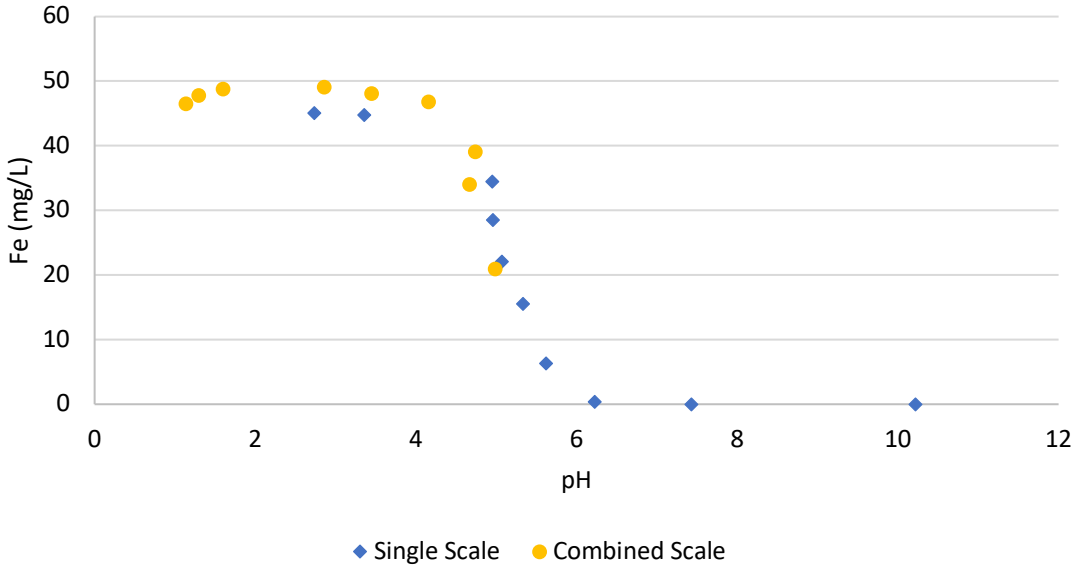

Figure 7.14 Comparison between the autoscaling profiles of FeS in single or combined scale solution in Khuff Na & Ca brine ($[Fe^{2+}]_i$= 50 mg/L, $[S^{2-}]_i$= 100 mg/L)

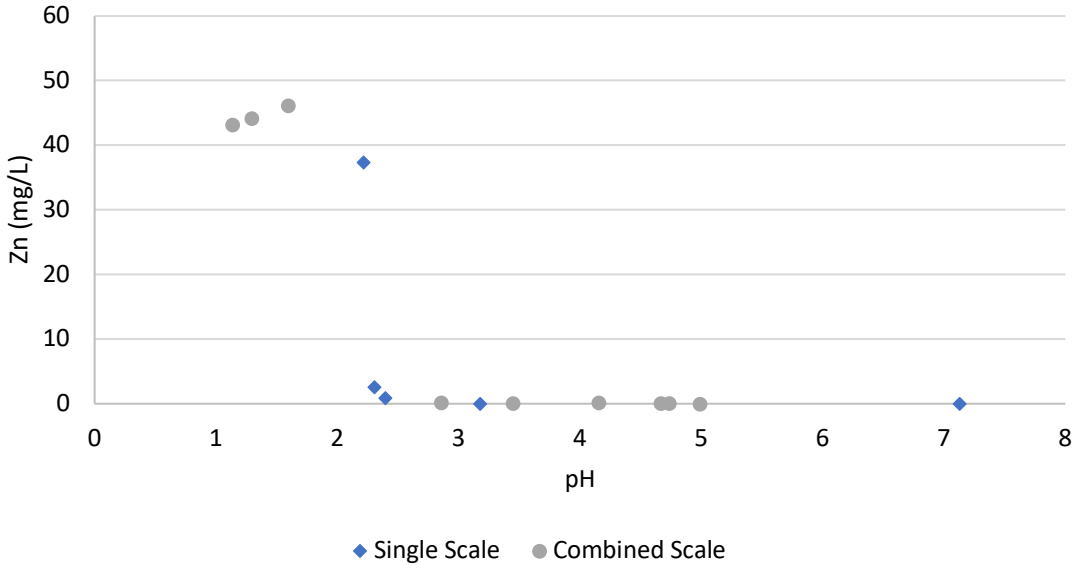

Figure 7.15 Comparison between the autoscaling profiles of ZnS in single or combined scale solution was inconclusive because of missing data points between pH 1.5 – 2.8 ($[Zn^{2+}]_i$= 50 mg/L, $[S^{2-}]_i$= 100 mg/L)

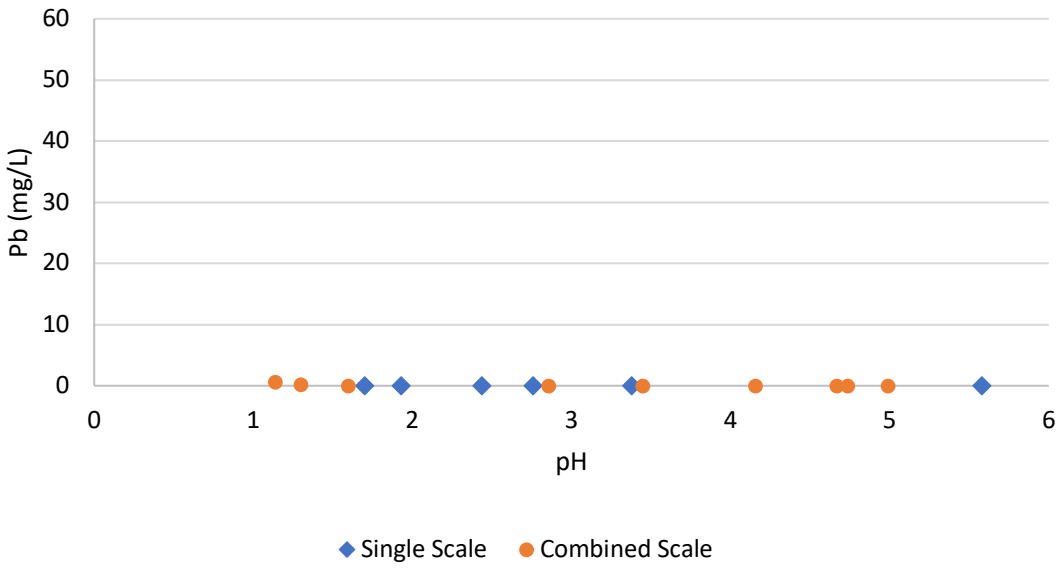

Figure 7.16 Comparison between the autoscaling profiles of PbS in single or combined scale solution both showing the extreme low solubility of PbS in brine at pH > 1 ($[Pb^{2+}]_i$= 50 mg/L, $[S^{2-}]_i$= 100 mg/L)

The experimental data shown in Figure 7.1 to Figure 7.16 provide evidence on the advantageous use of the newly developed anaerobic setup. The accurate pH adjustment of sulphide solutions, containment of H_2S, and isolation of oxygen were a critical set of features that ensured the reliable outcome for such sensitive tests. In addition, it was remarkable that these experiments were carried out on a bench-top setup (in a fume cupboard) without using anaerobic chambers or pressurised systems. A scale prediction model, discussed in the next section, was used to validate and clarify the autoscaling experimental data shown so far.

7.5 Experimental and Prediction Data Comparison

A prediction model was developed within FAST, Heriot-Watt University, which predicted the potential and mass of several oilfield scales including FeS, ZnS, PbS, and $BaSO_4$ (Silva, 2017). This model is based on finding solutions to a system of chemical equilibrium equations for the various reactions, charge and mass balance equations for the key species. Once this system is solved, an equilibrated output can be calculated using the reformed equation system to process the input data.

The model initially contained fixed (within the code of the model) solubility products values selected from the literature, which were essential to calculate the saturation ratios

and the scaling tendencies. The input data included the concentrations of various ions and initial pH value. The model calculated various potential solutions and produced the only converging (true) solution. The output was manifested in equilibrium values of a final pH, concentrations of ions in questions, masses of formed scales, and saturation ratios of all calculable scales. Figure 7.17 shows a screenshot of the model interface. The K_{sp} values used in this model for FeS, ZnS, and PbS were $K_{sp,\,FeS} = 8 \times 10^{-19}$, $K_{sp,\,ZnS} = 2.03 \times 10^{-25}$, *and* $K_{sp,\,PbS} = 3.80 \times 10^{-28}$. The autoscaling profiles could be generated, using this model, and compared to those obtained experimentally. The comparison of the prediction data to experimental results could provide validation of the model and analysis of the experimental results.

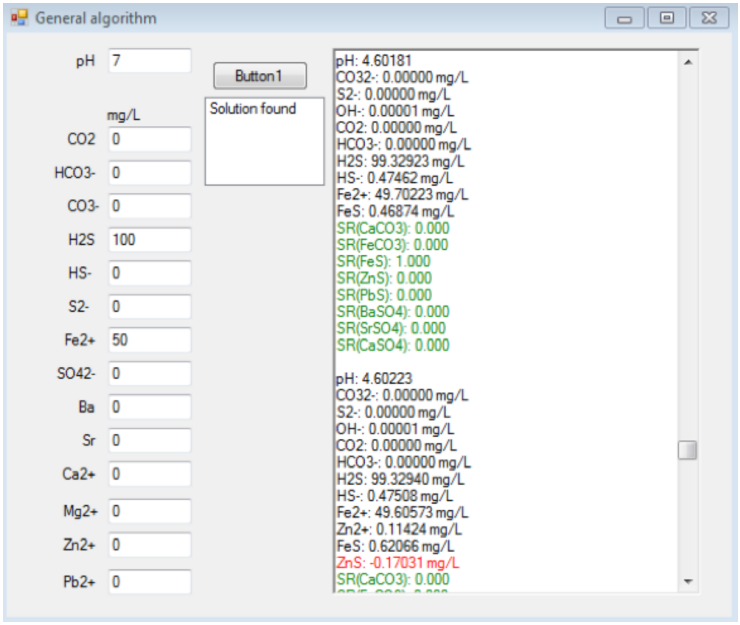

Figure 7.17 The interface of the scale prediction model showing the input fields and produced results

7.5.1 FeS Autoscale Profiles

The model was first used to predict the formation of FeS in Khuff Na & Ca brine, which contained 14,259 mg/L of Ca^{2+}, given that abundant experimental values were available from previous tests. The sodium concentration was not used as an input since sodium was considered to be inert to the scale formation process. Rigorously, the concentration of sodium, and other "inert" ions such as chloride etc., have an impact on the calculation of the activity coefficients, and thus on the system's thermodynamic equilibrium. However, the model makes the approximation that the species concentration equals their particular activity, and thus the sodium and chloride ions may be considered as "inert". Note that

the activity model based on the Pitzer equations (Pitzer, 1973) is currently being developed within FAST. Various initial pH values were used to initiate the iterations and find a converging solution representing all concentrations at equilibrium. Then, the predicted datasets were plotted with the experimental values against pH. Table 7.1 shows all the data points and initial pH inputs to produce such data. The initial sulphide concentration was set at 970 mg/L, which was the average of the measured concentration of the stock solution of the designed 1,000 mg/L, and iron's initial concentration was planned as 50 mg/L, while ICP analysis of stock solution registered 48 mg/L. This small variation in the initial concentration could help in correlating the experimental and predicted data more realistically than using designed experimental values.

Table 7.1 Scale prediction data for FeS in Khuff Na & Ca ($[Fe^{2+}]_i$ = 48 mg/L and $[S^{2-}]_i$ = 970 mg/L)

pH_i	pH_f	H_2S (mg/L)	HS^- (mg/L)	Fe^{2+} (mg/L)	FeS (mg/L)	$SR_{(FeS)}$
2	1.99998	969.98805	0.01159	48	0	0
3	2.99849	969.88096	0.11552	48	0	0.006
4.5	4.11324	968.45192	1.50239	48	0	0.993
4.9	4.11722	968.13268	1.51572	47.4994	0.78803	1
5	4.11755	968.08899	1.5168	47.42962	0.89787	1
6	4.1187	967.93669	1.52057	47.18693	1.27992	1
7	4.11882	967.92025	1.52099	47.16021	1.32198	1
8.5	4.11923	967.86689	1.52232	47.0751	1.45595	1
9	4.12011	967.75134	1.52522	46.89084	1.74601	1
10	4.13197	966.23048	1.56498	44.46833	5.55935	1
10.5	4.16315	962.57259	1.67512	38.66631	14.69255	1
10.7	4.19352	959.43724	1.79062	33.72876	22.46501	1
11	4.30241	950.91864	2.28045	20.61071	43.11504	1
11.1	4.38697	946.4067	2.75745	14.02985	53.47458	1
11.15	4.45487	943.65219	3.2147	10.29251	59.35791	1
11.25	4.73084	936.24907	6.02138	2.91064	70.97855	1
11.3	4.9788	930.33206	10.59011	0.93503	74.08861	1
11.5	5.65245	891.21123	47.85092	0.04387	75.4915	1
12	6.54158	658.35986	273.84261	0.00099	75.55901	1
12.3	7.19868	319.19553	602.83713	0.0001	75.56041	1
12.35	7.38378	236.23875	683.26973	0.00006	75.56048	1
12.4	7.65511	143.19145	773.56069	0.00003	75.56053	1
12.42	7.82016	102.8704	812.67168	0.00002	75.56054	1
12.44	8.07089	60.66111	853.61494	0.00001	75.56055	1
12.45	8.27525	38.82788	874.69777	0.00001	75.56056	1
12.46	8.65597	16.56031	896.39262	0	75.56057	1
12.47	10.30353	0.37934	912.06276	0	75.56057	1
12.5	11.36179	0.03317	911.93422	0	75.56057	1
13	12.84904	0.00108	912.39084	0	75.56057	1

The set of data in Table 7.1 was plotted to demonstrate the theoretical autoscaling profile, as seen in Figure 7.18. In this model run, the values of $[S^{2-}]$ were not recorded, as they

were less than 1 x 10^{-5}, while the current model version only showed five decimal places. From Table 7.1, the initial FeS formation was observed at pH 4.11, with H_2S, HS^- and Fe^{2+} equilibrium concentrations at 968.13, 1.51, 47.49 mg/L, respectively. Nearly 98% of the initial [Fe^{2+}] was consumed in the range between pH 4.11 and pH 4.97, after which the rate of FeS formation gradually decreased, as the concentration of [Fe^{2+}] decreased.

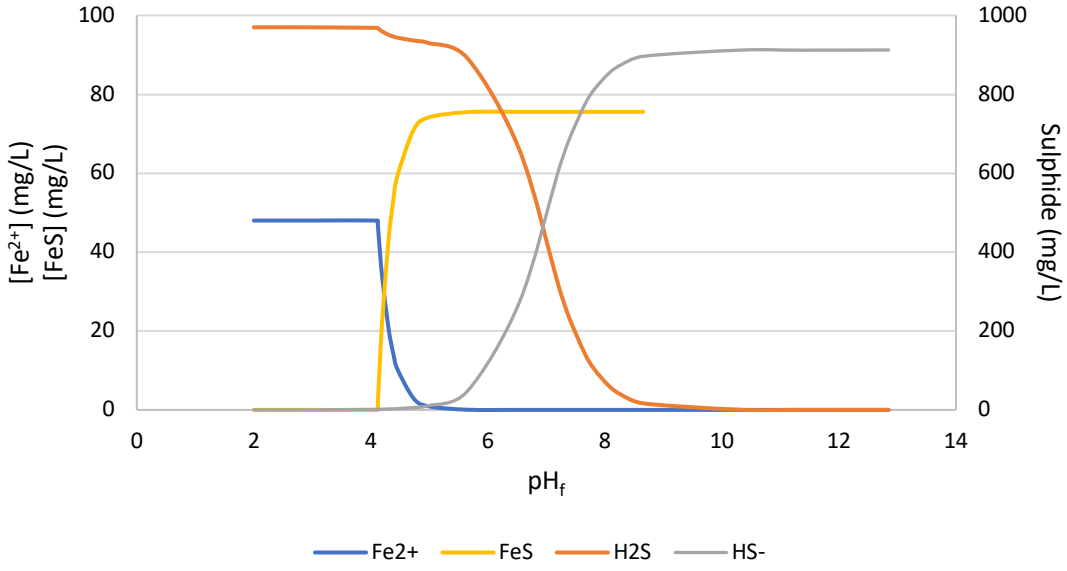

Figure 7.18 Plotted data from the scale prediction model listed in Table 7.1 ($[Fe^{2+}]_i$ = 48 mg/L and $[S^{2-}]_i$ = 970 mg/L)

Similar prediction runs were performed for total initial sulphide concentrations of 500, 200 and 100 mg/L, which were plotted in Figure 7.19, Figure 7.20, and Figure 7.21, respectively. These figures essentially revealed familiar trends, except for sulphide concentrations and the pH of the initial FeS formation. Since the formation of FeS is directly dependent on the concentration of one of the sulphide species (H_2S, HS^-, or S^{2-}) and pH, different autoscale profiles were produced.

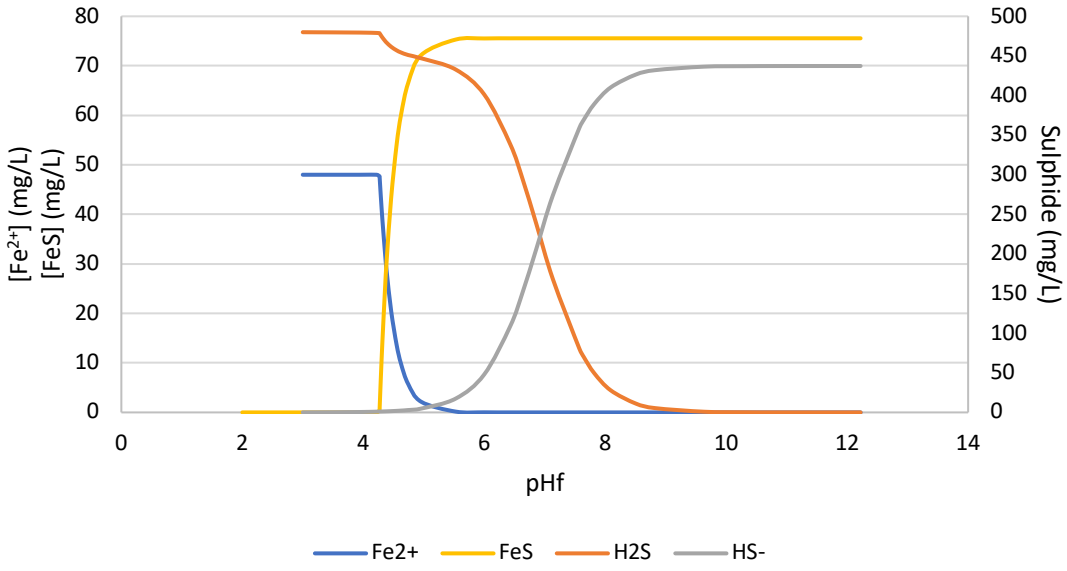

Figure 7.19 Plotted data from the scale prediction model ($[Fe^{2+}]_i$ = 48 mg/L and $[S^{2-}]_i$ = 480 mg/L)

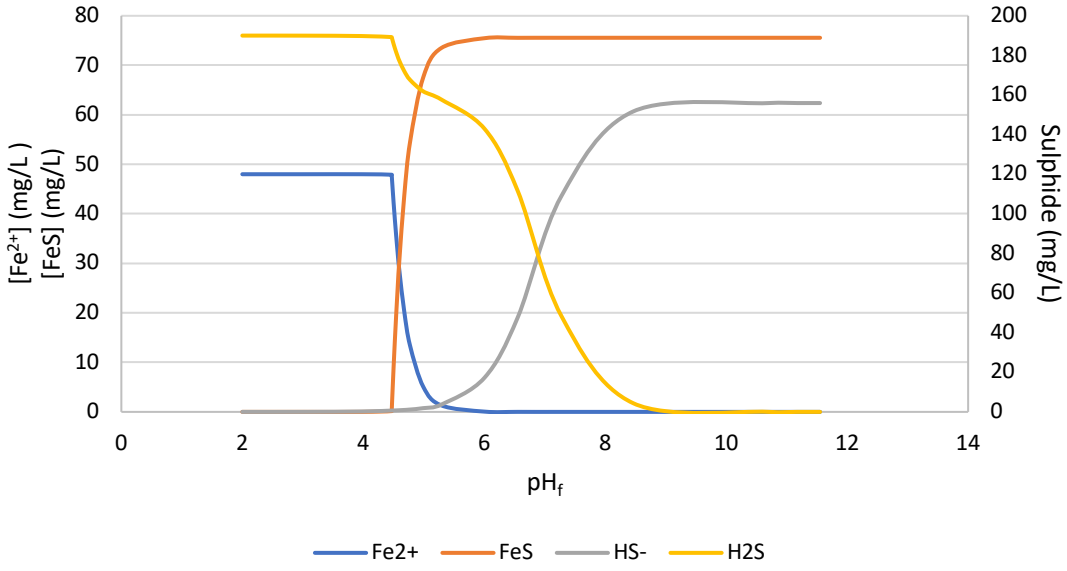

Figure 7.20 Plotted data from the scale prediction model ($[Fe^{2+}]_i$ = 48 mg/L and $[S^{2-}]_i$ = 190 mg/L)

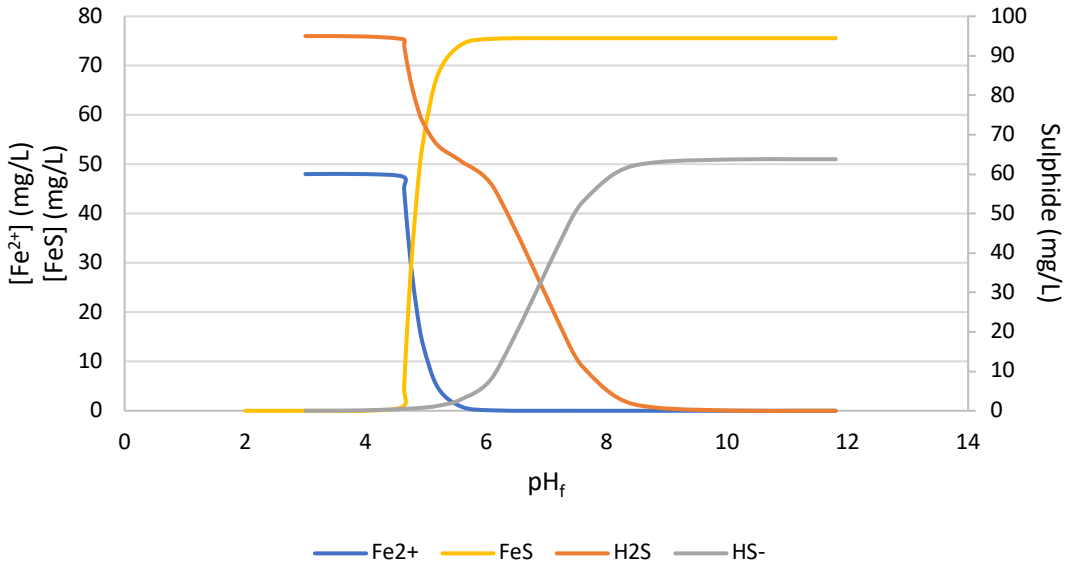

Figure 7.21 Plotted data from the scale prediction model ($[Fe^{2+}]_i$ = 48 mg/L and $[S^{2-}]_i$ = 95 mg/L)

The combination of the four autoscale profiles in terms of $[Fe^{2+}]$ against pH was plotted in Figure 7.22. As previously mentioned, the trends of dissolved iron depletion were similar yet spaced out by fractions of a pH unit. The pH difference between the initial FeS formation at 1,000 and 100 mg/L sulphide was nearly 0.51 of a pH unit. Another observation from the model data was the pH ranges at which most of $[Fe^{2+}]$ was consumed were varying from one set to another. Nearly 98% of $[Fe^{2+}]$ was depleted between pH 4.62 and pH 5.59 when 100 mg/L of initial sulphide concentration was used, compared to pH 4.11 and pH 4.97 for the 1,000 mg/L sulphide run. Such variation revealed the effect of initial sulphide concentration on the scale formation mass, which consequently might affect other scale properties such as particle size distribution.

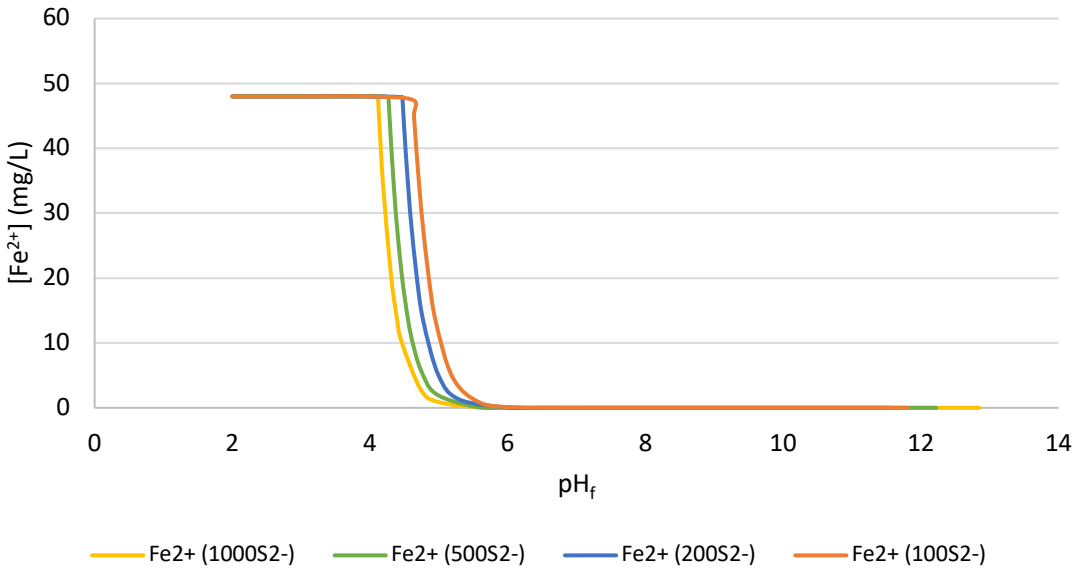

Figure 7.22 Prediction data of Fe^{2+} depletion during the FeS autoscale at various total sulphide concentrations showing different solubilities at pH 4 - 6

These autoscale profiles were directly compared to the experimental data obtained from the FeS autoscaling tests using Khuff Na & Ca brine. The experimental data in Figure 7.6, was overlaid on Figure 7.22 to produce Figure 7.23, which shows near-perfect matching for the 1,000, 500 and 200 mg/L sulphide sets, and shifted yet acceptable correlation for the 100 mg/L sulphide set.

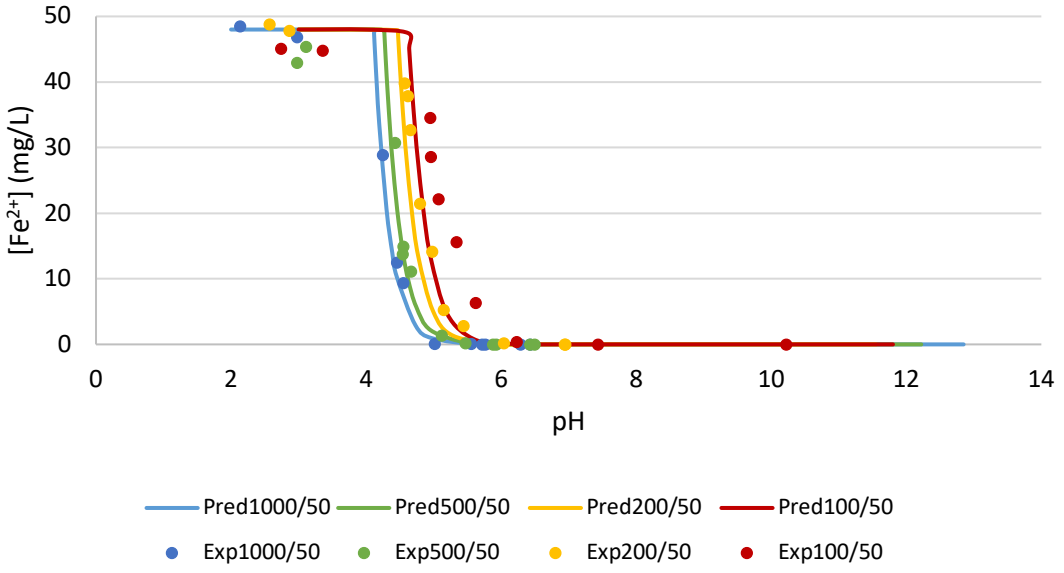

Figure 7.23 Experimental and prediction model data of Fe^{2+} depletion during FeS autoscale at various sulphide concentrations showing excellent agreement

This agreement between the prediction model and experimental data paved the way for further implementation for the model to represent theoretical data as a reference to which the experimental results could be compared. The complexity of the prediction runs could be varied to include different or multiple scales and compare the prediction data with the experiments discussed earlier in this section.

7.5.2 Direct FeS Formation vs FeS Autoscale

In an illustrative test was carried out to produce similar data points through the direct formation of FeS. The 10-mL aqueous sulphide solutions (1,000 mg/L) were pH-adjusted to various values between pH 4.26 – 5.93. The iron (II) chloride stock solution was added to create a final concentration of 50 mg/L of iron in solution. The supernatant solutions were analysed by ICP to determine the remaining iron concentration, as shown in Figure 7.24. The direct formation of FeS showed a slightly less solubility compared to the autoscale. Such behaviour was anticipated and could be justified by the mixing of two highly concentrated solutions, i.e. 1,000 and 5,000 mg/L of S^{2-} and Fe^{2+}, respectively, not necessarily following the designed test concentrations, i.e. 50 mg/L when completely diluted. Therefore, there could be a potential for forming iron sulphide in more forms than the equimolar composition FeS.

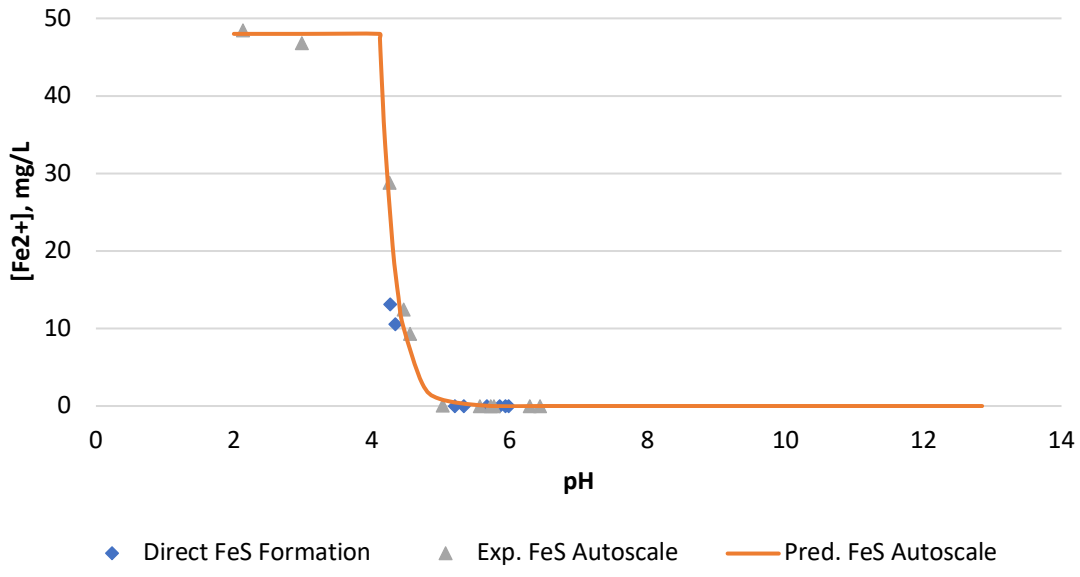

Figure 7.24 A Comparison between the direct formation and the autoscale of FeS at 1,000 mg/L of sulphide showing slightly lower solubility profile of the direct formation over the autoscale formation

7.5.3 PbS, ZnS and Multiple Scale

The initial attempt to overlay experimental data on top of predicted autoscale profiles for ZnS and PbS was not as successful as FeS. A significant shift in the pH of initial ZnS scale formation was observed in Figure 7.25, and the completely consumed [Pb^{2+}] in Khuff Na & Ca brine at pH 1.7 was expected to be around 4 mg/L according to the prediction, as seen in Figure 7.26. The shift in the prediction of ZnS scale formation could be attributed to the solubility constant value that was initially integrated in the first version of the prediction model, which was an absolute value from the literature, unlike the corrected $K_{sp,\ FeS}$. The autoscale of PbS in HCl had a better correlation, as seen in Figure 7.27, yet experienced a shift in pH. At pH 1, the model predicted no precipitation while the experimental value showed nearly 60% depletion of Pb^{2+}. As mentioned previously, the model's input fields did not include the chloride concentration; therefore, the various HCl dilutions were represented as DW with extremely low pH.

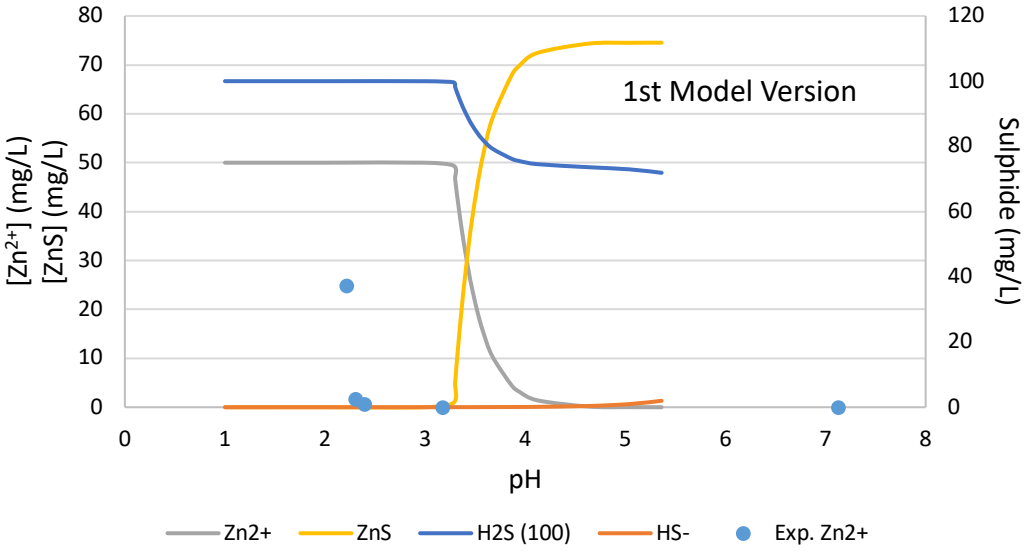

Figure 7.25 Overlaid experimental results on prediction data for ZnS autoscale profile in Khuff Na & Ca ($[Zn^{2+}]_i$ = 50 mg/L and $[S^{2-}]_i$ = 100 mg/L)

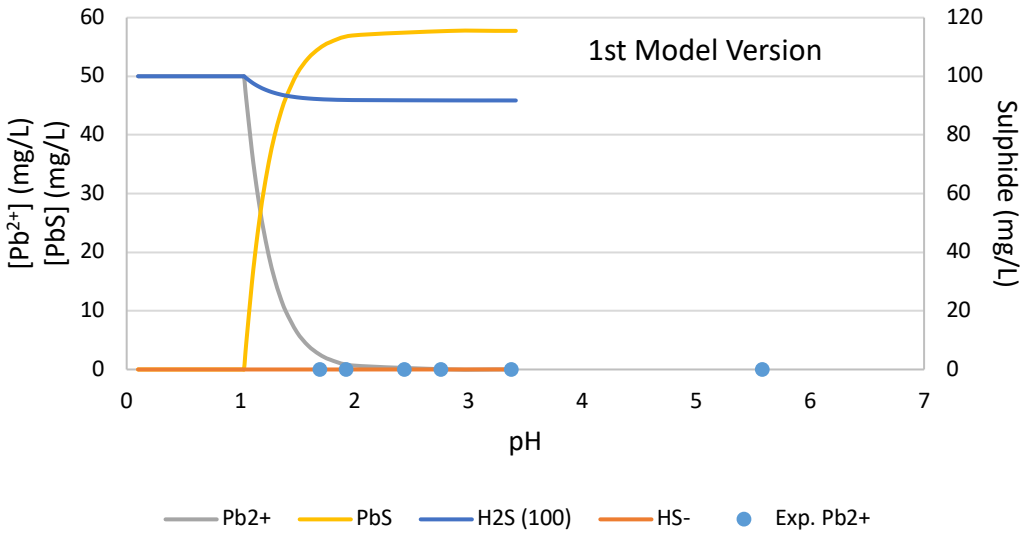

Figure 7.26 Overlaid experimental results on prediction data for PbS autoscale profile in Khuff Na & Ca ($[Pb^{2+}]_i$ = 50 mg/L and $[S^{2-}]_i$ = 100 mg/L)

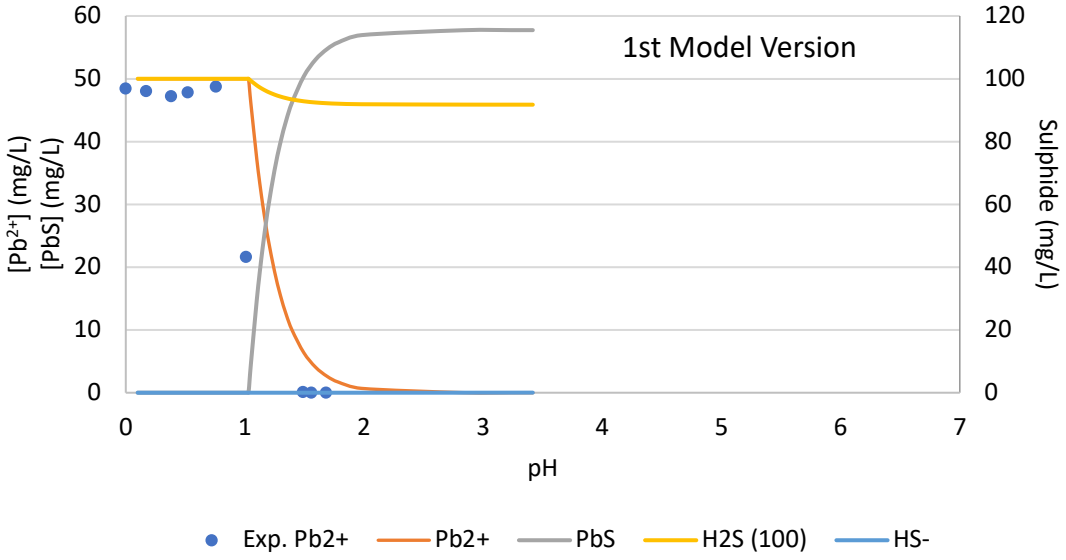

Figure 7.27 Overlaid experimental results on prediction data for PbS autoscale profile in DW ($[Pb^{2+}]_i$ = 50 mg/L and $[S^{2-}]_i$ = 100 mg/L)

The developer of this model has revealed that these discrepancies in the model were valid since the prediction calculations processes for FeS, ZnS and PbS were not exactly similar. In the first version of the model, the prediction of FeS included a correction factor to the solubility constant based on the activity coefficients. This correction was based on the Debye–Hückel theory, in which the mean activity coefficients are dependent on the

concentration and, subsequently, the inter-ionic attractions. An ideal solution should have ions distributed homogeneously within the solution based on the distribution of attraction-repulsion forces. However, the agreement between the Debye–Hückel theory and experimental data was only achieved for dilute solutions, and Scatchard (1925) has managed to extend the theory to 1 M using HCl in water and alcohol solutions. Pitzer (1973) has further improved the Debye-Hückel theory by accommodating concentrated electrolyte solutions, which laid out the core element of most developed activity models (Silva, 2017). These activity coefficients were highly dependent on the composition of the brine in terms of concentrations and charges, and the higher TDS and complexity of the brine produced slightly lower FeS solubility. In other words, FeS could form at pH values lower than what is thermodynamically anticipated if the TDS was higher or the brine composition was more complex. Unfortunately, the activity coefficient associated with PbS and ZnS required data that was not readily available in the literature, to the knowledge of the developer.

Since the first version of the model had fixed values of the solubility products, another modification was made which included input fields allowing the use of absolute thermodynamic K_{sp} values for PbS, ZnS, and FeS, without correction factors. This step enabled the evaluation of several reported values of the solubility products against the experimental data. However, such agreements, if any, between experimental and prediction data might not be accurate due to the lack of activity coefficients. Nonetheless, an experimental approach can be recommended to resolve this setback. Figure 7.28 shows a screenshot of the third model version which included additional fields to input the K_{sp} values of FeS, ZnS and PbS. In addition, the calculated concentrations of ions and molecules were represented scientifically, revealing extremely low concentrations, such as that of $[S^{2-}]$.

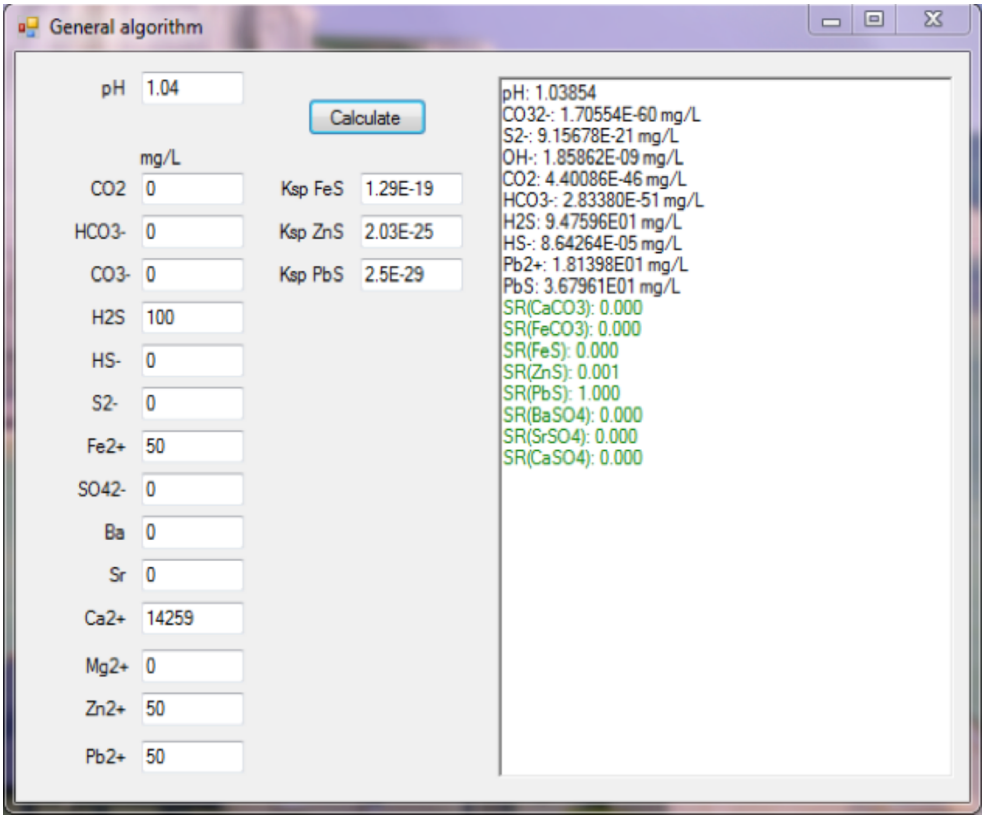

Figure 7.28 The interface of the 3rd version of scale prediction model showing the added input fields for K_{sp} values

In the following model runs, the values used were $K_{sp,\,FeS} = 1.29 \times 10^{-19}$, $K_{sp,\,ZnS} = 2.03 \times 10^{-25}$, *and* $K_{sp,\,PbS} = 2.50 \times 10^{-29}$. Additionally, the corrected value for $K_{sp,\,FeS} = 5.08 \times 10^{-21}$ was extracted from the 1st model version and used as a second iteration to verify the correction effect. The autoscale profiles for PbS and ZnS in Figure 7.29 and Figure 7.30 were noticeably different than the previously generated data, Figure 7.25 and Figure 7.27. The shift in the pH has been significantly reduced in the ZnS autoscale profile, whilst the formation of PbS has shown near-perfect match between the experimental and the prediction data. This enhancement in the scale prediction data was achieved solely by using lower K_{sp} values. Nonetheless, for the same brine composition (various dilutions of HCl), the used $K_{sp,\,PbS}$ can be efficient in the prediction calculations. Although HCl is not a common scaling brine, it might be useful in the case of using a prediction model for scale dissolution scenarios.

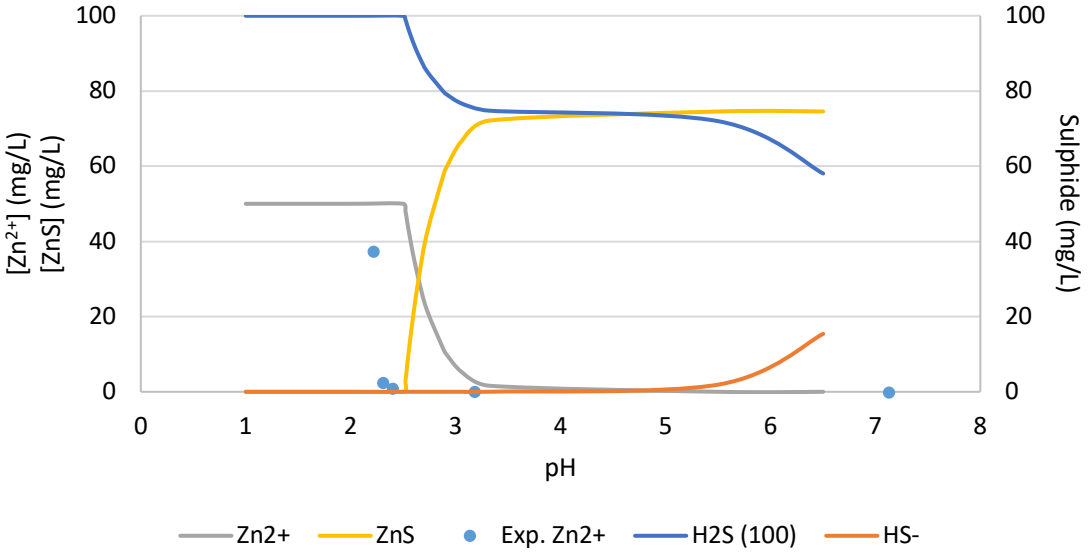

Figure 7.29 Data comparison of autoscale profiles of ZnS in Khuff Na & Ca using $K_{sp,\ ZnS} = 2.03 \times 10^{-25}$

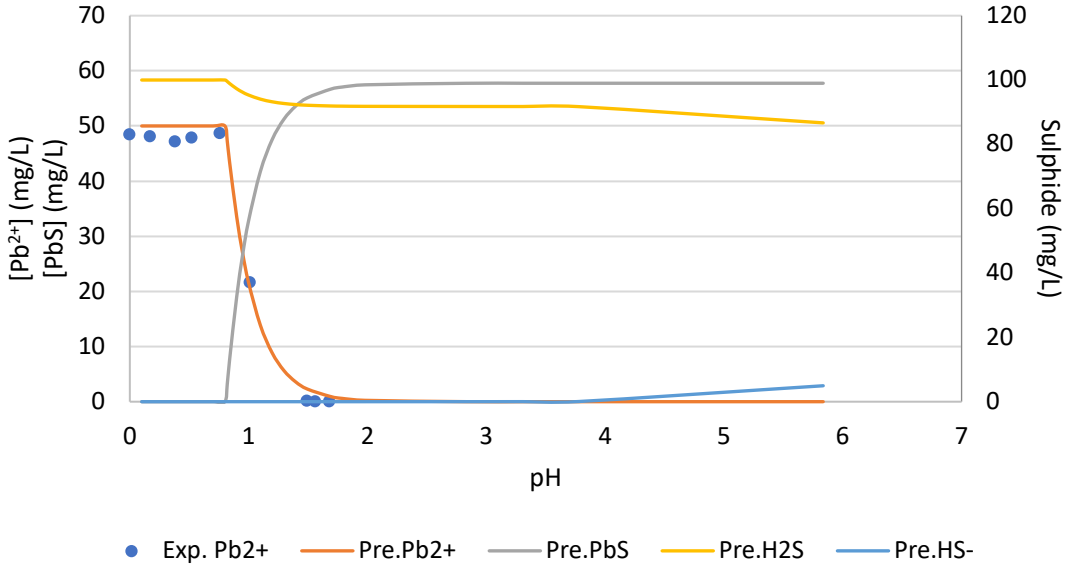

Figure 7.30 Data comparison (experimental and predicted) of autoscale profiles of PbS in HCl using $K_{sp,\ PbS} = 2.50 \times 10^{-29}$

The combination of the sulphide scales as mentioned above in one solution was tested in the experiments discussed earlier, and the data was overlaid on top of prediction model data of the metal cations depletion, as shown in Figure 7.31, Figure 7.32, and Figure 7.33. These sets of prediction data were generated using the 1st model version, and the 2nd model version with different K_{sp} values for FeS. The 1st model version, which corrected

$K_{sp,\ FeS}$, produced matching data for the depletion of Fe^{2+}, whilst the depletion profiles of Pb^{2+} and Zn^{2+} were far from ideal. This was also observed in earlier perditions of ZnS using the 1st model version.

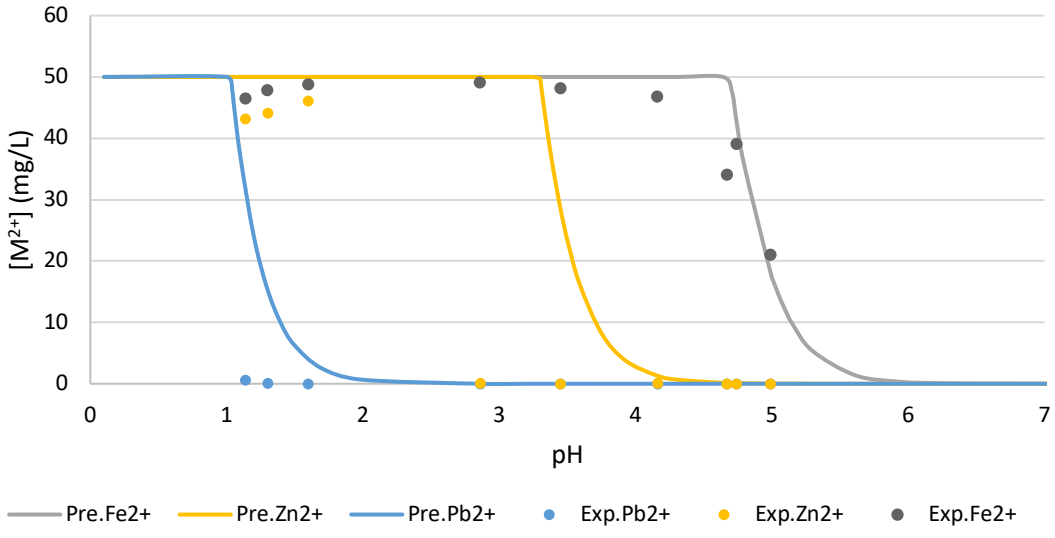

Figure 7.31 Experimental data from combined autoscale tests overlaid with 1st version of the prediction model showing discrepancies in the agreements with prediction data

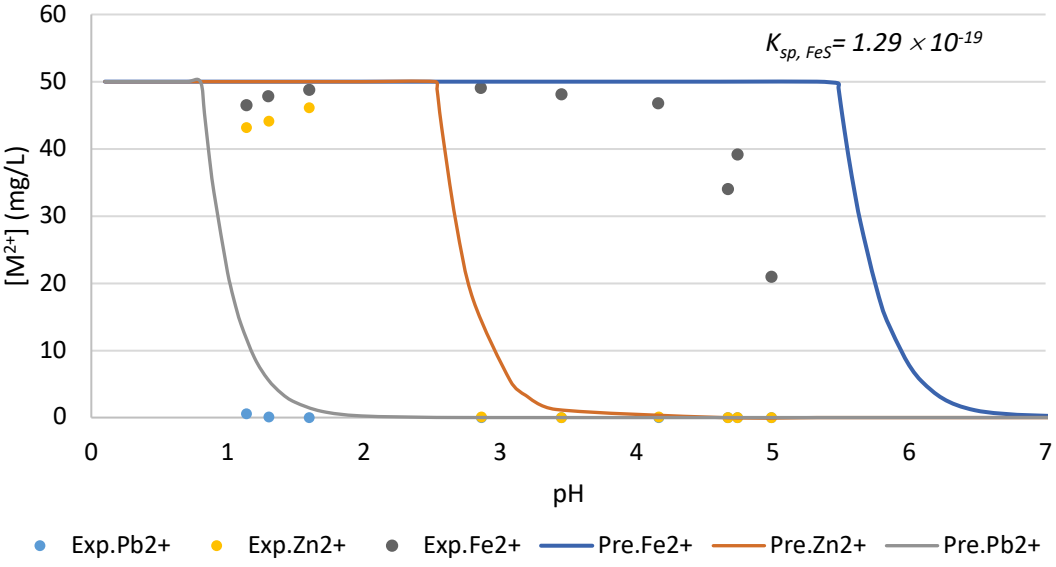

Figure 7.32 Prediction data of combined autoscale using $K_{sp,\ FeS}$= 1.29 × 10^{-19}, $K_{sp,\ ZnS}$= 2.03 × 10^{-25}, and $K_{sp,\ PbS}$= 2.50 × 10^{-29}

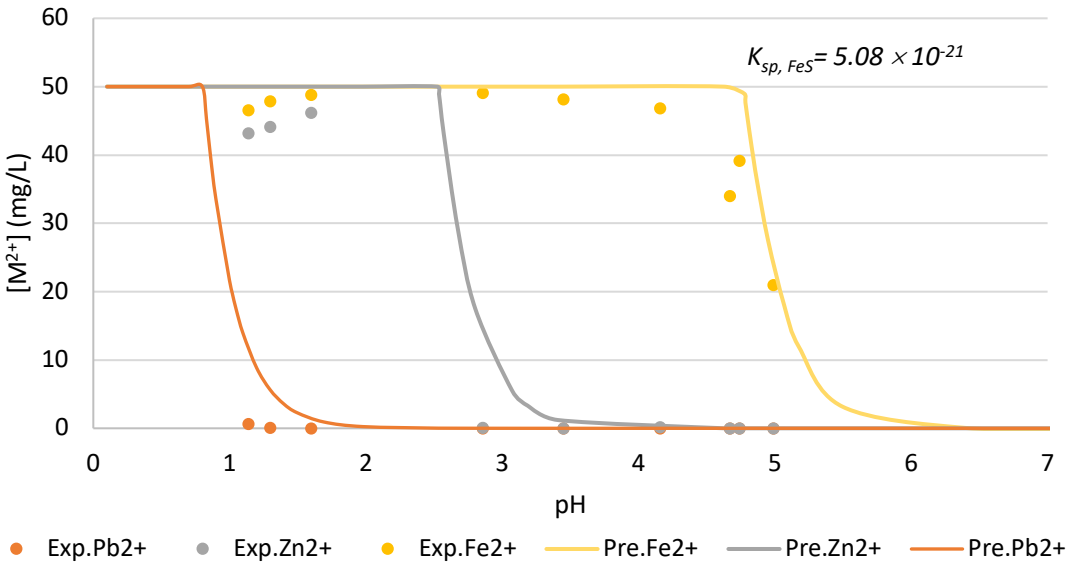

Figure 7.33 Prediction data of combined autoscale using $K_{sp,\ FeS}$= 5.08 × 10^{-21}, $K_{sp,\ ZnS}$= 2.03 × 10^{-25}, and $K_{sp,\ PbS}$= 2.50 × 10^{-29} showing better agreements than in Figure 7.31 and Figure 7.32

When the 2nd model version was used, and various values of K_{sp} could be implemented, an enhancement to the prediction of Pb^{2+} and Zn^{2+} depletion profiles was observed in Figure 7.32. However, the depletion of Fe^{2+} was shifted forward by nearly one pH unit, indicating that the theoretical formation of FeS should not occur at the range where it formed experimentally. Once the $K_{sp,\ FeS}$ corrected value (from the first model version) was used, the prediction and the experimental data of iron depletion were matching, whilst the zinc and lead profiles remained unchanged since the Zn and Pb sulphide scale formation would naturally be prior (i.e. at lower pH) to the formation of FeS.

7.6 Dynamic (Stirring) Tests of FeS Formation

All samples in this test initially contained 1,000 mg/L of sulphide and 50 mg/L of iron (II). After the formation of FeS, samples were stirred for various durations. The results from this test were analysed using the UV-Vis method to determine the sulphide concentration, ICP for the iron concentration, pH measurement, and ESEM-EDX for the composition of the formed FeS particles. The test set was repeated to validate the outcome trend. The first set included three samples, which were analysed after one minute, three and six days of mixing, whilst the second set was analysed after one hour, one, two and six days. Table 7.2 and Table 7.3 show the summary of the results from these two tests. Iron (II) was near completely consumed as FeS was formed. Furthermore, the decline in

the sulphide concentration with time was noteworthy. Plotting these losses of aqueous sulphide concentration versus time, as shown in Figure 7.34, revealed close trends. Both sets experienced loss of sulphide, even though FeS has formed instantaneously and the airtight vials were sealed during the mixing durations.

Table 7.2 1st Set - Final sulphide and iron concentrations and pH value after several mixing periods

Mixing duration	$[S^{2-}]_f$, mg/L	$[Fe^{2+}]_f$, mg/L	pH_f
1 Minute	868.4	0.024	6.84
3 Days	708.0	0.01	6.92
6 Days	385.1	0.016	6.82

Table 7.3 2nd Set - Final sulphide and iron concentrations and pH value after several mixing periods

Mixing duration	$[S^{2-}]_f$, mg/L	$[Fe^{2+}]_f$, mg/L	pH_f
1 Hour	845.8	0	6.32
1 Day	776.2	0	6.36
2 Days	520.1	0	6.51
6 Days	189.6	0	6.80

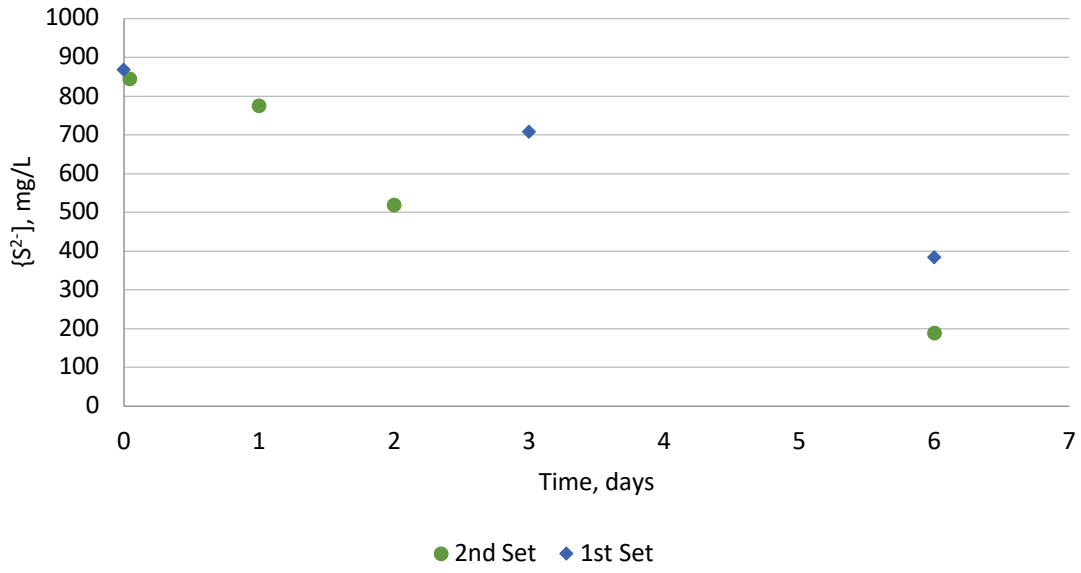

Figure 7.34: Decline in measured aqueous sulphide concentrations at different mixing durations

The formed scale particles were filtered through 0.45 µm filters, washed with distilled water and dried in the oven overnight before analysis. The ESEM-EDX provided semi-quantitative analysis of iron and sulphur atomic weights. Table 7.4 and Table 7.5 show ESEM images and the EDX analysis represented the corresponding iron-to-sulphur ratios calculated from the reported atomic weights. The first observation from these tables was the increase in S/Fe ratio as the mixing duration increased. The variation of Fe:S ratios was intense in the 1st set, whereas a subtler change in Fe:S ratio was observed the repeated 2nd set, even at comparable levels of magnification.

Table 7.4 ESEM analysis of FeS formed particles in the 1st set after mixing for various periods

Time	*Magnification*	*1)*	*2)*
One minute	1) 35x 2) 650x	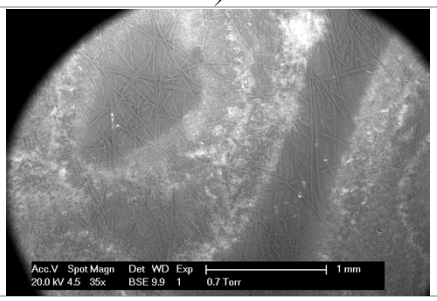	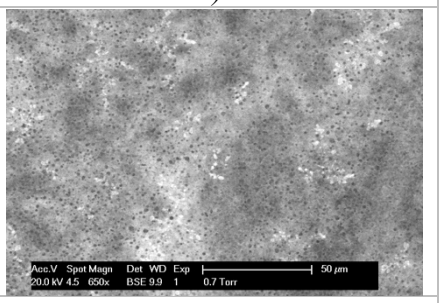
	Fe : S	1 : 0.28	1 : 0.42
Three days	1) 65x 2) 350x	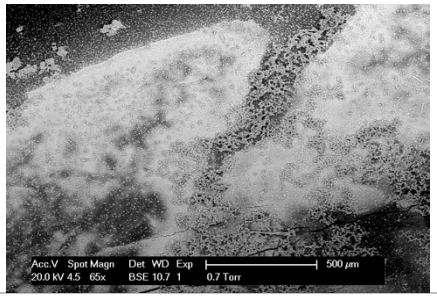	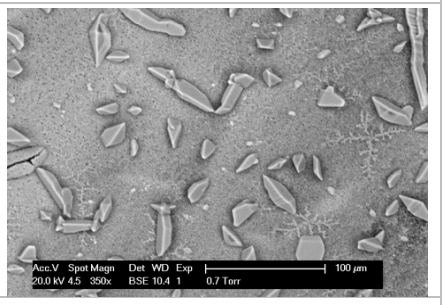
	Fe : S	1 : 1.66	1 : 1.08
Six days	1) 650x 2) 3500x	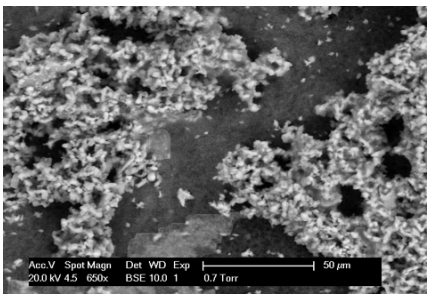	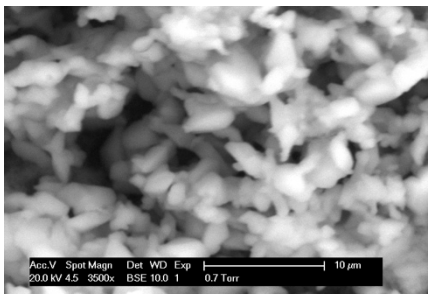
	Fe : S	1 : 10.15	1 : 23.60

Table 7.5 ESEM analysis of FeS formed particles in the 2nd set after mixing for various periods

Time	*Magnifications*	*50x*	*650x*
One hour	Image	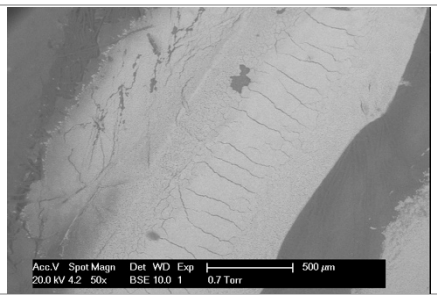	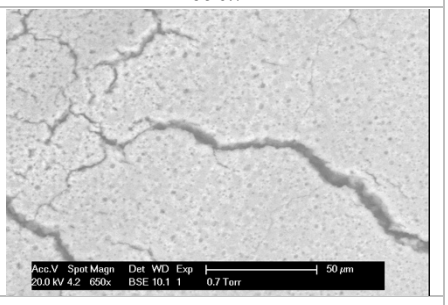
	Fe : S	1 : 1.31	1 : 0.96
One day	Image	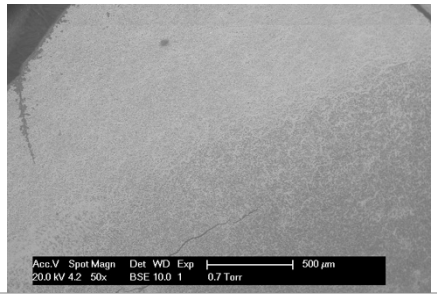	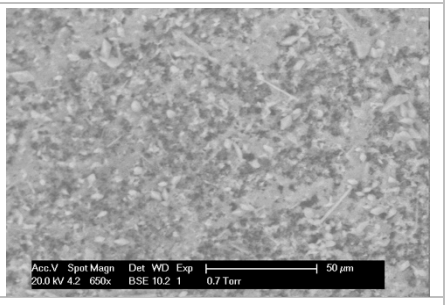
	Fe : S	1 : 2.22	1 : 2.22
Two days	Image	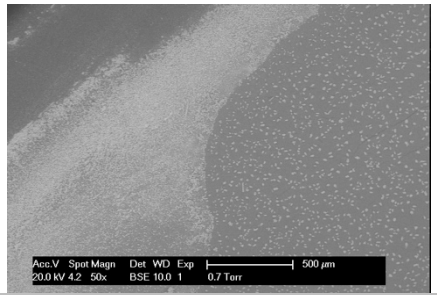	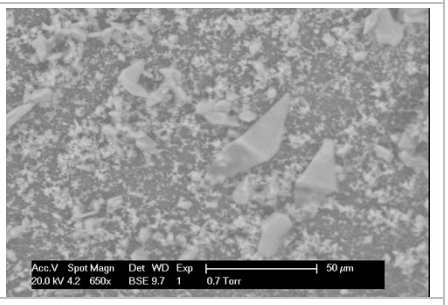
	Fe : S	1 : 2.04	1 : 1.95
Six days	Image	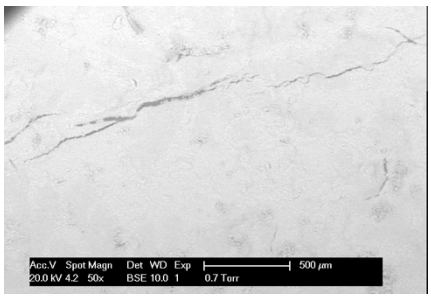	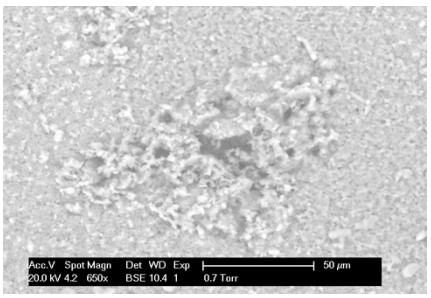
	Fe : S	1 : 1.99	1 : 2.67

The particles crystallography has shown obvious distinctions through various periods of mixing, which might suggest a continuous reaction or agglomeration taking place at the excess of sulphide. In the samples taken after 1 min and 1 hour of mixing, the particles appeared as a fine thin film, then more visible crystals were formed after 2 and 3 days of mixing. In both sets, denser crystals were observed after 6 days of mixing, which was

reflected as the highest S:Fe ratios. The solubility of iron deficient sulphide scale, such as pyrrhotites (FeS_2), in stimulation and clean out acids is known to be extremely low (Przybylinski, 2001). From a field perspective, such results could favour frequent low volume clean out treatments over the less frequent major clean out treatment.

It is common for the stoichiometry of iron sulphide to change under continuous exposure to a replenishing sulphide source. However, the high S/Fe ratios in Table 7.4 was considered abnormal. The main cause of sulphur increase from an experimental perspective could be the residue of the sulphide solution, which could have been not thoroughly washed with DW. The second set was conducted more systematically, and washed thoroughly, thus, reducing the vast excess of sulphur-to-iron ratio. Another source of the increase of sulphide/sulphur ratio in the ESEM analysis might be the elemental sulphur formation as an oxidative product of sulphide in the presence of oxygen. This source, however, is less probable given that the dissolved oxygen concentration did not exceed 30 μg/L in all experiments.

The formation of FeS in an excess iron environment was tested, where 2 mL of 1,000 mg/L sulphide was added to 38 mL of 5,000 mg/L iron solution. The final pH of the solution was pH 3, and consequently, FeS did not form in this solution. The solution required pH > 3.5 to form FeS, which can be achieved by adding NaOH to increase the pH. However, adding sodium hydroxide to a highly concentrated iron (ii) solution created a localised environment for iron hydroxide to form which was perceived as an incompatibility.

7.7 Conclusions

The formation of sulphide scale under various conditions, *i.e.* sulphide and iron concentrations, brines and pH values, has been investigated using static tests in Hungate-type tubes to prevent oxygen contamination and H_2S evolution. Highly repeatable results have been produced, and autoscale profiles have been established for one or more sulphide scales. The results were compared with prediction model data to verify the experimental results directly with theoretical results. Dynamic (stirring) iron sulphide formation tests were carried out to establish the effect of forming and exposing FeS to sulphide excess on the molecular composition of the scale. The findings from these tests have led to the following conclusions:

(i) The new static test setup was used to describe the formation of iron sulphide (mixing two brines and autoscaling) at variable conditions.

(ii) The developed setup revealed the different solubilities of FeS at variable sulphide concentrations and extremely low pH values, which was described briefly in previous studies using advanced pressurised anaerobic setups.

(iii) The new anaerobic setup unprecedently provided insight into the autoscale profiles of FeS, ZnS and PbS, which was validated theoretically using a scale prediction model.

(iv) The change in iron sulphide composition into iron-deficient forms could suggest more frequent clean out treatment to increase the acid dissolution efficiency.

8 – Inhibition of FeS

Executive Summary

The effect of varying the sulphide concentrations has been observed in Chapter 7, and such effect could be vital to scale inhibitors in terms of performance and loadings. In this chapter, a high molecular weight polymeric scale inhibitor has been tested at various conditions, such as varying sulphide and iron concentrations, temperatures, brine compositions, and time. Apart from the latter factor, each of these conditions has shown significant effect on the scale inhibition efficiency, with the sulphide excess concentration and the complex brine composition having the highest impacts. Longer exposure of inhibited FeS particles to excess of sulphide has shown minimal effect, especially when compared to the uninhibited FeS. This emphasised the crystal growth inhibition and dispersant capabilities of the tested scale inhibitor. Such findings must be taken into consideration when designing scale inhibitor recipes to achieve highest optimisation.

8.1 The Inhibition of FeS inhibition at various conditions

The inhibition of iron sulphide was investigated as a continuation of the evaluation of the versatility and effectiveness of the introduced anaerobic experimental setup (using airtight tubes and vials). The focus of this investigation was directed toward the various conditions under which the inhibitors could be examined using this setup, more than the inhibition chemistry of iron sulphide scale. So far, the anaerobic setup has provided significant advances in terms of the pH adjustment of aqueous sulphide, autoscaling of sulphide scales, containment of gaseous H_2S, and isolating atmospheric oxygen.

Scale inhibition efficiency is contingent on factors such as the pH, scaling cation (Fe^{2+}, Pb^{2+}, and Zn^{2+}) concentration, scale inhibitor concentrations, temperature, and time. Przybylinski (2001) has used a similar anaerobic setup to evaluate FeS scale inhibitors. However, the solutions involved in his experiments were not pH adjusted, yet he used a buffer to bring the final pH of the mixed solution to circumneutral. Therefore, the anaerobic experimental setup in this study was taken a step further by enabling the evaluation of inhibition at various conditions using pH-adjusted aqueous sulphide solutions.

8.2 Descriptions of MIC Determination Tests at Various Conditions

The tests included different concentrations of sulphide, iron and scale inhibitor to form FeS and determine the MIC. In addition, various salinities, temperatures and pH values were evaluated. The required threshold of MIC was set at 80% of the initial iron concentration remaining in solution either as dissolved Fe^{2+} or as formed and suspended FeS, which was analysed using ICP. For each sulphide concentration, *i.e.* 100, 200, 500 and 1,000 mg/L, groups of 6 x 12 mL Hungate-type tubes were filled with 10 mL of a de-oxygenated sulphide solution and pH adjusted (pH 4 – 6) to examine the total consumption of Fe^{2+}. Different loadings of the scale inhibitor (a high molecular weight sulphonated copolymer, SI-2) were injected into each group, to achieve final scale inhibitor concentrations ranging from 10 to 200 mg/L. Finally, the tubes were injected with 100 µL of 5,000 mg/L iron chloride to form FeS. A blank solution, without the scale inhibitor, was used as a reference for total iron consumption. The iron concentration was determined using ICP analysis conducted 24 hours after forming FeS. Filtered samples, through 0.2 µm filters, and unfiltered samples represented dissolved Fe^{2+} and total iron (dissolved Fe^{2+} and suspended FeS), respectively. The final pH values were measured after taking the ICP samples.

For some initial total sulphide concentrations, several repeats had to be executed to ensure total iron consumption. A duplicate of the 100, 200 and 1,000 mg/L sulphide and 50 mg/L iron (II) sets was repeated at 50ºC using a water bath. A doubled iron concentration (100 mg/L) was tested against 1,000 mg/L total sulphide to determine the effect of increasing iron on the MIC. Another set of 1,000 mg/L S^{2-} and 50 mg/L Fe^{2+} was left for one week before analysis to investigate the dispersion efficiency with time. Finally, a second scale inhibitor, SI-3, was tested to establish a comparison in performance to the SI-2. The results were plotted in terms of iron concentrations and pH, against scale inhibitors loadings.

It is essential to define the scale inhibition concept to clarify the evaluation criteria of the scale inhibitor's performance. The scale inhibition mechanisms vary from preventing the formation, to stopping the crystals growth, or dispersing the formed scale in solution. The tested scale inhibitor (SI-2) is a dispersant, which can be evaluated based on the combined concentration of dissolved Fe^{2+} and dispersed FeS (Al-Harbi *et al.*, 2018).

8.2.1 Effect of the Initial Sulphide Concentration on the MIC

The following tests were designed to have a constant [Fe^{2+}] whilst varying the concentration of total aqueous sulphide to explore the effect of initial total sulphide concentration on the MIC. The loadings of the scale inhibitor ranged from 10 – 200 mg/L. At a later stage, three temperatures and brine salinities were used to establish their effect on the MIC. Table 8.1 shows all sets prepared to determine the MIC of SI-2 at various initial sulphide and iron concentrations, and the final pH values. The concentrations of sulphide were 100, 200, 500 and 1,000 mg/L, and were adjusted with the intent to reach pH ~ 6. The results were plotted as the percentage of iron in solution over $[Fe^{2+}]_i$. Figure 8.1 shows a comparison between MICs at $[S^{2-}]_i$ = 200, 500 and 1,000 mg/L and at room temperature. The efficiency of the SI can be calculated using the following equation:

$$SI\ efficiency\ \% = \frac{([Fe]_{unfiltered} - [Fe]_{filtered}) \times 100}{[Fe]_{initial}} \quad (8.1)$$

An accurate determination of a scale inhibitor efficiency should be done at pH values where iron (II) has been completely depleted. Figure 8.1 shows the determined MICs as ~ 20, 20 and 40 mg/L for $[S^{2-}]_i$ = 200, 500 and 1,000 mg/L, respectively, whilst the set of 100 mg/L of S^{2-} could not be conclusive as iron (II) was not completely consumed. Figure 8.2, Figure 8.3, Figure 8.4, and Figure 8.5 show the inhibition efficiencies and dissolved iron concentration in filtered and unfiltered samples at varying pH values at $[S^{2-}]_i$= 100 and 200 mg/L.

Table 8.1 Details of the MIC determination sets of samples (concentrations, pH, brine, and temperature)

Set number	*$[S^{2-}]_i$ (mg/L)*	*$[Fe^{2+}]_i$ (mg/L)*	*Average pH_f*	*Comments*
1	1,000	50	6.25 ± 0.026	RT (3.5% NaCl)
2	1,000	50	6.15 ± 0.050	RT (3.5% NaCl)
3	1,000	100	6.11 ± 0.160	RT (3.5% NaCl)
4	500	50	6.93 ± 0.019	RT (3.5% NaCl)
5	200	50	5.18 ± 0.074	RT (3.5% NaCl)
6	200	50	5.39 ± 0.088	RT (3.5% NaCl)
7	200	50	6.20 ± 0.079	RT (3.5% NaCl)
8	200	50	6.39 ± 0.048	RT (3.5% NaCl)
9	200	50	6.62 ± 0.093	50°C (3.5% NaCl)
10	100	50	4.96 ± 0.081	RT (3.5% NaCl)
11	100	50	5.12 ± 0.032	RT (3.5% NaCl)
12	100	50	5.41 ± 0.053	RT (3.5% NaCl)
13	100	50	5.64 ± 0.208	RT (3.5% NaCl)
14	100	50	5.75 ± 0.075	50°C (3.5% NaCl)
15	200	50	6.82 ± 0.022	50°C (Khuff)
16	100	50	6.17 ± 0.053	50°C (Khuff)
17	1,000	50	6.36 ± 0.077	50°C (Khuff Na & Ca)
18	1,000	50	6.29 ± 0.040	50°C (Khuff Na & Ca)
19	1,000	50	6.53 ± 0.024	50°C (Khuff Na & Ca)
20	1,000	50	6.53 ± 0.030	50°C (Khuff Na & Ca)

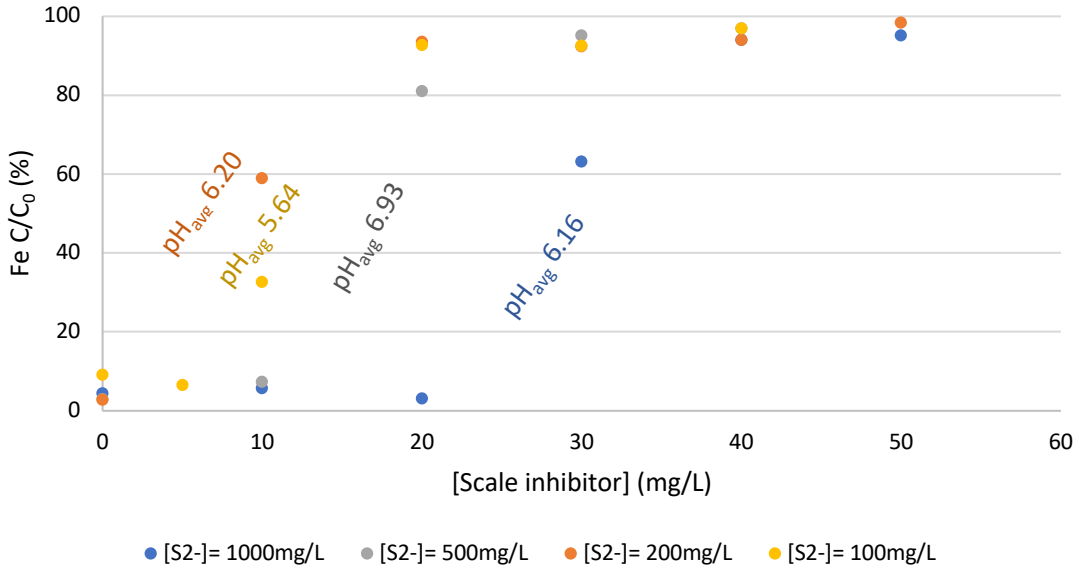

Figure 8.1 Determining MIC (80% or more Fe C/C_0 – Eq 8.1) of SI-2 to inhibit FeS at various pH and initial total sulphide concentrations in 3.5 wt.% NaCl ($[Fe^{2+}]_i$= 50 mg/L)

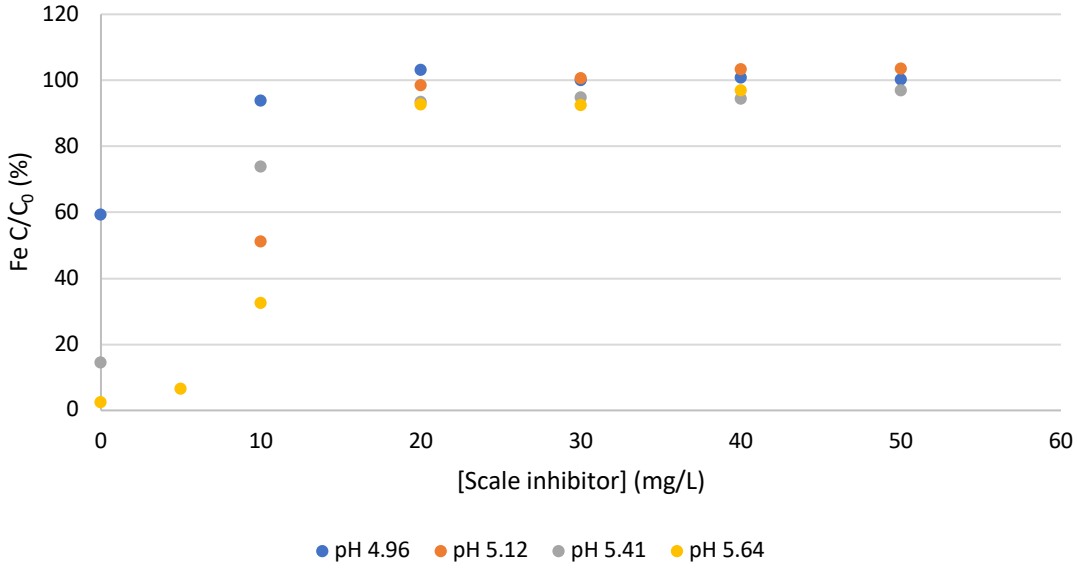

Figure 8.2 Effect of pH on total iron in solution (percentage) against the scale inhibitor concentration at $[S^{2-}]_i$ = 100 mg/L, $[Fe^{2+}]_i$ = 50 mg/L in 3.5 wt.% NaCl (Unfiltered samples)

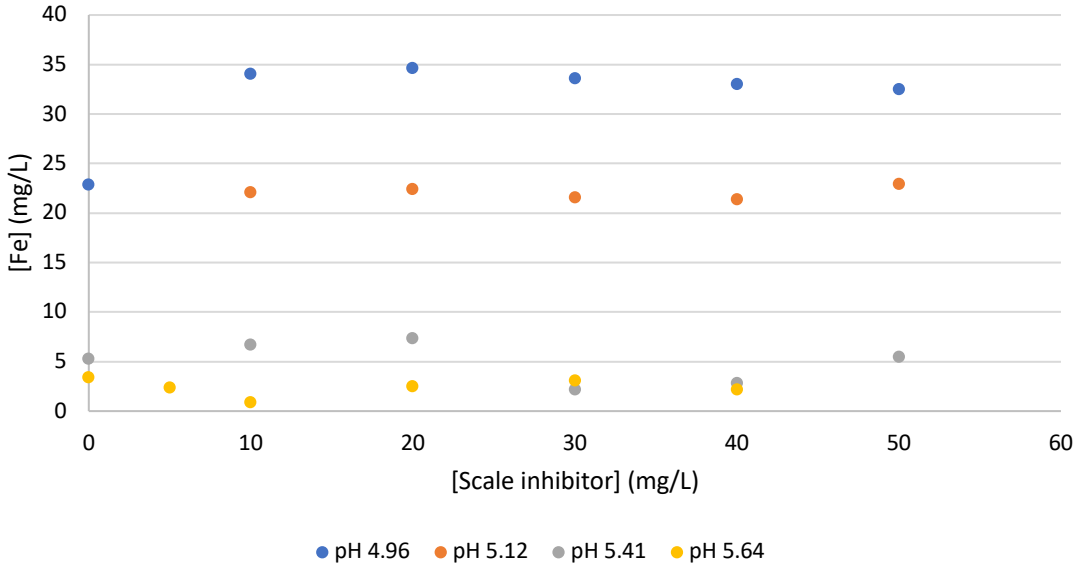

Figure 8.3 Effect of pH on iron concentration in filtered samples (through 0.2 µm filter size) against the scale inhibitor concentration at $[S^{2-}]_i$ = 100 mg/L, $[Fe^{2+}]_i$ = 50 mg/L in 3.5 wt.% NaCl

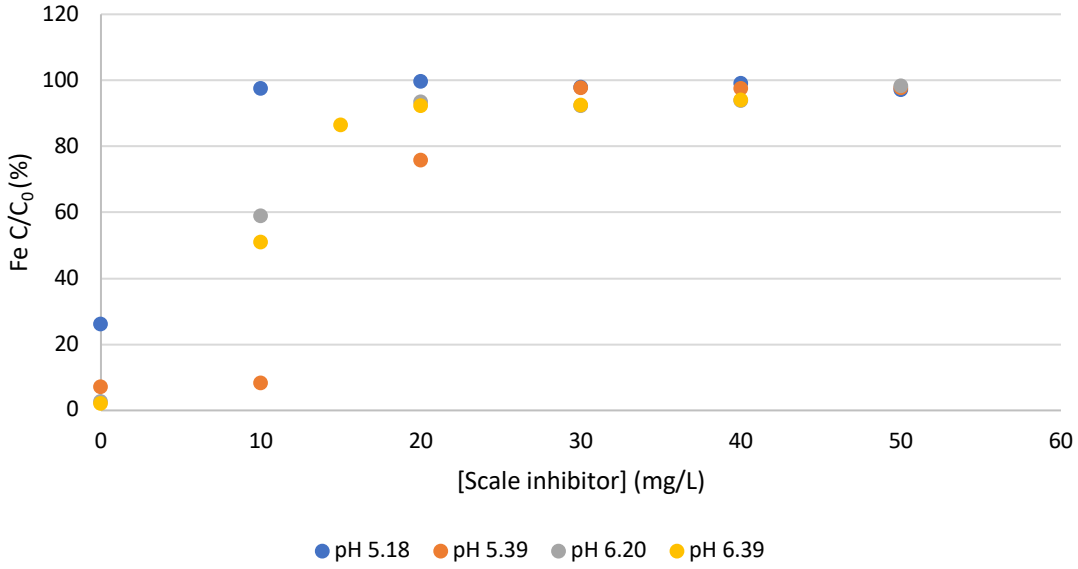

Figure 8.4 Effect of pH on total iron in solution (percentage) against the scale inhibitor concentration at $[S^{2-}]_i$ = 200 mg/L, $[Fe^{2+}]_i$ = 50 mg/L in 3.5 wt.% NaCl (Unfiltered samples)

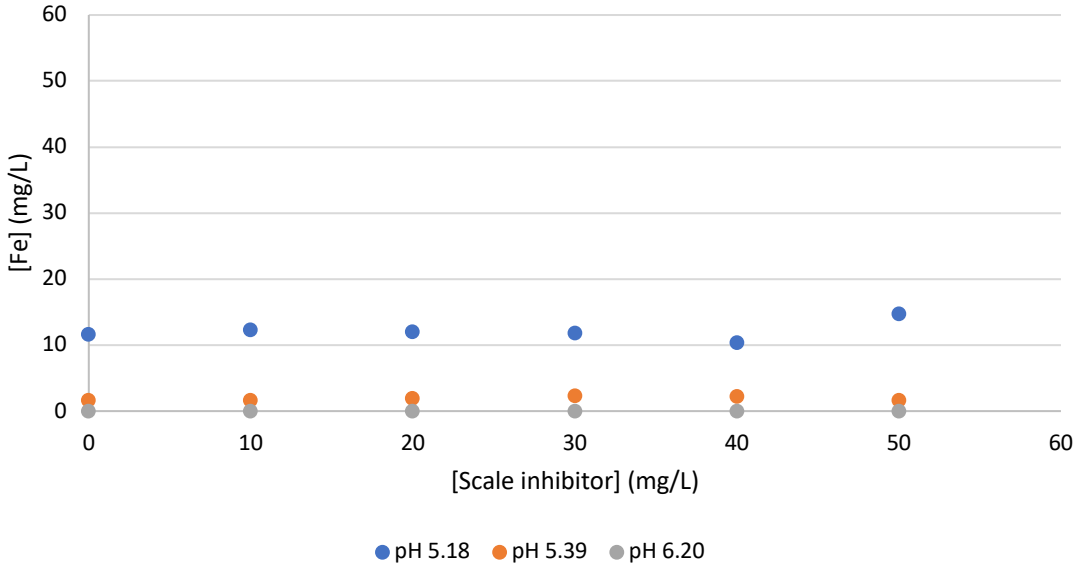

Figure 8.5 Effect of pH on iron concentration in filtered samples (through 0.2 µm filter size) against the scale inhibitor concentration at $[S^{2-}]_i$ = 200 mg/L, $[Fe^{2+}]_i$ = 50 mg/L in 3.5 wt.% NaCl

From Figure 8.1, the initial total sulphide concentrations significantly affected the efficiency of scale inhibitor in dispersing FeS particles. The possible causes of the impact of varying total sulphide concentrations could be changes in the size or mass of formed

FeS particles, or a direct reduction in the effectiveness of the scale inhibitor through chemically degrading the functional groups associated with the dispersing features. As a result, the inhibition of iron sulphide requires factoring the sulphide concentration as well as the iron concentration to provide an optimal inhibition efficiency.

8.2.2 Effect of Increasing the Iron Concentration on the MIC

The effect of increasing the iron concentration was investigated, and the results were plotted in Figure 8.6. Using a 1,000 mg/L of total sulphide and 100 mg/L of Fe^{2+} at pH 6.1 resulted in increasing the MIC by nearly 50% compared to the MIC at an initial [Fe^{2+}] of 50 mg/L. The mass of formed FeS should have doubled by using double the iron concentration in excess of sulphide. However, forming twice the mass of FeS did not necessarily require double the MIC, suggesting that the scale inhibition mechanism is capable of dispersing twice the scale with only 50% more of the inhibitor concentration. The outcome of this test could propose further optimisations to the inhibition treatment design.

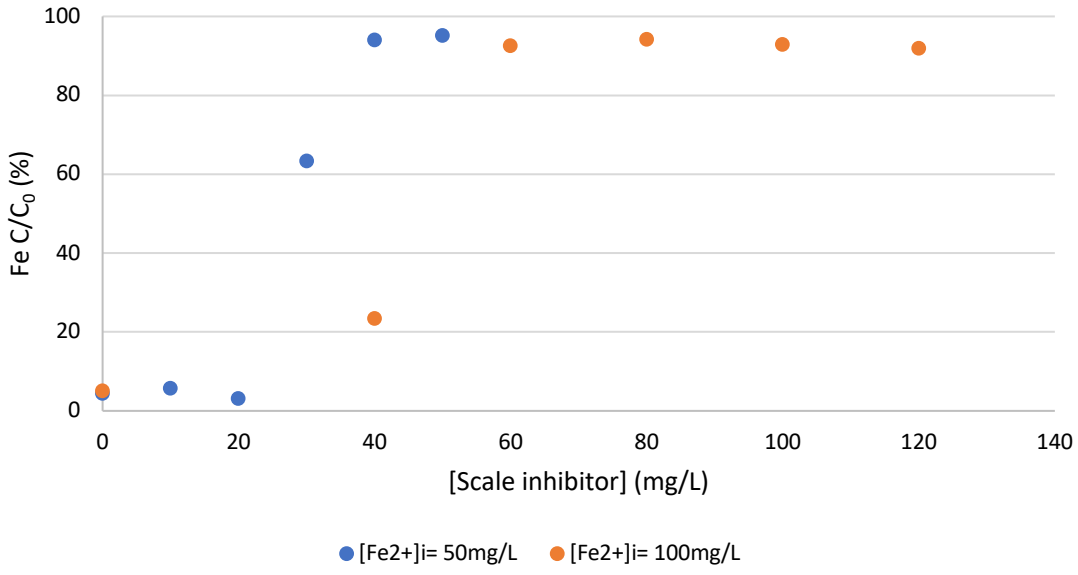

Figure 8.6 The scale inhibition efficiency (percentage) at 50 and 100 mg/L Fe^{2+}, pH ~ 6.1, and $[S^{2-}]_i$ = 1,000 mg/L in 3.5 wt.% NaCl at room temperature

The initial concentrations of sulphide and iron had an impact on the MICs from different perspectives since varying the limiting reactant was different than varying the ion in excess. In other words, changing the concentration of the excess ion did not produce different FeS masses (assuming the 1:1 molar ratio) as did the variation of the limiting

reactant. However, there could be a possibility of producing FeS with stoichiometric ratios other than 1:1 at various excesses of sulphide, resulting in different particle masses and sizes.

8.2.3 Effect of Extending the Inhibition Duration on the MIC

Other possible influential factors were investigated, such as the temperature, salinity, and time. The dispersion efficiency of the tested scale inhibitor was evaluated over an extended period, one week, and compared to the 24-hour test results. Figure 8.7 shows that the scale inhibitor's efficiency, i.e. the dispersion's efficiency of SI-2, is time-dependent, and more extended dispersion periods required higher MIC to disperse the formed scale in solution.

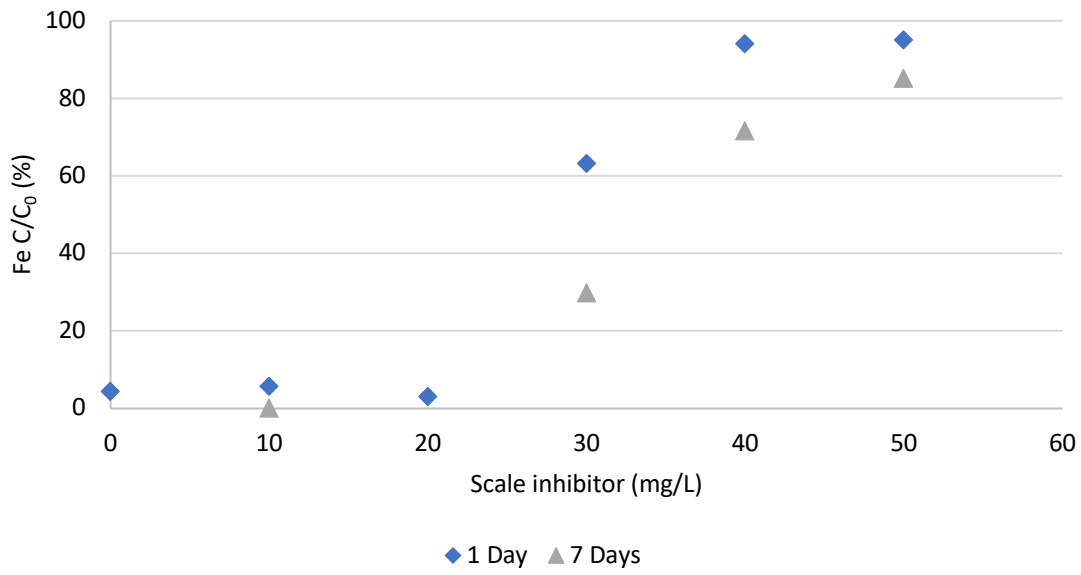

Figure 8.7 Scale inhibition efficiency (percentage) after two durations at $[Fe^{2+}]_i$ = 50 mg/L, pH 6, and $[S^{2-}]_i$ = 1,000 mg/L in 3.5 wt.% NaCl at room temperature

8.2.4 Effect of Temperature on the MIC

In addition to the tests at room temperature and 3.5 wt.% NaCl brine, the scale inhibitor was tested at 50 and 95°C and various brine salinities to examine the extent of the effects of temperature and brine composition on scale dispersion. Initially, 100 and 200 mg/L of total aqueous sulphide were tested against 50 mg/L Fe^{2+} at room temperature and 50°C using 3.5 wt. % NaCl. The average final pH values of these two sets at 50ºC were pH 5.75 (yellow dashed line) and pH 6.62 (amber dashed line) for the 100 and 200 mg/L of S^2, respectively, as shown in Figure 8.8. The final pH values for the sets at room

temperature were 5.63 (light blue line), 6.19 (blue dashed line), and 6.39 (grey line) for 100 mg/L, 200 mg/L in RT1 and RT2 (repeats), respectively. The room temperature sets are represented by dashed lines in Figure 8.8, while solids lines represent the sets tested at 50ºC. A slight improvement in the scale inhibition was observed in the 200 mg/L of total sulphide at 50ºC compared to the room temperature sets. This improvement was manifested by nearly 33% more inhibition at [SI]= 10 mg/L, and 96% and 88% of inhibition at [SI]= 15 mg/L, for the 50ºC and room temperature sets, respectively.

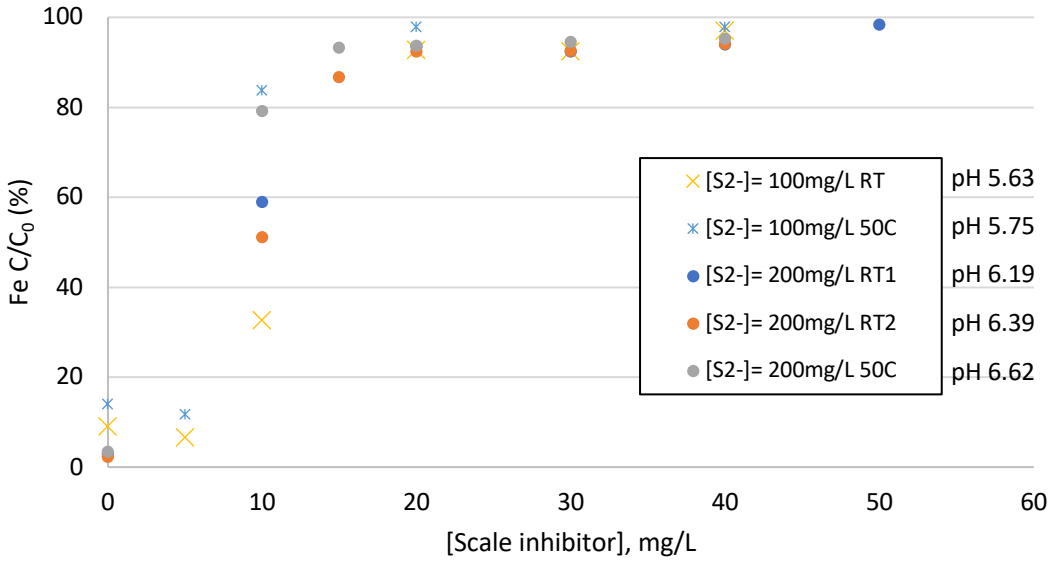

Figure 8.8 Scale inhibition efficiency at 50ºC and room temperature in 3.5 wt.% NaCl to show the effect of temperature on inhibition at various sulphide concentrations

8.2.5 Comparison of Two Scale Inhibitors at Two Temperatures in Terms of MIC

Another four sets of 1,000 mg/L of total sulphide and 50 mg/L Fe^{2+} were tested at room temperature and 50ºC using two scale inhibitors: SI-2 and SI-3. The objectives were to compare the effect of increasing the temperature on the scale inhibition efficiency while also comparing the performances of both scale inhibitors. For these tests, Khuff Na & Ca brine was used, while the total composition of Khuff formation brine was used on limited tests as its complex composition could add to the severity of FeS formation, which will be discussed in following experiments.

Figure 8.9 shows the scale inhibition efficiencies of SI-2 at both temperatures. In this test, the temperature effect was contradicting that noticed at 3.5 wt.% NaCl with lower total sulphide concentrations. Nonetheless, the difference in MIC levels was recorded as

5 mg/L as the temperature increased from 21.5 to 50ºC. The overall inhibition was marginally higher at room temperature. It was also noticeable that the MIC of SI-2 at room temperate was lower in Khuff Na & Ca compared to that found in 3.5wt. % NaCl (Figure 8.1). The increase in TDS (~192,000 mg/L) and the inclusion of $CaCl_2$ have (unexpectedly) enhanced the scale inhibition efficiency, however, the reason for such enhancement was still unclear.

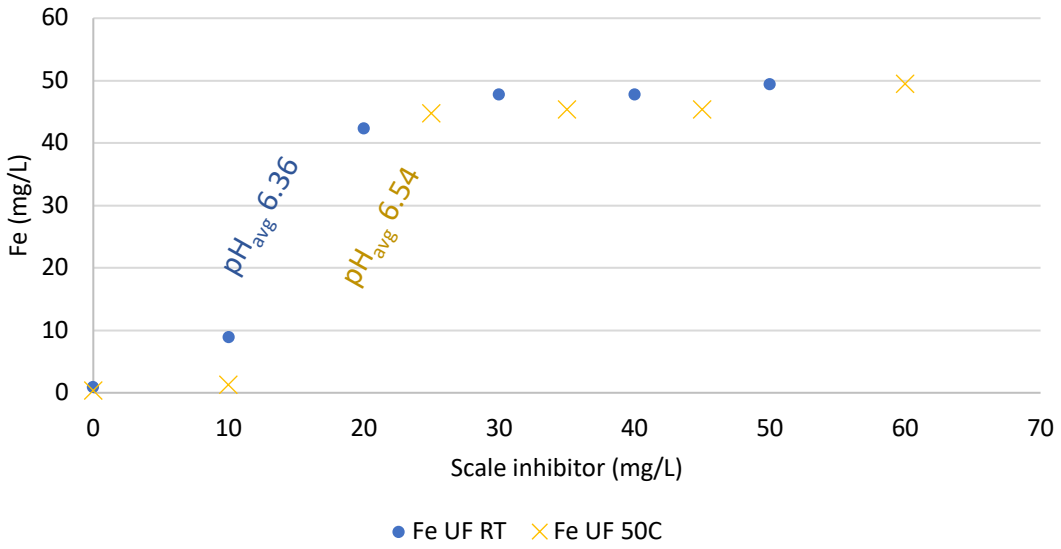

Figure 8.9 The effect of temperature on the MIC of SI-2 in Khuff Na & Ca ($[Fe^{2+}]_i$ = 50 mg/L and $[S^{2-}]_i$ = 100 mg/L)

On the other hand, the performance of SI-3 was not as successful as that of SI-2. At room temperature, concentrations of 0 - 50 mg/L of SI-3 were used and formed FeS completely deposited throughout that range of the inhibitor loadings. At 50ºC, higher dosages were tested, and 40% inhibition efficiency was achieved at $[SI]_{SI-3}$= 200 mg/L, as seen in Figure 8.10. The mechanism of SI-3 was not disclosed by the manufacturer which complicated comprehending the low performance of the inhibitor. An additional inhibition test was conducted at 95ºC using 1,000 mg/L of sulphide and 50 mg/L of Fe^{2+}. However, the high temperature affected the integrity of the Hungate tube screw-caps, as seen in Figure 8.11, which caused a loss of sulphide concentrations.

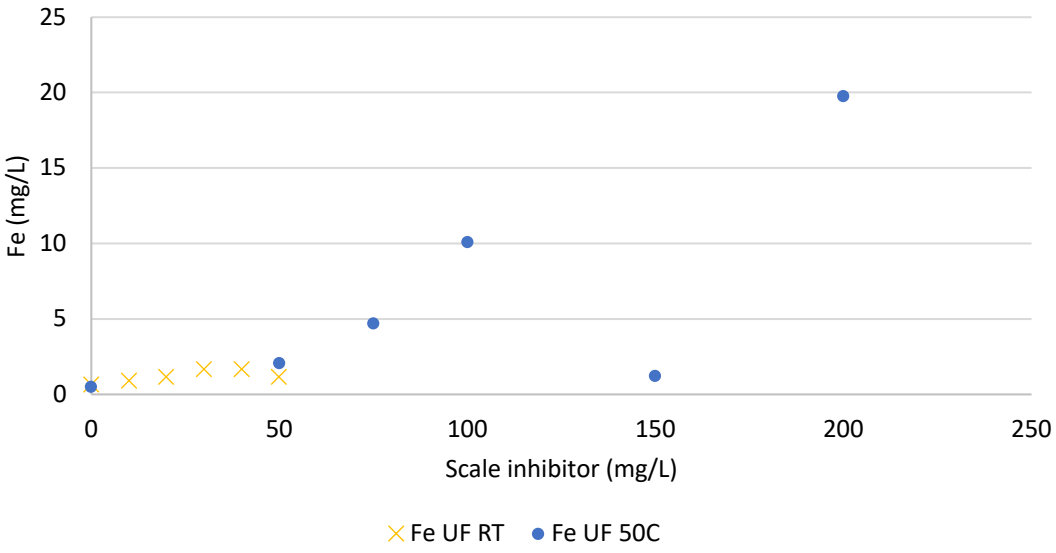

Figure 8.10 The effect of temperature on the MIC of SI-3 in Khuff Na & Ca ($[Fe^{2+}]_i$ = 50 mg/L and $[S^{2-}]_i$ = 100 mg/L)

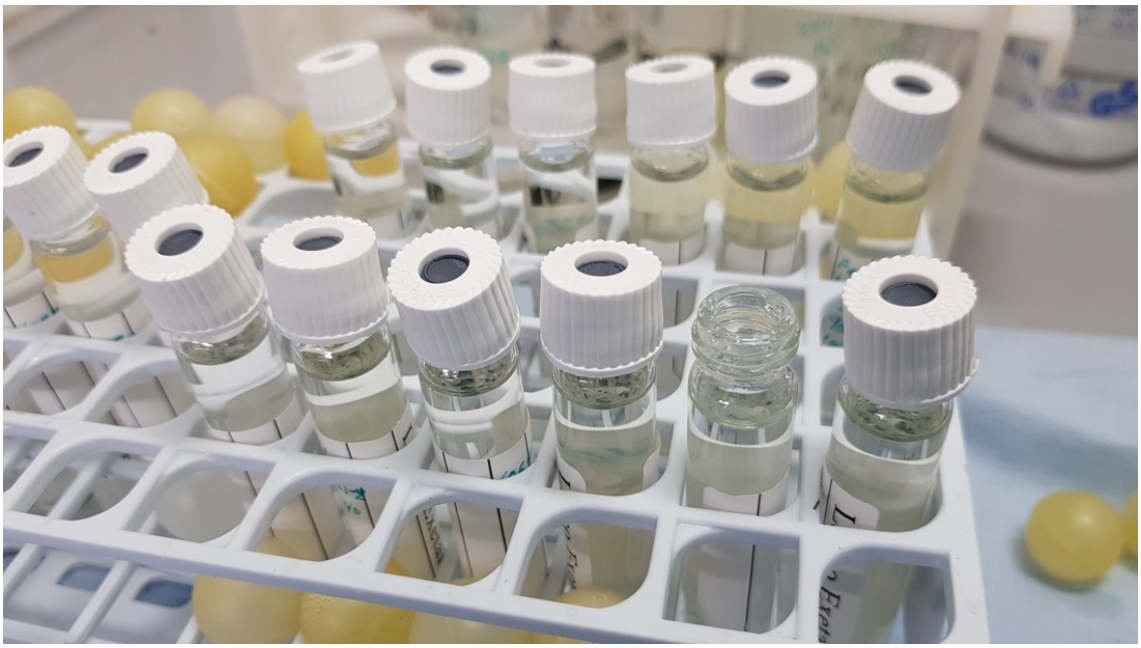

Figure 8.11 Tube lids loosened/removed as a result of high temperature (95ºC) and pressure

8.2.6 Effect of Salinity on the MIC

Adjacent inhibition tests using Khuff formation brine at 50ºC showed a more severe FeS formation compared to the scale formed at room temperature, as seen in Figure 8.12. Furthermore, the MIC of SI-2 was significantly higher for the 100 and 200 mg/L of total

sulphide compared to 1,000 mg/L in Khuff Na & Ca shown in Figure 8.9. The increase in MIC suggested that the formation of FeS was profoundly influenced by the brine composition, since the increase of TDS, as mentioned earlier, using only calcium and sodium chloride, was found enhancing the scale inhibition efficiency. The complexity of the tested Khuff formation water brine has solely increased the MIC four folds, which could be explained either as an effect on formed FeS sizes or as a hindrance to the inhibition mechanism, *i.e.* incompatibility.

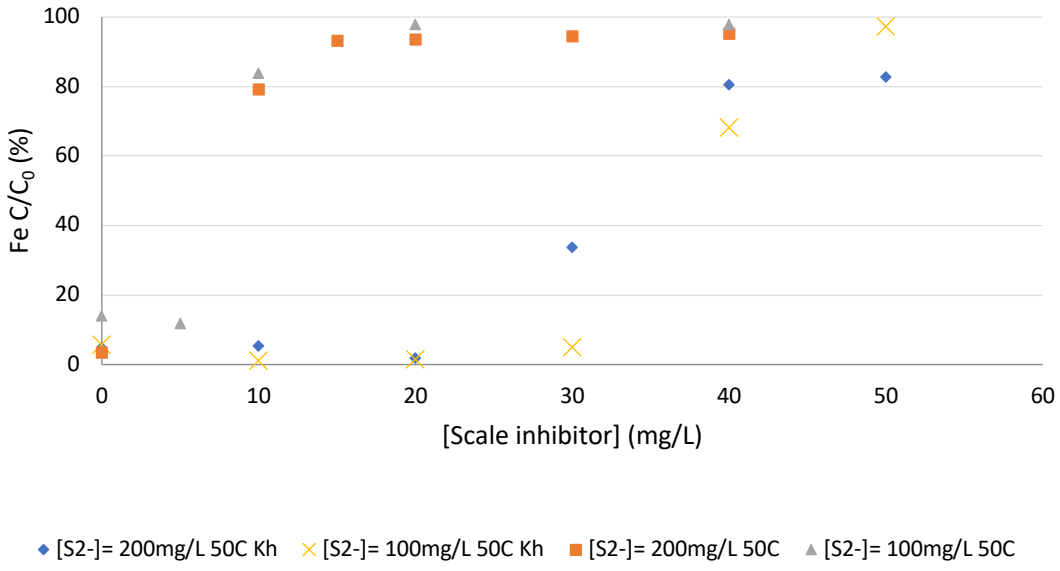

Figure 8.12 Scale inhibition efficiency of SI-2 at room temperature and 50ºC using 3.5 wt.% NaCl and Khuff formation brine to show the effect of brine composition on inhibition

8.3 The Effect of Dissolved Oxygen on the Inhibition Efficiency at [SI] = 40 mg/L

The effect of using an oxidised sulphide solution in the formation of FeS has been found minimal during the investigation in Section 7.3. A similar approach was followed to examine the effect of oxygen on the inhibition efficiency during an autoscale of FeS using an inhibitor concentration of 40 mg/L, found in Figure 8.1. The aqueous sulphide solution was prepared using aerated brine (Khuff Na & Ca) and 1M HCl. The iron concentration was analysed via ICP for filtered and unfiltered samples to illustrate the efficiency of the tested inhibitor.

The oxidised sulphide solution did not show a visible effect on the inhibition of FeS, as seen in the unfiltered data set in Figure 8.13. The iron concentrations at tested pH values

were between 90 – 96 % of the initial iron concentration, which was similar to the 93 % found in Figure 8.1 at pH 6.16. At these test conditions, the effect of sulphide oxidation was found negligible, even in the potential presence of elemental sulphur due to the low adjusted pH of the aqueous sulphide solution.

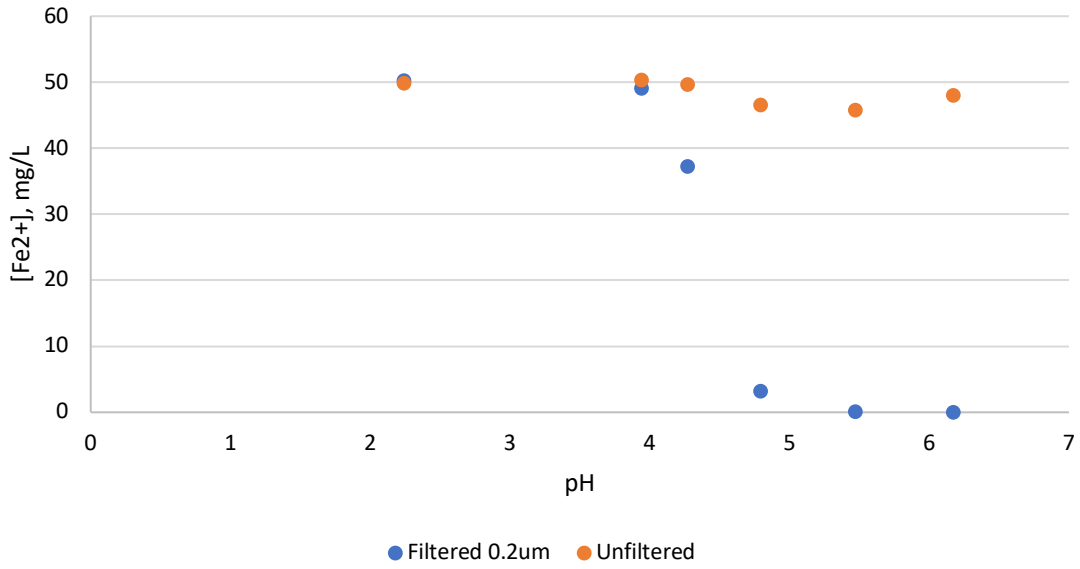

Figure 8.13 The scale inhibition of FeS in terms of $[Fe^{2+}]_{aq}$ at various pH levels using an aerated aqueous sulphide solution and [SI] = 40 mg/L

8.4 Dynamic (Stirring) Test of Inhibited FeS

Similar to the tests in Section 7.6, a dynamic (stirring) test was carried out with the addition of scale inhibitor at the MIC (~ 35 mg/L SI-2) determined from the tests listed in Table 8.1. The samples from this experiment were analysed for iron (ICP), pH and scale composition using ESEM-EDX, as shown in Table 8.2 and Table 8.3.

Table 8.2 Final iron concentrations and pH values of the inhibited FeS solutions after several mixing periods

Mixing duration	*$[Fe^{2+}]_f$, mg/L (filtered through 0.2 μm)*	*pH_f*
1 Hour	0	6.46
1 Day	0	6.55
2 Days	0	6.41
6 Days	0	6.53

Table 8.3 ESEM analysis of the inhibited FeS formed particles in the 3rd set after two days of mixing

Time	*Magnifications*	*50x*	*650x*
Two days	Image	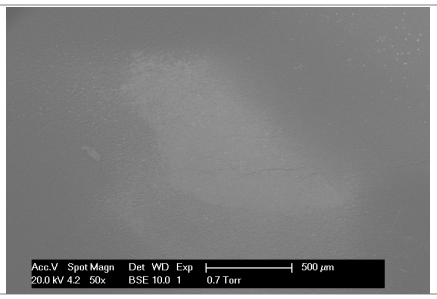	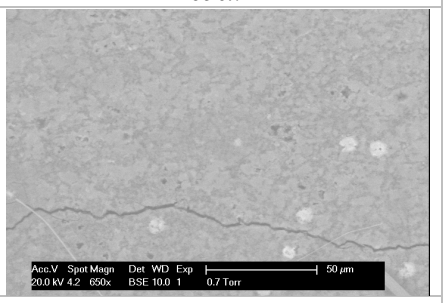
	Fe : S	1 : 0.97	1 : 0.44

The sulphide analysis for inhibited solutions is still under development since the supernatant solutions require filtration or centrifuge to acquire clear and colourless solutions, which caused losses in sulphide count before the analysis. Nonetheless, an example of the ESEM analysis of the sample after two days of mixing, Table 8.3, showed significant differences from un-inhibited sets in Table 7.4 and Table 7.5. The iron-to-sulphur ratios were significantly lower than that of the 1st and 2nd sets, especially at 650x magnification, where the ratio suggested a stoichiometry of *inhibited* Fe_2S. The crystallography of inhibited FeS after two days of mixing appeared similar or even of a smaller size than that observed at one minute and one hour in the two sets shown in Table 7.4 and Table 7.5. This observation emphasised the mechanism of inhibition, where after two days, the inhibitor successfully stopped/slowed the FeS crystal growth, preserving a particle size as small as those formed in less than one hour of mixing.

8.5 Conclusions

The alternative anaerobic experimental setup using airtight Hungate-type tubes and culture vials enabled the examination of the effects of varying the test conditions on the minimum inhibition concentration. A high molecular weight sulphonated co-polymer scale inhibitor has been used in these tests to develop a static evaluation method of the inhibition performance. The conditions investigated in these tests included the initial concentrations of sulphide and iron (II), salinity, pH, temperature, and inhibition duration. In addition, a dynamic (stirring) inhibition test was performed to examine the effect of exposing inhibited FeS to sulphide excess on the particle size and the scale composition

and in terms of sulphur-to-iron atomic ratio. Based on the findings of these tests, the following conclusions were drawn:

(i) The apparent inhibition efficiency of FeS was investigated at various conditions, including sulphide concentrations (100 – 1,000 mg/L) and brine pH (pH 2.24 – 6.93) in anaerobic static bottle test.

(ii) The effect of sulphide concentration directly and positively impacts the inhibition treatment design to increase in the efficiency of inhibited sulphide scale.

(iii) The anaerobic setup produced unprecedented results for a bench-top experimental system and agreed with the results generated in anaerobic chambers and pressurised systems, in terms of the effect of pH on inhibited FeS particle size.

(iv) The collective impact of the pH-adjustment, the conservation of sulphide concentrations, and the vast practicality have provided greater reliability and confidence in the results produced through the use of the new anaerobic setup.

9 – Conclusions and Recommendations

The conventional static test for the sulphide scale formation and inhibition is based on the common barium sulphate jar test. Several modifications have been made and described in the literature to address the requirements of the oilfield sulphide scale studies. However, a few areas of improvements have been identified and modified in the conventional static test setup. These improvements have led to the development of an alternative anaerobic setup based on airtight tubes and vials and gastight syringes. The new anaerobic setup was accompanied by an analytical method, consisting of a copper reagent and a UV-Vis spectrophotometer, specifically modified to accommodate the samples of sulphide scale studies.

The new anaerobic setup was employed in the investigation of sulphide oxidation due to the exposure to oxygen. Furthermore, the formation of iron, zinc and lead sulphide was investigation primarily in a single solution, i.e. autoscale, using the anaerobic setup and the results were validated against theoretical data generated from a scale prediction model. The scale inhibition of FeS was also tested in the anaerobic static setup, and the findings were compared to similar studies in the literature which utilised anaerobic chambers and pressurised systems.

Based on the findings of this study, the alternative anaerobic chamber was confirmed to be excelling at the challenging pH-adjustment process of the aqueous sulphide solutions, providing scaling conditions closer to the in-situ conditions. The setup has also provided unprecedented flexibility in terms of test design and accessibility to sampling and injection, as well as paramount safety measures even at elevated sulphide concentrations and low pH levels. The autoscaling profiles of FeS, ZnS and PbS were positively validated through a scale prediction model, which offered further confidence in the produced results overall. Such autoscaling profiles provide insight of the pH-dependent scale at various conditions, which 1) supports model training, and 2) leads to pinpointing the potential formation and deposition segments in the production lines.

This anaerobic setup has also enabled the examination of the effect of various conditions, including the dependency on initial sulphide concentration, on the inhibition efficiency and the MIC of FeS. In field applications, such accurate and reproducible scale inhibition tests should lead to the optimisation of inhibition treatments. These milestones were

achieved in a bench-top setup at a cost that was significantly lower than the conventional anaerobic chambers and pressurised systems. With increasing production from highly sour reservoirs, the developed setup enables accurate, accessible and safe investigations of, primarily, sulphide scales and, secondarily, elemental sulphur depositions. These studies are critical to provide resolutions to existing sulphide scaling challenges, assess scaling potentials, and proactively provide best practices and prevention means in new field developments. Ultimately, these studies should factor in the operational cost reduction and optimizing the production processes of sour hydrocarbons.

Further improvements and recommendations to the anaerobic setup, the analytical method and the new testing methodologies, which are listed as recommendations and follow up items for future research:

(i) Further investigation in the sulphur formation and deposition mechanisms, as well as sulphur-hydrocarbon interactions.
(ii) Development and evaluation of environmentally friendly dissolvers and solvents for sulphide scales and elemental sulphur, respectively.
(iii) Investigation of scale formation and inhibition in fracturing applications.
(iv) Development of analytical techniques to extract and quantify sulphur- compounds and sulphide ion species.
(v) Further developments of the current setup, which include:
    a. Enhancing the detection limits and automation of the UV-Vis method could be modified for high TDS brine by reducing the dilution factor.
    b. The preparation of aqueous sulphide solutions might be enhanced by using de-oxygenated brines to dissolve the sodium sulphide salt, which is followed by further de-oxygenation.
    c. There might be a potential for the scale prediction model to calculate the dissolution of sulphide scales using the results acquired through new anaerobic experimental setup.
    d. The determination of MIC and autoscaling profiles could be more representative if carried out at higher temperatures, i.e. +90ºC, since most field challenges, such as lead and zinc sulphide scale, occur at high-pressure and high-temperature conditions.

References

US Environmental Protection Agency, 1996. *"Potentiometric Determination of Sulfide in Aqueous Samples and Distillates with Ion-Selective Electrode"*, Test Methods for Evaluating Solid Waste: Physical/Chemical Methods.

Al-Duailej, Y.K., Al-Khaldi, M.H., and AlKulaibi, S., 2012. "*Triazine-Based Scavengers: Can They Be a Potential for Formation Damage?"*, SPE 157109 presented at the International Production and Operations Conference & Exhibition. Doha, Qatar, 14-16 May. doi:10.2118/157109-MS

Al-Duailej, Y.K., Al-Mutairi, S.H., and Al-Humaidan, A.Y., 2010. *"Evaluation of Triazine-Based H_2S Scavengers for Stimulation Treatments"*, SPE 136915 presented at the Saudi Arabia Section Technical Symposium and Exhibition. Al-Khobar, Saudi Arabia, 04-07 April. doi:10.2118/136915-MS

Al-Harbi, B.G., Graham, A.J., and Sorbie, K.S., 2017. "*Zinc and Lead Interactions in Combined Sulphide Scales*", SPE 184509 presented at the International Conference on Oilfield Chemistry, Montgomery, Texas, 3-5 April.

Al-Harbi, B.G., Graham, A.J., and Sorbie, K.S., 2018. *"Laboratory investigation of zinc and lead sulphide inhibition"*, SPE 189572 presented at the International Conference and Exhibition on Formation Damage Control, Lafayette, Louisiana, USA, 07-09 February.

Al-Jaberi, J., Al-Azani, K., and Fraim, M., 2017. *"Calculation of Sulfur Deposition in Gas Condensate Wells in Middle East"*, SPE 188000 presented at the Kingdom of Saudi Arabia Annual Technical Symposium and Exhibition, Dammam, Saudi Arabia, 24-27 April. doi:10.2118/188000-MS

Al-Mutairi, S.A., Abdulhadi, A.I., and Al-Taie, I.M., 2007. *"Sour Gas Dehydration System: Corrosivity And Selection in the Presence of Elemental Sulfur"*, NACE 7397 presented at the Corrosion Conference & Expo, Nashville, Tennessee, USA, 11-15 March.

Almgren, T. and Hagström, I., 1974. *"The oxidation rate of sulphide in sea water"*. Water Research. Vol.8, p395–400. doi:10.1016/0043-1354(74)90069-4

Avrahami, M. and Golding, R.M., 1968. *"The oxidation of the sulphide ion at very low concentrations in aqueous solutions"*. Journal of the Chemical Society A: Inorganic, Physical. Theoretical. Vol.68, p647–651. doi:10.1039/j19680000647

Baraka-Lokmane, S., Hurtevent, C., Tillement, O., Simpson, C., and Graham, G.M., 2015. *"Development and Qualification of New Zinc and Lead Sulphide Scale Inhibitors for Application under Harsh Conditions"*, SPE 173761 presented at the International Symposium on Oilfield Chemistry, The Woodlands, Texas, USA, 13-15 April. doi:10.2118/173761-MS

Baraka-Lokmane, S., J. Charpentier, T. V, Neville, A., Hurtevent, C., Ordonez-Varela, J.R., Moeller Nielsen, F., Eroini, V., Olsen, J.H., Ellingsen, J.A., and Bache, O., 2014. *"Comparison of Characteristic of Anti-Scaling Coating for Subsurface Safety Valve for Use in Oil and Gas Indsutry"*, IPTC 17953 presented at the International Petroleum Technology Conference, Kuala Lumpur, Malaysia, 10-12 December.

Barré, G., Gaucher, E., Hoareau, G., and Elias-Bahnan, A., 2018. *"Unravelling the Processes of the H_2S Generation in the North-western Pyrenees (France)"*, Th SRM 04 presented at EAGE/IFPEN Conference on Sulfur Risk Management in

E&P, Rueil-Malmaison, France, 18-20 September.

Barrett, T.J. and Anderson, G.M., 1988. *"The solubility of sphalerite and galena in 1–5 m NaCl solutions to 300°C"*, Geochimica et Cosmochimica Acta, Vol.52, p813–820. doi:10.1016/0016-7037(88)90353-5

Barzegar, M., Jabbari, A., and Esmaeili, M., 2003. *"Kinetic Spectrophotometric Determination of Trace Amounts of Sulfide"*, Bull. Korean Chemical Society Vol.24, p1261–1264. doi:10.5012/bkcs.2003.24.9.1261

Bhandari, N., Kan, A.T., Ruan, G.G., Liu, Y., Zhang, F., Yan, F., Alsaiari, H.A., Zhang, Z., Dai, Z., Lu, Y., Deng, G, and Tomson, M.B., 2016. *"Iron Sulfide Scale Control : A Novel Chemical for Growth Inhibition and Dispersion"*, SPE 179872 presented at the International Oilfield Scale Conference and Exhibition, Aberdeen, Scotland, UK, 11-12 May.

Bignell, L.G.E., 1930. *"Review of Oil-field Corrosion Problems for 1929"*, Transactions of the AIME, Vol.86, p392–395. doi:10.2118/930392-G

Boivin, J. and Oliphant, S., 2011. *"Sulfur Corrosion Due To Oxygen Ingress"*, NACE 11120 presented at the Corrosion Conference & Expo. Houston, Texas, USA, 13-17 March.

Boschee, P., 2014. *"Taking on the Technical Challenges of Sour Gas Processing"*, Oil and Gas Facilities. Vol.3, p21–25. doi:10.2118/1214-0021-OGF

Broderius, S.J. and Smith, L.L., 1980. *"Direct Determination and Calculation of Aqueous Hydrogen Sulfide"*, Analytical Chemistry, Vol. 49, p424–428.

Brunner, E., and Woll, W., 1980. *"Solubility of Sulfur in Hydrogen Sulfide and Sour Gases"*, Society of Petroleum Engineers Journal, October, p377–384.

Burt, I. and Susanna, L., 2015. *"Managing 23 % H_2S during Appraisal Well Drilling & Testing Operations in an Area with Adjacent Population and Infrastructure"*, SPE 177772 presented at Abu Dhabi International Petroleum Exhibition and Conference, Abu Dhabi, UAE, 09-12 November.

Bybee, K., 2001. *"Inhibition of Lead and Zinc Sulphide Scale Deposits"*, Journal of Petroleum Technology, Vol.53, p61–62. doi:10.2118/0301-0061-JPT

Canty, D., 2012. *"The Middle East Sour Oil & Gas Upstream Profile"*, [WWW Document]. *http://www.arabianoilandgas.com/article-10245-the-middle-east-sour-oil-gas-upstream-profile/1/*

Casella, I.G., Guascito, M.R., and Desimoni, E., 2000. *"Sulfide measurements by flow injection analysis and ion chromatography with electrochemical detection"*, Analytica Chimica Acta, Vol.409, p27–34.

Chen, K. and Morris, J., 1972. *"Kinetics of Oxidation of Aqueous Sulfide by O_2"*. Environmental Science Technology, Vol.6, p529–537. doi:10.1021/es60065a008

Clever, H.L., Derrick, M.E., and Johnson, S.A., 1992. *"The Solubility of Some Sparingly Soluble Salts of Zinc and Cadmium in Water and in Aqueous Electrolyte Solutions"*, Journal of Physical and Chemical Reference Data, Vol.21, p941–1004. doi:10.1063/1.555909

Clever, H.L. and Johnston, F.J., 1980. *"The solubility of some sparingly soluble lead salts: An evaluation of the solubility in water and aqueous electrolyte solution"*, Journal of Physical and Chemical Reference Data, Vol.9, p 751. doi:10.1063/1.555628

Cline, J., 1969. *"Spectrophotometric Determination of Hydrogen Sulfide in Natural Waters"*, Limnology and Oceanography. Vol.14, p454–458. doi:10.4319/lo.1969.14.3.0454

Cline, J.D. and Richards, F.A., 1969. *"Oxygenation of Hydrogen Sulfide in Seawater at Constant Salinity, Temperature and pH"*, Environmental Science and Technology, Vol.3, p838–843. doi:10.1021/es60032a004

Collins, I.R. and Jordan, M.M., 2001. *"Occurrence, Prediction, and Prevention of Zinc Sulfide Scale Within Gulf Coast and North Sea HighTemperature/High-Salinity Production Wells"*, SPE 68317 presernted at the Third Internationl Symposium on Oilfield Scale, Aberdeen, UK, 30-31 January.

Collins, I.R. and Jordan, M.M., 2003. *"Occurrence, Prediction, and Prevention of Zinc Sulfide Scale Within Gulf Coast and North Sea High-Temperature and High-Salinity Fields"*. SPE Production and Facilities. Vol.18, p200–209. doi:10.2118/84963-PA

Cord-Ruwisch, R., 1985. *"A quick method for the determination of dissolved and precipitated sulfides in cultures of sulfate-reducing bacteria"*, Journal of Microbiological Methods, Vol.4, p33–36.

Crabtree, M., Eslinger, D., Fletcher, P., Miller, M., Johnson, A., and King, G., 1999. *"Fighting Scale — Removal and Prevention"*. Oilfield Review. Automn, 30–45.

Crowe, C.W., 1987. *"Method of preventing precipitation of ferrous sulfide and sulfur during acidizing"*. US 4633949 patent.

Cutter, G.A. and Radford-knoery, J., 1993. *"Carbonyl sulfide in two estuaries and shelf waters of the western North Atlantic Ocean"*, Marine Chemistry, Vol.43, p225–233.

Devine, J.M., Wilhelm, C.J., and Schmidt, L., 1934. *"Comparative Resistance of Certain Commercial Ferrous Materials to Corrosion by Gaseous Hydrogen Sulfide"*, Transactions of the AIME, Vol.107, p106–110. doi:10.2118/934106-G

Ellenberger, A.R. and Holben, J.H., 1959. *"Flood Water Analyses and Interpretation"*, Journal of Petroleum Technology, Vol. 11, p22–25. doi:10.2118/1199-G

Emami, M., Mousavi, M.F., and Barzegar, M., 2004. *"Determination of sulfide in spring and wastewater by a new kinetic spectrophotometric method"*, Journal of the Chinese Chemical Society, Vol.51, p517–521. doi:10.1002/jccs.200400078

Fadairo, A.A., Ako, C.H., and Falode, O.A., 2012. *"Elemental Sulphur Induced Formation Damage Management in Gas Reservoir"*, SPE 154980 presented at the International Conference on Oilfield Scale, Aberdeen, UK, 30-31 May. doi:10.2118/154980-MS

Fishman, M.J. and Friedman, L.C., 1985. *"Sulfide, titrimetric, iodometric"*, Methods for the Determination of Inorganic Substances in Water and Fluvial Sediments. the United States Geological Survey, Vol. 5, Chapter A1.

Franco, C., Solares, J., Al-Marri, H., Mukhles, A., Ramadhan, N., and Al-Saihati, A., 2010. *"Analysis of Deposition Mechanism of Mineral Scales Precipitating in the Sandface and Production Strings of Gas-Condensate Wells"*, SPE Production & Operations, Vol.25, p15–18. doi:10.2118/120410-PA

Ghaderi, S.M., Keith, D.W., Lavoie, R., and Leonenko, Y., 2011. *"Evolution of hydrogen sulfide in sour saline aquifers during carbon dioxide sequestration",* International Journal of Greenhouse Gas Control, Vol.5, p347–355.

doi:10.1016/j.ijggc.2010.09.008

Graham, G.M., Sorbie, K.S., and Jordan, M.M., 1997. *"How scale inhibitors work and how this affects test methodology"* presented at the IBC International Conference on Solving Oilfield Scaling, Aberdeen, UK, 22-23 January.

Guo, X., Du, Z., Zhang, Y., and Wang, L., 2006. *"Laboratory and simulation-investigation of sulfur deposition in sour gas reservoir"*, SPE 103810 presented at the International Oil and Gas Conference and Exhibition, Beijing, China, 05-07 December. doi:10.2118/103810-MS

Hajj, H. El, Peng, Y., Fan, C., Alburaikan, R., Leal, J., and Chang, F., 2015. *"A Systematic Approach to Dissolve Iron Sulfide Scales"*, SPE 172794 presented at the SPE Middle East Oil & Gas Show and Conference, Manama, Bahrain, 08-11 March.

Halfyard, J.E. and Hawboldt, K., 2011. *"Separation of elemental sulfur from hydrometallurgical residue: A review"*. Hydrometallurgy, Vol.109, p80–89. doi:10.1016/j.hydromet.2011.05.012

Hands, N., Oz, B., Roberts, B., Davis, P., Sulphur, A., and Minchau, M., 2002. *"Advances in the Prediction and Management of Elemental Sulfur Deposition Associated with Sour Gas Production from Fractured Carbonate Reservoirs"*, SPE 77332 presented at the Annual Technical Conference and Exhibition, San Antonio, Texas, 29 September - 02 October.

Harmandas, N.G., Navarro Fernandez, E., and Koutsoukos, P.G., 1998. *"Crystal Growth of Pyrite in Aqueous Solutions. Inhibition by Organophosphorus Compounds"*, Langmuir, Vol.14, p1250–1255. doi:10.1021/la970354c

Hartog, F. A., Jonkers, G., Schmidt, A.P., and Schuiling, R.D., 2002. *"Lead Deposits in Dutch Natural Gas Systems"*, SPE Production and Facilities, Vol.17, p122–128. doi:10.2118/78147-PA

Headlee, A.J.W., 1945. *"Interactions Between Interstitial And Injected Water-A Review"*, Drilling and Production Practice. American Petroleum Institute, New York, USA, p59-64.

Henni, A., 2013. *"Sour Gas Interest Grows in Middle East"* Journal of Petroleum Technology, Vol.65, 54–55. doi:10.2118/0713-0054-JPT

Jordan, M.M. and Mackay, E.J., 2005. *"Integrated Field Development For Effective Scale Control Throughout the Water Cycle in Deep Water Subsea Fields"*, SPE 94052 presented at the Europec/EAGE Annual Conference. Society of Petroleum Engineers, Madrid, Spain, 13-16 June. doi:10.2118/94052-MS

Jordan, M.M., Sjursaether, K., Bruce, R., and Edgerton, M.C., 2000. *"Inhibition of Lead and Zinc Sulphide Scale Deposits Formed During Production From High Temperature Oil and Condensate Reservoirs"*, SPE 64427 presented at the Asia Pacific Oil & Gas Conference,Brisbane, Australia, 16-18 October. doi:10.2118/64427-ms

Kamyshny, A. and Ferdelman, T.G., 2010. *"Dynamics of zero-valent sulfur species including polysulfides at seep sites on intertidal sand flats (Wadden Sea, North Sea)"*, Marine Chemistry, Vol.121, p17–26. doi:10.1016/j.marchem.2010.03.001

Kamyshny, A., Zilberbrand, M., Ekeltchik, I., Voitsekovski, T., Gun, J., and Lev, O., 2008. *"Speciation of polysulfides and zerovalent sulfur in sulfide-rich water wells in Southern and Central Israel"*, Aquatic Geochemistry, Vol.14, p171–192.

doi:10.1007/s10498-008-9031-6

Kan, A. and Tomson, M., 2012. *"Scale Prediction for Oil and Gas Production"*, SPE Journal, Vol.17, p362–378. doi:10.2118/132237-PA

Kasnick, M.A., and Engen, R.J., 1989. *"Iron Sulfide Scaling and Associated Corrosion in Saudi Arabian Khuff Gas Wells"*, SPE 17933 presented at the Middle East Oil Show, Manama, Bahrain, 11-14 March. doi:10.2118/17933-MS

Kelland, M.A., 2011. *"Effect of various cations on the formation of calcium carbonate and barium sulfate scale with and without scale inhibitors"*. Industrial & Engineering Chemistry Research, Vol. 50, 5852–5861. doi:10.1021/ie2003494

Kelland, M.A., 2016. *"Production Chemicals for the Oil and Gas Industry"*. CRC Press.

Keogh, W., Charpentier, T., Neville, A., O'Brien, A., Eroini, V., Olsen, J.H., Nielsen, F.M., Ellingsen, J.A., Bache, O., and Baraka-Lokmane, S., 2017. *"Evaluation of Anti-Fouling Surfaces for Prevention of Lead Sulfide Scaling in Single and Multiphase Conditions"*, NACE 9658 presented at the Corrosion Conference and Expo. New Orleans, Louisian, USA, 26-30 March.

Kerr, J., Aarag, I., and Williams, E., 2017. *"The Evaluation and Development of Exotic Scale Dispersants Using Kinetic Turbidity Testing"*, Proceedings in Tekna Oil Field Chemistry Symposium, Gielo, Norway, 26-29 March.

Khan, R., Nighswander, J., Ponminissery, J., Stankiewicz, A., Okoh, B., Ashtekar, S., and Pollard, R., 2017. *"H_2S Losses in Reservoir Fluid Sample Chambers – A Case Study"*, OTC 27871 presented at the Offshore Technology Conference, Houston, Texas, USA, 1-4 May. doi:10.4043/27871-MS

Kolthoff, I.M., 1930. *"The Solubilities and Solubility Products of Metallic Sulphides in Water"*, The Journal of Physical Chemistry, Vol.35, p2711–2721. doi:10.1021/j150327a019

Lamoureux-Var, V., Ameur, Z.O., Michel, P., Lévêque, I., Ravin, A., Pillot, D., Ayache, S., and Preux, C., 2018. *"Characterizing Sulfur in Foster Creek Bitumen Using Rock- Eval Sulfur , for Assessing H_2S Production Risk in SAGD Operations"*, Th SRM 03 presented at the EAGE/IFPEN Conference on Sulfur Risk Management in E&P, Rueil-Malmaison, France, 18-20 September.

Lawrence, N.S., Davis, J., and Compton, R.G., 2000. *"Analytical strategies for the detection of sulfide : a review"*, Talanta, Vol.52, p771–784.

Leal, J., Solares, J.R., Nasr-El-Din, H.A., Franco, C., Garzon, F., Marri, H.M., Aqeel, S.A., and Izquierdo, G., 2007. *"A systematic approach to remove iron sulphide scale: A case history"*, SPE 105607 presented at the Middle East Oil Gas Show Conference, Bahrain International Exhibition Centre, Kingdom of Bahrain, 11-14 March.

Lefers, J.B., Koetsier, W.T., and Van Swaaij, W.P.M., 1978. *"The oxidation of sulphide in aqueous solutions"*, The Chemical Engineering Journal, Vol.15, p111–120. doi:10.1016/0300-9467(78)85003-5

Lehmann, M. and Firouzkouhi, F.F., 2008. *"A New Chemical Treatment to Inhibit Iron Sulfide Deposition and Agglomeration"*, SPE 114065 presented at the International Oilfield Scale Conference, Aberdeen, UK, 28-29 May. doi:10.2118/114065-MS

Liu, Q., Diaconu, A., and Grey, D., 2012. *"Elemental Sulfur Uptake and Corrosion Protection in Sour Gas Systems"*, NACE-2012-1090 presented at the Corrosion

Conference & Expo, Slat Lake City, Utah, USA, 11-15 March.

Liu, Y., Zhang, Z., Bhandari, N., Yan, F., Zhang, F., Ruan, G., Dai, Z., Alsaiari, H.A., Lu, A.Y., Deng, G., Kan, A.T., Tomson, M.B., 2017. *"Iron Sulfide Precipitation and Deposition under Different Impact Factors"*, SPE 184546 presented at the International Conference on Oilfield Chemistry, Montgomery, Texas, USA, 3-5 April.

Lopez, T.H., Yuan, M., Willamson, D. A, and Przbylinski, J.L., 2005. *"Comparing Efficacy of Scale Inhibitors for Inhibition of Zinc Sulfide and Lead Sulfide Scales"*, SPE 95097 presented at the International Symposium on Oilfield Scale, Aberdeen, Uk, 11-12 May. doi:10.2118/95097-MS

Luther, G.W., Findlay, A.J., MacDonald, D.J., Owings, S.M., Hanson, T.E., Beinart, R.A., and Girguis, P.R., 2011. *"Thermodynamics and Kinetics of Sulfide Oxidation by Oxygen: A Look at Inorganically Controlled Reactions and Biologically Mediated Processes in the Environment"*. Frontiers in Microbiology, Vol.2, 1–9. doi:10.3389/fmicb.2011.00062

Mahmoud, M., 2014. *"Effect of Elemental-Sulfur Deposition on the Rock Petrophysical Properties in Sour-Gas Reservoirs"*, the SPE Journal, August, p703–715.

Mahmoud, M.A. and Al-Majed, A.A., 2012. *"New Model to Predict Formation Damage Due to Sulfur Deposition in Sour Gas Wells"*, SPE 149535 presented at the North Africa Technical Conference and Exhibition, Cairo, Egypt, 20-22 February.

Mei, H., Zhang, M., and Yang, X., 2006. *"The Effect of Sulfur Deposition on Gas Deliverability"*, SPE 99700 presented at Gas Technology Symposium, Calgary, Alberta, Canada, 15-17 May.

Mills, R.V.A., 1926. *"Corrosion in Oil and Gas Wells - Its Causes and Prevention",* Transactions of the AIME*,* G-26, p589–597. doi:10.2118/926589-G

Mirza, M.S. and Prasad, V., 1999. *"Scale Removal in Khuff Gas Wells"*, SPE 53345 presented at the Middle East Oil Show and Conference, Bahrain, 20-23 February.

Morse, J.W., Millero, F.J., Cornwell, J.C., and Rickard, D., 1987. *"The chemistry of the hydrogen sulfide and iron sulfide systems in natural waters"*, Earth-Science Reviews, Vol.24, p1–42. doi:http://dx.doi.org/10.1016/0012-8252(87)90046-8

Murphy, H.D., 1949. *"Selection Maintenance of Lease Production Tanks in sulfide Areas"*, API-49-370, presented at Drilling and Production Practice, New York, USA, 1 January.

Nasr-El-Din, H.A.H., and Al-Humaidan, A.Y.A., 2001. *"Iron Sulfide Scale: Formation, Removal and Prevention"*, SPE 68315 presented at the International Symposium on Oilfield Scale, Aberdeen, United Kingdom, 30-31 January. doi:10.2523/68315-MS

Nielsen, A.H., Vollertsen, J., and Hvitved-Jacobsen, T., 2003. *"Determination of kinetics and stoichiometry of chemical sulfide oxidation in wastewater of sewer networks"*, Environmental Science & Technology, Vol.37, p3853–3858. doi:10.1021/es0340351

O'Brien, D.J. and Birkner, F.B., 1977. *"Kinetics of oxygenation of reduced sulfur species in aqueous solution"*, Environmental Science & Technology*,* Vol.11, p1114–1120. doi:10.1021/es60135a009

Oduro, H., Kamyshny, A., Zerkle, A.L., Li, Y., and Farquhar, J., 2013. *"Quadruple sulfur isotope constraints on the origin and cycling of volatile organic sulfur*

compounds in a stratified sulfidic lake", Geochimica et Cosmochimica Acta, Vol.120, p251–262. doi:10.1016/j.gca.2013.06.039

Okocha, C. and Sorbie, K., 2013. *"Scale Prediction for Iron, Zinc, and Lead Sulfides and Its Relation to Scale Test Design"*, SPE 164111 presented at the International Symposium on Oilfield Chemistry, The Woodlands, Texas, USA, 08-10 April. doi:10.2118/164111-MS

Okocha, C. and Sorbie, K.S., 2010. *"Effects of Sulphide Scales (PbS, ZnS & FeS) on $BaSO_4$ Crystal Growth and Dissolution"*, SPE 130391 presented at the International Conference on Oilfield Scale, Aberdeen, UK, 26-27 May. doi:10.2118/130391-MS

Okocha, C., Sorbie, K.S., and Boak, L.S., 2008. *"Novel Inhibition Mechanism for Sulfide Scales"*, SPE 112538 presented at the International Symposium and Exhibition on Formation Damage Control, Lafayette, Louisiana, USA, 13-15 February. doi:10.2118/112538-MS

Okocha, C.E., 2011. *"Mechanistic Evaluation of Sulphide Scale Formation in the Oilfield"*, PhD Dissertation, Heriot-Watt University, Edinburgh, UK.

Orski, K., Grimbert, B., Menezes, C.A., and Quin, E., 2007. *"Fighting Lead and Zinc Sulphide Scales on a North Sea HP/HT Field"*, SPE 107745 presented at the European Formatino Damage Conference, Scheveningen, The Netherlands, 30 May - 1 June. doi:10.2118/107745-MS

Pitzer, K.S., 1973. *"Thermodynamics of electrolytes. I. Theoretical basis and general equations"*, Journal of Physical Chemistry, Vol.77, p268–277. doi:10.1021/j100621a026

Plummer, F.B. and Walling, I.W., 1946. *"Laboratory Investigations of Chemical Changes in East Texas Oil-field Water Affecting its Injection into Subsurface Sands"*, Transactions of the AIME, Vol.165, p64–77. doi:10.2118/946064-G

Przybylinski, J., 2001. *"Iron Sulfide Scale Deposit Formation and Prevention under Anaerobic Conditions Typically Found in the Oil Field"*, SPE 65030 presented at the International Symposium on Oilfield Chemistry, Houston, Texas, 13-16 February. doi:10.2523/65030-MS

Przybylinski, J.L., 2003. *"Ferrous Sulfide Solid Formation and Inhibition at Oxidation-Reduction Potentials and Scaling Indices Like Those That Occur in the Oil Field"*, SPE 80260 presented at the International Symposium on Oilfield Chemistry Houston, Texas, 05-07 February. doi:10.2118/80260-ms

Ramachandran, S., Al-Muntasheri, G., Leal, J., and Wang, Q., 2015a. *"Corrosion and Scale Formation in High Temperature Sour Gas Wells: Chemistry and Field Practice"*, SPE 173713 presented at the International Symposium on Oilfield Chemistry, The Woodlands, Texas, USA, 13-15 April. doi:10.2118/173713-MS

Ramachandran, S., Al-muntasheri, G.A., Company, A.S., Al-ajwad, H., Gupta, A., Leal, J., and Jovancicevic, V. 2015b. *"Engineering Corrosion Protection in High Temperature High Pressure Sour Gas Wells"*, SPE 177882 presented at Abu Dhabi International Petroleum Exhibition and Conference, Abu Dhabi, UAE, 09-12 November.

Rickard, D., 2012. *"Sulfur Chemistry in Aqueous Solutions"*, Developments in Sedimentology, Vol.65, p31-83. doi:10.1016/B978-0-444-52989-3.00002-7

Rickard, D., 1989. *"Experimental concentration-time curves for the iron(II) sulphide precipitation process in aqueous solutions and their interpretation"*, Chemical

Geology, Vol.78, p315–324. doi:10.1016/0009-2541(89)90066-1

Rickard, D. and Luther, G.W., 2007. *"Chemistry of iron sulfides"*, Chemical Reviews, Vol.107, p514–562. doi:10.1021/cr0503658

Roberts, B., 1997. *"The Effect of Sulfur Deposition on Gaswell Inflow Performance"*, SPE Reservoir Engineering, Vol.12, p112-123 doi:10.2118/36707-PA

Rogers, W.F. and Rowe Jr., A., 1955. *"Corrosion Effects of Hydrogen Sulphide and Carbon Dioxide in Oil Production"*, Proceedings in the 4th World Petroleum Congress. Rome, Italy.

Savin, A.J., Adamson, B., Wylde, J.J., Kerr, J.R., Kayser, C.W., Trallenkamp, T., Fischer, D., and Okocha, C., 2014. *"Sulfide Scale Control: A High Efficacy Breakthrough Using an Innovative Class of Polymeric Inhibitors"*, SPE 169777 presented at the International Oilfield Scale Conference and Exhibition, Aberdeen, UK, 14-15 May. doi:10.2118/169777-MS

Scatchard, G., 1925. *"The activity of strong electrolytes. IV. The application of the debye-hückel equation to alcoholic solutions"*, The Journal of American Chemical *Society*, Vol.47, p2098–2111. doi:10.1021/ja01685a004

Shanthi, K. and Balasubramanian, N., 1996. *"A Simple Spectrophotometric Method for the Determination of Hydrogen Sulfide Based on Schiff ' s Reaction"*, Microchemical Journal, Vol.174, p168–174.

Shedid, S.A. and Zekri, A.Y., 2002. *"Formation Damage Due To Sulfur Deposition in Porous Media"*, SPE 73721 presented at the International Symposium on Formation Damage Control, Lafayette, Louisiana, USA, 20-21 February.

Silva, D.J., Sorbie, K.S., Ness, G., and Mackay, E.J., 2018. *"Carbonate and Sulphide Scale Prediction Modelling in Auto-Scaling Processes : Procedure for the Calculation of Reservoir Fluid Compositions and Scale Profiles in Production Systems using Topside Data"*, SPE 190711 presented in the International Oilfield Scale Conference, Aberdeen, Scotland, UK, 20-21 June. doi:10.2118/190711-MS

Silva, D.J.A. de C. e, 2017. *"Mineral Scale Prediction Modelling: Precipitation of $CaCO_3$ Scale in CO_2-Water Alternating Gas Production Systems"*, PhD Dissertation, Heriot-Watt University, Edinburgh, UK.

Steudel, R., 1996. *"Mechanism for the Formation of Elemental Sulfur from Aqueous Sulfide in Chemical and Microbiological Desulfurization Processes"*, Industrial & Engineering Chemistry Research, Vol.35, p1417–1423. doi:10.1021/ie950558t

Stumm, W. and Lee, G.F., 1961. *"Oxygenation of Ferrous Iron"*, Industrial & Engineering Chemistry, Vol.53, p143–146.

Sun, H., Fang, H., Davis, J., and Hudgins, R., 2011. *"Elemental Sulfur Corrosion and Inhibition in the Presence of Sulfur Solvent"*, NACE 11125 presented at the Corrosion Conference & Expo, Houston, Texas, 13-17 March.

Tang, Y., Voelker, J., Keskin, C., Xu, Z., Hu, B., and Jia, C., 2011. *"A Flow Assurance Study on Elemental Sulfur Deposition in Sour Gas Wells"*, SPE 147244 presented at the Annual Technical Conference Exhibition, Denver, Colorado, 30 October - 2 November.

Thakur, G.C. and Satter, A., 1998. *"Integrated Waterflood Asset Management"*. PennWell Books, ISBN 0878146067.

Verri, G., Sobie, K.S., Singleton, M.A., Hinrichsen, C., Wang, Q., Chang, F.F., and Ramachandran, S., 2017. *"Iron sulfide scale management in high H_2S and CO_2*

carbonate reservoirs", SPE Production & Operrations, Vol.32, p305–313. doi:https://doi.org/10.2118/179871-PA

Verri, G. and Sorbie, K., 2017. *"Iron Sources in Sour Wells: Reservoir Fluids or Corrosion?"*, NACE 8998 presented at the International Corrosion Conference & Expo, New Orleans, Louisiana, 26-30 March.

Wallace, K.J., Cordero, S.R., Tan, C.P., Lynch, V.M., and Anslyn, E. V, 2007. *"A colorimetric response to hydrogen sulfide"*, Sensors and Actuators B: Chemical, Vol.120, p362–367. doi:10.1016/j.snb.2006.02.031

Wang, B., Chen, T., Chen, P., Montgomerie, H., Hagen, T.H., Liu, X., and Yang, X., 2012. *"Development of Test Method and Environmentally Acceptable Inhibitors for Zinc Sulfide Deposited in Oil and Gas Fields"*, SPE 130926 presented at the International Conference on Oilfield Scale, Aberdeen, United Kingdom, 26-27 May. doi:10.2118/156005-MS

Wang, Q., Ajwad, H., Shafai, T., and Lynn, J.D., 2013. *"Iron Sulfide Scale Dissolvers: How Effective Are They?"*, SPE 168063 presented at the Saudi Arabia Section Technical Symposium and Exhibition, Khobar, Saudi Arabia, 19–22 May. doi:10.2118/168063-MS

Wang, Q., Leal, J., Syafii, I., Mukhles, A.E., Chen, T., Chang, F., and Espinosa, M., 2016. *"Iron Sulfide and Removal in Scale Formation Sour Gas Wells"*, SPE 179869 presented at the International Oilfield Scale Conference and Exhibition. Aberdeen, Scotland, UK, 11-12 May.

Weres, O. and Tsao, L., 1983. *"Reaction of hydrogen sulfide with oxygen in the presence of sulfite"*, Lawrence Berkeley Laboratory, California, United States. doi:10.2172/6131155

William, M. H., 2010. *"Solubility Product Constants"*, CRC Handbook of Chemistry and Physics 91st Edition. Taylor & Francis Group, pp. 127–129.

Wylde, J.J., Okocha, C., Bluth, M., Savin, A., and Adamson, B., 2015. *"Iron Sulfide Inhibition: Field Application of an Innovative Polymeric Chemical"*, SPE 173730 presented at the International Symposium on Oilfield Chemistry, The Woodlands, Texas, USA, 13-15 April. doi:10.2118/173730-MS

Xiao, G., Zhimin, D., and Li, W., 2010. *"Effect of Sulfur Deposition on Rock Permeability in Sour Gas Reservoir"*, SPE 136979 presented at the 34th Annual SPE International Conference and Exhibition, Tinapa – Calabar, Nigeria, 31 July - 7 August. doi:10.2118/136979-MS

Zangh, J.-Z. and Millero, F.J., 1992. *"Kinetics of oxidation of hydrogen sulfide in natural waters"*, Environmental Geochemistry of Sulfide Oxidation, Ch.26, 393–409.

Zekri, A.Y., Shedid, S.A., and Almehadeb, R.A., 2009. *"Sulfur and Asphaltene Deposition During CO_2 Flooding of Carbonate Reservoirs"*, SPE 118825 presented at the Middle East Oil and Gas Show and Conference, Manama, Bahrain, 15-18 March.

Zerkle, A.L., Kamyshny, A., Kump, L.R., Farquhar, J., Oduro, H., and Arthur, M.A., 2010. *"Sulfur cycling in a stratified euxinic lake with moderately high sulfate: Constraints from quadruple S isotopes*", Geochimica et Cosmochimica Acta, Vol.74, p4953–4970. doi:10.1016/j.gca.2010.06.015

Appendix A - Development of the UV-Vis Spectrophotometric method

The Repeatability of the 100 µL SGE™ Gastight Syringe (with and without Repeating Adaptor RAX) Against the 1,000 µL Volumetric Pipette

The UV-Vis method required an accurate technique of transferring the 0.1 mL of sulphide sample to the copper reagent. Initially, the Eppendorf volumetric pipette was used, and it was later compared to the SGE™ Gastight Syringe, which was further mounted with the repeating adaptor (RAX). Table (I) shows the repeatability of each dispensing technique using DW (ρ = 1 g/mL) and an analytical balance to measure the weight. Excluding the human error reduced the standard deviation in the Eppendorf volumetric pipette and the SGE™ syringe with mounted RAX, and the latter was preferred due to the use of anaerobic tubes with septa-caps.

Table (I) Repeatability of 0.100 µL using different analytical tools.

Runs	*Eppendorf Pipette*	*SGE™ syringe*	*SGE™ syringe w/ RAX*
1	0.1004	0.0996	0.1006
2	0.1002	0.0993	0.0999
3	0.1004	0.0990	0.1004
4	0.1005	0.0994	0.1002
5	0.1003	0.0991	0.1003
6	0.1006	0.0989	0.1000
7	0.1003	0.0994	0.1002
8	0.1002	0.0997	0.1000
9	0.1009	0.0987	0.1002
10	0.1008	0.0995	0.1002
11	0.1005	0.0990	0.1000
12	0.1006	0.0999	0.1002
STD	± 0.2126%	± 0.3427%	± 0.1863%

Appendix B – pH Measurement of Anaerobic Sulphide Solutions

The pH measurement of sulphide solutions was challenging due to the sensitivity to pH and H_2S evolution at low pH. A non-intrusive pH measurement technique was commercially available through Presens Online Optical pH measurement. Unfortunately, the dot sensors are only applicable in pH 4.0 – 7.5. Although such range was useful, it would have limitations in the pH ranges covered in the sulphide studies (pH 0 – 12).

Alternatively, a conventional pH probe was used to measure the pH in vials (40 mL) immediately after opening their caps, as seen in Figures IX and X. The measurement commonly lasted 30 – 90 seconds, depending on how rapid the pH meter validated the measurement.

Figure (IX) pH measurement of a high pH sulphide solution in a vial

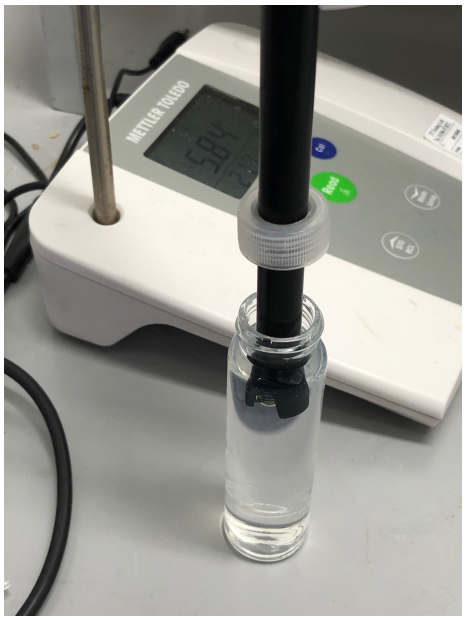

Figure (X) pH measurement of a low pH sulphide solution in a vial (notice the turbidity

To confirm that stable pH readings can be obtained during this period and to confirm that H_2S evolution is not impactful to the pH, a short test was devised. Two 40-mL samples of 100 mg/L of H_2S in DW were prepared, and their pH was measured initially (pH 11.26 and 11.25). Afterwards, 140 µL of 1M HCl was added to sample one through the septum, while sample two received 200 µL of 1M HCl. Samples were shaken and the pH was

measured immediately after opening the cap. Figure XI shows the pH measurements against time for each sample. Both samples became stable after ~ 60 - 90 seconds, and insignificant pH changes were recorded afterwards. The evolution of H_2S would theoretically increase the pH as the concentrations of hydrogen protons begin to decrease. However, such impact was not observed.

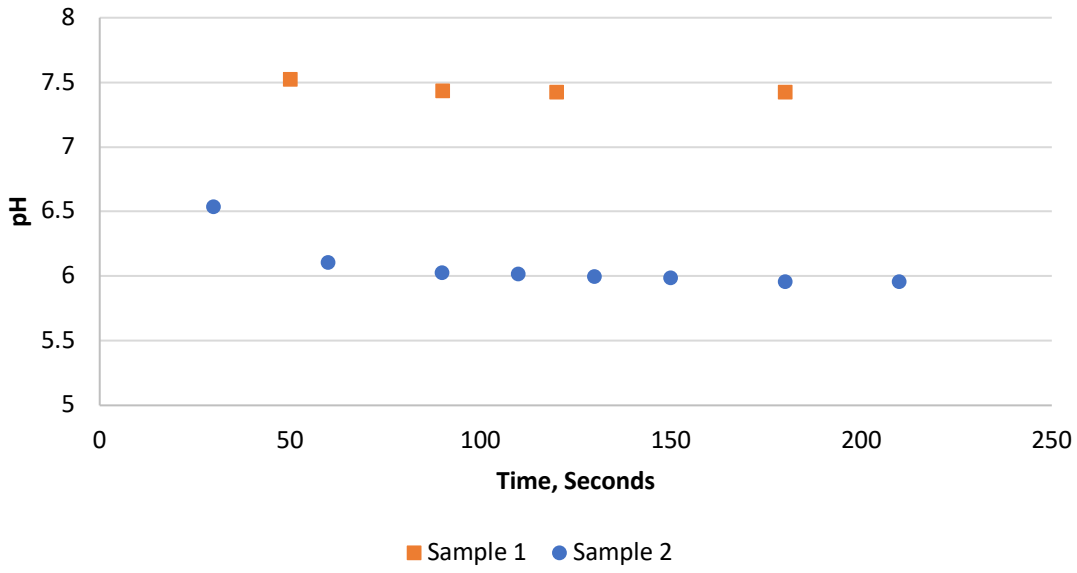

Figure (XI) pH Measurements against time for pH-adjusted sulphide solution after opening their caps showing no impact of H_2S evolution on pH

Appendix C - Experimental Procedures

The De-Oxygenation of Aqueous Solutions

Although anaerobic samples discussed in this report have shown insignificant oxidation results, it was discovered that these solutions might not have been entirely anaerobic. The followed procedure for nitrogen purging was 15 and 25 minutes for 11 and 40 mL, respectively, at a regulated pressure of 2 pounds per square inch (psi). However, monitoring the dissolved oxygen concentration has determined a drawback in this procedure, and two experiments were carried out to correct this step using 40 mL of NSSW in 40 mL culture vial. The first experiment was to find the best-regulated pressure that can be used to reach a minimum dissolved oxygen concentration in the shortest period, and the second experiment investigated the re-dissolution of limited and unlimited atmospheric oxygen. Figure (I) shows the results for the lowest oxygen concentration at the shortest purging period.

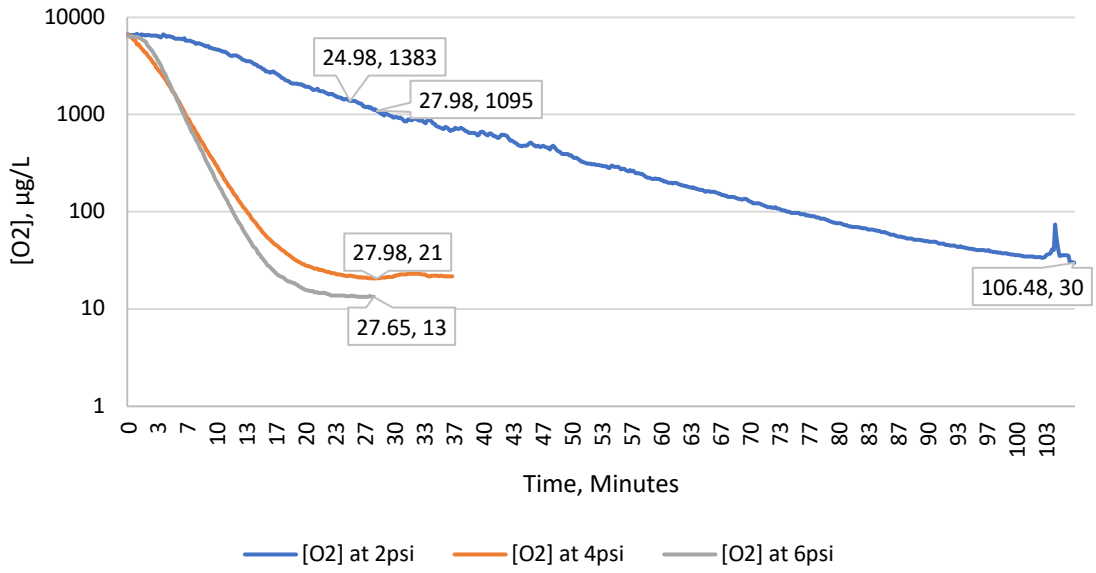

Figure (I): Concentrations of dissolved oxygen concentrations against time at different flow rates at different regulated pressure values, and atmospheric pressure and room temperature

Using 6 psi of regulated pressure has shown the optimum results so far. Increasing the pressure might produce favourable results; however, it could also be potentially unsafe while using narrow needles as inlets and outlets for the gas flow. From Figure (I), it could be assumed that 40 ml samples purged for 25 minutes at a flow rate of 2 psi regulated

pressure could have contained 1.3 - 1.4 mg/L of dissolved oxygen. Other samples of 11 ml volumes were purged for 15 minutes, thus, might not include similar oxygen concentration, but they definitely contain oxygen. Nonetheless, static oxidation reactions which lasted for one week showed an insignificant effect of such concentrations in the anaerobic solutions at test conditions.

The results from the second experiment, shown in Figure (II), further provided extra margins of flexibility when exposed to oxygen is concerned. At t = 106 minutes, dissolved oxygen level was at 29.7 µg/L, and the culture vial was opened briefly (~20-30 seconds) to allow the headspace to be filled with air, then it was closed again. At t = 138 (after 32 minutes from closing the vial's cap), the dissolved oxygen concentration reached 44.6 µg/L, then the concentration significantly increased to reach 500 µg/L at t = 166 minutes. After 34 minutes (t = 200 minutes), the vial was opened and left open until dissolved oxygen reached ~5,800 µg/L at t = 1366 minutes (22.7 hours).

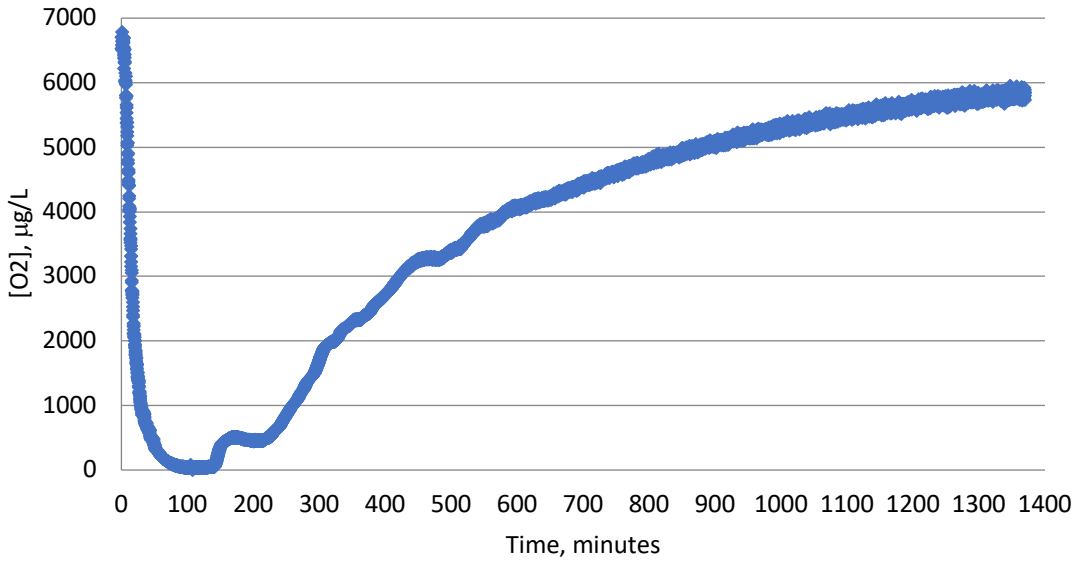

Figure (II) The re-dissolution rate of limited and unlimited atmospheric oxygen in 40 mL NSSW at atmospheric pressure and room temperature

Appendix D - Sulphide Oxidation

The Depletion of Aqueous Sulphide at Various Solutions

The oxidation of aqueous sulphide depends significantly on the concentration of dissolved oxygen in solution. Therefore, several sodium sulphide solutions were prepared distinctively to identify the impact of the preparation method on the oxidation of sulphide manifested as the depletion of the concentration of aqueous sulphide.

Two sulphide solutions of ~ 250 mg/L of aqueous sulphide (~ 0.0731 g of $Na_2S.9H_2O$ in 250 mL of NSSW) were prepared in aerated and degassed NSSW. The aerated sulphide solution was distributed in 5 mL aliquots into Hungate-type tubes and labelled as aerobic and semi-anaerobic. The degassed sulphide solution was distributed in 5 mL aliquots into Hungate-type tubes and labelled degassed and anaerobic. The anaerobic and semi-anaerobic solutions went through a de-oxygenation step prior to introducing HCl to adjust the pH. These solutions and the applied steps are shown in Table (II). Various volumes of 1 M HCl were injected in these solutions and the aqueous sulphide concentrations were measured using the UV-Vis method. The aqueous sulphide concentration at various HCl injected volumes have been normalised and demonstrated in Figure (III).

Table (II) Sulphide solutions and the corresponding applied preparation steps

	Duration			
Steps	*Aerobic*	*Semi-anaerobic*	*Degassed*	*Anaerobic*
De-oxygenation	-	15 minutes	-	20 minutes
Degassing	-	-	30 minutes	30 minutes

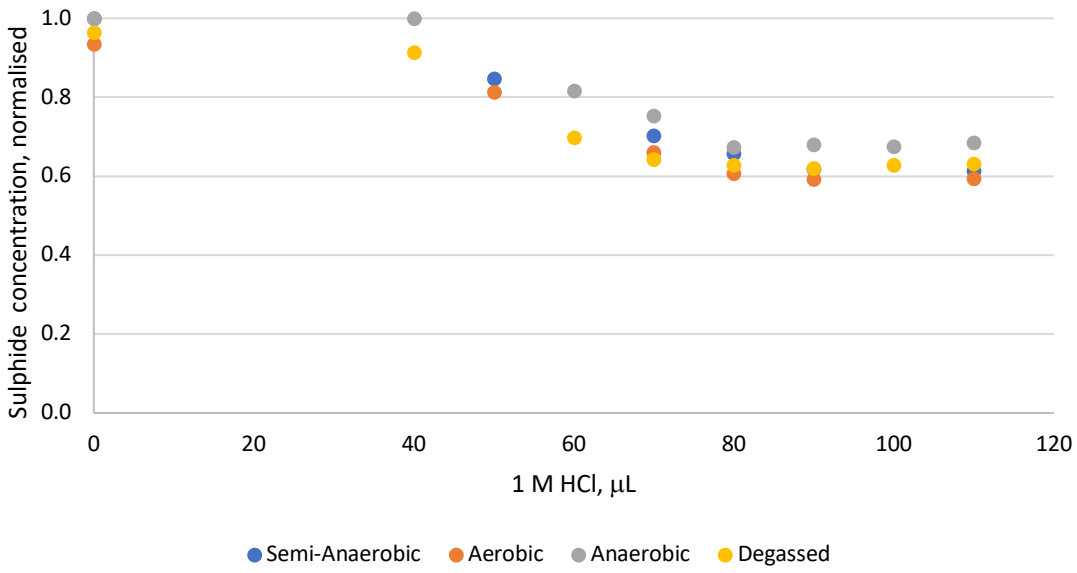

Figure (III) Normalised aqueous sulphide concentrations after injecting various volumes of 1M HCl into sulphide solutions with supposedly different dissolved oxygen levels.

The depletion of aqueous sulphide concentrations was found to be minimum in the anaerobic solution, which was 7.5 – 15 % higher than the sulphide levels in the aerobic solution. The sulphide concentrations in the degassed and the semi-anaerobic solutions were slightly higher than those in the aerobic solution, yet lower than the anaerobic sulphide concentrations. Nonetheless, the difference in sulphide concentrations (7.5 – 15 %) can be neglected if the total concentration is high, as in this test, and in excess to the metal cation (Zn or Pb). The impact is more significant at lower concentrations (e.g. less than 100 mg/L) of limiting sulphide in excess of the scaling cation.

Appendix E - Direct Formation of FeS at Variable-pH Solutions

The formation and solubility of FeS are highly dependent on the pH of solution. Adjusting the final pH of the FeS supernatant solution has been previously achieved (Okocha, 2011; Przybylinski, 2001, 2003). However, the instantaneous formation of FeS is thought to be quicker than the pH adjustment of the aqueous sulphide solution. Therefore, several tests were performed to form and inhibit FeS using pH-adjusted aqueous sulphide solutions.

The oxygen-free sulphide solutions were prepared in 1,000 mg/L concentrations and diluted further to achieve 500 and 100 mg/L of sulphide. These solutions were injected with 1M HCl to achieve pH levels below and above pH 4. The analysis of supernatant solutions included ICP to determine the residual iron concentrations, UV-Vis for the aqueous sulphide concentrations, and pH measurements. The results of these tests are shown in Figure (IV) - (VIII). The analysis of iron was not performed to all samples in Figure (IV) and (V).

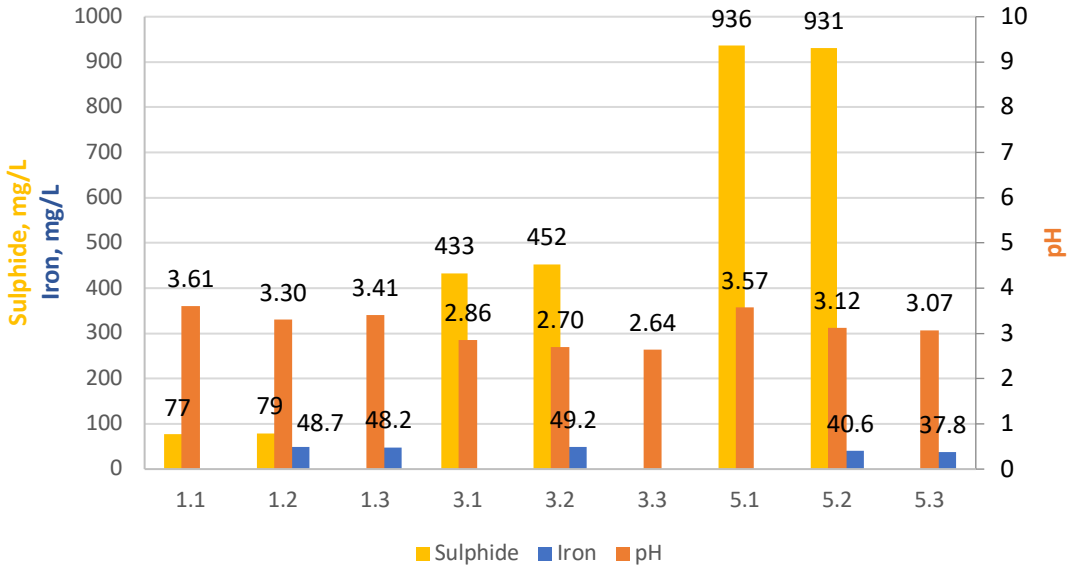

Figure (IV) The concentrations of aqueous sulphide and iron at pH < 4

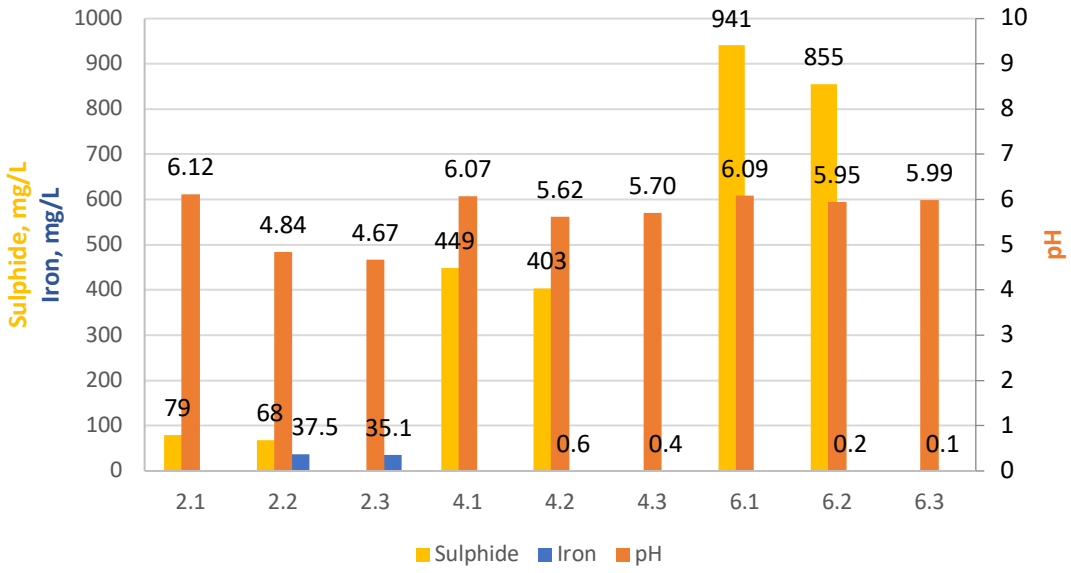

Figure (V) The concentrations of aqueous sulphide and iron at pH > 4

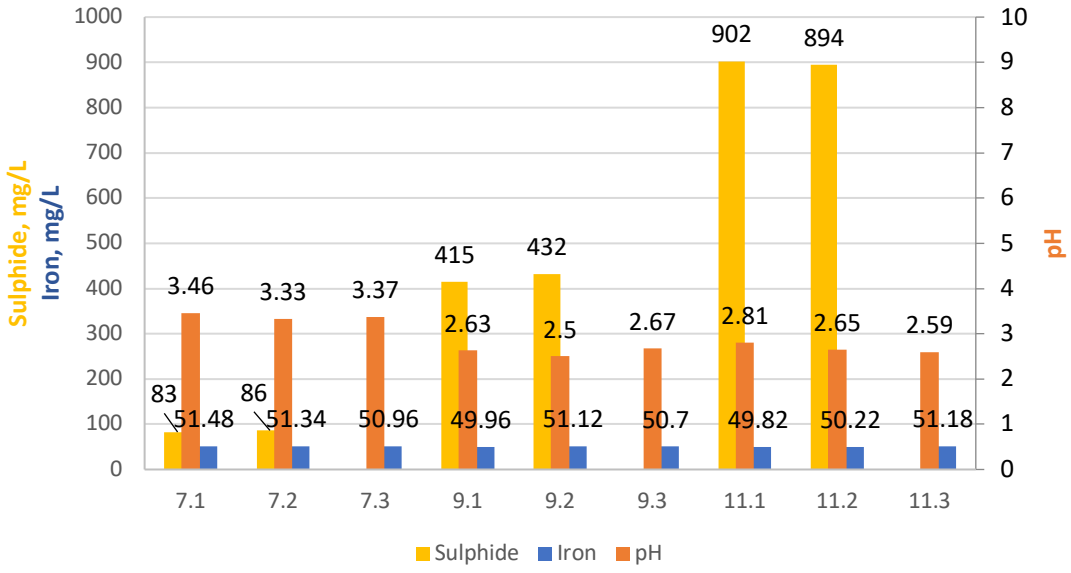

Figure (VI) The concentrations of aqueous sulphide and iron (SI = 50 mg/L) at pH < 4 after filtration through 0.2 µm filter

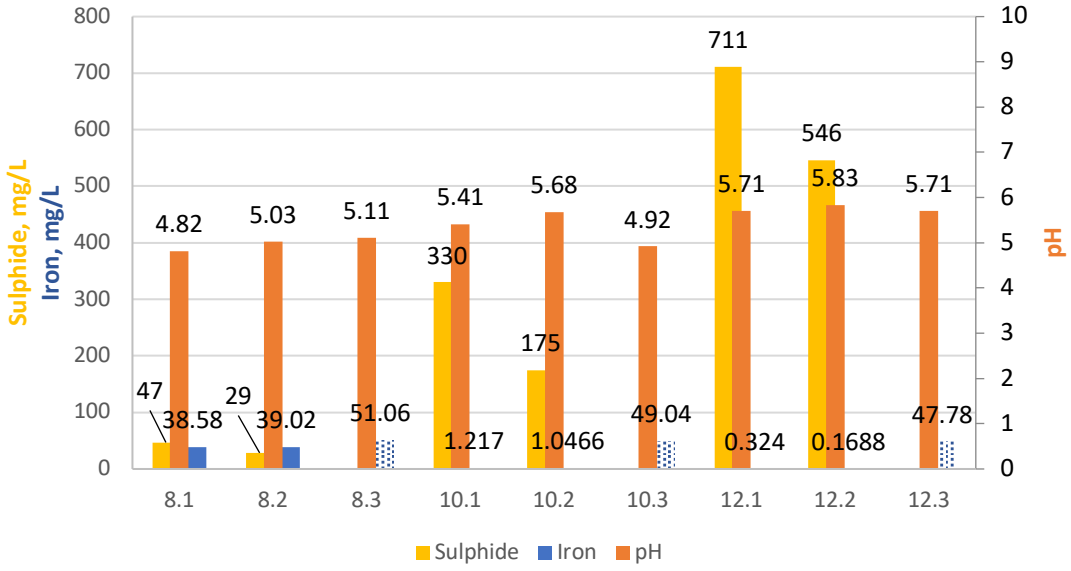

Figure (VII) The concentrations of aqueous sulphide and iron (SI = 50 mg/L) at pH > 4 after filtration through 0.2 µm filter (Dotted bars represent unfiltered samples)

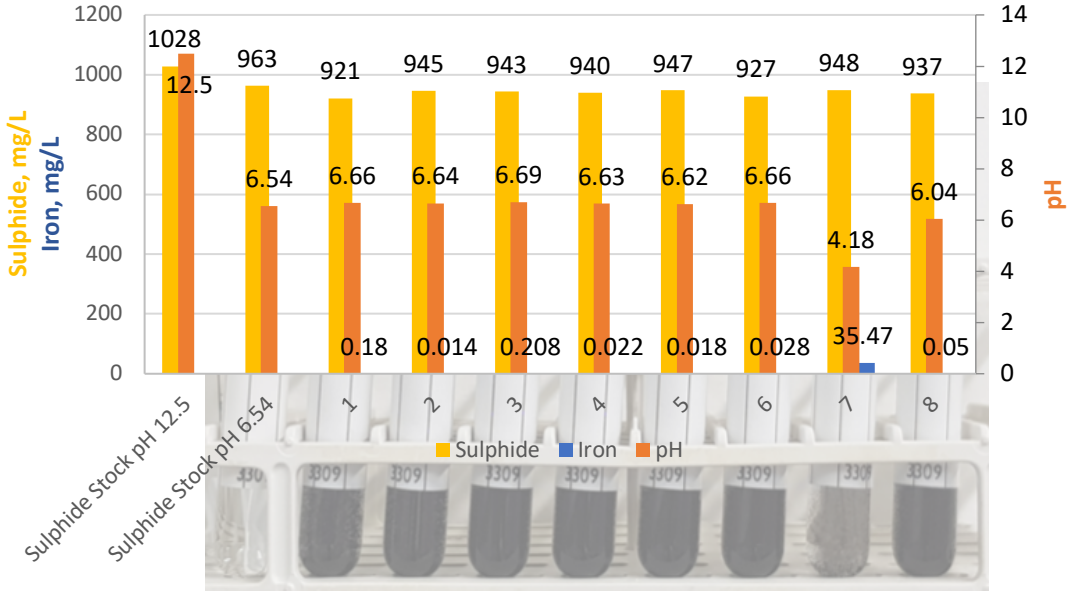

Figure (VIII) The repeatability of pH adjustment and the iron and aqueous sulphide concentrations at pH > 4

Appendix F – ICP Analysis Protocol (for TF-iCAP 6500DV and HJY-U2 Equipment)

The following protocol is cited from Heriot-Watt University's FAST internal General Laboratory Procedure and Risk Assessment (GLP RA) for ICP analysis:

1. Prepare the brines/solutions required for the procedure.
2. Prepare standards for each set of analysis. Refer to the note below for the iCAP internal standard.
3. Ensure the torch/sample introduction glassware and tubing have been clean.
4. Light the plasma and allow a warm up time of 1hr before initiating an analysis run. For the TF-iCAP 6500DV – a Zn stability needs to be performed after 10-15mins warm up and prior to starting the run – use the zinc stability method. A zinc stability std is 2ppm Zn & 0.01% methanol (2ml from a 1000ppm ICP std and 0.1ml of methanol) in 1L of distilled water.
5. Set up method and sequence.
6. **HJY – U2:** Run profiles to check background correction points for each element in the appropriate DW or brine. Set the backgrounds in the method for each element.
7. **TF – iCAP 6500DV:** Backgrounds are run automatically alongside the sample but can be manipulated afterwards.
8. **Both instruments:** Run a calibration and a set of repeats to check repeatability.
9. Check that the calibration for each element is successful and that the repeats for the standards are consistent with the expected values.

Samples could now be run. Samples at known concentrations are statistically analysed for their precision and accuracy, the definition of which are outlined below.

Note: In step 2, for the Thermofisher iCAP, an additional preparation of an internal standard is required. There are a number of factors to consider when choosing the internal standard:-

- The internal standard should behave similarly to the element of interest in the plasma. For best results, where possible, the atomic (I) or ionic (II) state of the element line should match that of the internal standard line. A similar wavelength should also be used. If the element line is a low wavelength (<235nm (4xx)) then the internal standard line should also be a low wavelength. If the element line is a high wavelength (>235nm (1xx or 0xx)) then the internal standard line should also

be a high wavelength. It is also advisable to match the viewing option i.e. a radial element line with a radial internal standard line

- The most commonly used wavelengths for the yttrium internal standard are 224.306nm (for low wavelengths) and 371.030nm (for high wavelengths). Other wavelengths that can be used, although less frequently, are 324.228nm and 360.773nm

The internal standard could contain a number of different elements such as Rhodium, Scandium, Indium, Gold, Yttrium, Caesium in 1% Nitric Acid or distilled water for sulphide/EDTA containing solutions. This internal standard is sprayed at a low flow rate at all times throughout the analysis run. **NOTE:** Do not include Gold or Rhodium in the internal standard solution used for sulphide sample analysis. The initial Gold and Rhodium standards are prepared in a strongly acidic matrix. The low acidity encourages sulphide deposition in the nebuliser line after the Y piece. There are two consequences from this; hydrogen sulphide gas is released – not good and if a deposit does occur, it is very difficult to remove and in fact the tubing needs to be replaced as opposed to cleaned. Caesium is sometimes present in the internal standard to reduce or stop ion suppression happening however if it does occur then the other elements can be used to account for this ion suppression. To ensure effective mixing and reduce any air bubble effects, Triton X100 is also added to the internal standard solution if a Y-piece setup is being used. The final concentration of Triton in the internal standard is 0.1%.

Preparation of Internal Standard

With Nitric Acid	**In Distilled Water Without Nitric Acid**
2ml 10,000ppm Y standard 400ml of 5% Nitric containing 0.1% Triton Additional 1.6ml Triton to give overall 0.1% Triton All in 2L of Distilled Water ⇨ 10ppm Y, 0.1% Triton in 1% Nitric Acid	2ml 10,000ppm Y standard 2ml Triton X100 ⇨ 10ppm Y, 0.1% Triton in DW
NOTE: When adding the Triton, have the solution already stirring with an excess of the background solution present. The Triton is extremely thick and this swirling helps it dissolution	

Accuracy is the degree of agreement between the measured value and the true value. An absolute true value is seldom known. A more realistic definition of accuracy then would be to assume it is the agreement between a measured value and the *accepted* true value.

Precision is defined as the degree of agreement between replicate measurements of the same quantity. It is the repeatability of the result. This is also known as standard deviation. However, good precision does not mean good accuracy, for instance, if there was a systematic error in the analysis. This error would not affect the precision but it does affect the accuracy.

10. Using the diluter or a pipette, do the appropriate dilution for the elements in question, so their concentrations fit within the calibration range of the corresponding element calibration standards.
11. Run the real samples.
12. Give data to personnel responsible for the plotting of results
13. Personnel will use the appropriate ICP macro to manipulate the data to determine the concentration of the analysed samples
14. Construct a summary table of results

Analysis Exceptions: Sulphide ion analysis cannot be performed by ICP-OES. The calibration standards and samples are potentially affected by the aspiration process of the nebuliser and drop in pressure as it flows through the torch assembly. This encourages further S^- ions to be produced which when analysed by ICP gives a higher sulphur concentration than expected. However, solutions containing sulphide ions but are not being analysed for sulphur concentration can be run through the machine but there are precautions to be taken;

1. Sulphide containing samples must only be run during the day and not stored in the analytical lab. A personal H_2S alarm unit and the local exhaust ventilation over the autosampler must be used when the samples have been removed from the local fume cupboard and uncapped for the run

2. Immediately after the run, samples must be capped and transferred back to the Sulphide laboratory and placed in the fume cupboard, This lab must have a fixed H_2S wall alarm which would detect any leaks of H_2S

3. During the analysis run, there must be no contact with the nitric acid rinse e.g. in tubes or waste container. A distilled water rinse must be used and the waste container emptied and rinsed prior to being used for this run
4. The waste container must be emptied into sulphide waste immediately after a run
5. Do not include Gold or Rhodium in the internal standard solution used for sulphide sample analysis. This is due to the strongly acidic matrix used for these standards. This is discussed in more detail earlier in this procedure.
6. **Note:** When using an internal standard throughout an analysis run, acceptable fluctuation for the internal standard intensities is regarded to be within 80 – 120% provided the results are reported accordingly. If the internal standard falls below 60% then a dilution of the sample is required or perhaps machine maintenance would be beneficial, depending on the cause of low recovery. With recoveries above 140%, the run should be stopped and then restarted if this has been caused by conditioning due to the sample matrix

Chemical Tick Forms Applicable with this Activity

Hazardous Substances Classification List of Individual Substances*	Hazard Classification √							
Nitric acid 69%: **Used at 5% for ICP acid rinse & 1% for internal std matrix** Corrosive. Causes severe burns. Do not breathe fumes. In case of contact with eyes, rinse immediately with plenty of water and seek medical advice. **Concentrated acids should be used in the fume cupboard.**	**Very toxic**	**Toxic**	**Harmful**	**Corrosive**	**Irritant**	**Dust**	**Carcinogen**	**Micro-organism**
			√	√				

Hazardous Substances Classification List of Individual Substances	Hazard Classification √							
Argon, refrigerated, liquid Contact with skin may cause burns or frostbite. Damage to eyes on contact. Asphyxiate at high concentrations. Containers should be kept out of doors away from excessive heat. High pressure gas.	**Very toxic**	**Toxic**	**Harmful**	**Corrosive**	**Irritant**	**Dust**	**Carcinogen**	**Micro-organism**
			√					

Hazardous Substances Classification List of Individual Substances	Hazard Classification √							
Nitrogen, refrigerated, liquid Contact with skin may cause burns or frostbite. Damage to eyes on contact. Asphyxiate at high concentrations. Containers should be kept out of doors away from excessive heat. High pressure gas.	**Very toxic**	**Toxic**	**Harmful**	**Corrosive**	**Irritant**	**Dust**	**Carcinogen**	**Micro-organism**
			√					

Hazardous Substances Classification List of Individual Substances*	Hazard Classification √							
Cesium Chloride Electran ® for Molecular Biology **Supplier: VWR** This substance is not classified as dangerous. Use PPE. If it does come into contact with the skin or eyes, wash thoroughly with water. If inhaled remove to fresh air but watch for tract irritation and seek medical help if swallowed. First Aiders are to pay attention to self-protection. In fire: hydrogen chloride gas liberated – fire fighters to wear breathing apparatus. Do not allow run off into drains or water courses. Collect up any spilt solid and dispose of suitably via contractor. Do not breathe dust. Use local extraction when handling the solid, if unavailable use under nitrogen gas. Store between 15-25ºC.	**Very toxic**	**Toxic**	**Harmful**	**Corrosive**	**Irritant**	**Dust**	**Carcinogen**	**Micro-organism**
					√	√		

Hazardous Substances Classification List of Individual Substances*	Hazard Classification √							
Gold 1000ppm ICP standard **Supplier: Romil** **MSDS no: RSE3025** Contains 10-25% HCl. Causes burns. Irritating to eyes, respiratory system and skin. In case of contact with eyes rinse immediately with plenty of water and seek medical advice. In case of accident or if you feel unwell, seek medical advice immediately. Fire: produces toxic fumes. Wear PPE. Neutralise spills with sodium carbonate then use large quantities of water and flow to drain. Avoid; water as there are strong reactions. Environmental toxicity unknown	**Very toxic**	**Toxic**	**Harmful**	**Corrosive**	**Irritant**	**Dust**	**Carcinogen**	**Micro-organism**
				√	√			

Hazardous Substances Classification List of Individual Substances*	Hazard Classification √							
Rhodium 1000ppm ICP standard **Supplier: Romil** **MSDS no: RSE3025** Contains 10-25% HCl. Causes burns. Irritating to eyes, respiratory system and skin. In case of contact with eyes rinse immediately with plenty of water and seek medical advice. In case of accident or if you feel unwell, seek medical advice immediately. Fire: produces toxic fumes. Wear PPE. Neutralise spills with sodium carbonate then use large quantities of water and flow to drain. Avoid; water as there are strong reactions. Environmental toxicity unknown	**Very toxic**	**Toxic**	**Harmful**	**Corrosive**	**Irritant**	**Dust**	**Carcinogen**	**Micro-organism**
				√	√			

Hazardous Substances Classification List of Individual Substances*	Hazard Classification √							
Scandium 1000ppm ICP standard **Supplier: Romil** **MSDS no: RSE3010** Contains < 5% Nitric. Causes severe burns. Contact with combustible material may cause fire. Irritating to eyes - rinse immediately with water or saline solution for at least 15mins and seek medical advice. Wear PPE. Neutralise spills with sodium carbonate then use large quantities of water to wash site of spillage to drain. Avoid; water as there are strong reactions. Environmental toxicity unknown	**Very toxic**	**Toxic**	**Harmful**	**Corrosive**	**Irritant**	**Dust**	**Carcinogen**	**Micro-organism**
				√	√ **eyes**			

Hazardous Substances Classification List of Individual Substances*	Hazard Classification √							
Indium 1000ppm ICP standard **Supplier: Romil** **MSDS no: RSE3010** Contains < 5% Nitric. Causes severe burns. Contact with combustible material may cause fire. Irritating to eyes - rinse immediately with water or saline solution for at least 15mins and seek medical advice. Wear PPE. Neutralise spills with sodium carbonate then use large quantities of water to wash site of spillage to drain. Avoid; water as there are strong reactions. Environmental toxicity unknown	**Very toxic**	**Toxic**	**Harmful**	**Corrosive**	**Irritant**	**Dust**	**Carcinogen**	**Micro-organism**
				√	√ **eyes**			

Hazardous Substances Classification List of Individual Substances*	Hazard Classification √							
Yttrium 10,000ppm ICP standard **Supplier: Romil** **MSDS no: RSE7010** Contains < 5% Nitric. Causes severe burns. Contact with combustible material may cause fire. All ingredients at concentrations not classified as hazardous. Irritating to eyes - rinse immediately with water or saline solution for at least 15mins and seek medical advice. Wear PPE. Neutralise spills with sodium carbonate then use large quantities of water to wash site of spillage to drain. Avoid; water as there are strong reactions. Environmental toxicity unknown	**Very toxic**	**Toxic**	**Harmful**	**Corrosive**	**Irritant**	**Dust**	**Carcinogen**	**Micro-organism**
				√	√ **eyes**			

Hazardous Substances Classification List of Individual Substances*	Hazard Classification √							
Triton X100 (Polyethylene glycol mono [4-(1, 1, 3, 3-tetramethylbutyl)phenyl] ether **Supplier:** Fisher Scientific Harmful if swallowed – seek medical help. Causes burns. Harmful to aquatic life. Causes serious eye damage. Toxicological properties have not been fully investigated. Avoid release to the environment – long term adverse effects. Expected to be biodegradable Fire: irritating gases/vapours i.e. CO, CO_2 – fire brigade to wear breathing apparatus. Ensure adequate ventilation and shower/eye wash facilities are available. Avoid heat, exposure to air (explosive peroxides formed), exposure to light (degradation), incompatible products such as strong oxidising/reducing agents and strong acids	**Very toxic**	**Toxic**	**Harmful**	**Corrosive**	**Irritant**	**Dust**	**Carcinogen**	**Micro-organism**
			√ ingest enviro	√	√ Fire:gas			